DISTRIBUTED SERIES REACTANCE: A NEW APPROACH TO REALIZE GRID POWER FLOW CONTROL

A Thesis
Presented to
The Academic Faculty

by

Harjeet Johal

In Partial Fulfillment
of the Requirements for the Degree
Doctor of Philosophy in the
School of Electrical and Computer Engineering

Georgia Institute of Technology
December 2008

DISTRIBUTED SERIES REACTANCE: A NEW APPROACH TO REALIZE GRID POWER FLOW CONTROL

Approved by:

Prof. Deepakraj M. Divan, Advisor
School of Electrical and Computer Engineering
Georgia Institute of Technology

Prof. Miroslav M. Begovic
School of Electrical and Computer Engineering
Georgia Institute of Technology

Prof. Ronald G. Harley
School of Electrical and Computer Engineering
Georgia Institute of Technology

Prof. Wayne H. Wolf
School of Electrical and Computer Engineering
Georgia Institute of Technology

Prof. Marilyn Brown
School of Public Policy
Georgia Institute of Technology

Date Approved: 11/10/2008

To my loving parents and my sweet brother

ACKNOWLEDGEMENTS

My PhD at Georgia Tech has helped me immensely to lay a foundation for my future professional life. I have received invaluable support from my teachers, colleagues, and friends, without whom this journey would not have been possible.

First, I would first like to express sincere gratitude for my advisor Professor Deepak M. Divan. His guidance and support has always helped me to think creatively and instigated a philosophy of "always believe in yourself." I will always be indebted to him for helping me choose my career path. I am also thankful to Professor Ronald G. Harley and Professor Miroslav M. Begovic for being wonderful teachers and for their support to my thesis work. I would also like to extend my gratitude to Professor Marilyn Brown and Professor Wayne H. Wolf for serving on my PhD defense committee and for their valuable suggestions.

I am extremely grateful for the help and support from Mr. Frank Lambert and Mr. Paul Springer. Their suggestions, guidance, and help have helped immensely for this thesis work. I would also like to thank other NEETRAC personnel, especially Jorge Altamirano and Mr. Thomas Parker for helping me with the experimental work. My thanks to Ms. Deborah King for always being so patient with me, and helping me with the lab orders and organization of events. This thesis work was supported under research contract from TVA, ABB, ConEd, and DOE. I would like to acknowledge their financial support for my graduate studies.

Additionaly, I would like to thank all my family and friends who have always helped me and have been a source of inspiration. I would especially like to thank my sister, Yamille Del Valle and my friend Dr. Navin Elango for their support and for always being there for

me. My heartfelt gratitude for Jean Carlos, Dr. Afroz Imam, Dr. Satish Rajagopalan, Jyoti Sastry, Anish Prasai, Yi Yang, Debrup Das, and Frank Kreikebaum for their wonderful friendship. It was a pleasure for me to be with you all.

Finally, I would like to thank my parents and my brother for their unconditional love, support, and confidence that has always helped me through difficult times.

TABLE OF CONTENT

LIST OF TABLES

LIST OF FIGURES

SUMMARY

The objective of the proposed research is to develop a cost-effective power flow controller to improve the utilization and reliability of the existing transmission, sub-transmission, and distribution networks. Over the last two decades, electricity consumption and generation have continually grown at an annual rate of around 2.5% [1]. At the same time, investments in the Transmission and Distribution (T&D) infrastructure have steadily declined. Further, it has become increasingly difficult and expensive to build new power lines. As a result, the aging power-grid has become congested and is under stress, resulting in compromised reliability and higher energy costs. In such an environment it becomes important that existing assets are used effectively to achieve highest efficiency.

System reliability is sacrosanct and cannot be compromised. Utility system planners are moving from radial towards networked systems to achieve higher reliability, especially under contingency conditions. While enhancing reliability, this has degraded the controllability of the network, as current flow along individual lines can no longer be controlled. The transfer capacity of the system gets limited by the first line that reaches the thermal capacity, even when majority of the lines are operating at a fraction of their capacity. The utilization of the system gets further degraded as the lines are operated with spare capacity to sustain overloads under contingencies. Market efficiency is also sub-optimal, with congestion on key corridors restricting the low-cost generators to connect to the end users, resulting in higher electricity prices for the consumers.

The proposed technology offers the capability to realize a controllable meshed-network, with the ability to utilize static and dynamic capacity of the grid to provide system-wide benefits, including- increased line and system-capacity utilization, increased reliability, improved operation under contingencies, and rapid implementation. It would allow a broadening of the energy market, permitting owners to direct how energy flows on their wires, and making it easier to connect to new sources of generation.

CHAPTER 1

OBJECTIVE OF RESEARCH

1.1 Introduction

Increasing demand of electricity has put unprecedented pressure on the US power-grid. Transmission bottlenecks and congestion have become a frequent sight for the network operators. The conventional method of reinforcing network capacity through building additional lines has become difficult to implement, with long delays in siting and approval process. To compound the situation, the utilities often do not possess detailed information on the status and operating margins on their various geographically-distributed power-line assets, resulting in sub-optimal use. In today's competitive environment, the ability to use its assets efficiently becomes an important component of a utility's profitability.

While radical changes in infrastructure may seem attractive, and in line with transformations that have occurred in the telecom and internet areas, the analogies are likely to be misleading at best. Unlike in telecom where society's bandwidth requirements have grown exponentially, no metrics can be identified in the power delivery industry; although the performance has improved by several orders of magnitude over the last decade. With the exception of a few high growth opportunities, e.g. China and India, where building new infrastructure is a priority, enormous legacy investments exist in the existing power delivery infrastructure and one can only posit incremental improvements on the existing infrastructure.

A few critical requirements can clearly be defined. System reliability is sacrosanct and cannot be compromised. Utility system planners are moving away from radial systems towards networked systems to achieve higher reliability, especially under contingency conditions. While enhancing reliability, this degrades controllability of the network, as current flow along particular lines cannot easily be controlled. The situation is exacerbated when a contingency such as loss of a line or generator results in overload and tripping of lines, increasing the possibility of a cascading blackout. Finally, rapid load growth leads to congestion on key lines connecting low-cost generation to load centers, leading to an inefficient operation of energy markets.

The answer seems to lie in the implementation of a 'Smart Grid', that is reliable, self-healing, fully controllable and asset efficient. The research outlined in this thesis introduces a power flow controller that can enhance T&D system reliability, increase asset utilization, and improve operational efficiency of the power market.

1.2 Objective

The objective of this research is to develop a power-flow control solution that can provide the ability to utilize static and dynamic capacity of the grid, to provide system-wide benefits, including- increased line and system-capacity utilization, increased reliability, improved operation under contingencies, and rapid implementation.

Proof of concept is first shown by benchmark studies on simplified power networks. Various metrics are suggested to quantify the performance of the solution in terms of improvement in system utilization and reliability. Economic impact of the proposed technology on the welfare of various market stakeholders is presented and some

public finance mechanisms are proposed for creating investment opportunities for the technology. Finally, a design of the prototype is outlined to match its unique magnetic, electrical, and mechanical requirements and detailed experimental results are presented

1.3 Outline of Chapters

Dissertation begins by outlining the problem statement in Chapter 2. A comprehensive literature survey on the available solutions of power flow control is presented, detailing their control and operation. Limitations of the existing techniques are documented and required features for the proposed power flow controller are outlined.

Chapter 3 introduces the proposed power flow controller. The module structure and design features are outlined. A control strategy is presented for implementation of the technology on a system. Simulation studies are shown the robustness of the technology under non-idealities of operation.

The impact of the technology on improvement in system utilization, transfer capacity, and reliability is presented in Chapter 4. Various metrics are suggested to quantify the performance of the solution. A system wide deployment of DSR technology is only possible if all issues of interference to system operation are fully resolved. Chapter 5 presents anticipated interactions between DSR modules and system operation and discusses them in detail.

The transmission market is not open and is regulated by federal government and state utility commissions. Development of a new technology under such conditions cannot be done in isolation and without studying its economic impact on the market operation. Chapter 6 presents the current market policies and discusses the economic

impact of the DSR technology on the various stakeholders. The chapter puts forward some social business models and public finance mechanisms that can be used for creating a market for the DSR technology.

A detailed design of the prototype is outlined in Chapter 7. Module design revolves around the unique magnetic, electrical, and mechanical requirements of the application. Detailed results from experimental validation of the prototype are documented.

Chapter 9 presents a technique to control power flow along a designated path between a generator and a consumer. DSR technology offers the simplest implementation of the approach. Creating a pipeline flow of electrons is shown to support new market functions by specifying and validating the path taken by the electrons.

Conclusions, contributions, and recommendations for future work are presented in Chapter 10.

CHAPTER 2

ORIGIN AND HISTORY OF PROBLEM

2.1 Introduction

The US power sector can be broadly classified into three main sectors- generation, transmission, and distribution. The electricity produced by the generators is first transmitted over high voltage lines (66 KV to 765 KV) and then distributed at low voltage levels (below 66 KV) to the end consumers. The transmission network spans the entire country with more than 150,000 miles of lines and is geographically demarcated by three main interconnected regions, as shown in Figure 2.1 [1]. Within each of these interconnections, the control and operation of the transmission network is maintained by system operators and transmission organizations. Further, eight regional councils coordinate with the North American Reliability Corporation (NERC) to maintain a reliable and secure operation of the grid.

The US power grid is aging and under increasing stress. The modern industrial infrastructure demands increasing amounts of affordable and reliable electricity. After restructuring of the power sector, electricity generation is now driven by the free market forces and has responded well to the growth of electricity demand. However, a regulated transmission and distribution (T&D) sector has failed to keep pace with the generation sector and to comply with the increasing electricity needs. Congestion and transmission bottlenecks have become a regular issue for the system operators. The aging power-grid is under stress, resulting in compromised reliability and higher energy costs. The

following section outlines the problems and issues that we are facing today in the T&D sector.

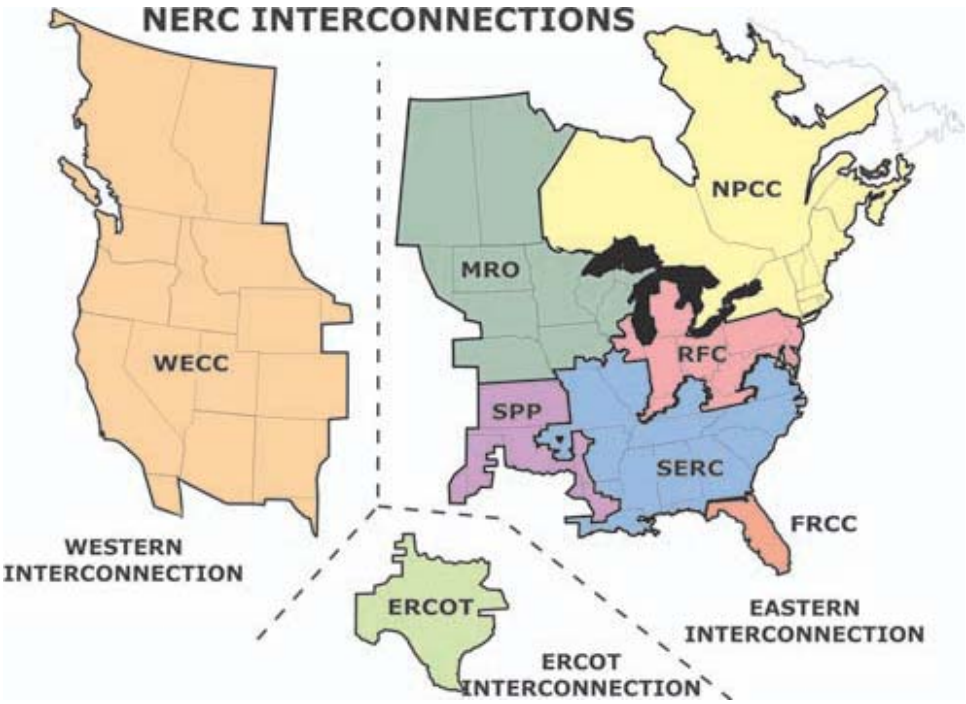

Figure 2.1 Geographical operation of reliability councils in the three interconnections

2.2 Transmission and Distribution: Problems and Issues

2.2.1 Declining Transmission Investment

With the restructuring of the power system currently underway and stalled partway through the process, tremendous risk and uncertainty exists about the structure of the industry. As a result, the investments in the transmission and distribution sector have been decreasing over the years. Figure 2.2 shows the steady rate of decline in the transmission investments until 2000. A recent pick-up in transmission investments has still not erased deficits from two decades of declining investments. This has resulted in an

increased loading on the existing transmission lines, making the grid very fragile to disturbances.

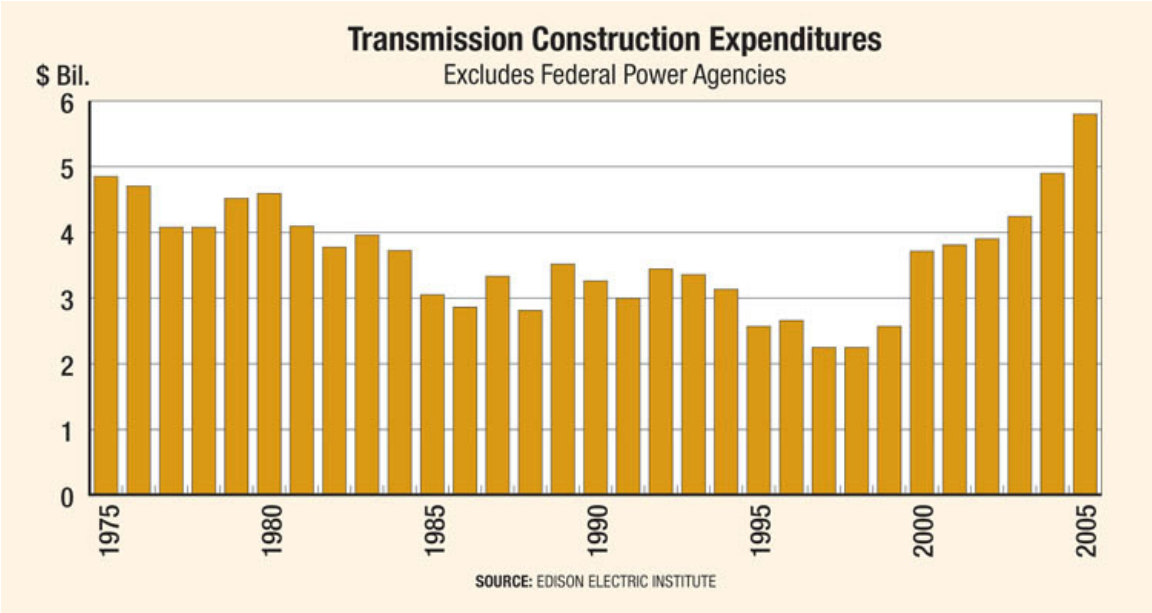

Figure 2.2 Transmission investments over the last 30 years

2.2.2 High Cost of Building Transmission Lines

Over the recent years there has been increasing public sentiment against locating power lines close to their communities. Acronyms such as NIMBY (Not In My Backyard) and BANANA (Build Absolutely Nothing Anywhere Near Anyone) have become more and more popular. Long delays in siting and approval of new transmission lines, makes the process very expensive. This is especially true for urban areas where the cost of land is very high. A recent study conducted by the Department of Energy (DOE) highlights increasing number of congested corridors near metropolitan areas [2].

2.2.3 Under Utilization of Existing Assets

Traditionally, the transmission systems were radial in structure, primarily because they were easier to build and provided fully controllable operation. However, such systems suffer from poor reliability because a single fault results in an extended outage for all downstream customers, severely compromising system reliability. Utilities are moving from radial systems to meshed networks at the distribution, sub-transmission, and transmission levels in an effort to enhance system reliability. In a meshed network, a fault results in the isolation of a single line segment, with alternate paths maintaining power to all other customers. This results in significantly higher reliability levels. Many urban centers, such as New York, have vast networks at the distribution level and consistently deliver some of the most reliable power in the US [3].

A major limitation of meshed networks is the inability to control the flow of power. The current always flows on the path of lowest impedance, which may result in an uneven loading of the network. The first line to reach the thermal capacity limits the power transfer capacity of the system, even though majority of the system may be operating much below the limit. Network reliability also demands that reserve margins be assigned to transmission lines to carry additional power so that no degradation of service occurs with a (N-1) contingency. This further lowers the available transfer capacity of the transmission system and results in a sub-optimal operation of the grid.

The utilization of a meshed grid can be improved if the power-flow can be controlled through the lines of the network. By steering the current in an appropriate manner, it is possible to equally distribute the loading on the lines, making the overall system operate at its theoretical maximum capacity. Numerous algorithms and controllers

have been suggested to achieve this objective. The following section gives an overview of these solutions and highlights their impact and limitations on power-flow control.

2.3 Existing Solutions to Improve T&D Capacity

The conventional solution used by the utilities to improve the T&D capacity has been building of additional lines. This involves long term planning as the siting and approval process can take up to 10 years. To improve the capacity and reliability of the grid in the short run, it is imperative to develop solutions that can use the available infrastructure and asset base more effectively. Providing the ability to control the flow of current can help the system operators to use the network resources more efficiently. State estimation is one such technique that adjusts line flows, by monitoring the prevailing system conditions, to extract the unused capacity from the grid.

2.3.1 State Estimation

A complete knowledge of the operating conditions of the system can help to route the flow of power in an optimal way and enhance the overall utilization of the grid at all times. For instance, if all the line currents in a network are known, then by controlling transformer tap settings and adjusting the generator dispatch, the currents can be steered in a way to improve the utilization of the lines.

The objective of state estimation is to estimate the unknown network quantities, which can be voltage magnitudes, phase angles, etc., from the quantities that are easily measurable such as generator's injected power, line reactance, transformer tap settings, etc. As an example, if the net power injection at each node is known, along with the

network reactance matrix, then equation (2.1) can be used to calculate the voltage magnitudes and phase angles. Once the voltage magnitudes and phase angles are known, then the current/power flowing on individual lines can easily be calculated. Equation (2.1) is a non-linear equation and must be solved using numerical algorithms [4]-[5].

$$\begin{aligned} P_k + jQ_k &= \tilde{E}_k \sum_{m=1}^{N} \tilde{Y}_{km}^{*} \tilde{E}_m^{*} \\ \tilde{E}_k &= |E_k| \angle \delta_k \\ \tilde{E_m} &= |E_m| \angle \delta_m \end{aligned} \tag{2.1}$$

Here P_k and Q_k are the real and reactive powers entering node k, $|E_k|$ and $|E_m|$ are the magnitude of the voltages at nodes k and m respectively, δ_k and δ_m are the voltage phase angles at nodes k and m respectively, Y_{km} is the admittance matrix, N is the number of nodes in the network, superscript ~ means that the associated quantities are vectors, and * refers to the complex conjugate.

Most of the times, the measured quantities are not error free and may get corrupted by digitization noise. Under these conditions, the estimated parameter may not correlate to the true value and the adjusted power-flow might not meet the objective. However, if additional measurements are provided, it is possible to produce a statistical estimate of the system state [6]-[7]. These additional measurements can be node voltages, line currents, etc.

State estimation problem is formally defined by equation (2.2). It takes M measurements to estimate N states of the system (M>N). Once the states of the system are know with some degree of accuracy, it is possible to dispatch the resources optimally to improve the controllability of power through the network.

$$z = h(x) + \varepsilon \tag{2.2}$$

Here z is a vector (M x 1) of measured quantities, x is the system state vector (N x 1) given by the voltage magnitudes and angles, h is a vector function defining the relation between the states and the measurements, and ε is the measurement error.

It must be noted that communications between the control centers and sensors/monitoring units on the grid is the basic requirement for the operation of the state estimation algorithms. Once the state of the system is known, then network resources can be adjusted in a way to improve the efficiency of operation. A similar technique of improving the utilization of lines and transfer capacity of the existing network is optimal power-flow control.

2.3.2 Optimal Power Flow Control

Optimal power flow (OPF) gives the optimal dispatch of power through a network, satisfying a given objective function [8]-[9]. The objective function is formulated so as to improve the efficacy of the grid-operation and can be minimization of line losses, fuel costs, or reactive power generation. The optimization is done satisfying

the system constraints, which can be specified as limits on the line current flows, voltage magnitudes, reactive powers of shunt VAR compensators, etc. Two variables are used in an OPF simulation. They are described as below:

1. State variables (specified by a vector [x]): These are the dependent system variables to which the OPF finds a solution. Bus voltages and angles are the state variables in an OPF problem. State variables are sometimes constrained within certain limits (e.g. the range of feasible voltage magnitude is specified for a PQ bus), as shown in equation (2.3).

$$\left[V_{\min}\right] \leq [V] \leq \left[V_{\max}\right] \tag{2.3}$$

Here V is the state variable denoting a bus voltage, specified to be within a certain range.

2. Control variables (specified by a vector [u]): These are the independent system variables such as transformer tap settings, generating unit's reactive power, etc. These variables can be controlled during the OPF analysis. However, their permissible values are constrained (e.g. a maximum upper limit may be specified for reactive power generation from a shunt capacitor), as given by equation (2.4).

$$\left[u_{\min}\right] \leq [u] \leq \left[u_{\max}\right] \tag{2.4}$$

Here u is a control variable, specified to be within a certain range.

An OPF problem is outlined by equation (2.5) and is expressed as minimization of an objective function subject to equality and inequality constraints and the permissible

values of the control variables. The problem is solved using the classical Lagrangian function [10], and minimization techniques such as steepest gradient descent [11].

$$\begin{aligned} &Min_u\ f(x,u) \\ &s.t.\ \ g[x,u]=0 \\ &s.t.\ \ h[x,u]\le 0 \end{aligned} \tag{2.5}$$

Here x is a vector of state variables and u is a vector of control variables, f is the cost or the objective function, g gives the nodal power-flow equations as described by (2.1), and h gives the system operating constraints.

The solution finds the optimal operating point for the system, satisfying the given objective function and utilizing the existing network resources to the fullest. Security constraints are also included in the analysis to guarantee that the given operating point would give a secure system operation under any (N-1) contingency condition. These constraints refer to the additional equality and inequality constraints associated with contingency conditions. This augmented OPF problem is sometimes referred to as the security constrained optimal power flow (SCOPF) [12]. If the optimal operating point of the 'intact system' does not does not satisfy the security constraints, then the objective function is augmented with new penalty terms for each violation and a new optimal operating point may be obtained. It should be noted that while OPF can find an optimum, given the degrees of freedom possible in terms of control elements, it may not represent the best performance that is achievable.

OPF simulations must be carried out every time the loading or the operating conditions on the network changes. A central control and communication unit is required to compute the new state of the system and adjust the control variables. Computational complexity and the requirement of an extensive communication capability make this approach practically infeasible for very large power networks.

The requirements for communications can be minimized if the objective is restricted to optimize the utilization of the lines locally over a region. Under-utilized lines can be compensated in a way to carry more power through them, while overloaded lines can be controlled to limit additional current intake. Various power-flow controllers work on this principal and are given a generic name of flexible AC transmission systems or FACTS.

2.3.3 Power-Flow Control by FACTS Devices

FACTS devices can dynamically improve the transmission capacity and utilization of existing lines by controlling the flow of current through them. They change system parameters such as voltage magnitude, voltage angle, or the line reactance to achieve this objective. Figure 2.3 shows a simple two bus system, with the associated parameters. The basic equation governing the flow of real and reactive power between the two buses/nodes is described by equation (2.6).

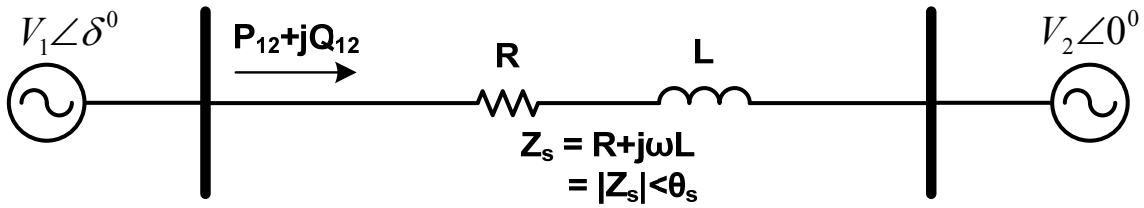

Figure 2.3 Two bus system

$$P_{12} = \frac{V_1 V_2}{|Z_s|}\cos(\theta_s - \delta) - \frac{V_2^{\,2}}{|Z_s|}\cos(\theta_s) \quad watt / phase$$
$$Q_{12} = \frac{V_1 V_2}{|Z_s|}\sin(\theta_s - \delta) - \frac{V_2^{\,2}}{|Z_s|}\sin(\theta_s) \quad watt / phase \qquad (2.6)$$

Here P_{12} and Q_{12} is the flow of real and reactive power from Bus 1 to Bus 2, V_1 and V_2 are the voltage magnitudes at the two buses, δ is the phase difference between the voltages at the two buses, $|Z_s|$ is the absolute value of line impedance, and θ_s is the angle of the line impedance

The equations can be further simplified if the line resistance (R) is neglected. This assumption holds true if the reactance of the line (X_L) is much greater than the resistance (R). In most transmission and distribution circuits, an X_L/R ratio of 4-8 is observed. Therefore, it may not be practically correct to ignore the resistance of the line but for the simplicity in understanding the theoretical analysis we shall ignore it for now. The simplified power-flow equations are described in (2.7).

$$
\begin{aligned}
P_{12} &= \frac{V_1 V_2}{X_s}\sin(\delta) \\
&= \frac{V^2}{X_s}\sin(\delta), \quad if \ |V_1| = |V_2| = |V| \\
Q_{12} &= \frac{V_1 V_2}{X_s}\cos(\delta) - \frac{{V_2}^2}{X_s} \\
&= \frac{V^2}{X_s}(\cos(\delta) - 1), \quad if \ |V_1| = |V_2| = |V|
\end{aligned}
\tag{2.7}
$$

Here X_s is the line reactance.

The equation highlights that both the real and reactive power flows between any two buses can be controlled by changing the voltage magnitudes, voltage phase difference, or the reactive impedance of the line. All FACTS devices alter one or more of these system parameters to control the flow of power. In the subsequent sections, the term 'power' would be used to implicitly refer to real power. The terms 'real power' and 'reactive power' would be used only to make a distinction between the two.

2.3.3.1 Controlling Power-flow through Voltage Magnitude

Power-flow through a line can be increased by increasing the terminal voltage magnitude and vice versa, provided the impedance and voltage phase difference across the line remains the same. Voltage magnitude of a bus or in general of a particular node can be increased by generating shunt Vars and can be decreased by absorbing shunt Vars. As transmission and distribution lines are predominantly reactive, shunt Vars adjust the reactive power flowing through series line reactance, controlling the series voltage drop across the line and consequently the node voltage.

Traditionally, shunt capacitors and inductors have been used with electromechanical switches for this purpose. For example, if the bus voltage needs to be increased, a shunt capacitor is used to generate Vars so as to reduce the reactive power flowing through the line. On the other hand if the node voltage needs to be decreased, a shunt inductor can be connected to absorb more Vars from the system and consequently increase reactive current flowing through the line.

A simple two bus system is used, as shown in Figure 2.4, to illustrate the power-flow control using shunt Var compensation. The magnitude of the voltage sources at the sending and receiving points are assumed to be the same, i.e. $|V_s| = |V_r| = V$. A shunt compensator is placed at the middle of the transmission line, which is an ideal location as the voltage sag is highest at this point. The compensator is programmed to boost the midpoint voltage (V_m) and increase it to the level of the sending and receiving end voltages. The phasor diagram of the system before and after compensation is shown in Figure 2.5 and the modified power-flow equations are given by equation (2.8).

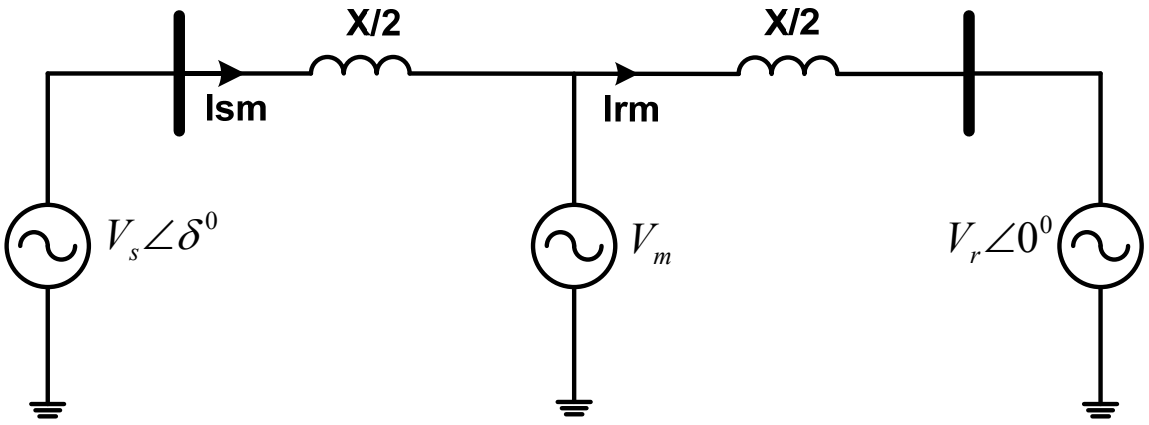

Figure 2.4 Two bus system with a shunt compensator connected to the mid point

$$P_{sr} = 2\frac{V^2}{X}\sin\left(\frac{\delta}{2}\right)$$
$$Q_{sr} = \frac{4V^2}{X}\left(1-\sin\left(\frac{\delta}{2}\right)\right) \tag{2.8}$$

Here P_{sr} is the real power transmitted through the line and Q_{sr} is the reactive power generated at the sending end.

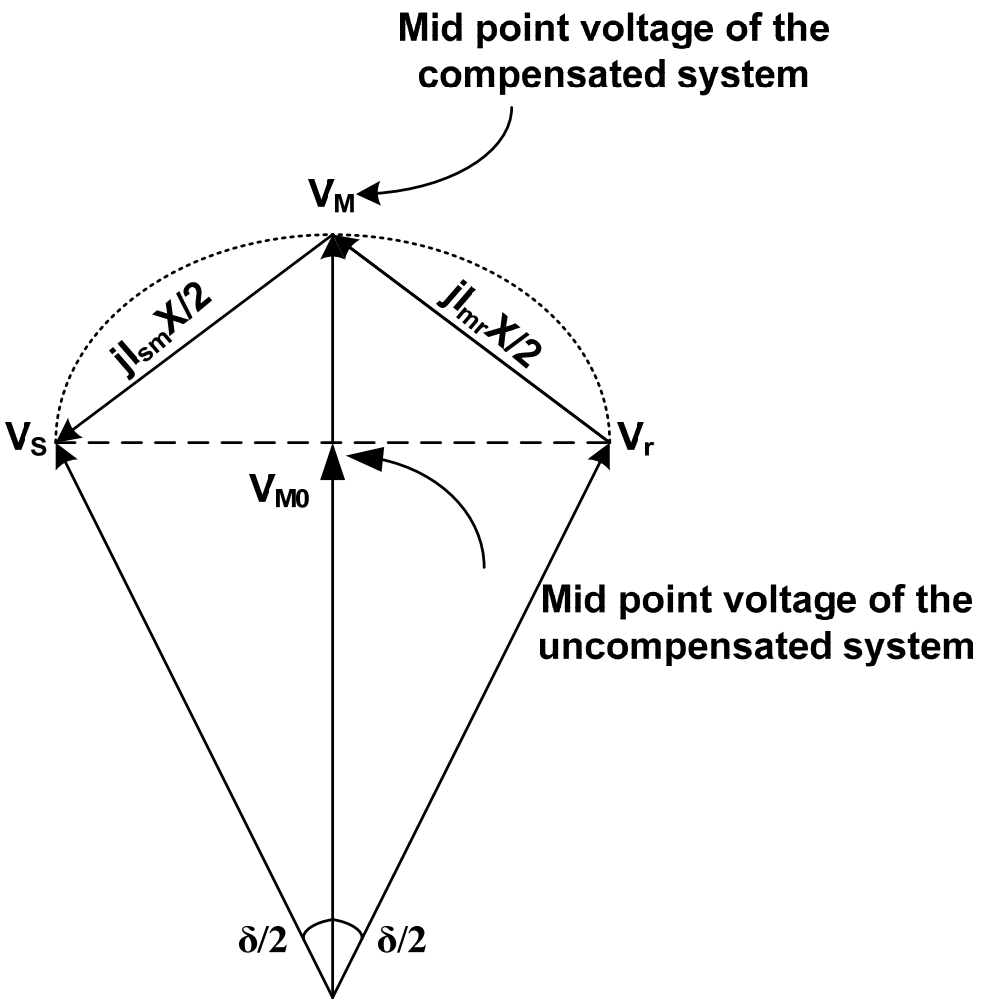

Figure 2.5 Phasor of the two bus system with a shunt compensator at the mid-point

It can be seen that with additional voltage boost at the midpoint, the maximum real power transmitted through the line can be increased by two times. However the peak reactive power demand of the system is seen to increase by as much as four times, implying a higher rating for the generating units. It is possible to segment the line further and employ shunt compensators at these locations so as to obtain an almost constant voltage profile throughout the line. The increase in transmittable real power would show a direct correspondence with the number of segments, provided there is unlimited capability to generate reactive power. Such a system would be practically infeasible to implement because of the cost implications on the size of the generators and the shunt compensators.

The primary role of shunt compensators is thus limited to providing voltage support to the system during normal conditions, when the Var requirements are expected to be within a certain range, and to increase the stability margin of the system under transient conditions [13]. However, to complete the analysis on shunt Var compensation, a brief overview of the available technologies is presented here.

With advances in power electronics, high power semiconductor switches (predominantly thyristors) are increasingly used to provide controlled reactive power to the grid. These shunt compensators are termed as Static Var Generators (SVGs), which can appropriately control the Var output from maximum capacitive to maximum inductive [14]-[15]. Figure 2.6 shows different combination of thyristor-controlled reactances for Var generation and absorption. The switching of reactances is controlled by the firing angle of the thyristors.

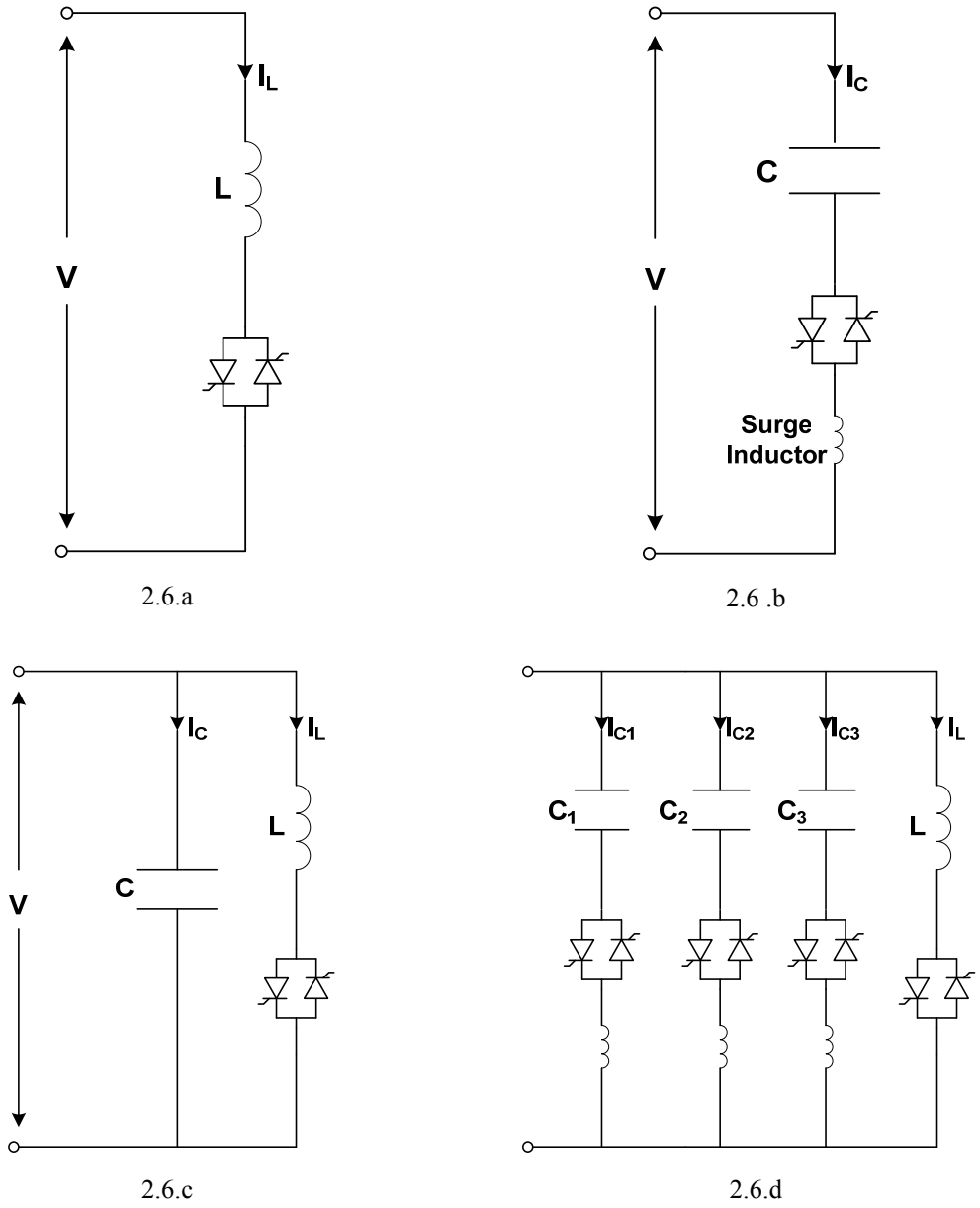

Figure 2.6 Basic Static Var Generators (a) thyristor controlled reactor, (b) thyristor switched capacitor, (c) fixed capacitor-thyristor controlled reactor, and (d) thyristor switched capacitor-thyristor controlled reactor

A thyristor-controlled reactor (Figure 2.6.a) provides inductive Vars from zero to a maximum value, which is limited by the system voltage and the inductive impedance at the fundamental frequency. Similarly a thyristor-switched capacitor (Figure 2.6.b) can be

controlled to provide capacitive Vars from zero to a maximum value. The capacitors are switched at the time instant when the voltage across the thyristor is zero, so as to avoid any transients. A combination of thyristor-controlled reactor and thyristor-switched capacitor can also be used to provide variable Vars. An arrangement such as the one shown in Figure 2.6.c can be used to control the capacitive Vars with suitable switching of the inductor. A complete vernier control over the Var generation and absorption can be accomplished by the arrangement of Figure 2.6.d.

One of the biggest concern with the use of SVGs is that they pollute the power-system with harmonics [16]. In a three phase system, the shunt banks are normally connected in a delta configuration to cancel the triplen harmonics. However, harmonics at $(6k\pm1)*f$ Hz, where k is a positive integer and f is the fundamental frequency, are still injected into the system. Another associated problem with employing a shunt capacitor is the possibility of resonance with the line inductances [17].

The biggest disadvantage of using SVGs, besides their slower response, is the fact that their ability to provide Var support is voltage dependent. Shunt Vars are normally required when the system voltage is depressed and during these periods the ability of SVG to provide Var support is also seen to decrease. For this reason, voltage-source based Var generators, also known as Static Compensators (STATCOMs), were introduced in 1988 [18]. Their operation is akin to that of a synchronous condenser, which exchanges reactive power at its terminals by varying the field excitation. They employ a four a four quadrant inverter (Figure 2.7) to generate a voltage in phase with system voltage so that only reactive power can be exchanged with the system.

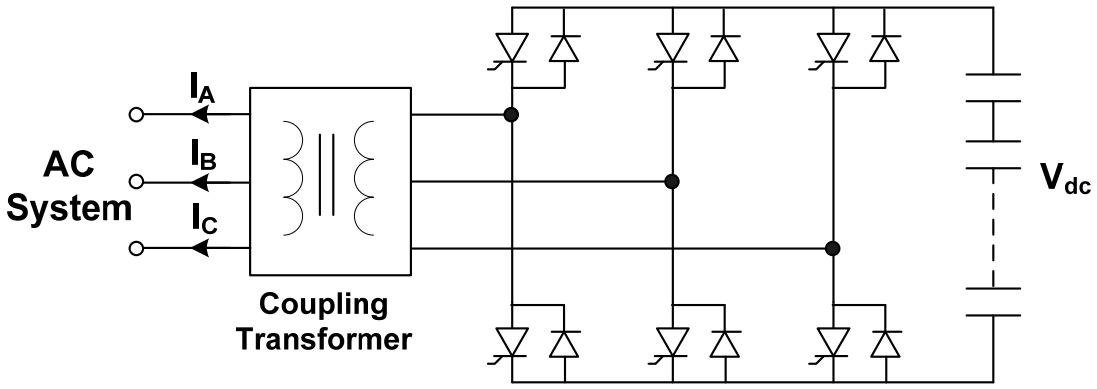

Figure 2.7 Six pulse voltage-source inverter bridge

A phase shift between the inverter and the system voltage would imply exchange of real power, which would require a DC energy storage to be connected at the input of the inverter. By controlling the magnitude of the generated voltage, reactive Vars can be controlled from full inductive to full capacitive. In particular, if the generated voltage magnitude is greater than the system voltage, capacitive Vars are injected into the system and when the generated voltage magnitude is smaller than the system voltage, inductive Vars are absorbed. Only a small real power is needed to compensate for the internal losses of the inverter and this can be achieved by phase shifting the generated voltage from the system voltage by a few degrees. The harmonic content of the injected voltage can also be controlled more effectively by using multi level inverters.

STATCOMs are seen to be more robust in providing reactive support to the network as their level of injection is independent of the variations in system voltage. The operational range of STATCOM is compared with that of thyristor-controlled compensator in Figure 2.8.

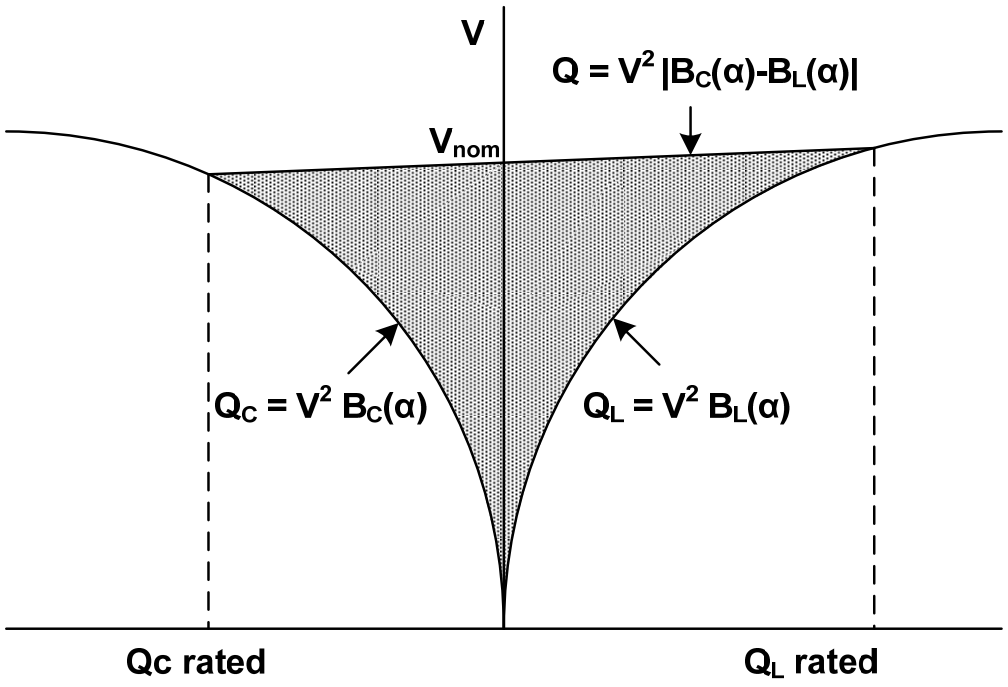

2.8.a

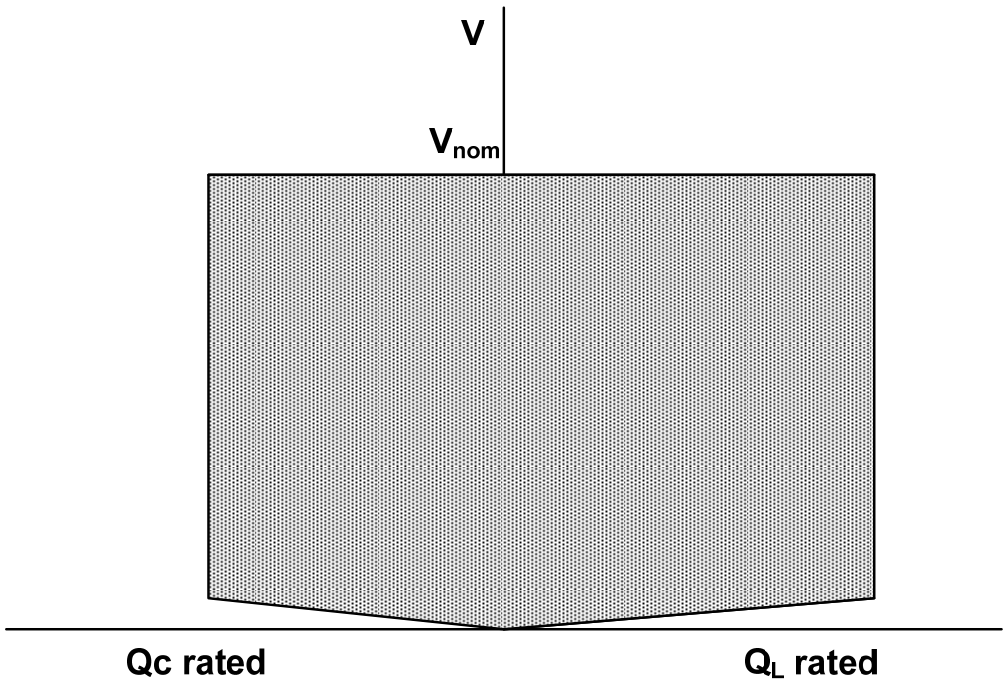

2.8.b

Figure 2.8 Voltage and reactive power characteristics for (a) Static Var Generator and (b) STATCOM

As can be seen, a STATCOM can generate full rated capacitive (Q_C) or inductive (Q_L) Vars even the system voltage drops down to almost zero. On the other hand, the reactive power capability of a thyristor-controlled reactor varies directly with the square of the system voltage. As system voltage drops, the output Vars are seen to drop significantly and the value is limited by the maximum susceptance of the shunt capacitor (B_C) or the inductor (B_L).

2.3.3.2 Controlling Power-flow through Series Impedance Control

Power-flow through a line can also be altered by changing the series line reactance. The flow of current is dictated by the lowest impedance path, and hence the power-flow through a line can be decreased by inserting a series inductor, or can be increased through insertion of a series capacitor. The modified power-flow equation for the two bus system of Figure 2.4 is given by equation (2.9), when capacitive compensation is induced in the line.

$$P_{12} = \frac{V_1 V_2}{X_s - X_c}\sin(\delta) = \frac{V_1 V_2}{X_s (1-s)}\sin(\delta) \tag{2.9}$$

Here, X_C is the magnitude of the capacitive reactance and s is the compensation ratio.

For inductive compensation with reactance X_L, the sign of s will be negative and its value will be given by $-X_L/X_S$. Figure 2.9 graphically depicts the effect of series compensation, at different compensation ratios, on the flow of active power through a line. It can be seen that series compensation increases the transmitted power by a fixed

percentage of that transmitted by an uncompensated line, at a particular value of transmission angle or the voltage phase difference (δ).

In a radial transmission structure, the power transfer capacity of the network can only be increased through capacitive compensation of transmission lines. In other words, to pull more current into a transmission line connecting a source to a sink, the impedance of the line has to be decreased by adding series capacitance. As a result, most of the research effort in the past has been devoted to series capacitive compensation. Series capacitive compensation can also help to improve the voltage stability of the system by cancelling a portion of the series line reactance.

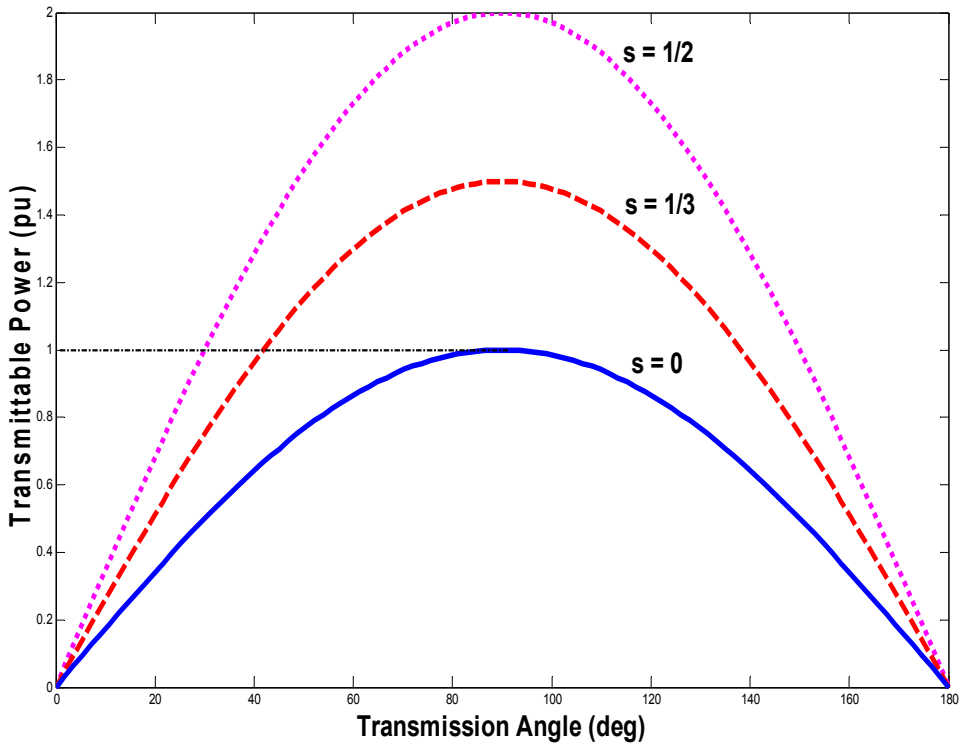

Figure 2.9. Effect of series compensation on power vs. angle profile

Figure 2.10 shows the basic implementation of thyristor-switched series capacitor (TSSC) [19]. Here a string of n capacitor banks, each shunted by a thryistor switch is used. The capacitors are by-passed when the thyristor-switch is closed and can be injected into the transmission line by opening it. In this way the compensation reactance can be varied in a step like manner from zero to $n*X_C$.

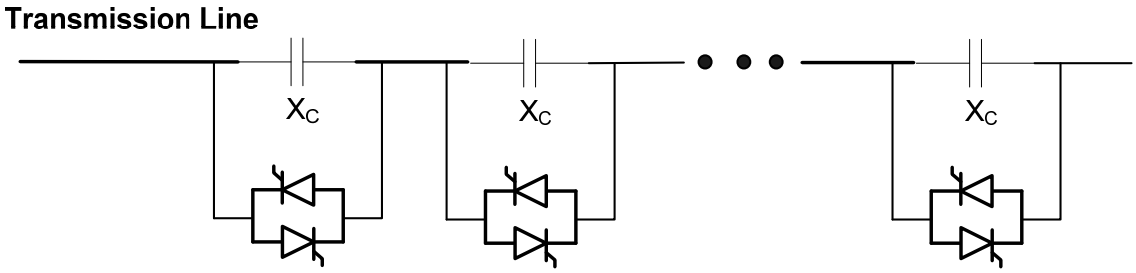

2.10.a

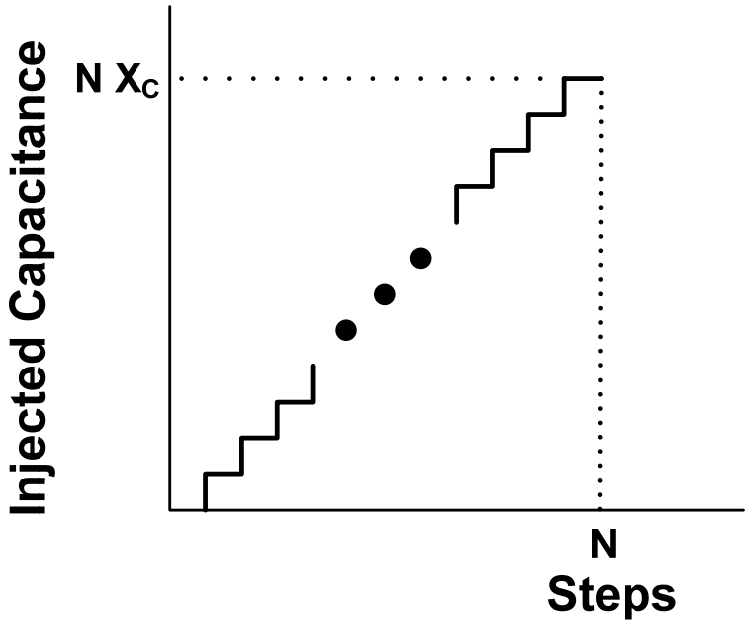

2.10.b

Figure 2.10 (a) Basic implementation of TSSC, (b) injected impedance profile

The injection capacity of TSSC can be increased by employing a small reactor in the shunt path. By varying the conduction angle of the thyristors, the voltage on the capacitor can be increased beyond 1 pu (implying a higher total capacitance value), because of the circulating current set up between the inductor and the capacitor. This topology is referred to as the Thyristor-Controlled Series Capacitor (TCSC) [20]-[21]. The basic circuit arrangement of TCSC is shown in Figure 2.11.

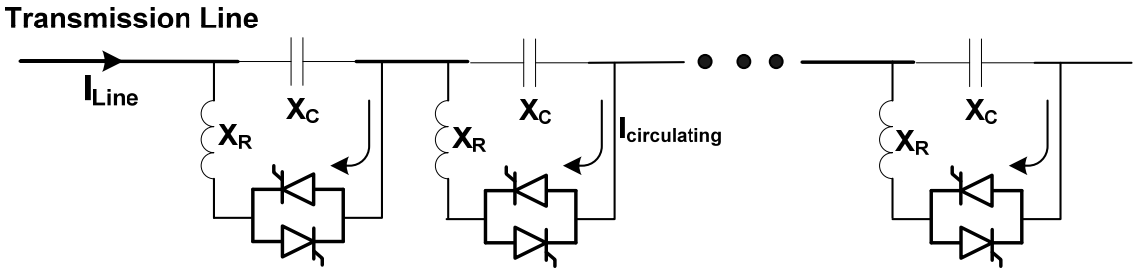

Figure 2.11 Basic implementation of TCSC

There are several issues associated with the use of a series capacitor on a power line. Series installation of the capacitor has to be done at a substation and requires additional infrastructure such as isolation platforms, cooling systems, and other protection devices [22]. As the fault currents at substations can be as high as 50 kA, series capacitors are by-passed to avoid generation of excessive voltages across them. However to increase the stability margin of the system, the capacitors must be reinserted within a few cycles (3-5), after the fault is cleared [23]. This requires elaborate control and protection strategies. Another issue of concern is sub-synchronous resonance with the turbine-generator unit. The series capacitor can form a resonant circuit with the line reactances under fault or nominal conditions, such that the resonant frequency gets tuned

to the complement of the rotor torsional frequency. Under such conditions, torque amplifications occur and can cause damage to the turbine-generator shaft [24]. Further, the thyristor-switches must also be designed with a fault ride through capability of 50 kA and peak voltage rating of twice the peak voltage stresses on the capacitor. These design requirements increase the cost and complexity of the solution. As a result, the penetration of this technology has been limited to a few project demonstrations sponsored by utilities.

A series capacitor or inductor reflects a voltage, which is orthogonal to the line current. Therefore, a series reactance can be realized through a series voltage, leading or lagging the line current by 90^o. A voltage lagging the line current would translate into a series capacitor while a voltage leading the line current would imply a series inductor. A synchronous voltage-source inverter with a series transformer can serve this purpose [25]. This approach is referred to as the Static Series Synchronous Compensation (SSSC) and the topology is described in Figure 2.12. Equation 2.10 gives the modified power-flow when the two bus system, shown earlier in Figure 2.4, is compensated with a voltage V_q, lagging the line current by 90^o. The sign of V_q is negative when it is made to lead the line current by 90^o.

$$P_{12} = \frac{V_1 V_2}{X_s}\sin(\delta) + \frac{V_1 V_q}{X_s}\cos(\delta/2) \tag{2.10}$$

Figure 2.13 compares the impact of SSSC to that of TCSC, on the power-flow through the line. V_q is chosen so as to give the same value of transmitted power at $\delta = 90^0$, as series compensation with TCSC would have provided. It can be seen that SSSC

has a greater effect on increasing the transmitted power in the important angle range $0 \leq \delta \leq 90^{o}$.

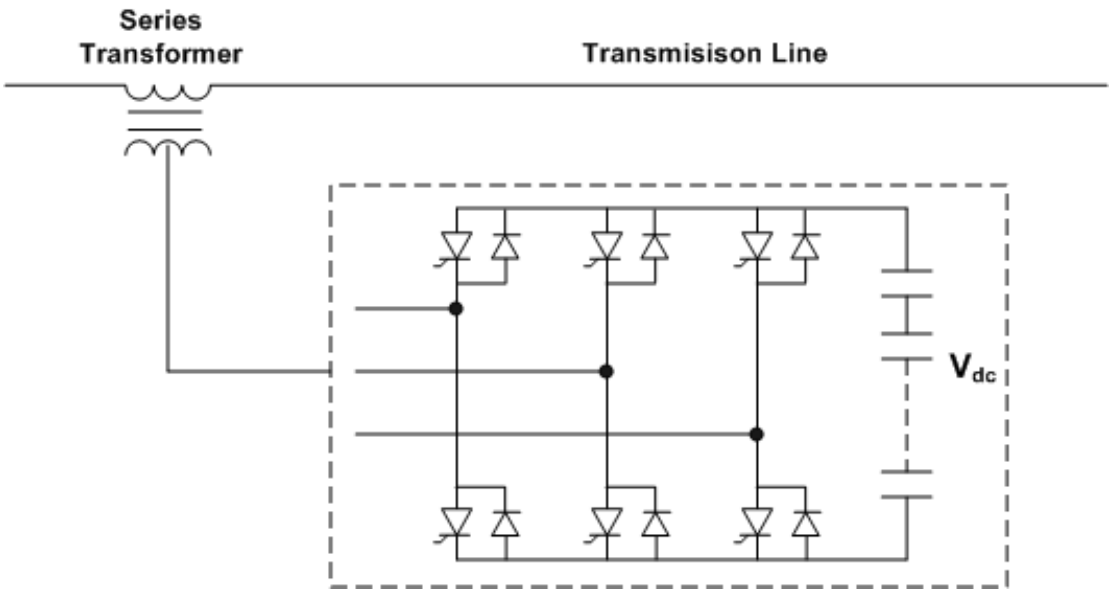

Figure 2.12 Basic implementation of SSSC

Similar to a STATCOM, a SSSC has the ability to provide a constant reactive compensating voltage, independent of the system conditions. SSSC can also be used to reduce line losses, by injecting a voltage out of phase with the line current; the power losses in the series line resistance are then supplied by the SSSC. The capability of injecting a voltage at any angle to the line currents allows independent control of real and reactive power. However, the exchange of real power with the system necessitates the use of DC energy storage. As the SSSC is essentially a voltage-source and not an impedance, it also eliminates the possibility of series resonance with line reactance. However, practical implementation of the technology is limited by the cost of coupling transformers, inverter circuit, and DC energy storage. Also, the use of DC capacitors and semiconductor switches brings into question the reliability of the solution.

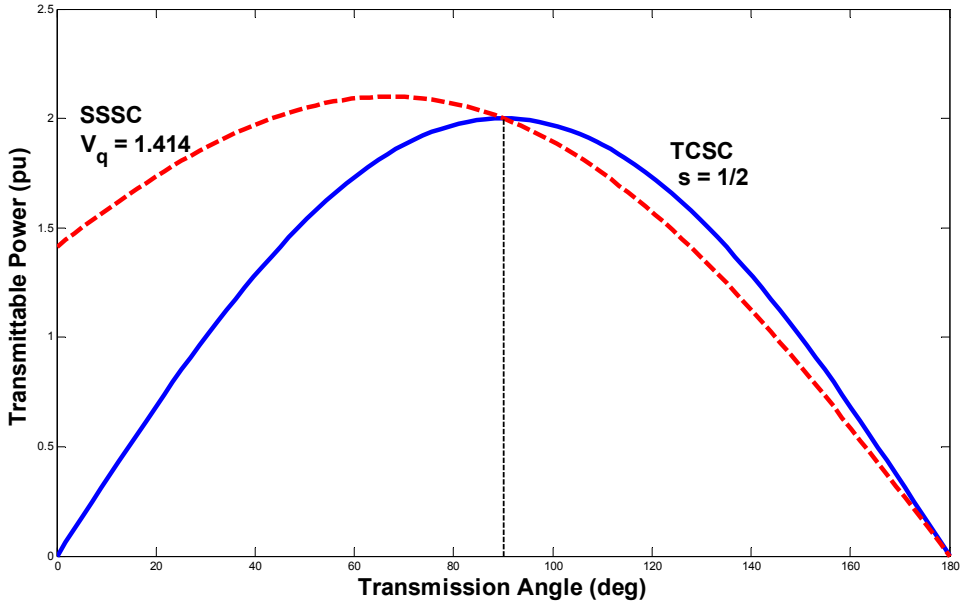

Figure 2.13 Effect of SSSC on the transmitted power vs transmission angle profile

2.3.3.3 Controlling Power-flow through Phase Angle Control

The direction of real power-flow along a transmission line is in the direction of decreasing voltage phase angle. In a radial network, the power-flow along a transmission line can be altered or even reversed by changing the phase difference. In meshed networks, phase shifting technology can be used to control unscheduled power flows and increase transfer capacity of the network with the aid of communications.

There are different ways of realizing a voltage phase shift along a transmission line. The standard delta-wye connection provides a fixed phase difference of 30^o between the primary and secondary voltages. Polygon transformers can be used to obtain phase shifts of $\pm 15^o$. Phase shifting transformers or phase angle regulators can provide a continuous phase control range [26]-[27]. One such configuration for the phase shifting

transformers is shown in Figure 2.14, with the associated phasor diagram to show the phase shift between the output (V_A') and the input (V_A') voltage.

Phase shift is implemented by injecting a voltage in quadrature (leading or lagging by 90^o) with the corresponding phase to neutral voltage of the system. In Figure 2.14 (a), a quadrature voltage (V_{bc}) is generated from phases 'B' and 'C' and is injected into phase 'A', to generate a phase shift of α, while maintaining the magnitude of the primary and secondary voltages the same. Two different transformer units are used for this purpose. The exciting unit generates the required quadrature voltage using tap changers. The primary winding of the exciting unit is connected to the midpoint of the primary winding of the series unit. The secondary windings of the two units are interconnected in a way so as to inject the generated quadrature voltage into the correct phase. A continuous variable range of approximately $\pm 25^o$ can be provided by the conventional phase shifting transformers [28]. Both the MVA rating of the transformer and the amount of phase shift affects the cost and size of the transformer. The mechanical tap changer on the exciter unit can be replaced by a thyristor-controlled tap changer to realize high speed operation under transient conditions [29].

A modified phase shifting transformer is shown in Figure 2.15. The primary of the transformer consists of a shunt-connected three phase winding. The secondary voltage is generated through auto-transformer action and is injected in series with the line. The arrangement eliminates the need of the exciting unit, decreasing the cost of the solution. These are called 'Sen' Transformers, named after the inventors [30]. The control range for the injected voltage magnitude and the phase angle is shown in Figure 2.15.b.

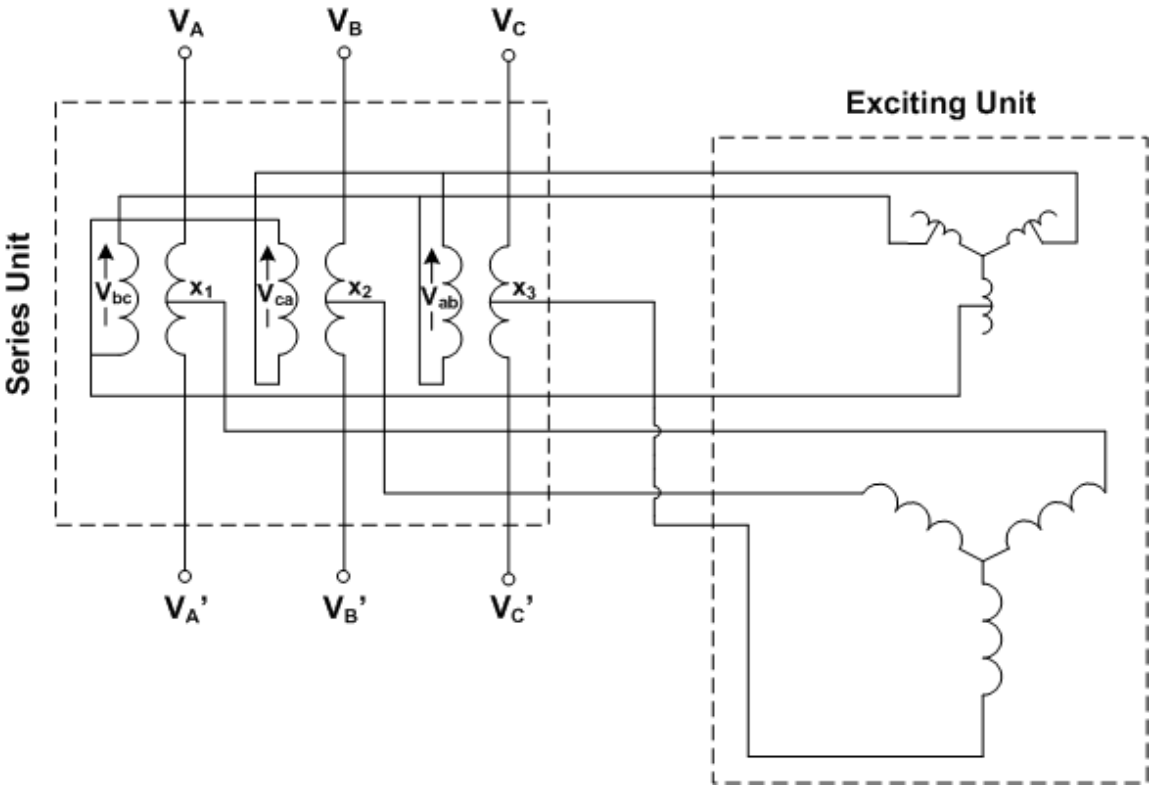

2.14.a

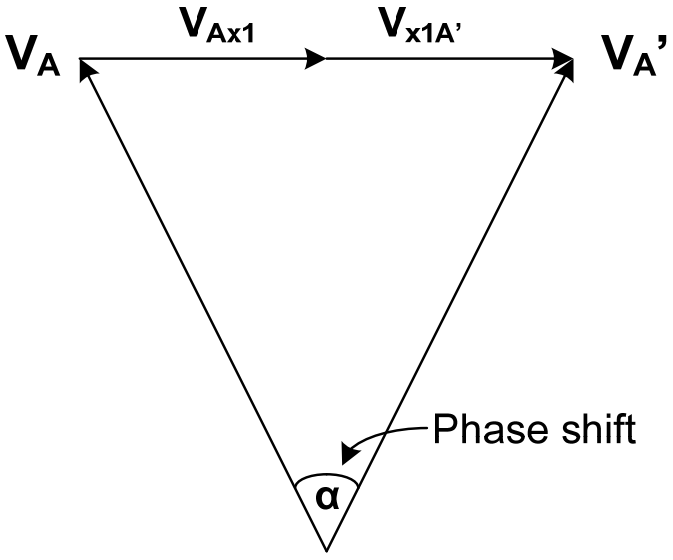

2.14.b

Figure 2.14 (a) Basic implementation of a phase shifting transformer, (b) associated phasor diagram

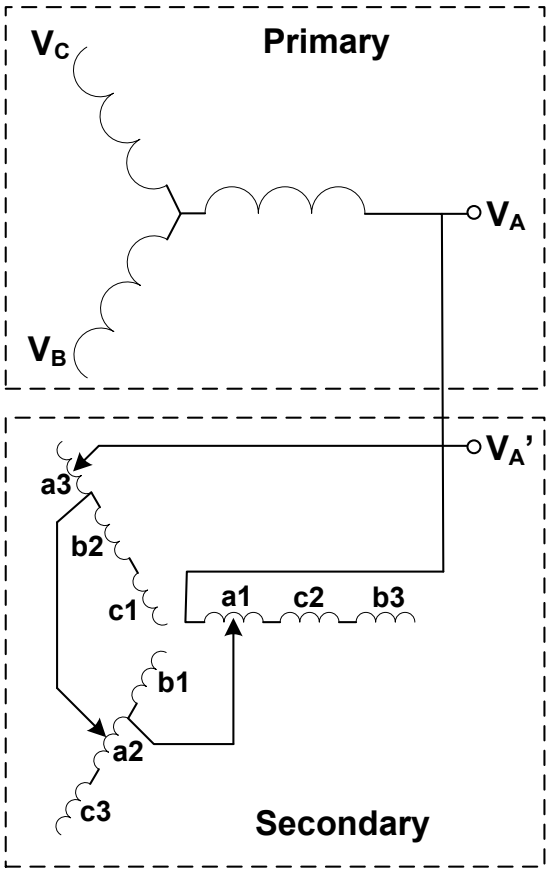

2.15.a

Magnitude Reg. 0-V_r

Phase Reg. $0 \leq \alpha \leq 360^o$

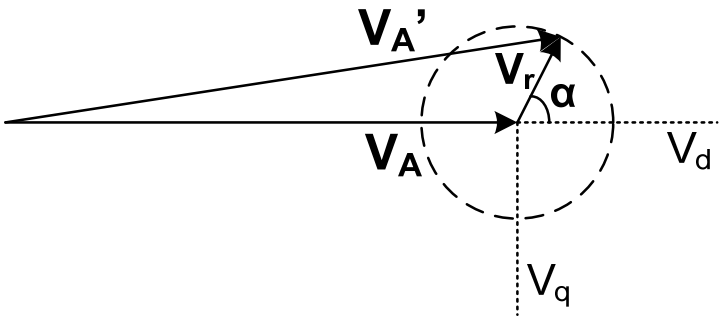

2.15.b

Figure 2.15 (a) Basic implementation of a 'Sen' Transformer, (b) associated phasor diagram

The primary winding is energized by the system voltage (V_A). Each phase of the secondary consists of three windings, magnetically coupled to each phase of the primary. The secondary voltage (V_A') is induced through auto-transformer action and is a phasor sum of the voltages on windings 'a1', 'b1', and 'c1'. By choosing the number of turns on each of the phase windings, the magnitude of the compensating phase voltage can be varied from zero to a maximum value, given by V_r, and the phase angle can be regulated from 0^o to 360^o.

The capability of injecting a voltage at any angle and with a controlled magnitude range, allows independent control of real and reactive powers through the line. The transformer can also be used to give voltage support to the system, if the injected voltage is in phase with the system voltage. However, there are certain issues with the use of 'Sen' Transformers. The injected series voltage increases the loading of the lines, as both real and reactive currents flow through the shunt-connected primary winding. To compensate for these loading effects, a separate shunt-connected reactance compensator may be required. This further increases the complexity and cost of the technology. Use of mechanical tap changers reduces the speed of operation and the response time. This can be improved by using solid state tap changers, but at higher cost and lower reliability. Under fault conditions, the entire magnitude of current must flow through the transformer unit, particularly through the taps. This reduces the reliability of the solution and requires extensive fault protection strategies for a safe ride- through under such conditions.

Recently, a concept of Controllable Network Transformer (CNT) has been proposed [31]. CNT provides simultaneous control of voltage magnitude and phase angle by augmenting an existing tapped transformer with a small rated converter, as shown in

Figure 2.16. The vernier control requirements of the system allow for the converter to be rated fractionally with respect to the rating of the transformer. The converter includes two ac switches, a small filter capacitor and inductor. It may be assumed initially that the switches are controlled with fixed duty cycles D and (1-D). For a transformer with a tap ratio N, the voltage magnitude of the output voltage can be varied between (1+N) pu for D=1 to (1-N) pu for D =0. This can be implemented using well known pulse width modulation techniques.

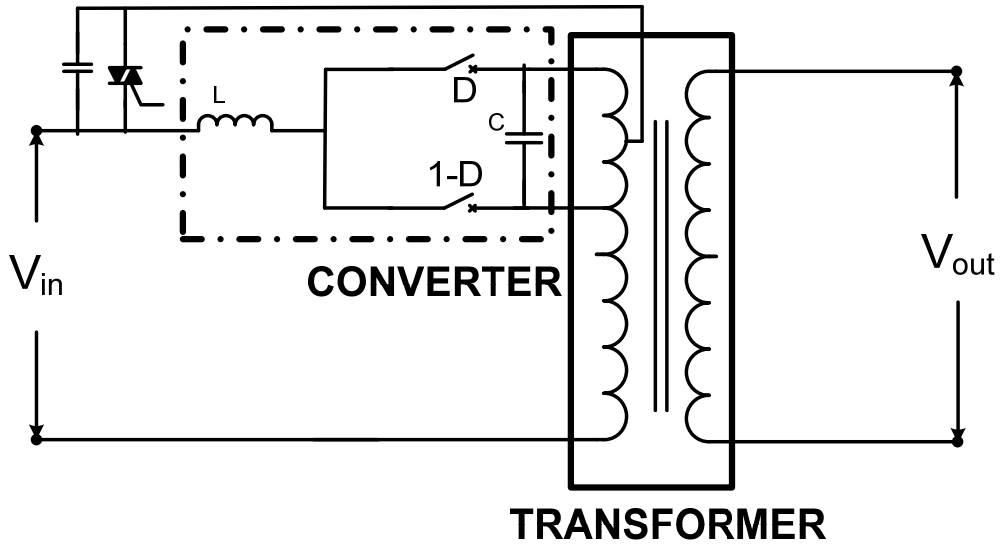

Figure 2.16 Circuit schematic of a Controllable Network Transformer

By applying conventional pulse-width modulation techniques only half the desired functionality is achieved, i.e. voltage magnitude control. The ability to control phase angle is not possible as there are no energy storage elements that can provide the required energy during the zero crossings of the input voltage. Phase angle control in a

CNT is made possible by applying the technique of "Dual Virtual Quadrature Sources" [32].

CNT has been demonstrated to control branch currents and bus voltage magnitudes in a power network; thus providing the functionality of series and shunt compensators. However, the control problem is seen to be very complex and has not been validated on a large scale power system.

2.3.3.4 Unified Power Flow Controllers

Unified power flow controllers (UPFC) can control all three line parameters: voltage, angle, and impedance to affect the power-flow [33]-[34]. Basic circuit arrangement of UPFC is shown in Figure 2.17.

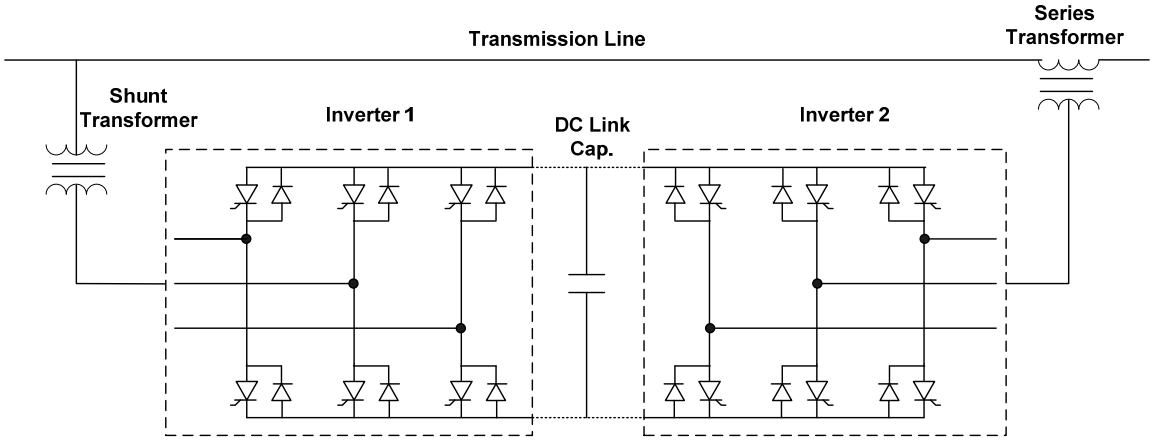

Figure 2.17 Basic circuit arrangement of UPFC

Inverter 2 is used to inject a voltage of desired magnitude and phase angle in series with the transmission line, with the use of a series-connected transformer. The injected voltage magnitude can be controlled from zero to some maximum value, while

the phase angle can be controlled form 0^o to 360^o. Inverter 1 operates to supply the real power demand of inverter 2, at the DC link. It can also be used as an independent shunt reactive compensator to give voltage support to the line. There is bi-directional flow of real power between the two inverters. However, the reactive power is exchanged independently at the inverter output terminals and is internally generated by the operation of the solid state switches.

The maximum value of the injected voltage is limited by the rating of the inverter. It is further limited by the leakage reactance of the series transformer. The transformers and the inverters must be designed for peak voltage and peak currents, even though they may not occur at the same time. Fault management is a critical issue, and the complete unit must be by-passed to protect the electronics from excessive currents and voltages. For a safe ride-through, all the switches in inverter 1 must be opened, while a by-pass switch must be used across the series transformer.

A ± 160 MVA UPFC was installed in Inez, Arizona in 1998 [35]. Each leg of the inverter is composed of several gate turn-off thyristors (GTOs), each rated for 4000 A, 4.5 kV and connected in series. Two intermediate transformers, each rated for 80 MVA are used at the inverter output terminals to remove the harmonics. The entire unit is housed in a 200' by 100' building, with water cooling pumps and liquid to air exchangers.

Although, UPFC is the most versatile power-flow controller, its penetration into the utility market has been limited by the high installation and operation costs. It requires skilled professionals for its control and maintenance, and also suffers from low reliability of the electronics.

2.3.4 Distributed FACTS

FACTS devices have proved to significantly increase the transfer capacity and the utilization of the power-system. However, their commercial success has been limited and only a few project demonstrations have been done in the past. The following points outline the difficulties in convincing the utilities for making investments in FACTS technology.

1. High Cost: Converter complexity and semiconductor ratings make FACTS devices an expensive solution. Moreover, the maintenance and repair calls for skilled labor, which further increase the cost.
2. Low Reliability: A single component failure can prove to be fatal in the overall performance of the module. Further, currently available power electronic components are not suitable for operation in the hostile utility environment.
3. Custom Engineering: Most FACTS devices are custom-designed and have long build times. They further require additional infrastructure such as mounting platforms and isolation transformers.

The limitations listed above can be attributed to the lumped nature of FACTS devices. The reliability of the technology can be increased and the cost can be decreased, if the same control objective is served by replicating a lumped controller into smaller controllers and distributing them over the grid. With this thought in mind, the concept of Distributed FACTS (D-FACTS) was proposed by Divan, et al. [36]. Figure 2.18 shows a conceptual visualization of D-FACTS on a transmission line. It consists of single phase devices that can clamp onto existing conductors, providing easy installation procedure

and the possibility for on-site repairs. The cost of the technology is lower, as off-the-shelf components can be used to meet the rating of the individual controllers/devices and can be further scaled down with volume production. The reliability of the solution is also improved as the failure of a single component or even a complete device is seen to have limited impact on the overall functionality of the solution.

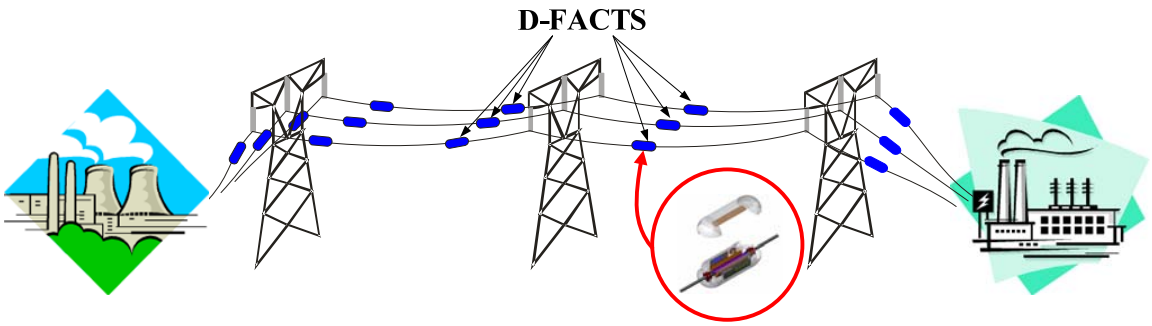

Figure 2.18 D-FACTS on power line

The concept was first extended to implement the functionality of a static series compensator (SSSC), with a single phase, 5 kVA inverter. Figure 2.19 shows the basic circuit schematic of a distributed static series compensator (DSSC). A single-turn transformer is used to magnetically couple and mechanically attach the module to the line. The required quadrature voltage is injected into the line through this coaxial transformer. The module is powered from the line to generate a regulated DC power supply for the controls and electronics. An additional current transformer is attached to the line to give feedback signals for the controls. A communication device is provided to receive instructions using wiresless or power-line communication technique, allowing the module to adjust according to changing operating conditions.

The module is by-passed by a normally closed relay (R_1), until the line current is below 150 A. Once the power supply and controls get activated (above line currents of 150 A), the inverter can inject an orthogonal voltage in the range of ± 4.6 volts, up till currents of 1000 A. The single-turn transformer is designed with a higher number of turns ratio (75:1), to reduce the line current to lower levels, sustainable by the semiconductors on the secondary. Even under fault conditions, when the line current can be as high as 50 kA, the inverter only sees a current of 667 A, well within the capability of commercially used semiconductor devices. It was anticipated that the total weight of the module would be less than 100 lbs, making it suitable for clamp-on applications. A lab prototype of DSSC can be seen in Figure 2.20.

Figure 2.21 shows a lab demonstration on control of power-flow between two parallel transmission lines. DSSC is attached on Line 1, while Line 2 is left uncompensated. When DSSC impresses inductive voltage on Line 1, the effective impedance of this line increases and the excess current gets diverted to Line 2. Capacitive voltage injection on Line 1 reduces its impedance and increases the current flow through it.

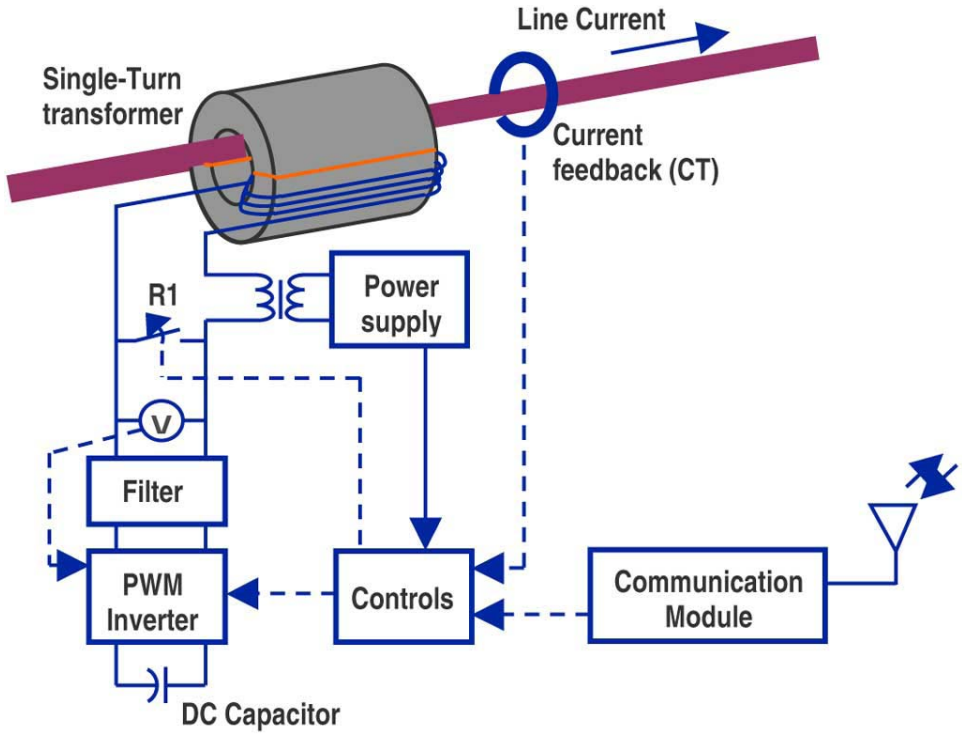

Figure 2.19 Circuit schematic of a DSSC

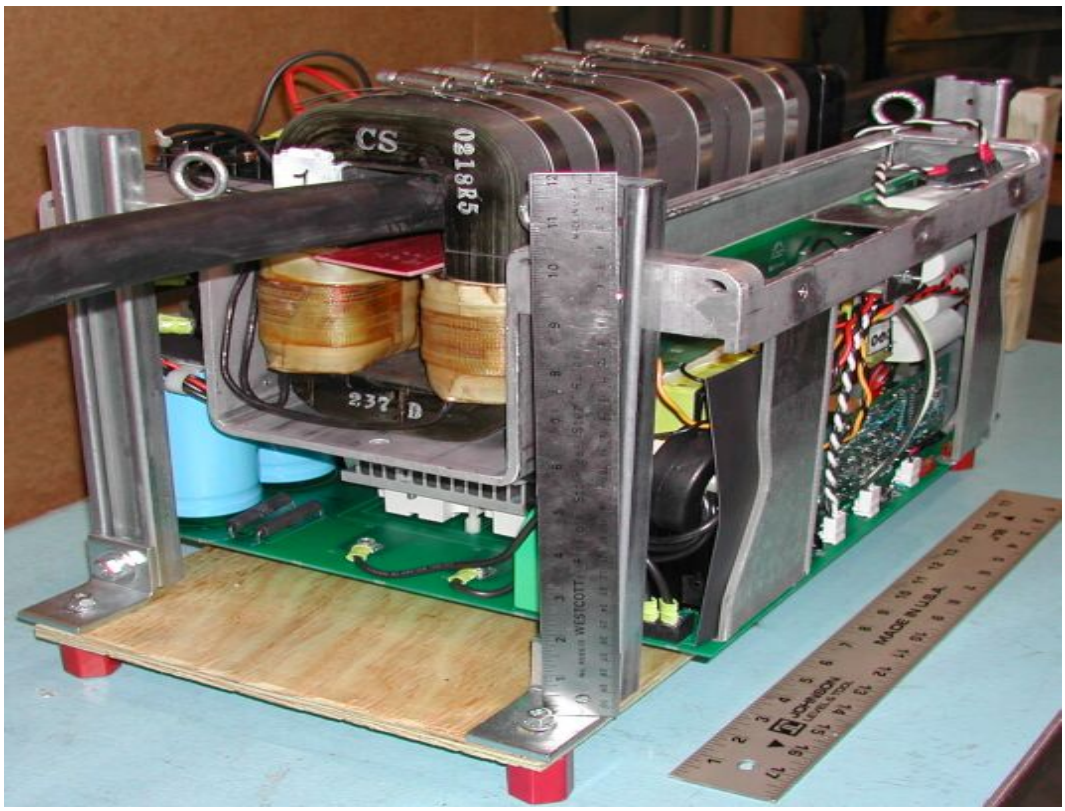

Figure 2.20 Lab prototype of DSSC

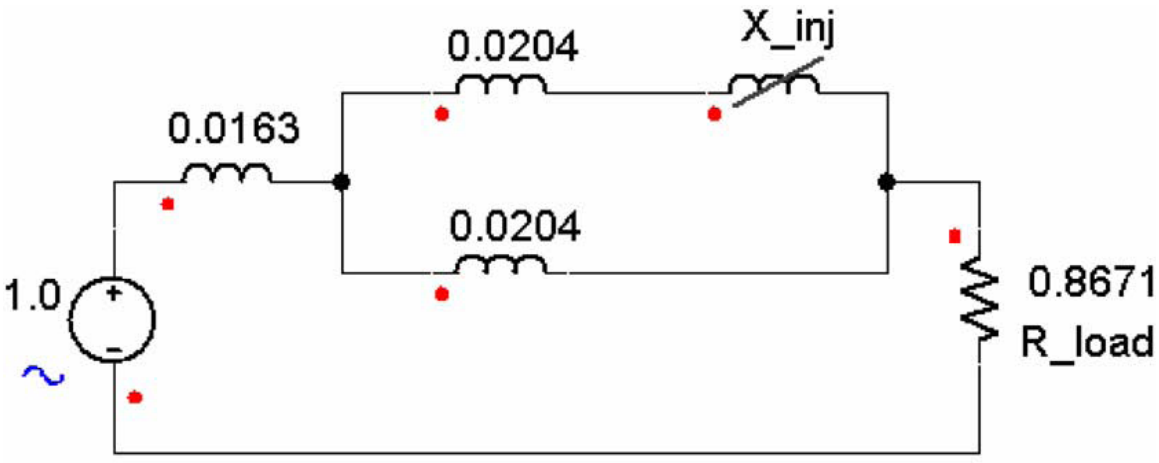

2.21.a

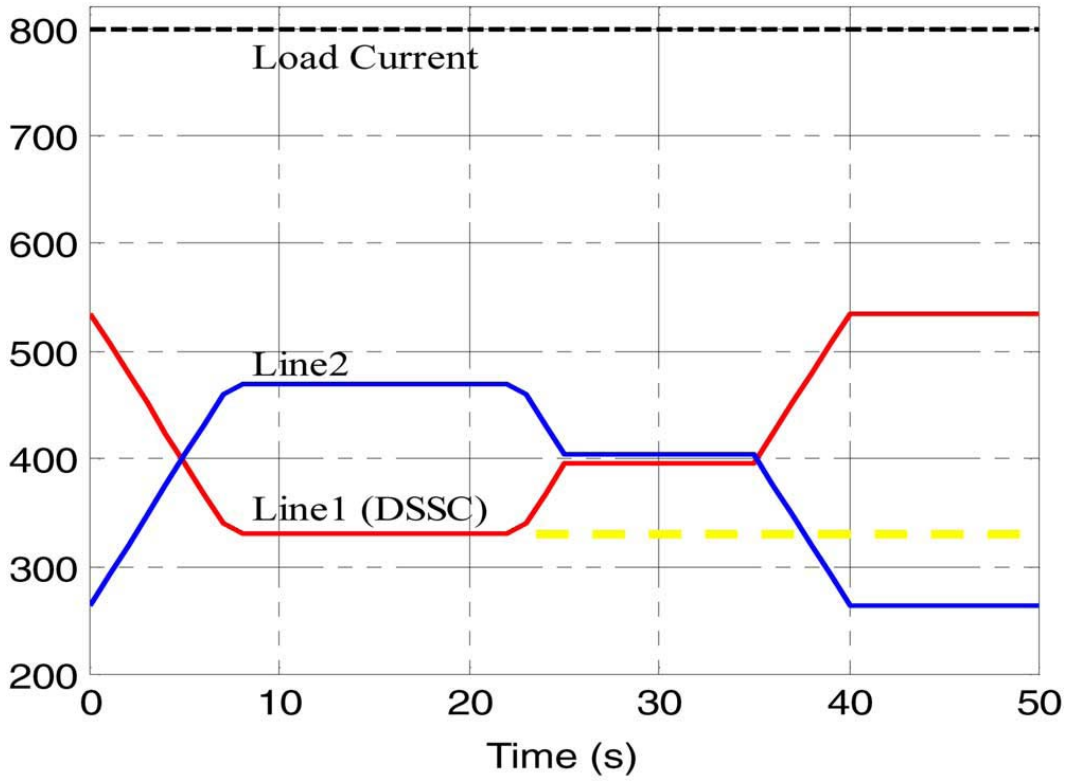

2.21.b

Figure 2.21 (a) Lab set-up of two parallel transmission lines, (b) current steering effect of DSSC

The current steering property of the technology opens the possibility of controlling the power-flow in a meshed network. On a under-utilized line, the modules can be controlled to inject a lagging voltage, so as to reduce the effective impedance of the line and to pull additional current into it. In congested areas, the control objective would be to increase line impedance with leading voltage injection so as to push excess current into other parallel paths. This can have significant increase in system capacity and line utilization, and can be used as a simple scalable tool to improve network capacity. Utilities can reduce the uncertainty and risk in investing lump sum amounts in building new transmission lines, while incrementally increasing system capacity at a lower cost.

DSSC presents an attractive solution for power-flow control at the transmission, sub-transmission, and distribution level. However, being an inverter-based technology, it opens up issues of robust and reliable operation in tough utility environment. Commercially available semiconductor switches and electrolytic capacitors may not be able to sustain extreme weather conditions and system requirements. Further a communication infrastructure is essential for the coordinated operation of the modules on the network. This would further delay the adoption of the technology in the market. The research outlined in this proposal advances the concept of D-FACTS and tries to overcome the limitations of this technology. The proposed research presents a low cost D-FACTS technology at higher operational reliability and without the need of any communications or centralized control. The module is designed with unique electrical, magnetic, and mechanical properties to match utility requirements.

2.4 Conclusion

Increasing demand for electricity is putting increasing pressure on the existing transmission and distribution structure, creating bottlenecks and congestion. The conventional solution of increasing system capacity by building additional lines has become expensive and is subject to regulatory delays. Under such conditions, it becomes imperative to use the existing asset base more effectively, improving line capacity and system reliability.

This chapter presents an overview of the existing technologies for controlling power-flow through a network, to increase utilization of the existing lines. State estimation and optimal power-flow techniques increase the efficacy of grid-operation by efficient deployment of network resources. However, they require extensive computing power and communication capabilities for their operation. As a result, these techniques are not economically and practically feasible for large power networks.

FACTS devices change network parameters (voltage magnitude, phase angle, and line impedance) to affect power-flow. Shunt Var compensators can control the active power-flow but at the expense of increasing the reactive power flows on the system. Their primary value has been limited to provide voltage support to the grid. Series compensators change effective line impedance to alter the active and reactive power flows. However, problems of resonance between line inductance and the series capacitance, difficulties in fault management, and low reliability of voltage-source converters have restricted their implementation on a large scale. Another technique to control the power-flow is to alter the voltage phase difference across the line. ‘Sen’ Transformers can inject a series voltage of controllable magnitude and phase angle to

affect the power-flow. Again, fault management is difficult and complex, which reduces the operational-reliability of the solution. Unified power flow controllers are the most versatile in the sense they can change all three network parameters to achieve independent control of real and reactive powers. However, the installation and operational costs are high and the reliability of power electronics is low.

Utility project demonstrations have shown that FACTS devices can have significant impact on improving the transfer capacity of the system. However, they have had limited penetration into the utility market. This is primarily because of their low operational-reliability and high investment costs. D-FACTS offers the possibility of overcoming these limitations by providing a distributed solution. DSSC, for instance, serves the objective of a conventional SSSC, at a lower cost and higher reliability. However, the need for a communication infrastructure can delay the adoption of this technology in the near future. The proposed research will present an improved DFACTS solution, which will operate at a lower cost, higher reliability, with minimal power electronics, and without the need of communications.

CHAPTER 3

DISTRIBUTED SERIES REACTANCE: A NEW APPROACH TO REALIZE GRID POWER FLOW CONTROL

3.1 Introduction

The objective of the proposed research is to develop a cost-effective power flow controller for releasing trapped and unused T&D system capacity, and to enhance system reliability and utilization. Several power flow control solutions exist and have been proven to have a significant impact on increasing the capacity of the existing T&D assets, but these are expensive and complex, and a single point of failure can bring down the entire system. These solutions are custom engineered with long lead times and high operating and maintenance costs. As a result, while they are technically viable, they have not been widely applied. The proposed technology can increase the capacity of meshed transmission, sub transmission, and distribution networks at low cost. The technology is more robust and provides for uninterrupted operation in the event of a unit failure, giving high reliability and availability. Moreover, the proposed technology provides the possibility of having incremental and reconfigurable investment opportunities, making it unique and more promising as compared to the currently available solutions.

3.2 Optimum Configuration of a Power Flow Controller

Power flow through a line can be altered by changing the series line impedance, voltage bus magnitude, or the phase of the bus voltage. Discussion in chapter 2 reflects that either a series compensator or a shunt compensator or a combination of the two can

adjust one or more of the above mentioned system parameters to control the power flow. This raises the question: "What is the optimum configuration of a power flow controller?" An optimum configuration would be one, which requires minimum control effort to achieve the desired objective. By way of an example, the impact of series compensation on the power flow is compared with that of shunt compensation.

A two bus network is shown in Figure 3.1, with two generators, connected by two transmission lines. The voltage and angles of the generators are fixed so that any change in the power flow can only be attributed to the injection of shunt or series VARs. Line 2 is shorter and is the preferred path for current flow. Therefore to realize an increase in the power transfer capacity of the system, utilization of Line 1 must be improved by directing additional power transfer through it. This is done by connecting a variable capacitor in shunt or series configuration to Line 1, to provide shunt or series VARs respectively.

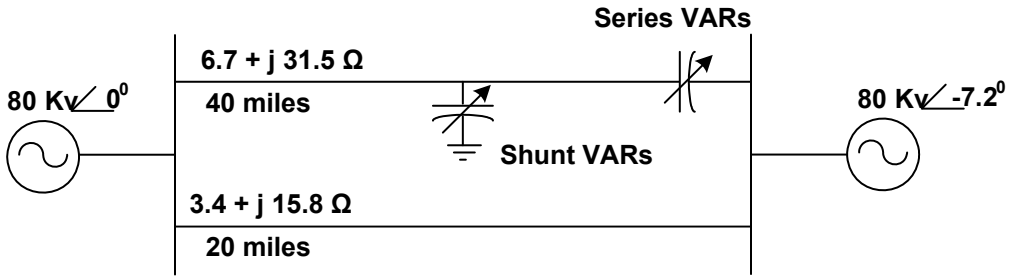

Figure 3.1 Two bus network

Figure 3.2 shows the effect of shunt and series compensation on the increase in power flow through Line1. A performance metric, given by equation (3.1), is suggested to compare the efficacy of the two technologies. The increase in power throughput is

normalized by the control effort to give a performance index of the respective compensators. Higher the performance index, higher is the efficacy of the solution.

$$PI = \frac{\Delta MW}{\Delta MVAR} = \frac{Increased\ Power\ Throughput}{MVARs\ Applied} \tag{3.1}$$

Here PI refers to the performance index of the compensators.

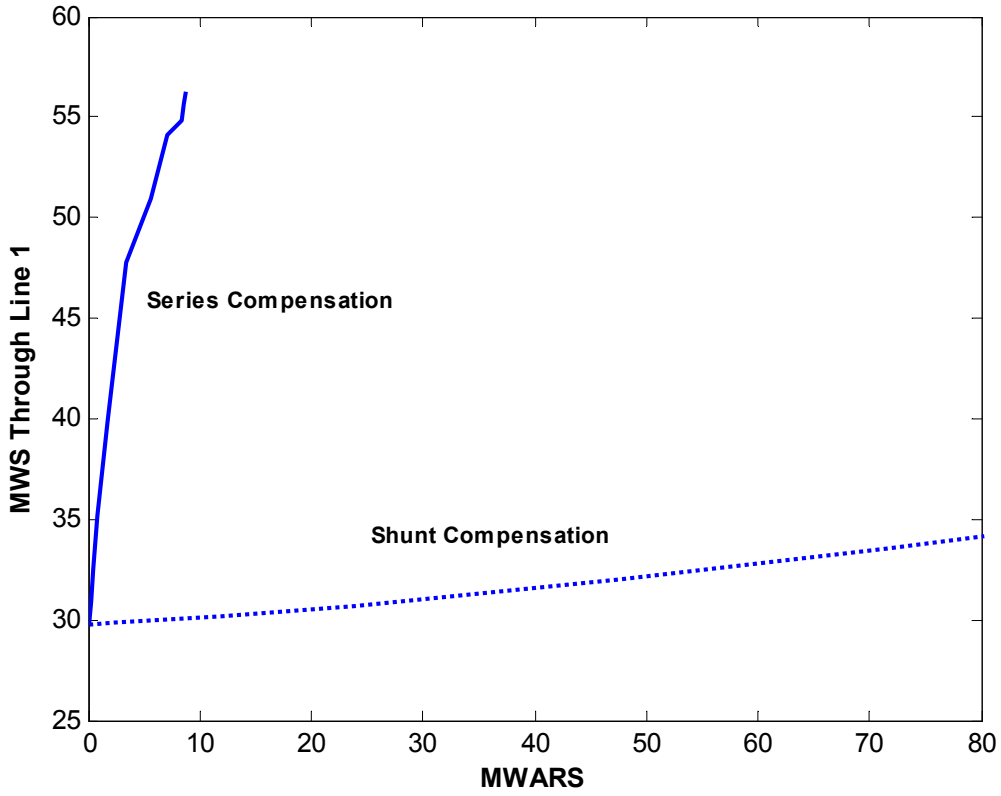

Figure 3.2 Effect of Shunt and Series compensation on power flow

Shunt injection can realize 5 MWs of additional power flow through Line1 with 81 MVARs injection, giving a performance index of 0.05. Series compensator on the

other hand can achieve 26.5 MWs of additional power flow with only 8.6 MVARs of injection, suggesting a performance index of 3. This suggests that series compensation is a more effective tool to control the power flow. In a similar way it can be shown that shunt Vars provide a more effective approach for voltage regulation of the system.

3.3 Proposed Power Flow Controller

The concept of using a distributed series compensator to control the power flow has been suggested earlier [36]. A distributed series compensator is capable of providing the same control capability as that of conventional series FACTS devices but at high module reliability and lower cost. However, the technology is based on a voltage source inverter, implying a high dependency on power electronics and electrolytic capacitors. The current power electronics devices are generally not suited for use in the utility environment. The safe operating temperature range of the commercially available power electronic and control devices is between 80^{o}C to 125^{o}C, while the temperature extreme for power line conductors (100^{o}C) can result in unsafe operating temperatures. Moving parts such as fans are not desirable making thermal management a major challenge as well. Further, the long projected life (~30 years) suggests that dependence on electrolytic capacitors must be reduced. It is thus required to keep the power electronics at a minimal level to ensure a reliable system operation. Further, to realize the full control range of a distributed series compensator, a communication interface is required. In particular, a capacitive voltage injection can only be induced on a line if local information about the operating limits of other lines is made available to the controller. Communication adds another layer of cost and complexity, and degrades the system reliability.

The distributed compensator was proposed with the objective of providing a continuous control range, which translates into varying the impedance of the entire line over a desired range. The proposed power flow controller is based on this idea and is introduced as a subcategory of Distributed FACTS devices. The injection of series VARS is made possible through injection of series impedance (inductor or a capacitor).

3.4 Distributed Series Impedance

A Distributed Series Impedance (DSI) can control active power flow by realizing variable line impedance. The transfer capacity and consequently the grid utilization can be improved by routing the power flow from overloaded lines to underutilized parts of the network. Capacitive compensation on under-utilized lines makes them more receptive to the inflow of current, while inductive compensation on over-loaded lines makes them less attractive to current flow. In both the cases, the throughput of the system is increased by diverting additional power flow from the congested parts of the network to the lines with available capacity.

The series injection of impedance at each module can be accomplished using a single turn transformer (STT), which uses the line conductor itself as a winding of the transformer. Figure 3.3 shows the circuit schematic of a Distributed Series Impedance module. The STT is normally bypassed by the normally-closed electro-mechanical switch S_M, while opening S_M allows injection of the desired impedance into the line. Switch S_1 is closed to inject an overall inductance, while S_2 is closed to inject capacitance X_C. This then allows the module to inject zero impedance in the bypass mode, X_L in the inductive mode, or $-X_C$ in the capacitive mode. With a suitable turns ratio on the secondary of the

transformer (say 1:25), the operating value of the secondary current can be reduced to values small enough to allow the use of mass manufactured parts. A control circuit is powered off the line, and monitors the line current.

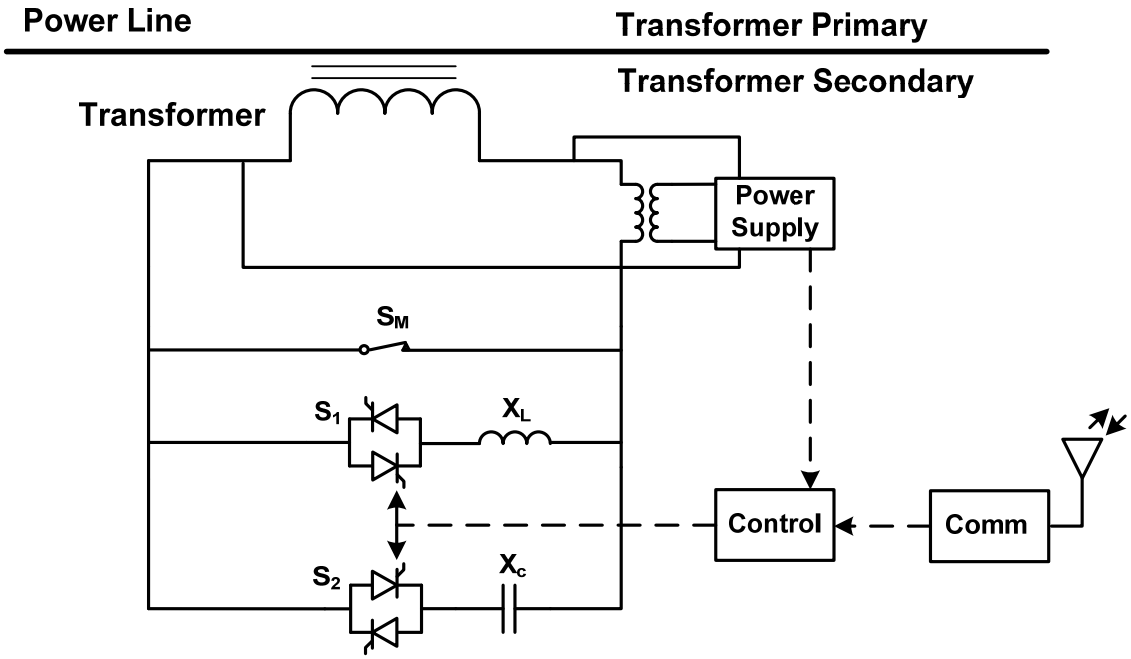

Figure 3.3 Circuit schematic of DSI

Figure 3.4 shows that with a total of N DSI modules on a single power line, the line impedance can be changed from ($N.X_L$) to ($-N.X_C$) in a total of 2N steps. If N was a large number, say 100, the impedance could be changed with 0.5% resolution, approximating linearly varying line impedance.

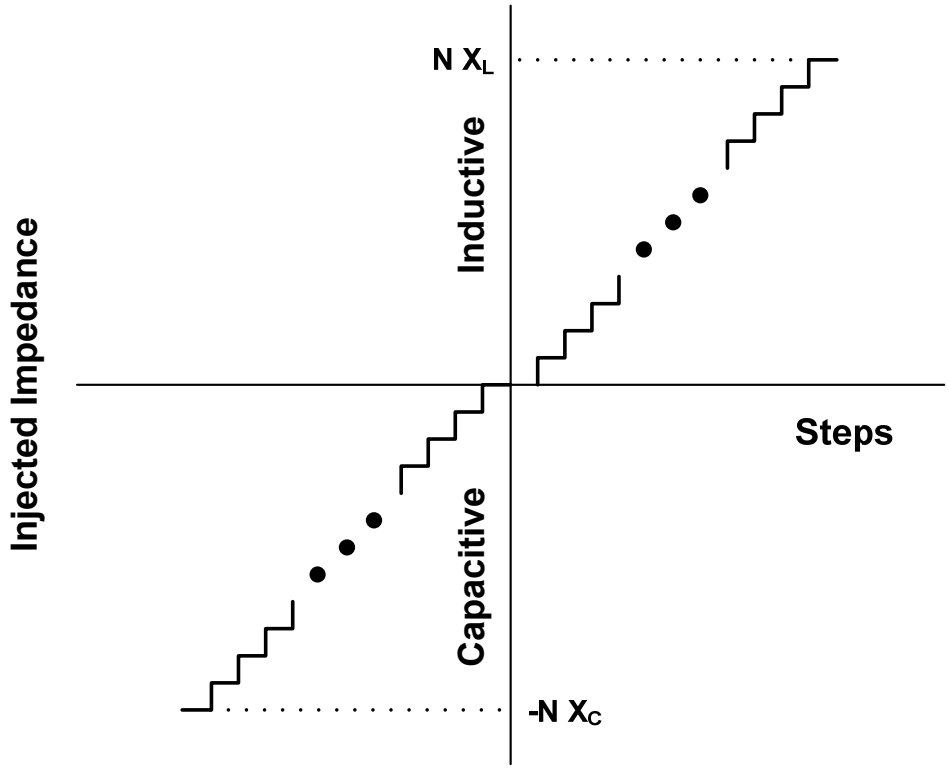

Figure 3.4 Profile of injected impedance as the modules are switched

However, as in the case of DSSC, bidirectional control capability requires a communication interface to instruct the device to operate in the particular mode. Communication adds another layer of complexity to the network and can further delay the adoption of the technology. A desirable control objective would be to make the modules switch in or out at a predetermined point, thus eliminating the need for centralized control. This can be easily realized if the control is made unidirectional, and the amount of injection can be related to locally measured quantities, namely current and/or voltage. The particular case that exhibits this characteristic is that of purely inductive injection. This implementation, where the injected impedance can only increase the line impedance is referred to as the Distributed Series Reactance. The control strategy

is unidirectional and the devices can be made to operate autonomously based on the measured line current.

3.5 Distributed Series Reactance

Figure 3.5 shows the circuit schematic of a Distributed Series Reactor (DSR). As in the case of DSI, a normally closed electromechanical switch (S_M) is used to bypass the module when it is not energized. With S_M open, the STT magnetizing inductance (tuned to a desired value) is inserted into the line. With S_M closed, the module is bypassed and a minimal level of reactance (corresponding to the STT leakage reactance) is inserted in the line. S_1 is a thyristor switch, which is used to provide a sub-cycle response, to by-pass the module quickly under fault conditions. This prevents the thyristor pair from having a sustained loss and also allows enhancement of contact life for the relay.

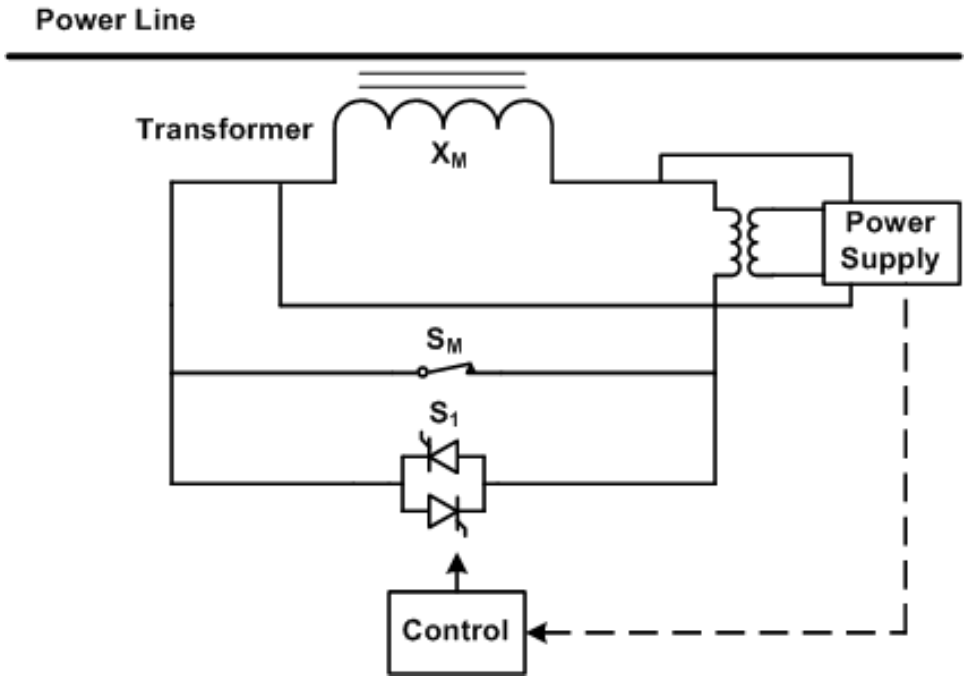

Figure 3.5 Circuit schematic of DSR

At a system level, as the current in a particular line exceeds a predetermined value, increasing numbers of DSR modules are switched in, gradually increasing line impedance and diverting current to under-utilized lines. Pre-selected lines that are likely to see overload conditions at certain times of the day or under defined contingency conditions can be modified with DSR modules to automatically control the current flow. Deployment of DSR modules on a power system can thus help to steer current from one part of the network to the other. The utilization of all the lines in the network can be gradually increased, bringing the system to its maximum power transfer capacity. Reliability of the system is also enhanced with the ability to share the overload between lines. A DSR system can not only restore a secure system operation under contingency conditions by diverting the excess current to other lines, but can also improve the transmission capacity under such conditions. Thus a self-healing network with controllable valves can be obtained. However the benefits from the DSR modules can only be realized if a stable system operation is guaranteed without any interaction between the modules and the network.

3.6 Control Strategy

As the overall control objective is to keep the lines from thermal overload, the control strategy is seen to be very simple. The control algorithm is given by the linear relation between line current and injected inductance, as shown in Figure 3.6 and explained by equation (3.2). The same controller, but with different set points is located on each module.

$$L_{inj} = L_f \frac{\left(I - I_0\right)}{\left(I_{thermal} - I_0\right)} \tag{3.2}$$

Here L_{inj} is the required injection, L_f is the final value of inductance with all the DSR modules on the line active, I_0 is the threshold value of current, and $I_{thermal}$ is the thermal limit beyond which there is no injection.

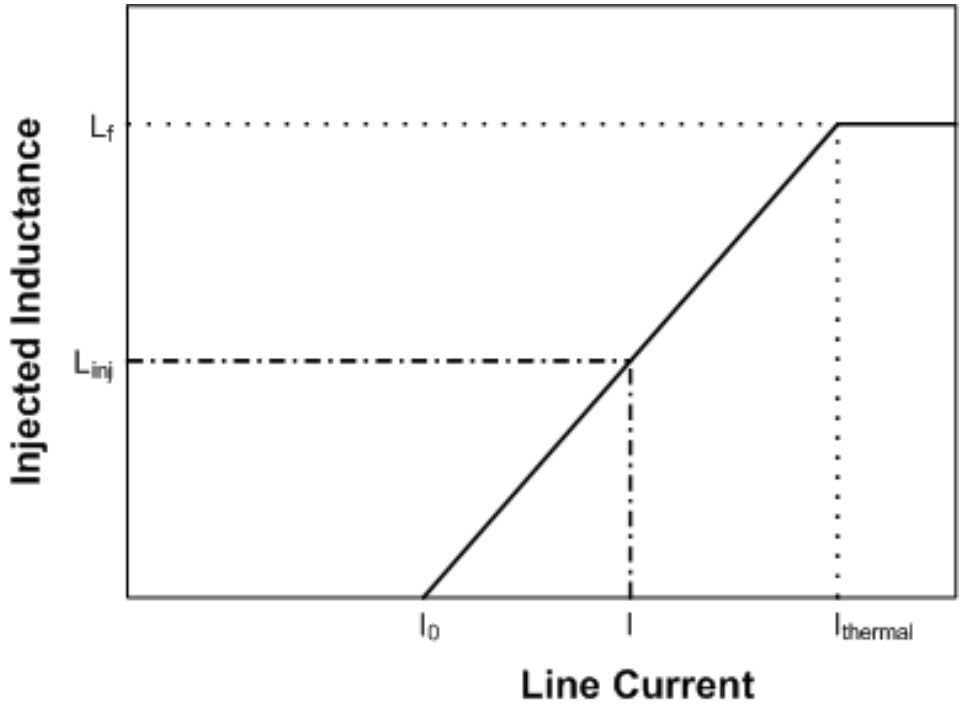

Figure 3.6 Relation between injected inductance and line current

The range for inductance injection (L_f) is determined by an apriori system simulation to assess worst case requirements of thermal overload. A small hysteresis band is introduced in each module to separate the turn-on value of a module from its turn-

off value by a few amperes. Without hysterisis, a module may continuously turn-on and turn-off at its trigger point. The value of the threshold limit (I_0) is dependent on $I_{thermal}$ and L_f. It is chosen so as to allow sufficient margin between the turn-on of one module and the turn-off value of the next module. Otherwise, there exists the possibility of interaction between the modules as they turn-on and-off at the same line current value.

As the line current increases above the threshold value (I_0), the first module is turned on. With further increase in current through the line, subsequent modules click-in at predefined line current values, realizing a stair case like increase in the line inductance. This is shown in Figure 3.7, where the total line inductance increases from an initial value of L_0, corresponding to inductance of the uncompensated line, to a final value of L_0+L_f, where all the modules on the line are turned on. While this seems simple to implement on a single line, it opens up important questions of potential interactions between modules, when multiple lines have to be compensated.

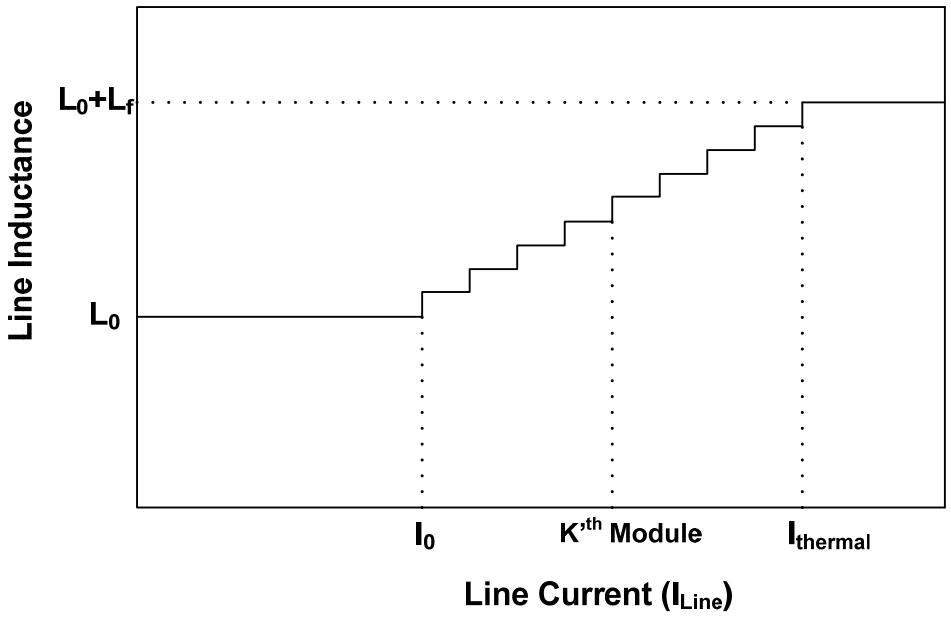

Figure 3.7 Increase in line inductance with switching in of DSR modules

3.6.1 Control Issues

Control of DSR modules, when implemented on multiple lines, has to ascertain that no line-current oscillations occur when the modules switch-in on different lines. A control strategy with a simple click-in and click-off of the modules, as the line current crosses their triggering value can lead to steady state oscillations or system instability. This is demonstrated by way of an example on a simple four bus system, which is shown in Figure 3.8.

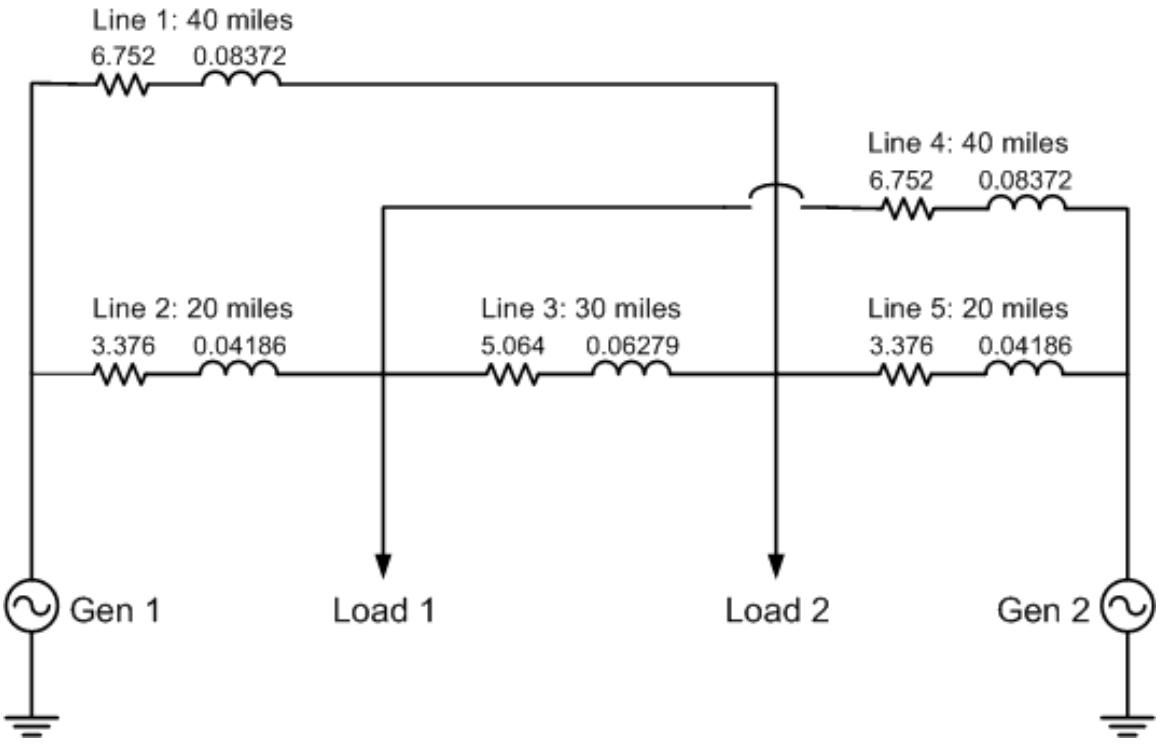

Figure 3.8 Detailed schematic of the 4 bus system

The system comprises of two generation sources, two load points, and five power lines. The DSR modules are programmed as fixed inductors such that each module can change the line reactance by roughly 10%. For instance, on Line 5 each DSR module is

modeled with an inductance value of 4.1 mH. The thermal limit of each the lines is assumed as 750 A (typical for 138 KV-161 KV transmission lines) and the threshold level for the turn-on of the first module is defined to be 600 A. A total of 15 modules are placed on each line, with their triggering values of current separated by 10 A. A hysterisis of 5 A is also included in each module. The line current is sampled at a period of 25 μsec and the injection is induced after every 75 msec, so as to allow sufficient time for the system to settle down before changing the line inductances again.

As the load of the system is increased, the operating level of Line 2 and Line 5 goes past the threshold limit of 600 A. Figure 3.9 shows that as the DSR modules are made active on these lines, the current in these two lines is brought down. However, steady state oscillations are observed, as the modules on these two lines start fighting each other to push the current away from the respective lines. Such oscillations can increase and become more significant as the current increases and multiple lines get into the inductance injection range.

In a highly meshed network, the interactions between the modules on different lines will be seen to be more predominant. Decreasing the granularity of injection does improve the response, but does not guarantee stability. A modified control strategy is clearly required to improve the response and reduce such interactions.

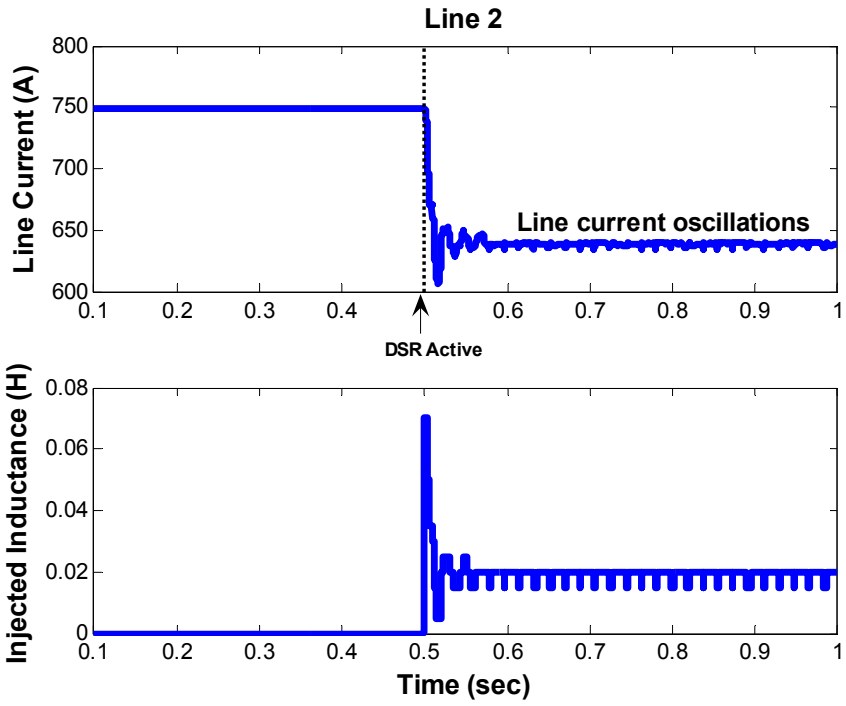

3.9.a

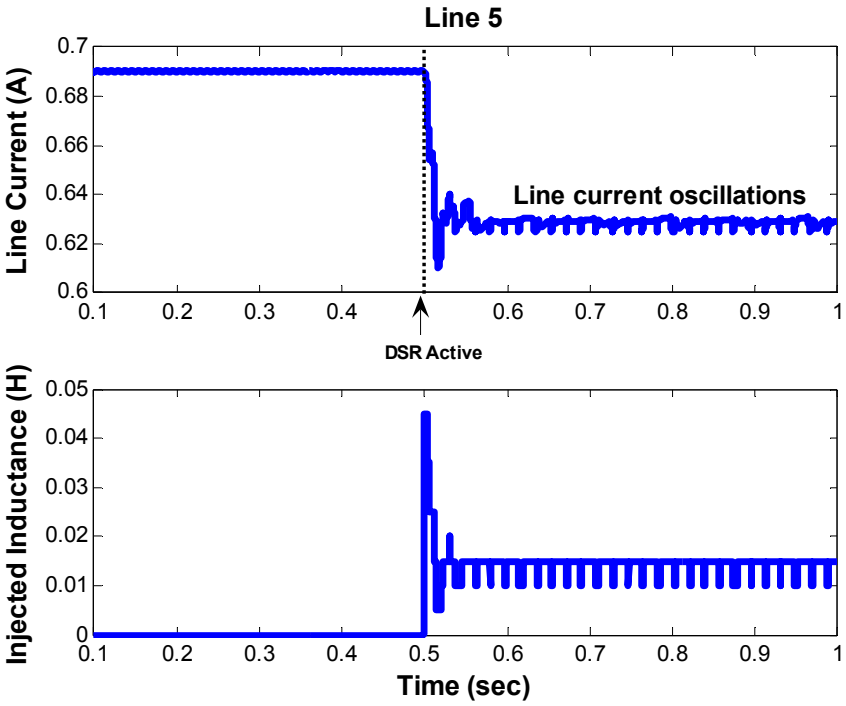

3.9.b

Figure 3.9 Line currents under DSR injection

3.6.2 Problem Formulation

A first order differential equation, given by equation (3.3), can be used to describe a meshed power network containing only inductances and resistances. The state vector x(t) represents the line currents in the network and the control vector u(t) represents the desired inductive injection. The objective of the controller is to find an optimal trajectory of the input u*, which will bring the system to a desired and stable, but unknown state.

In the problem at hand, the relation between the final state of the system and an input u* can only be known through the well established state estimation algorithms. State estimation requires a central computation facility and fast communication infrastructure. Communications is susceptible to delays and channel failure, and requires GPS technology for synchronization. This would seem to be the most significant impediment to the implementation of a truly distributed control system, such as the one proposed here. It is thus desired that the controller must be able to self-correct itself to reach the desired state in an optimal way.

In the next sections, the word "controller" would be used to represent a single control unit on a particular line that will give switching signals to all the modules on that line, but at different values of line current. The control function is based on the local measurement of the line current value and must be distinguished from the system level control function of a state estimator.

$$\dot{x}(t) = f(x(t), u(t), t) \tag{3.3}$$

Here *x(t)* is the state vector, *u(t)* is the control input, *f()* is a function defining the relation between the system states and the control input, and *t* is the time.

In section 3.6.1, the control effort was based solely on the measured value of line current in that time instant. At each sampling instant the controller finds the value of injection according to equation (3.2), and accordingly increases or decreases the control effort. The controller has to iterate between the two modes (increase in injection and decrease in injection) before it can find a stable equilibrium point and in some cases, as in Figure 3.9, the controller may not be able to find one. In a meshed network, the current on a particular line is not only governed by the parameters of the line itself, but also by the parameters of the other lines. To introduce stability to the control response, it is desired that the controller modifies the injection homeostatically or in harmony with the changes in line current.

3.6.3 Homeostatic Control

The philosophy of homeostatic control is based on a cooperative action between different interdependent processes to achieve a continuous state of equilibrium. The origins can be traced to the biological world, where the term '*homeostasis'* refers to a state of dynamic equilibrium between different but interdependent elements of an organism.

Homeostatic control has been applied successfully in the field of robotics and cybernetics to develop autonomous robot architecture. Robots with this capability can dynamically re-plan their actions to adapt to the changing environmental and internal conditions [37]-[38]. In 1980's the concept of homeostatic control was introduced in the utility market to dynamically balance the forces of demand and supply, so as to achieve better market equilibrium conditions [39]. A concept of Frequency Adaptive Power

Energy Rescheduler (FAPER) was suggested to homeostatically adjust the consumer demand under peak load conditions with the available supply of electricity. This is illustrated by the following example of a consumer heating appliance. A typical operational logic of the appliance is given by equation (3.4) and is shown graphically in Figure 3.10. The appliance is turned on when the temperature drops below a minimum allowable temperature (T_{min}) and is turned off when the temperature of the unit goes above a certain maximum allowable temperature (T_{max}).

$$u(t+\Delta t)=\begin{cases} u(t) & T_{\min} < T(t) < T_{\max} \\ 1 & T(t) \le T_{\min} \\ 0 & T(t) \ge T_{\max} \end{cases} \tag{3.4}$$

Here *t* refers to time, *u(t+Δt)* is the present thermostat control logic, *u(t)* is the thermostat control logic in the previous time instant, *T(t)* is the appliance temperature, T_{min} is the minimum allowable temperature, and T_{max} is the maximum allowable temperature.

A FAPER would dynamically adjust these temperature points in harmony with the system loading conditions. Thus under heavy loading on the system, T_{max} would be made closer to T_{min} so that the temperature of the unit is maintained at the minimum allowable temperature and minimum possible energy is withdrawn from the system. Similarly, under light operating conditions, when there is surplus available energy, T_{min} can be shifted close to T_{max}. With such a demand side response, the generators can benefit from the savings on the extra capital they have to invest to keep large spinning reserves, while the consumers can benefit by reducing their demand under heavy system loading

when the energy price is high. As the frequency deviation from its nominal value is an indication of the loading on the system, FAPER involves changing the operational logic of the heating appliance based on the frequency response characteristic shown in Figure 3.11. The new temperature thresholds are outlined in Table 3.1.

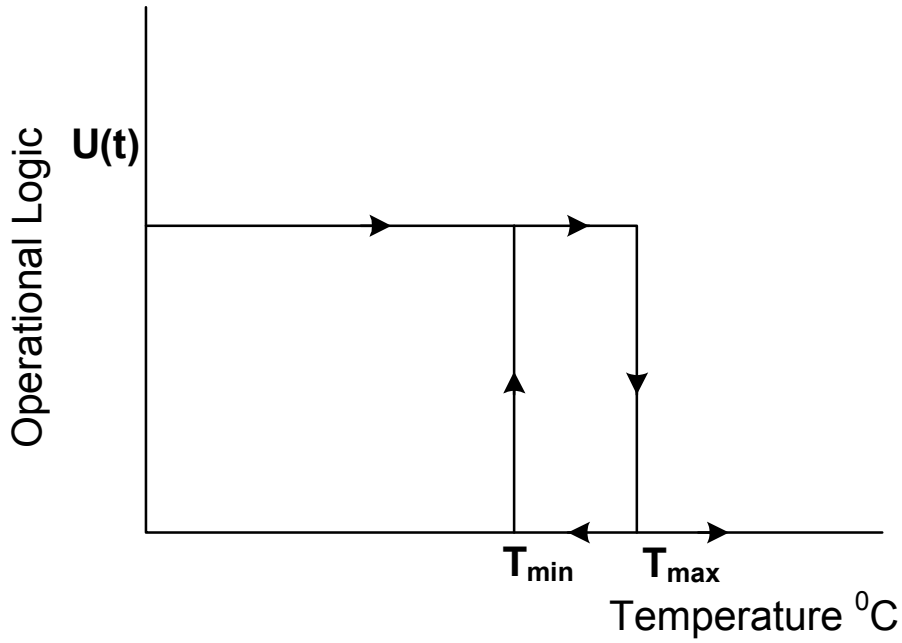

Figure 3.10 Operational logic of a consumer heating appliance

Table 3.1 Variation of temperature thresholds with frequency

	$\Delta f(t)<0$	$\Delta f(t)<0$
T_U	$T_{max} + g[\Delta f(t)]$	T_{max}
T_L	T_{min}	$T_{min} + g[\Delta f(t)]$

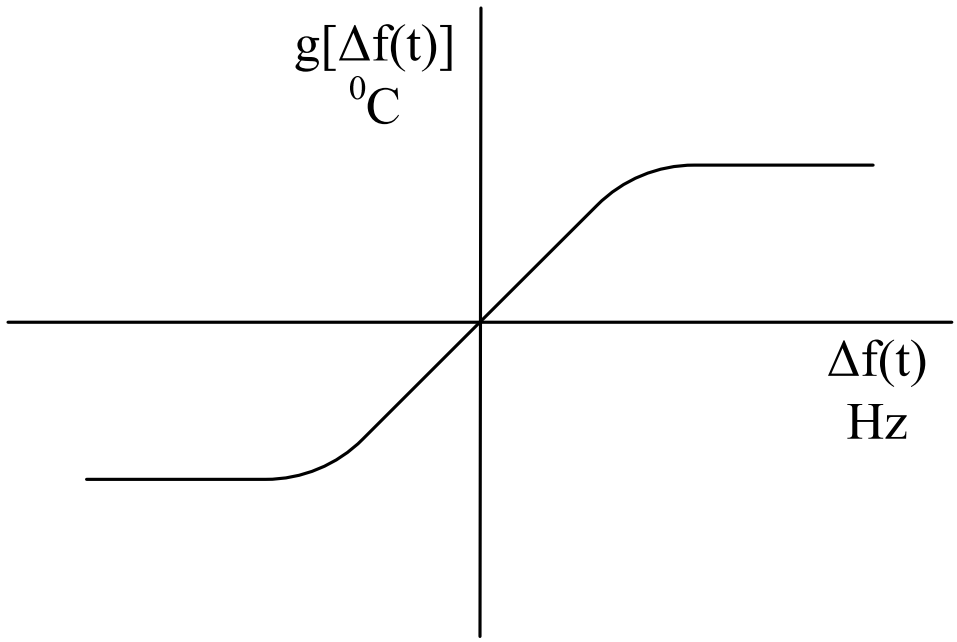

Figure 3.11 Frequency response characteristic used in FAPER

Looking at the problem of defining an optimal control strategy for the DSR modules, a homeostatic state is the desired end objective between the currents on different lines of the network. To achieve this, the controller must be able to internally correct itself and control the rate of injection by looking at the system state at each sampling instant. This self-correcting mechanism eliminates the need of communication between the controllers on different lines of the network. In the previous example, a FAPER unit installed at each customer load point would independently control the operation of the heating appliance by looking at the frequency deviation of the system. In a similar way, a DSR controller on each line must adjust the injection looking at the line currents at each time instant.

One strategy that can realize this objective is to make the controllers on each line to reach their desired injections asymptotically over time. This allows the controllers to

adjust their actions according to the dynamics of the system. Figure 3.12 shows a simple control schematic to implement this strategy. The controller calculates the desired injection (u_k) at each sampling instant, based on the measured line current (I_{Line}). The difference between u_k and the injection value at the previous time instant (u_{k-1}) gives the residual injection requirement of the line. The controller then self-adjusts the injection rate (u_t), according to some time varying function. This injection rate is valid over the next Δt sec, in a way that only if $\Delta t \rightarrow \infty$, the injection $\rightarrow$ u_k. In this way, at each sampling instant the rate of injection is updated such that the controller reaches the desired injection asymptotically over time.

One possibility for implementing such a self adjusting control rate is to use a time decaying exponential profile. The time constant of the exponential must be chosen to be very large as compared to the sampling time period to make sure that the injection varies slowly over time. We would refer to this exponential function as a decaying exponential estimator in the remainder of the document.

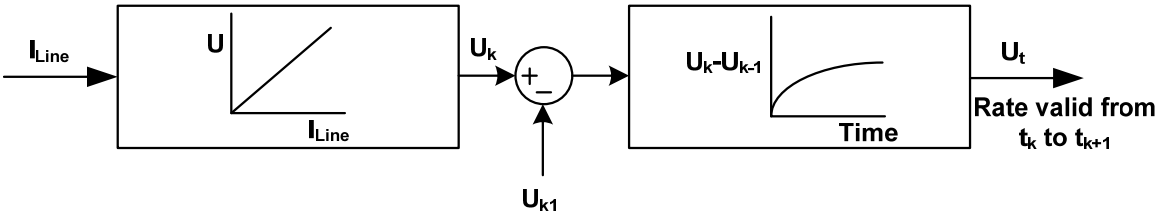

Figure 3.12 Control schematic for the modified control strategy

3.6.4 Decaying Exponential Estimator

A decaying exponential rate of injection is suggested to reduce interactions between modules on different lines. The required injection is calculated at every

sampling time instant according to equation (3.2). The injection over the next time period is governed by the exponential time response of the estimator. For instance, assume a sampling time of 1 sec and an exponential time constant of 10 sec. If the injection requirement at time t = 0 sec is 1 unit of inductance, then the inductance that will be injected at the next sampling time, i.e. at time t = 1sec, will be 0.0952 units of inductance. Thus, the exponential estimator conservatively increases line inductance by taking into account the response of the line current. As the line current settles to a different value, the estimator is updated with the new injection and in this way it tries to reach the desired injection without any steady state interactions. Equation (3.5) describes the trajectory of the exponential estimator over the interval of Δt sec.

$$L_{\exp} = \left(L_{inj} - L_{prev}\right)\left(1 - \exp^{-\left(t - t_0\right)/\tau}\right) + L_{prev} \tag{3.5}$$

Here, L_{exp} corresponds to the injection profile (valid over $t \le t_0 \le \Delta t$), L_{prev} is the injected inductance in the previous sampling instant, L_{inj} refers to the current injection demand, and τ is the exponential time constant.

Again assuming that a single controller is giving switching signals to the various modules on a line, this modified control strategy is used on the four bus system under similar conditions of overload as in Figure 3.9. The simulation results in Figure 3.13 show that the line currents are brought down with no steady state interactions between the controllers on different lines. Each of the lines is programmed to have a reasonably large number of modules, which turn on subsequently at their triggering value.

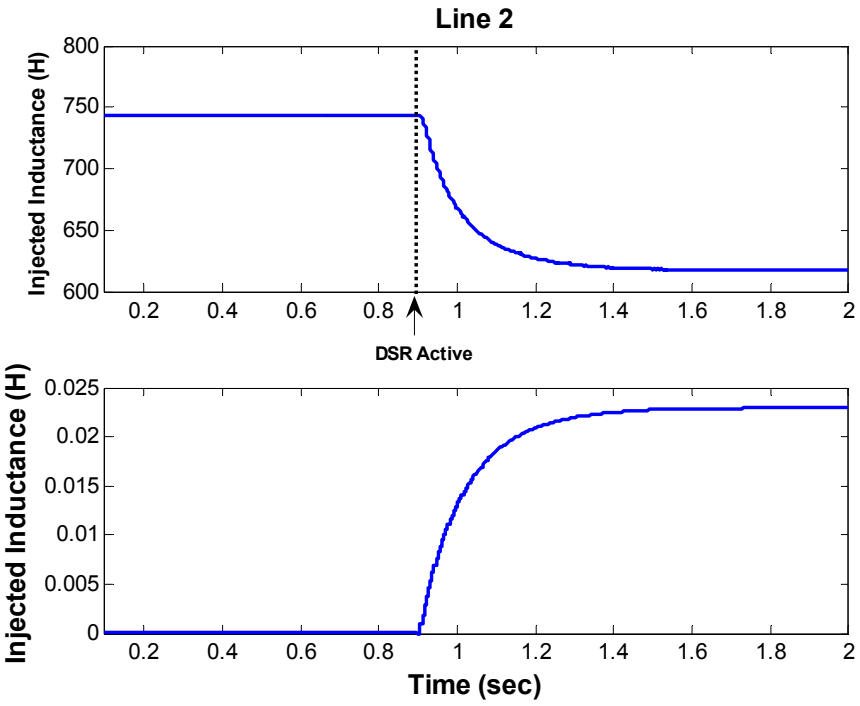

3.13.a

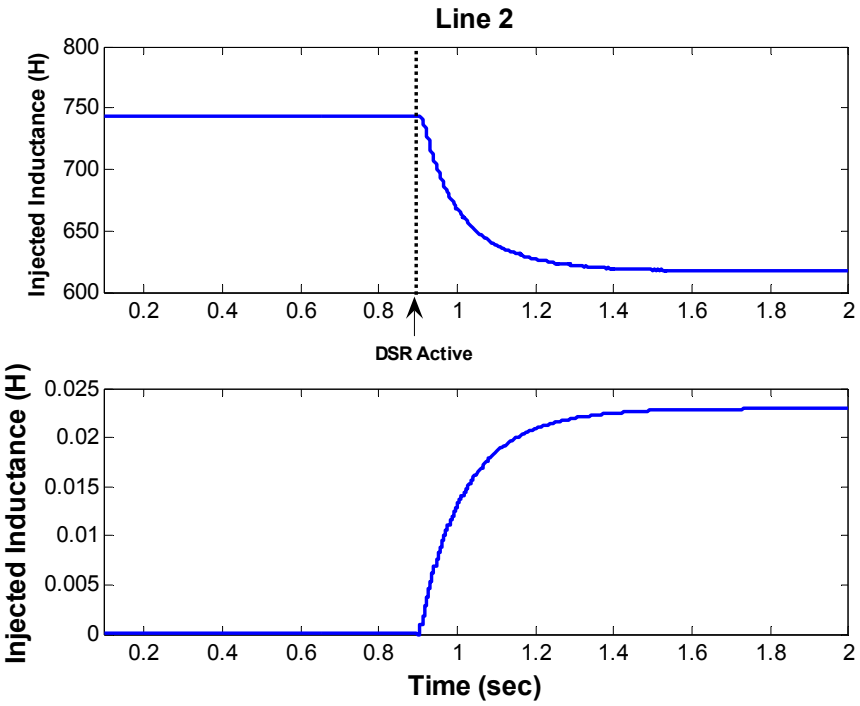

3.13.b

Figure 3.13 Line currents and injected inductance with the modified control strategy

The total injection on the lines is seen to follow a decaying exponential profile towards a steady state value. Again a sampling time period of 25 μsec is used and the injection is introduced after every 10 msec. The time constant of the estimator is taken as 1 sec. As mentioned before, an important design parameter of the control strategy is the time constant of the exponential estimator. If the time constant is made smaller and comparable to the sampling time period, then the controller might not able to vary the injection in sympathy with the changes in line current. This is seen by the simulation results in Figure 3.14, where line interactions come into play as the time constant is decreased to 1 msec and further to 10 μsec. The sampling period and the injection time are maintained at their previous values of 25 μsec and 10 msec respectively.

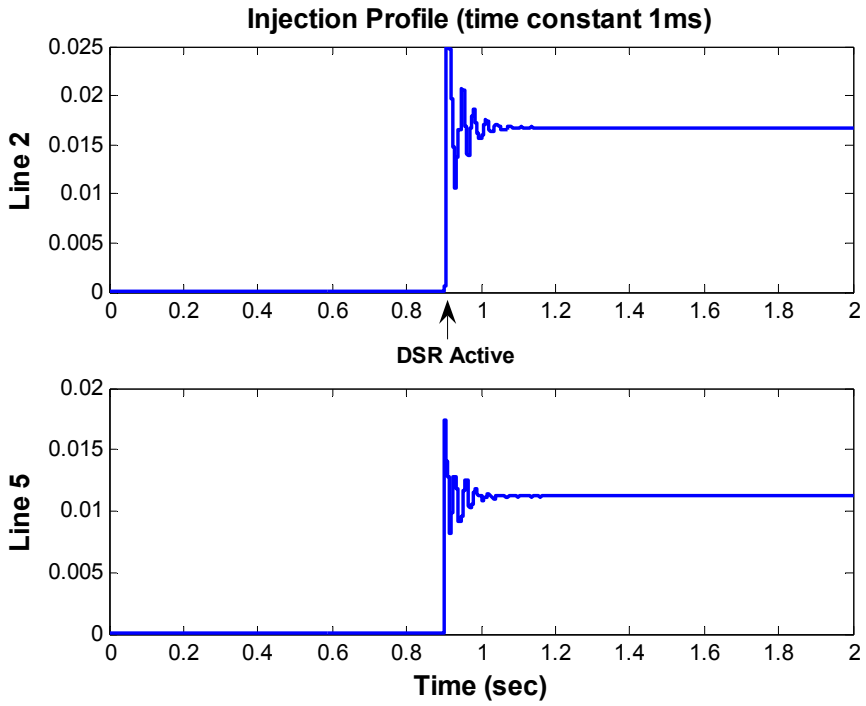

Figure 3.14.a Injection profile with a time constant of 1 msec

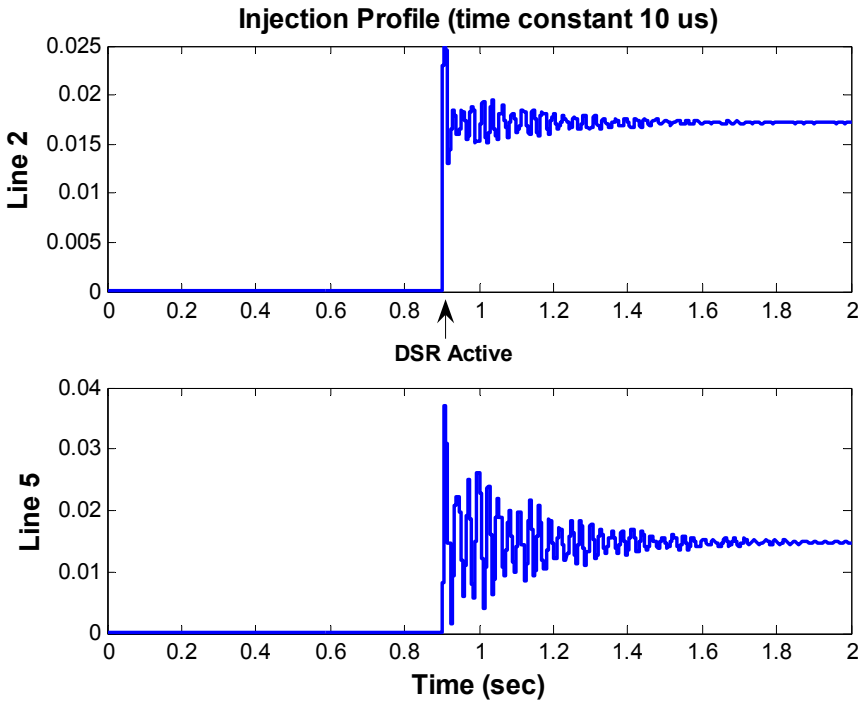

3.14.b

Figure 3.14.b Injection profile with a time constant of 10 μs

In a practical scenario, a finite number of DSR modules will be added to the critical lines of a network. Each module will have an identical controller that will calculate the total injection requirement of the line based on the measured current. The exponential estimator would then translate the injection vs current profile to injection vs time profile. The triggering signal would be given to the k'th module when the time profile of injection becomes equal to k times the inductance of a single module. This is explained by Figure 4.15, which shows the triggering of the k'th module on a line. The module is programmed to turn on at line current value of I_K and has an inductance value of X_K. It should be noted that each of the modules have identical inductance, say X. The value X_K simply refers to the k'th module with an inductance of X. The controller

calculates the injection requirement (X_{Line}) based on the line current (I_{Line}). By subtracting the value injected in the previous time instant (X_{prev}), the additional injection requirement of the line is obtained. The estimator then tries to reach this value exponentially over time. At time t_k, when the value of the exponential estimator becomes equal to k*X, the trigger is given to the module.

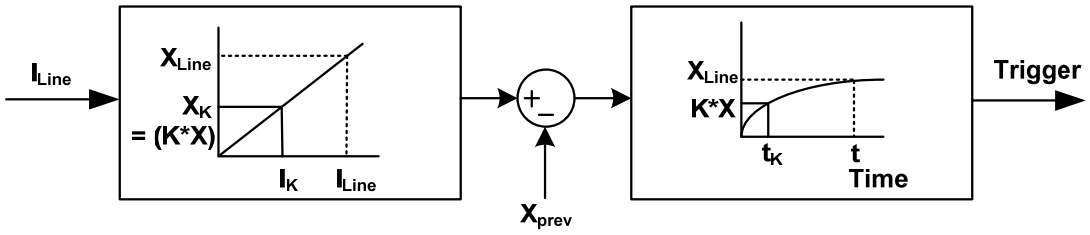

Figure 3.15 A schematic showing the functionality of a DSR controller

To show the practical feasibility of the control strategy, twenty DSR units are placed on each of the five lines of the four bus system. Each DSR module is rated for 10 KVA (at a line current of 750 A), which is also the design rating for the actual DSR prototype, as will be discussed later. This makes the inductance value of a single module to be 0.05mH. The first unit on each line is programmed to trigger at a line current value of 700 A and the last unit turns on when the current becomes 800 A. Thus, for example if the line current is 750 A, half the modules on that line must turn-on. A hysterisis band of 2 A is included in each module. The time constant of the exponential estimator for each module is taken as 1 sec. However, a random variation of ±10% is introduced in their values. This allows us to verify the robustness of the control strategy under non-idealities.

With this simulation set up, Figure 3.16 shows the turn-on of the required modules on two different lines (Line 2 and Line 5). Seventeen modules are triggered on Line 2 and seven modules on Line 5, as these modules receive actuating signals at different times. Only a small reduction is seen in the line currents as the total injection on the lines does not significantly increase the line inductances. However, the purpose of this simulation study is to show the triggering of individual modules on a network without any interactions. As part of future research work, investigation of a similar control strategy is required, exploring the conditions under which instability can be initiated.

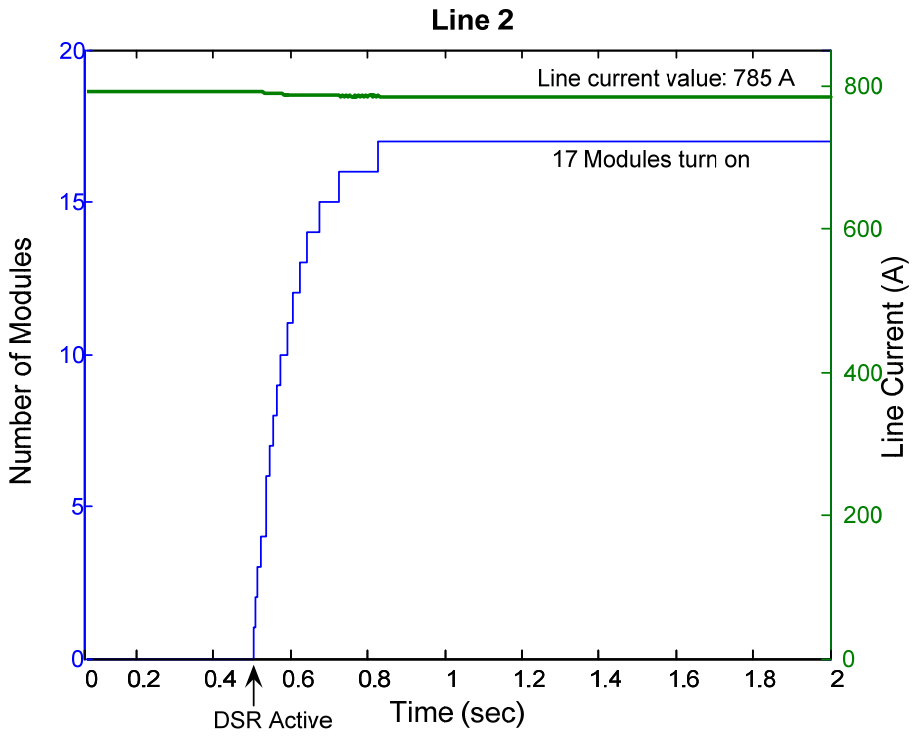

Figure 3.16.a Turn-on of DSR modules on Line 2

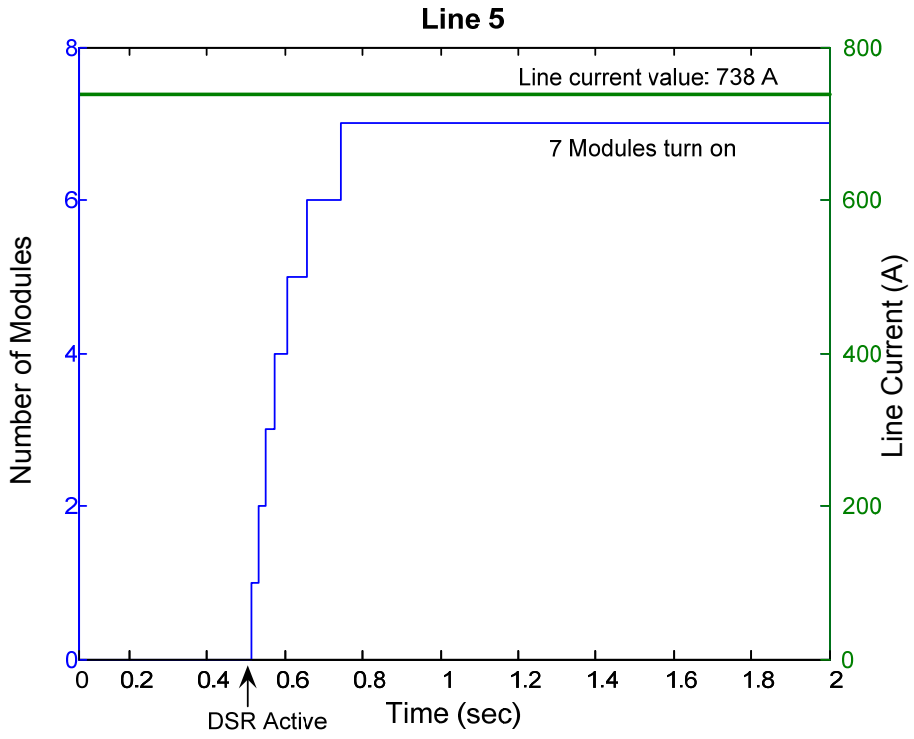

Figure 3.16.b Turn-on of DSR modules on Line 5

3.7 Conclusion

This chapter describes a simple passive solution that can increase power system capacity and reliability, in particular for meshed transmission, sub-transmission, and distribution networks. This approach of varying the line impedance is referred to as a Distributed Series Impedance (DSI) or Distributed Series Reactance (DSR). DSR technology eliminates the requirement of communication, making it compatible with the existing utility infrastructure. Communication can be used to optimize the system performance but is not essential for a stable system performance. The proposed control strategy allows the DSR devices to be switched in a coordinated manner, without any line interactions. It can be visualized that automatic steering of line currents in power network

can improve the power transfer capacity and reliability of the network. Simulation results in the next chapter demonstrate the system impact of DSR technology on improving grid utilization and reliability.

CHAPTER 4

SYSTEM IMPACT OF DSR MODULES

4.1 Introduction

The objective of this chapter is to demonstrate the impact of DSR technology in enhancing the control and operation of power system under nominal and contingency conditions. A reliable system operation is the primary concern of network planners and operators. Advanced simulation techniques such as optimal power flow and state estimation are normally used to reserve spare capacity on the lines to handle (N-1) contingency conditions. Further the capacity of the system also gets limited by the first line that hits the thermal limit, even though most of the lines may be operating at only a fraction of their capacity. Thus only sub-optimal system operation can be obtained with regard to the available capacity of the system. DSR system offers the capability to dynamically control the flow of power, resulting in improved system utilization under nominal and contingency conditions. Simulation studies on a simplified four bus and the IEEE 39 bus system confirms that system wide gains can be realized. Various metrics are suggested to quantify the performance of the technology.

4.2 Simulation Results on the Four Bus System

A simplified single phase model of a meshed transmission system is represented by the four bus system, shown earlier in Fig 3.8. The generators are modeled as fixed voltage sources and the loads as constant impedances with unity power factor. Each of the lines has a thermal rating of 750 A and an impedance of $0.1688 + j0.789\,\Omega/mi$. The

network is made perfectly symmetrical so that the system behavior and the performance of the DSR modules can be explained analytically. The system simulation was done using PSCAD software.

4.2.1 Increase in System Capacity

System capacity can, in principle and up to a point, be increased by diverting current flow from the overloaded parts to the underutilized parts of the network. Thus, the entire system can be gradually pushed to the 'absolute' thermal limit. Simulation studies on the four bus system show that even when Line 2 is operating at the thermal limit, the next critical line (Line 5) is operating at a much lower capacity (64% of the rated ampacity). Hence there is a lot of margin to push additional power through the rest of the power lines. The increase in line utilization thus represents an important metric for understanding the increase in system transfer capacity. Equation (4.1) defines the line utilization factor (LUF) to capture the average utilization of the lines. A higher LUF implies that transmission lines are being used more effectively.

$$LUF = \frac{\sum_{i=1}^{n} I_i}{\sum_{i=1}^{n} I_{thermal\_i}} \tag{4.1}$$

Here, I_i represents the operating line current, $I_{thermal\_i}$ corresponds to the thermal rating of the i^{th} line in the network, and n gives the number of lines in the network.

Figure 4.1 shows the line utilization factor as the loading of the system is

increased. For simplicity, the loading levels at the two load points were assumed to vary equally. The maximum transfer capacity of the uncompensated system is limited to 140 MW. With the DSR technology, the system capacity can be increased to 215 MW, before increasing line impedances push the system past its maximum power point (resulting in large reactive power flows on all lines). An increase of 30% in the line utilization factor is observed.

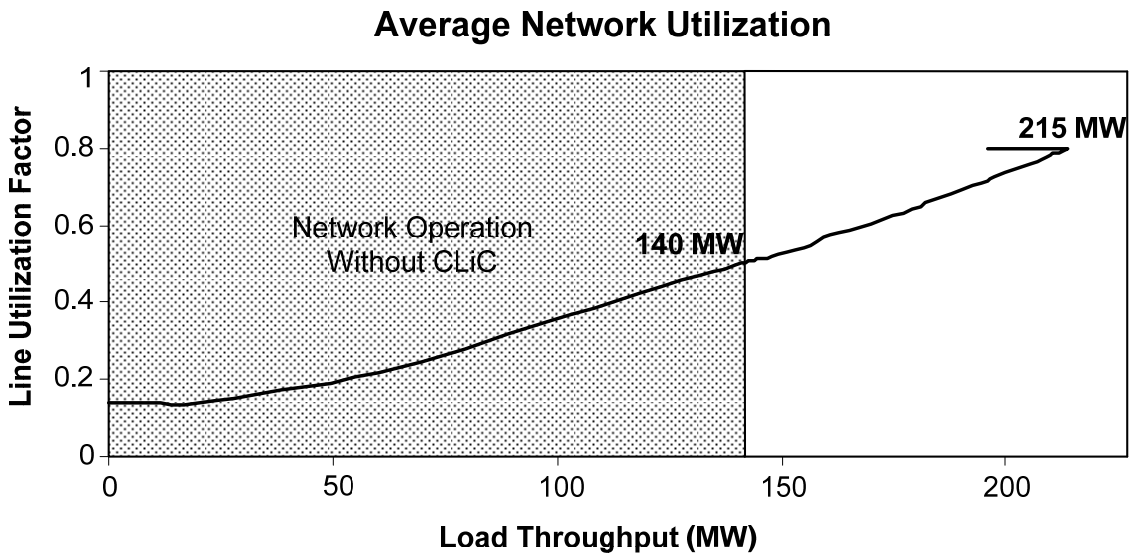

Figure 4.1 Increase in line utilization with DSR modules

A direct impact of the increase in line utilization is the additional megawatts that the system can deliver. With only two loads, it is easy to represent system capacity on a single plot, as shown in Figure 4.2. The original system capacity is limited by the overloads on Line 2 or Line 5. With the addition of DSR module, an increase in the load throughput by as much as 75% can be realized when the load is concentrated at Load 1.

This shows that DSR devices are able to control the level of current in the grid, automatically operating the power lines so as to keep them out of thermal overload.

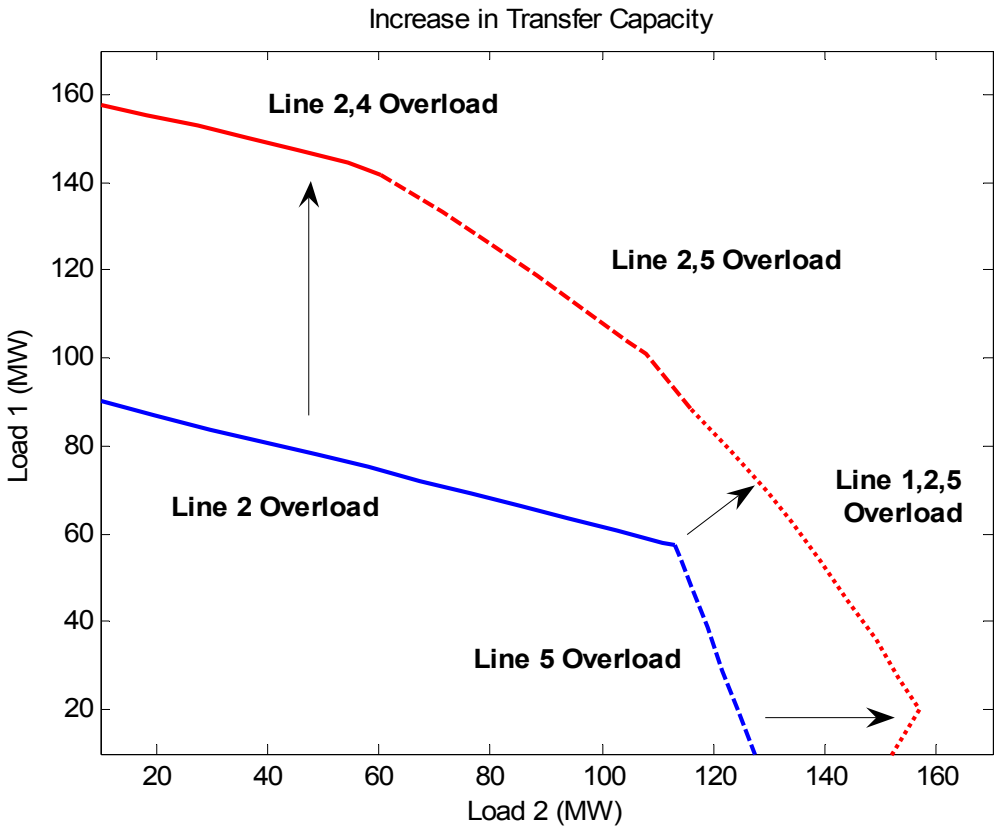

Figure 4.2 Increase in ATC with injected MVARs

The benefits of the DSR modules need to be analyzed taking into account the required control effort (MVARs) to realize the increase in system capacity. Performance index, defined by equation (3.2), measures the additional MWs that can be delivered to the load for each additional series MVAR injected. A higher performance index implies higher benefit to cost ratio. Figure 4.3 shows the plot of the performance index and the injected MVARs as a function of the total load power.

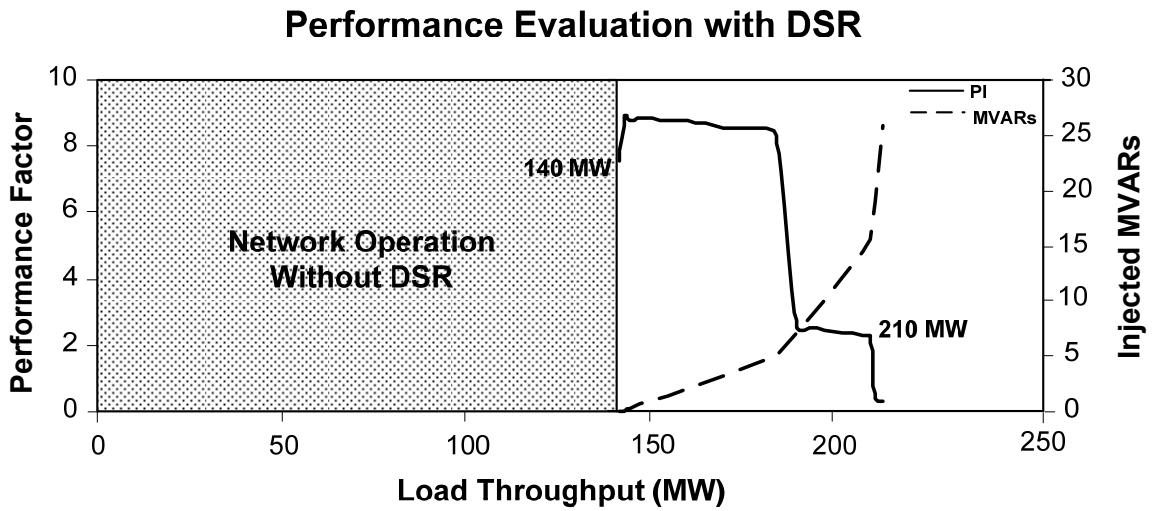

Figure 4.3 Network performance index with DSR

As DSR modules begin to operate on the first overloaded line, the load throughput increases by as much as 8.9 MW for every MVAR of injection. The DSR modules increase the impedance of the overloaded line, making other parallel paths more attractive for the flow of current. Additional power flows through these parallel paths increasing the transfer capacity of the system. The performance index remains practically constant until the next line gets overloaded. As the DSR modules on this line are made active, a sharp decrease in the performance index and a rapid increase in the injected MVARs are seen. The performance index drops further as the next line gets overloaded. These sharp drops in the performance index occur because as the system gets more and more overloaded, a greater control effort is required to make the underutilized lines of the network more receptive to the current flow.

When the system capacity has been increased by 29% (at a load throughput of 210 MW), the performance index becomes less than one, suggesting diminishing returns to scale with the further compensation of the system. It is anticipated that under realistic

system conditions, similar steps in performance index will be obtained, allowing selection of 'reasonable limits' on the deployment of DSR modules.

4.2.2 Increase in System Reliability

Another important aspect of the DSR modules is the capability to automatically and dynamically redistribute the line current under unanticipated contingencies. Figure 4.4 shows system operation under contingency condition when Line 2 is tripped because of a fault. This causes a thermal overload on Line 5. It is seen that with the DSR modules, the current is rapidly reduced, keeping the line within its thermal limit, preventing a possible cascading blackout or load shedding.

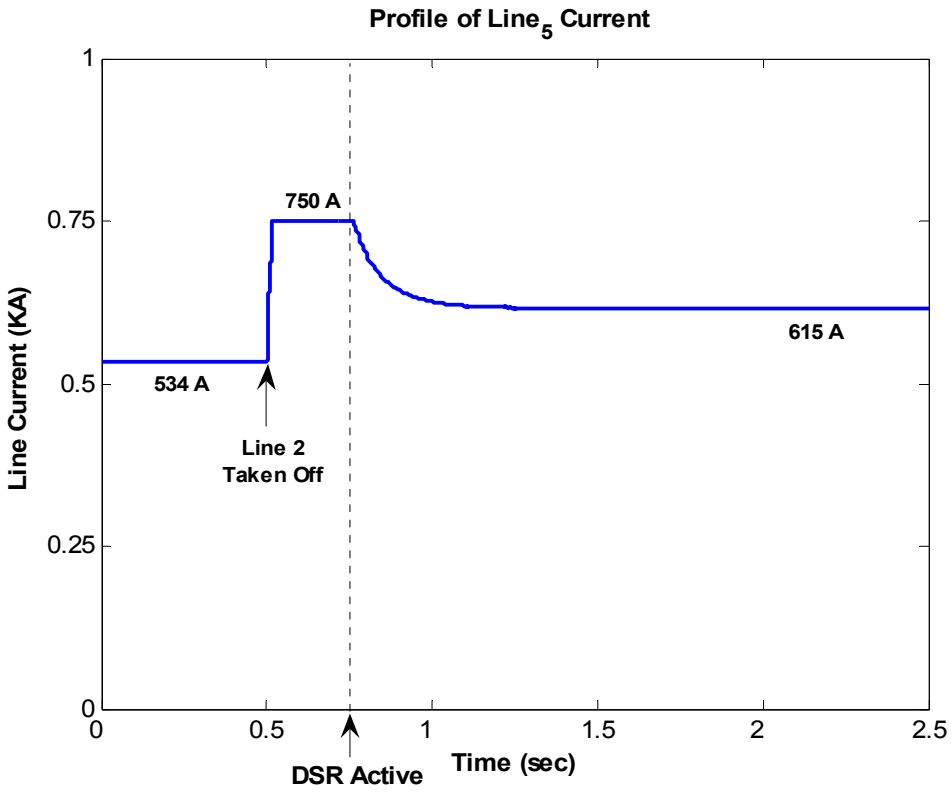

Figure 4.4 Performance under line outage

Another (N-1) contingency condition is simulated by taking off Generator 2. This causes the current in Line 2 to reach its thermal limit. Once again, as the DSR modules turn on, the line returns to a safer operating level of 624 A, as illustrated by Figure 4.5. It should be noted that the above mentioned contingencies were not pre-calculated in any way. The DSR modules make the network 'self-healing' by allowing the system to share the overload and settle to a new operating point. Further improvement in system reliability and operation may be possible with communication enabled DSI technology. While a significant number of papers have discussed the desirability of 'self-healing' networks, this is possibly the first example of an autonomously operating 'self-healing' network [40].

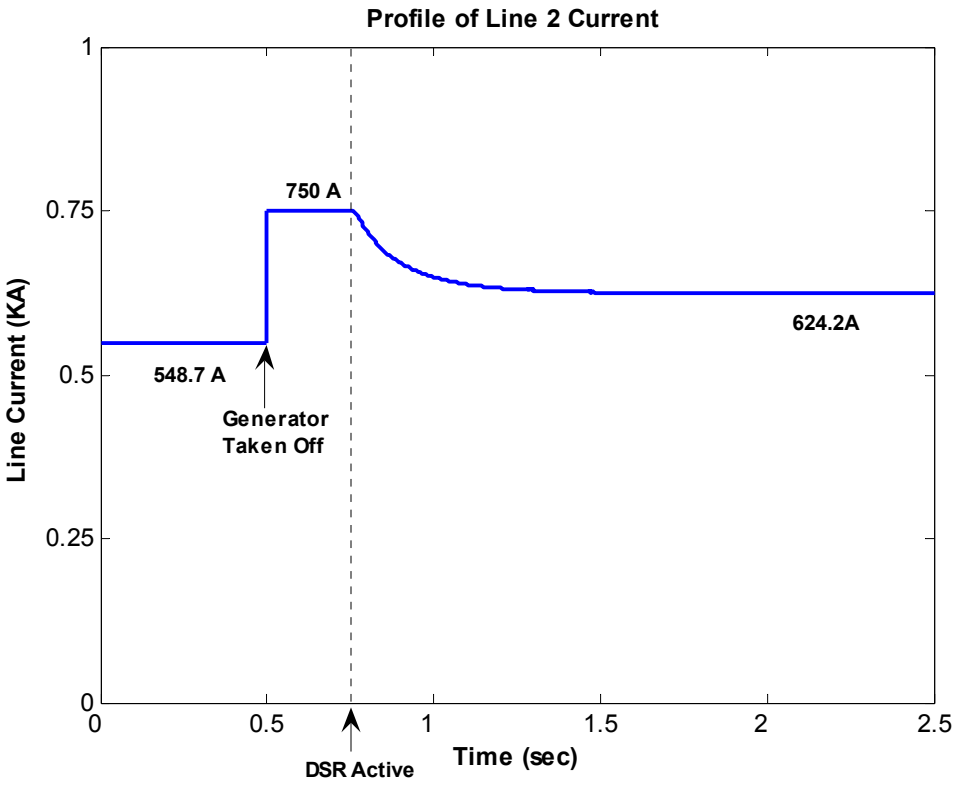

Figure 4.5 Performance under generator outage

4.2.3 Comparative Performance of DSI and DSR Technology

As we opt for a simpler technology, there exists a trade off between lower cost and reduced system gains. If communication could provide visibility to the state of the network, optimal power flow techniques could be used to determine an optimal control strategy. With complete information of the network or a part of the network, DSI technology is bound to have a superior performance than DSR. It is important to note that the DSI technology operates without any optimal power flow or system wide optimization techniques, but only with communications. Here we again use the four bus system (Figure 3.8) to study and compare the performance of the two strategies. Percentage increase in the transfer capacity of the system is used as the performance metric.

Each DSI module is modeled to have information about the operating values of all the line currents. A number of control strategies are possible. The adopted control strategy makes DSI to start off as a DSR module with only inductive injection. As the loading of the system is increased, a line or set of lines are identified, which start operating closer to the thermal limit. DSI modules are made active on these lines and inductive injection is introduced to keep these lines at the thermal limit by diverting additional power away from them. The injection is stopped once the injected inductance reaches 100% of the original line inductance. Up till this point, all the increase in the transfer capacity of the system can be attributed to DSR technology. With further increase in load growth, DSI modules on the neighboring lines are required to inject capacitance to pull the additional current flow towards them, to help increase power throughput of the network. A sensitivity analysis is done by injecting a small value of

capacitance on all of the neighboring lines and measuring the change in the line currents. Equation (4.2) gives the metric used for calculating the sensitivity of each line towards capacitive injection. The line with the highest sensitivity is selected and capacitive injection is induced with the constraint that the overloaded lines still continue to operate at their thermal limit.

$$I_{sensitivity} = \frac{\left(I_{current} - I_{prev}\right)}{I_{prev}} \tag{4.2}$$

Here $I_{sensitivity}$ measures the percentage change in current when a capacitor of a fixed value (2000 uF) is inserted into the line, $I_{current}$ refers to the value of line current after the capacitance injection, and I_{prev} is the value of line current prior to capacitance injection.

Capacitive injection is increased in a line with increasing granularity and is stopped once it brings down the line inductance by 50% of its original value. Equation (4.3) shows the different brackets of injection on Line 2. The inductance of the uncompensated line is 0.04186 H, and thus the maximum capacitance injection on this line is limited to 340 uF. It must be noted that a smaller series capacitance can compensate the line inductance to a larger extent. Therefore the capacitance injection is started with a larger value say 50000 uF and is subsequently decreased.

$$C_{new} = \begin{cases} C_{prev} - 500uF; & C_{prev} > 2000uF \\ C_{prev} - 10uF; & 500 < C_{prev} \le 2000uF \\ C_{prev} - 2uF; & 350 < C_{prev} \le 500uF \\ C_{prev} - 0.1uF; & 346 \le C_{prev} \le 350uF \end{cases} \quad (4.3)$$

Here C_{new} and C_{prev} refer to the current and previous injection values on Line 2.

The process is continued until further increase in capacitive injection brings down operating level of the overloaded lines from the thermal limit. The utilization of the network at this point is said to be optimized. Simulation results in Figure 4.6 show that the bulk of the increase in transfer capacity can be realized from the DSR technology (curve B-B'). By measuring the area under the curves, we can estimate the improvement in system capacity relative to the uncompensated system. It is seen that DSR modules can increase the power throughput of the network by as much as 96%. Communication enabled DSI technology optimizes the injection and improves the transfer capacity of the system further by 50% (curve C-C'). These additional gains from the DSI modules can only be obtained at the expense of added communication costs. This clearly indicates the superiority of DSR technology to realize improved system capacity at a much lower cost.

So far the value addition from the DSR technology has been shown on a simple system, so as to provide the visibility in terms of how the modules control the current flow to realize improvement in system utilization, transfer capacity, and operational reliability. In the next section, the gains from the DSR technology are presented on a more complicated system, which will provide resemblance to those that can be obtained on a real power network.

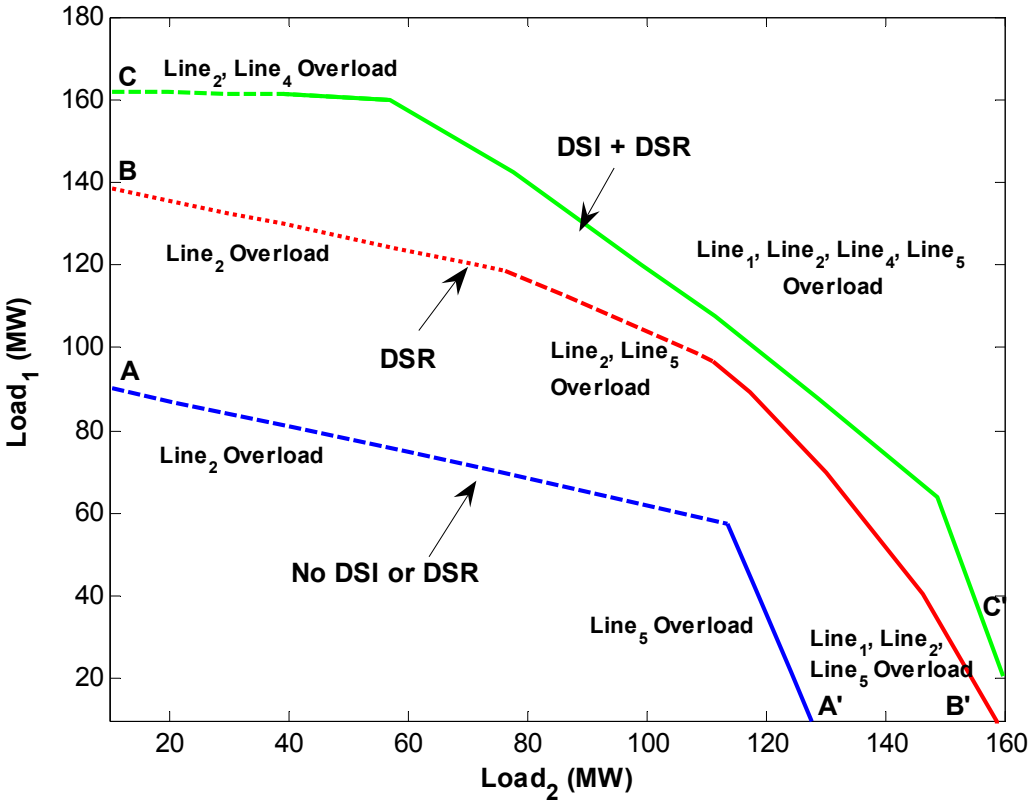

Figure 4.6 Comparison of increase in system capacity with DSI and DSR

4.3 Simulation Results on the IEEE 39 Bus System

To demonstrate the robustness of the proposed strategy, the concept of DSR was extended to a more complex system such as the IEEE 39 bus system. The system is shown in Figure 4.7 and has 10 generators, 19 load points, and 45 transmission lines. The generators are modeled as fixed voltage sources and the loads as constant impedances with unity power factor. Each of the lines is modeled to have a thermal rating of 750 A. The system data can be obtained from [41]. The simulation studies were done in PSCAD software, with an operating voltage of 80 KV (line to ground).

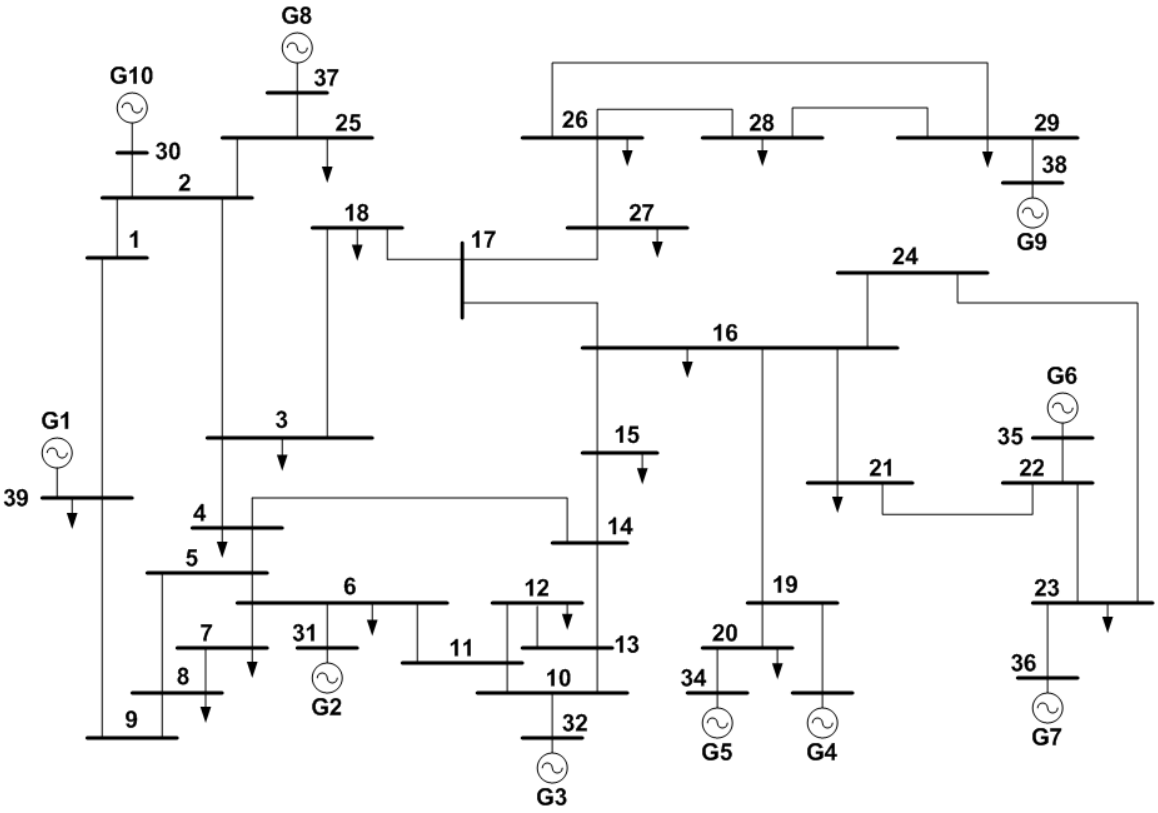

Figure 4.7. IEEE 39 bus system

4.3.1 Increase in System Capacity

To identify the transfer capacity of the uncompensated system, the loading of the network was increased uniformly till one of the lines (Line 22_21) reached its thermal limit. On a three phase basis, the maximum capacity of the IEEE 39 bus system was obtained to be 1904 MW. A set of 14 power lines were identified as the most critical to the system and most likely to suffer congestion. The utilizations of these lines at the maximum system capacity are highlighted in Figure 4.8. It can be seen that individual line utilization varies from 5% to 100%, with an average of ~59%. The real situation is even worse as it is driven by the need to have spare system capacity and to ensure system integrity and reliability under (N-1) or (N-2) contingency conditions. This reduces the

allowed line current levels under normal operating conditions to well below nominal thermal limits, and further degrades system utilization. A contingency study on the IEEE 39 bus system showed that the outage of Line 19-16 was the worst case (N-1) contingency. Under this line outage, the transfer capacity of the system gets limited to only 1469 MW.

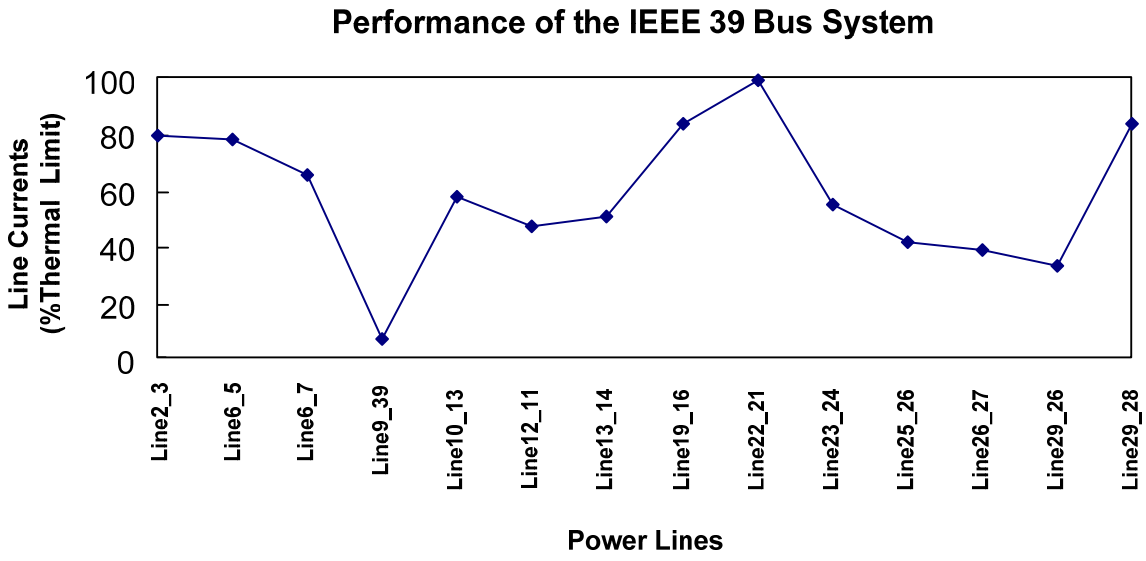

Figure 4.8 Network utilization when the first line reaches thermal limit

To increase the transfer capacity of the system, DSR modules were added onto each of these lines. DSR modules were modeled as fixed inductors of 50 uH, rated for 10 KVA @750 A. This is an ideal model, without incorporating losses and nonlinearities. However, it captures the impact of DSR technology on improving system capacity and reliability and the study provides an estimate on the number of modules required to realize the required gains.

Figure 4.9 illustrates an increase in line usage from 59% to 93.3% that can be realized from a redistribution of the current through the network, as the system load is increased. This increase in utilization was obtained without addition of new lines, and while ensuring that all lines operate within their thermal limit.

The system capacity was seen to improve from 1904 MWs to 2542 MWs, an increase of 33.5%. The control effort required to realize this improvement in system capacity is shown in Figure 4.10. As the modules are initially deployed on the Line 22-21, a performance index of 7.4 is observed. Thus each DSR module (with a rating of 10 KVA) can increase the transfer capacity of the system by as much as 74 KW initially. This is indicated by the initial slope of the line in each of the curves in Figure 4.10.

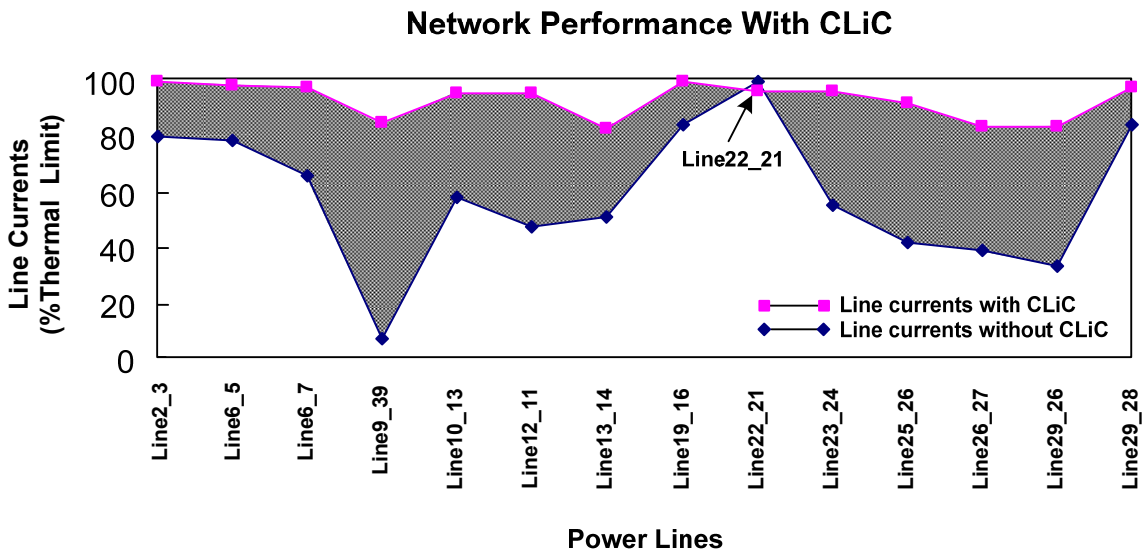

Figure 4.9 Increase in Line Usage

As the impedance of the overloaded line is increased, the current easily redistributes to nearby lines with lower impedance. As more and more lines see overload, greater control effort is required to push the currents to far away lines with spare capacity. The performance index drops as more modules are required to realize a given improvement in system capacity and this shows up as a decreasing slope in Figure 5.10.

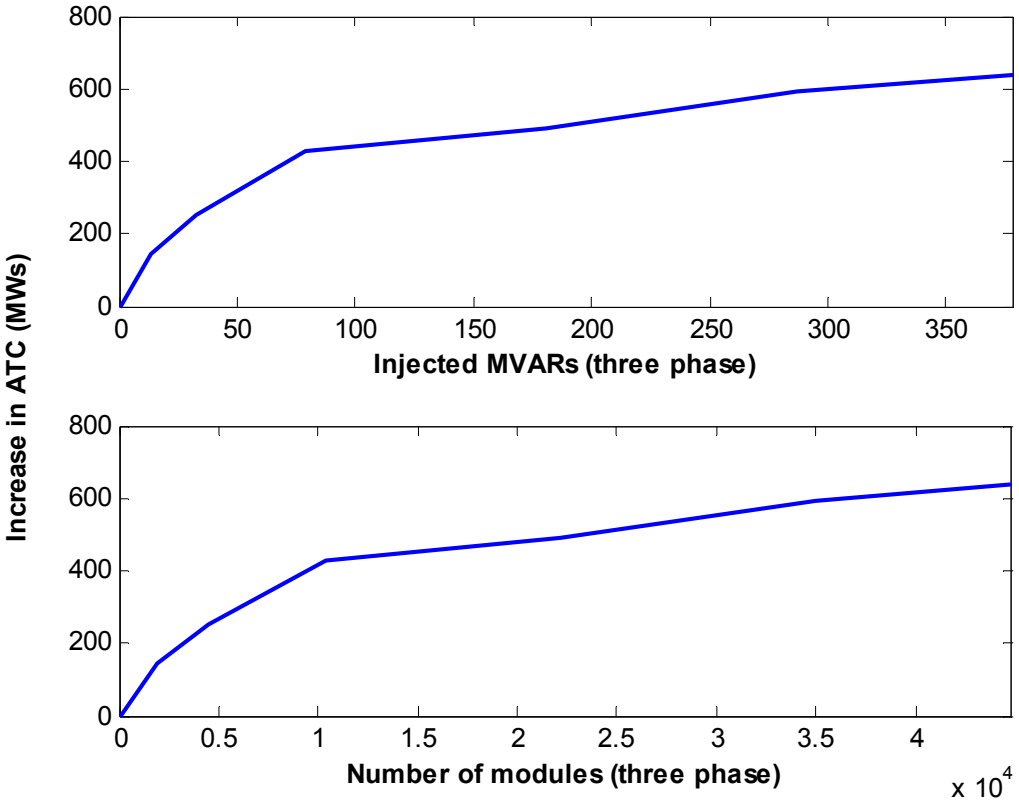

Figure 4.10 Increase in system capacity vs control effort

Figure 4.11 shows the corridors of the IEEE 39 bus where DSR modules were deployed to improve the system capacity by 33.5%. Without the use of DSR technology, additional transmission lines would be required to reinforce the capacity of these

congested links. Increasing transmission capacity by building additional lines does not promise an increase in the line utilization. Simulation results show that if new lines are built on these congested corridors, the line utilization factor merely increases from 59.4% to 64.4%. This demonstrates the efficacy of improving system capacity through DSR modules compared to building additional transmission lines.

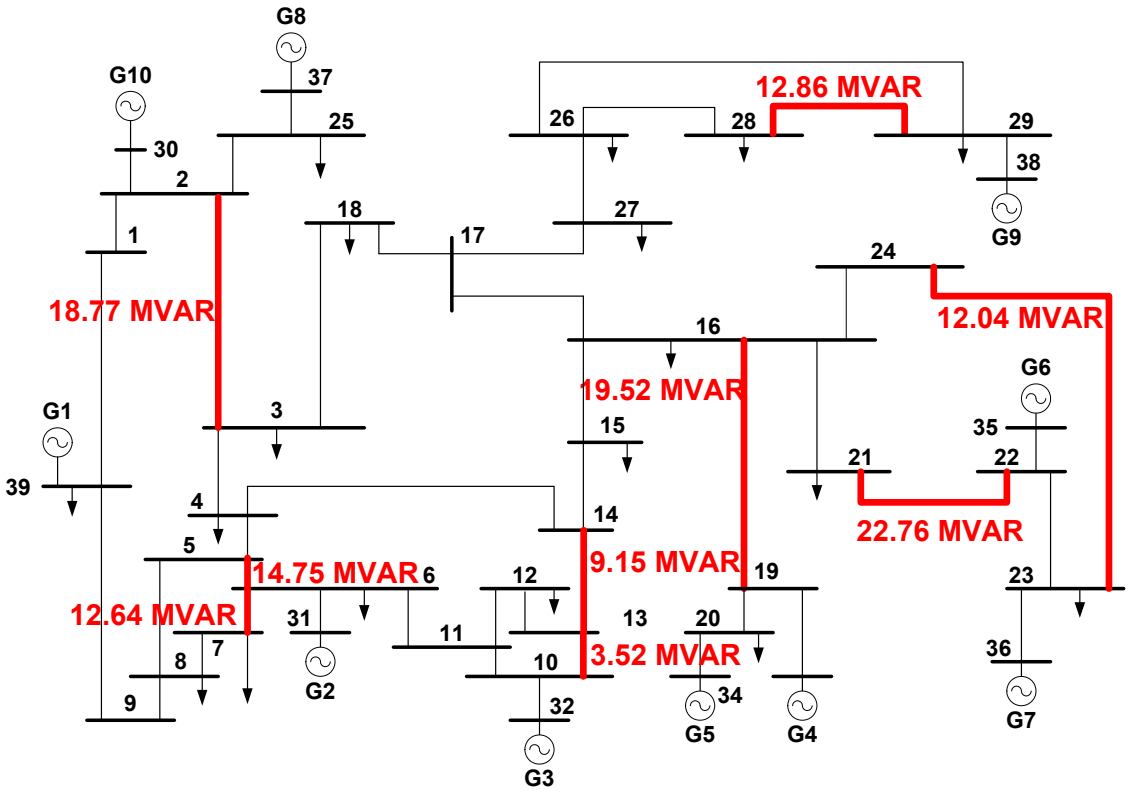

Figure 4.11 Congested corridors of the IEEE 39 bus system

4.3.2 Increase in System Reliability

Planning for contingency conditions requires system operators to reserve extra margin on the critical lines, so that a secure and stable system operation is guaranteed at any time. This further reduces the available transfer capacity of the system. Sensitivity

analysis tests on the IEEE 39 bus system showed the outage of Line 19-16 as the worst case contingency that affects the transfer capacity of the system. Under this contingency condition, the power throughput of the network is limited to 1469 MW, compared with 1904 MW under nominal operating conditions. As illustrated by Figure 4.12, DSR technology can provide significant gains in system reliability and utilization even under a contingency condition.

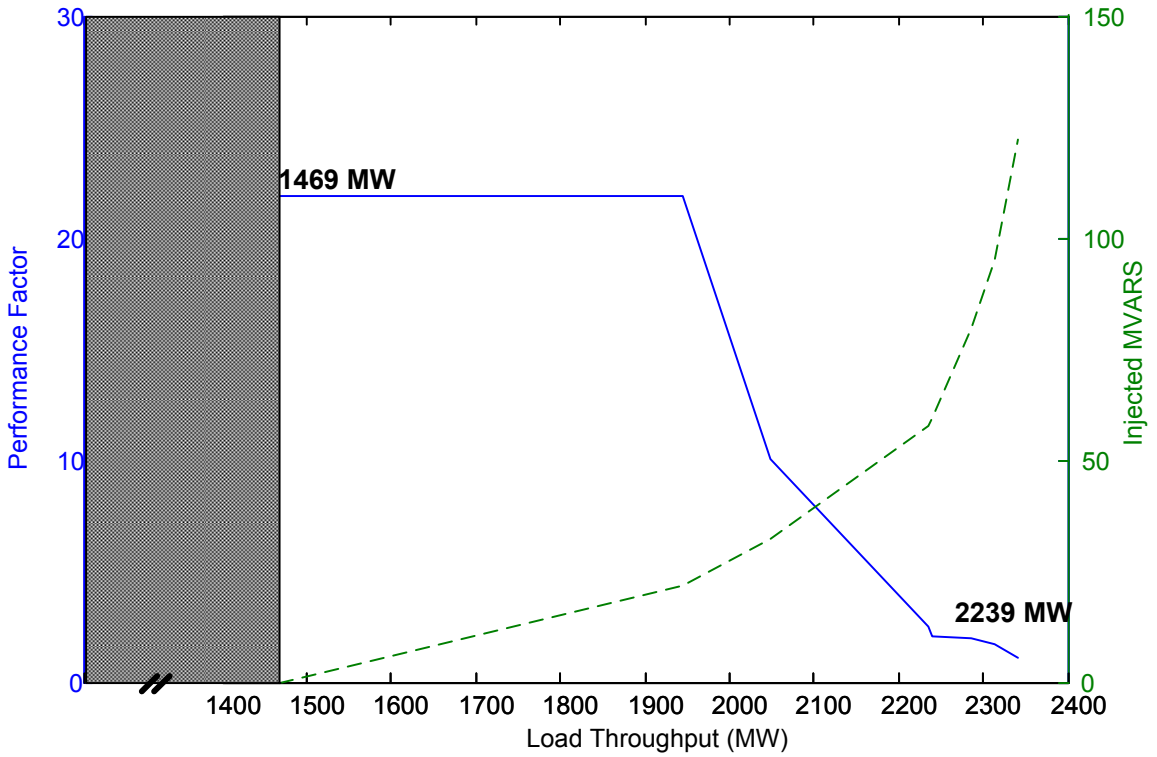

Figure 4.12 Performance index with DSR and outage of Line 19-16

The shaded portion in the figure shows the operation of the system without any DSR modules and under the mentioned contingency. As the DSR modules are applied to the overloaded lines, an initial performance index of as high as 22 is observed. This

suggests that under this contingency condition the DSR modules can realize an increase in power throughput by 22 MW for each MVAR of injection. The total system capacity can be increased by 870 MW (a percentage increase of 60) before the performance index drops below one and further deployment of DSR becomes uneconomical.

This result highlights that performance of DSR modules is topology-dependent. A summary of the results is presented in Table 4.1. It is important to note that under the mentioned (N-1) contingency, percentage increase in transfer capacity of the system and initial performance index is much higher than with no contingency.

Table 4.1 Summary of results on the IEEE 39 bus system

	Nominal Conditions	**Worst Case (N-1) Contingency**
System capacity with no DSR modules	1904 MW	1469 MW
System capacity with DSR modules	2542 MW	2339 MW
Initial Performance Index	7.4	22

4.3.1.1 Topology-dependent Performance of DSR Technology

Results in the previous sections show that for the system with no contingencies, each DSR module was able to realize 74 KW of increase in system capacity. Under a line contingency, 220 KW of additional system capacity can be obtained from each DSR unit. This clearly shows that the performance of the DSR technology is topology-dependent. This has a very important economic bearing on the system. When the planning studies predict a change in the topology or operating conditions of the system, DSR modules can be redeployed on the system to extract maximum benefits at a lower cost. Reconfigurable

investment opportunities can change the dynamics of the current transmission market and help to create investment opportunities for DSR technology.

4.4 Feasibility Study on a Utility Distribution Network

This section presents a feasibility study of DSR modules on a distribution network operated by a major utility in the North East. The network is a 4 kV distribution grid in Staten Island and is supplied by a number of unit substations fed from 33 kV systems. Under contingency conditions, such as the loss of a unit substation, some of the 4 kV feeders or other unit substations may experience overloads even though there maybe sufficient capacity in the grid. DSR modules were proposed as a potential means to improve the reliability of the grid under (N-X) contingency conditions. The Staten Island study was aimed at locating the best location on the 4 kV distribution grid for the field testing of DSR technology.

Network power system analysis software, 'DEW 8.2.0.0,' was used to study the power flows under normal and contingency conditions on the Staten Island. The DSR modules were modeled as lumped inductors in the simulations. A (N-1) contingency on the grid is defined by the loss of either a 33 kV feeder or a 4 kV distribution line while a (N-1-1) contingency is defined by the loss of a 33 kV feeder and a subsequent outage of a 4 kV line. A sample of (N-1) contingency conditions was provided by the utility for the feasibility study. Additional critical contingencies were also identified and are outlined in this section.

An interesting case is illustrated by the following scenario. This case simulates (N-1) contingency condition at the Port Richmond substation in the Staten Island area. The 4

kV distribution grid in the neighborhood of Port Richmond is shown by the schematic in Figure 4.13. Arlington2, Arlington4, Howlahk1, Howlahk2, and Mariners Harbor are the main substations in the vicinity of Port Richmond. Each of the distribution lines has an identification number, as can be seen in Figure 4.13. This case has also been suggested for a pilot demonstration of the DSR technology.

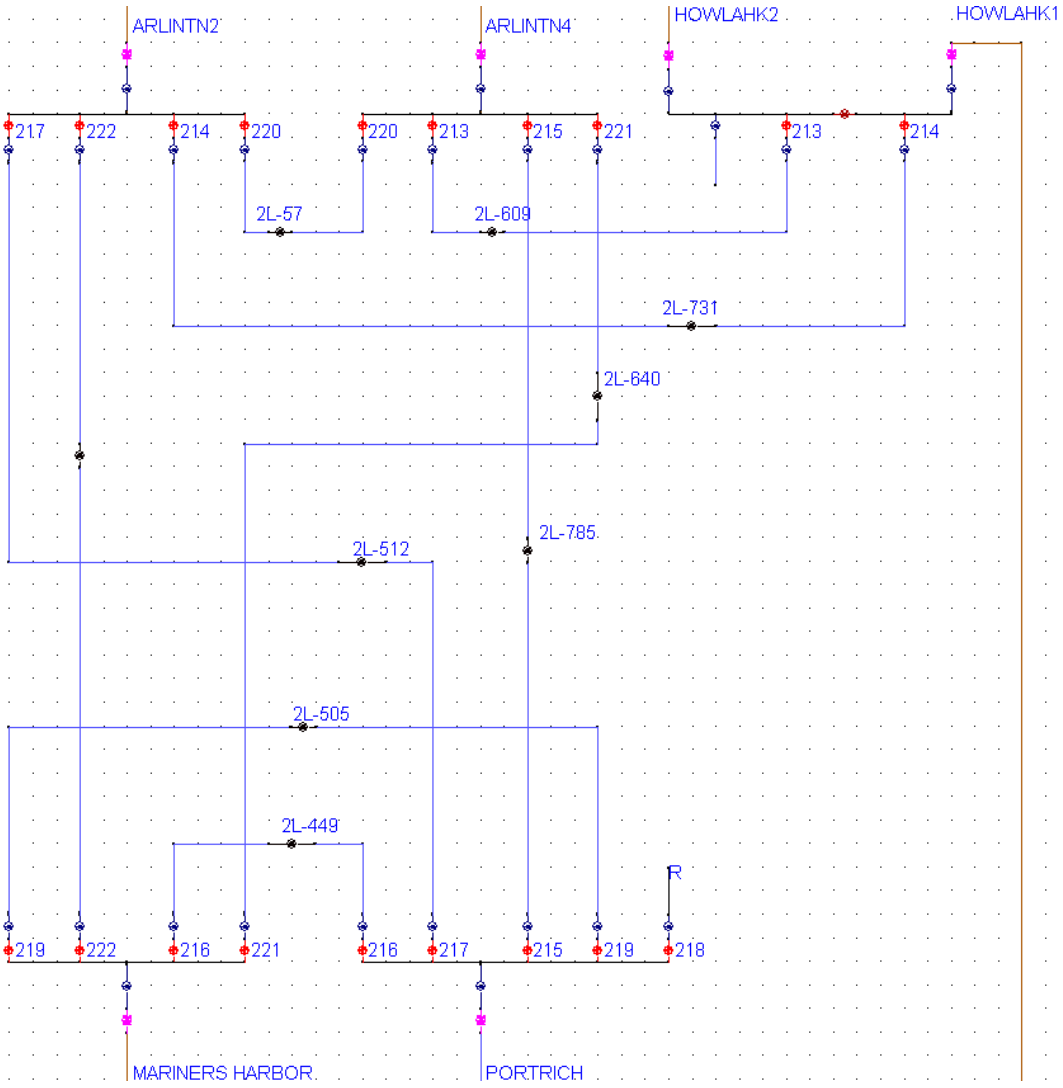

Figure 4.13 Schematic of the grid in the vicinity of Port Richmond

The study shows that the substations Mariners Harbor and Port Richmond are tightly 'coupled' to each other. The outage of the 33 kV feeder at Mariners Harbor causes a significant overload on Port Richmond 216. Table 4.2 shows the loading on Port Richmond 216 before and after the contingency. Port Richmond is seen to operate at 700 A under the mentioned contingency, well above its emergency rating of 585 A. The base case power flow (before contingency) corresponds to 8 pm of a weekday in August.

Table 4.2 Load flow results on Port Richmond 216

	Emergency Rating (A)	**Before Contingency (A)**	**After Contingency (A)**
Phase A	585	206	710
Phase B	585	193	685
Phase C	585	191	711

With the deployment of DSR modules on Port Richmond 216, the overload could be reduced to within the emergency rating of the line. A total of 1.38 MVAR (on a three phase basis) injection is required to maintain reliable operation of the system under such a severe contingency condition. For simplicity, the modules were lumped as an inductor with a value of 18.85 mH per phase near the substation. However, in practice the modules could be appropriately distributed over the line length of 12,000 feet connecting Port Richmond to Mariners Harbor. A summary of the results is shown in Table 4.3.

Table 4.3 Summary of results under (N-1) contingency condition at Port Richmond

(N-1) Contingency with a 33 kV feeder outage				
33 kV feeder out		**Overloaded Lines**		
Mariners Harbor		Port Richmond 216		
Load Flow Results for Port Richmond 216				
Emergency Rating (A)	Before Contingency (A)	After Contingency (A)	CLiC Modules Added (kVA)	Overload Relief (A)
585	206	710	460	587
585	193	685	460	566
585	191	711	460	588

It is interesting to see what would have happened if DSR modules were not used to bring down the current level on Port Richmond 216. As Port Richmond 216 begins to operate above its emergency rating under the feeder outage at Mariners Harbor, the over-current relays would signal the tripping of the line. Tripping of Port Richmond 216 would result in significant overloading of Port Richmond 219, taking it over its emergency rating as well. As over-current relays operate to trip this line (Port Richmond 219), the overload would be shifted to the next most sensitive line in the neighborhood and if appropriate measures are not taken, a cascading failure may result. This example highlights the value of securing the operation of Port Richmond 216 under the mentioned (N-1) contingency at Mariners Harbor, with the use of DSR technology.

Another example of overload relief under (N-X) contingency condition is presented below. Table 4.4 shows that with the simultaneous outage of a 33 kV feeder (Wardsworth 1) and a 4 kV line (Clifton 1_365), two lines of the system (Clifton2_366

and Wadsworth2_368) are seen to get severely overloaded, and require 320 kVA and 360 kVA of injections respectively to bring the overload within limits.

Table 4.4 Line overloads under (N-1-1) contingency

(N-1) Contingency with a 33 kV feeder and a 4 kV line out				
33 kV feeder out	4 kV line out	Overloaded Lines		
Wadsworth 1	Clifton 1_365	Clifton 2_366	Wadsworth 2_368	
Clifton 2_366				
Normal rating	Before contingency	After contingency	CliC modules added (kVA)	Overload relief
489	256.37	595.78	320	532.03
489	191.32	559	320	524.2
489	230.11	628.49	320	575.43
Wadsworth 2_368				
Normal rating	Before contingency	After contingency	CliC modules added (kVA)	Overload relief
577	101.45	494.74	360	444.39
577	233.53	674.88	360	577.28
577	164.1	635.39	360	552.86

The Staten Island study was aimed at locating the best location to demonstrate the DSR concept on the 4 kV distribution grid. The targeted line (Port Richmond 216) is fairly short and will require 1.38 MVAR of series injection to provide the overload relief. Based on target price point of $100/kVAR, it is expected that the commercial DSR solution will cost around $138,000.

4.5 Conclusion

The simulation results in this chapter demonstrate that DSR modules can increase the transfer capacity and reliability of a system by automatically diverting current flow from congested parts of the network to underutilized lines of the network. A metric that gives the average utilization of the lines in a network is used to show the improvement in system capacity. It is theoretically possible to increase the system capacity to the point where all the lines in the network start operating at their thermal limit. However the increased inductance of the system would demand increased amounts of reactive power from the generators, making such operating conditions impractical. Further, as the DSR modules can realize a very high performance index initially, only a reasonable number of modules are required to realize the gains from the technology. This also opens the avenue to redeploy DSR modules over the system to specifically increase transfer capacity in one part of the network, at a reduced cost.

System planning studies are dominated by contingencies, to allocate sufficient reserve margins on each line. The available transfer capacity of the system is seen to significantly suffer. The DSR technology can improve system reliability and can also increase the transfer capacity of the network under such conditions. Studies on Staten Island network have confirmed that reasonable level of injection can secure system operation and reliability under (N-X) contingency conditions and can alleviate a cascading failure.

Communications enabled DSR technology can further improve system utilization and reliability, but only to a limited extent. Simulation results have shown that with the

DSR technology, the network utilization can be brought to near optimal, without any changes to the existing infrastructure.

A system wide deployment of DSR technology is only possible if all issues of interference to system operation are resolved. The following chapter presents anticipated interactions between DSR modules and system operation and discusses them in detail.

CHAPTER 5

DESIGN CONSIDERATIONS TO MINIMIZE INTERFERENCE WITH SYSTEM OPERATION

5.1 Introduction

The objective of this chapter is to put forth the anticipated interactions between the operation of DSR modules with that of the power system, including other protection and control elements. Discussion with the utilities and other experienced professionals has suggested that primary issues of concern are:

- Interactions between the operation of modules, on the same or different lines, resulting in steady state line current oscillations
- Deterioration of system voltage profile with increase in line impedance
- Fault management and impact on the operation of protective relays
- Impact on the transient stability of the system

The scenarios listed above are specific to the operating conditions of the power system. A generic approach is taken wherever possible; otherwise, simulation studies on the four bus and the IEEE 39 bus system are used to illustrate the feasibility of using DSR modules on a power system without any interactions with the system operation.

The issue of interactions between switching of modules on the lines of a power system has been discussed in chapter 3. With the proposed control strategy, no interactions between the modules on the same line or on different lines are seen. Impact on bus voltage profiles, fault management, and transient stability of the system are

discussed in this chapter and it will be shown that DSR modules operate with no interference to the system control and operation.

5.2 Impact on Voltage Regulation

One of the major concerns with a system that increases line inductance is voltage regulation at the load buses. It is obvious that as the DSR modules are deployed, additional line voltage drop across the modules would reduce the bus voltages. Equation (5.1) defines the voltage regulation at a load bus as the drop across line impedance normalized by the sending end voltage. A higher value of voltage regulation implies a bigger drop in the load voltage magnitude from its nominal value.

The load voltage profile of the four bus system with increase in the loading of the system is shown in Figure 5.1. The load is increased uniformly at the two load buses, till one of the lines of the system reaches the thermal limit, at which point the system is said to operate at maximum power transfer capacity. The voltage regulation at the two load buses is shown with two different lines (represented as a band). As can be seen, the voltage regulation shows a continuous rise with increase in the loading of the system.

$$V_{reg} = \frac{\left|\tilde{V}\,sending - \tilde{V}\,receving\right|}{\left|\tilde{V}\,sending\right|} \times 100 \qquad (5.1)$$

Here V_{reg} is the voltage regulation in percentage, $\tilde{V}_{sending}$ is the sending end voltage phasor, and $\tilde{V}_{receving}$ is the receiving end or the load voltage phasor.

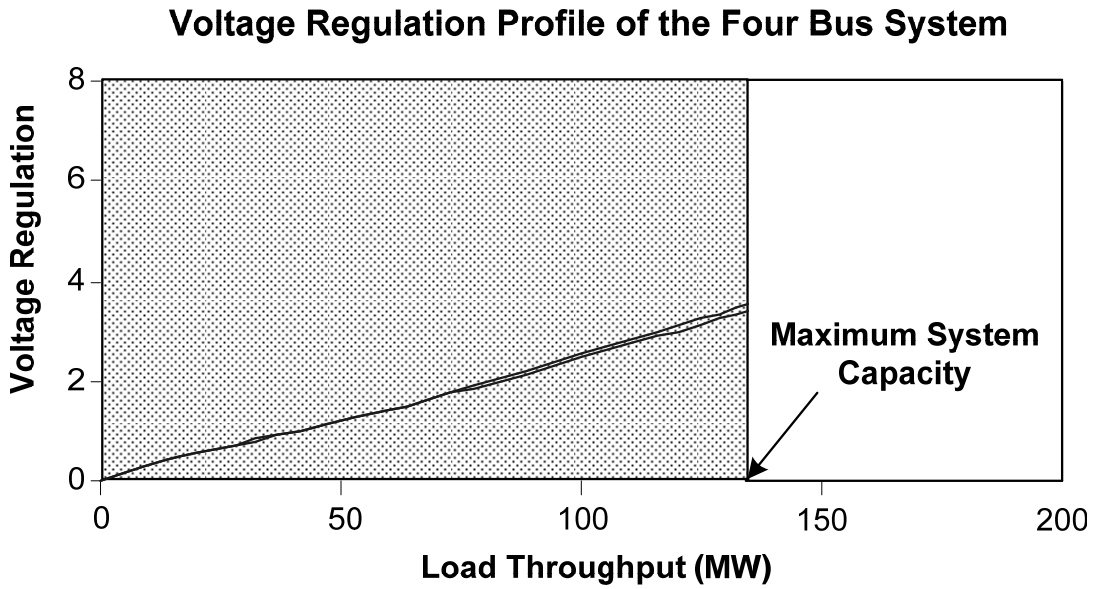

Figure 5.1 Voltage regulation profile at the two load buses

The deployment of DSR modules on the system increases the series line inductance and consequently the series voltage drop. The voltage regulation profile worsens and is seen to rise above the profile of the original uncompensated system. This is illustrated by the sharp increase in the voltage regulation band in Figure 5.2, when DSR modules are used on the power lines to extract unused capacity of the system, as the loading at the buses is increased beyond the point of maximum transfer capacity.

For most practical systems, a voltage profile within 0.95 pu to 1.05 pu is considered acceptable. A voltage drop of more than 0.05 pu from the nominal must be corrected by supplying the required VARs through capacitive shunt compensation. Referring again to Figure 5.2, the voltage profile of the load buses is seen to improve and becomes similar to the one with the original (uncompensated) system, after capacitive shunt compensation is used at the two load buses. This also shows that load voltage

regulation under series injection can easily be solved by coordinated shunt VAR injection, without any interference between the two control functions.

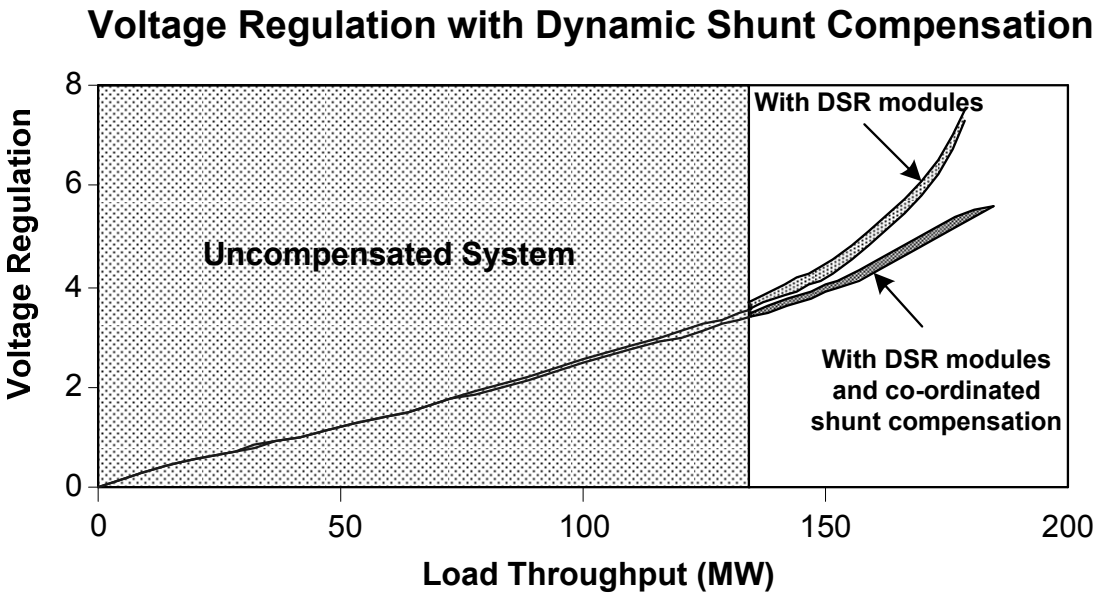

Figure 5.2 Voltage regulation profile with DSR modules

As stated before, DSR technology is able to realize maximum gains early-on, when the performance index is very high. Therefore, it seems that DSR modules will not deteriorate the system voltage profile significantly as long as the performance index is much greater than one. This is validated by a simulation study on the IEEE 39 bus system. Figure 5.3 depicts the voltage profile at the nineteen load buses of the IEEE 39 bus system for three different scenarios. The blue line corresponds to the bus voltages under light loading conditions (20% of the maximum capacity). As the system loading is increased to the maximum, the bus voltage profiles are seen to depress, as shown by the red line. This is because of the increase in the series voltage drop across the line

reactance. Finally, when DSR modules are deployed on the lines, the series voltage drop increases further because of increase in line inductance and the bus voltages show a further drop. This is shown by the pink line in Figure 5.3. The nominal system voltage is 80 kV and a band of ±%5 around the nominal voltage is shown to account for acceptable voltage variations.

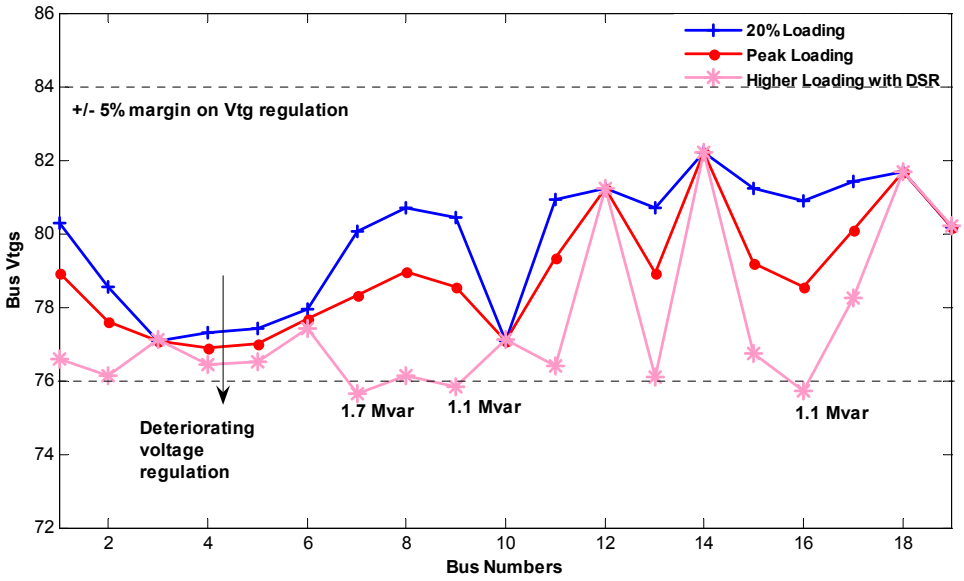

Figure 5.3 Voltage regulation profile on the IEEE 39 bus system

An increase in system capacity by 630 MW (equivalent to 33% increase in base capacity) is realized at the expense of 75 MVAR of series injection from DSR modules. At this point, the voltage at the three load buses is seen to marginally cross the acceptable regulation band of ±%5. This was easily corrected by shunt capacitive injection of a total of 11.7 MVAR (on a three phase basis) at these buses. It is thus seen that the issue of voltage regulation under DSR compensation can be easily resolved through capacitive

shunt VAR injection and will not pose any impediments to the application of DSR modules on the system.

5.3 Impact on Power System Protection

To ensure reliable and safe system operation, circuit breakers are commonly used for interrupting the fault and disconnecting the faulted transmission line or equipment. The trigger signal to these breakers is provided by relays, once they sense a fault on the system. The particular relay of interest is the distance protection relay. The relay calculates the impedance of the line to the fault by sensing the voltage and the current at the point of installation. If the impedance of the line or the equivalent length of the line to the fault is smaller than the zone of protection, a trigger signal is initiated. Figure 5.4 shows protection zones and tripping times of a typical distance relay installed at Bus A.

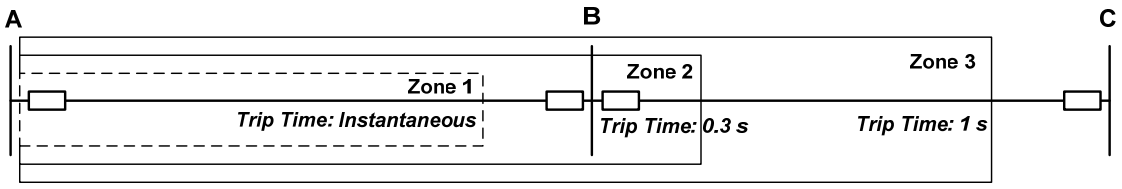

Figure 5.4 Zones of protection and tripping times for a distance relay installed at Bus A

The DSR modules increase the impedance of the line and as a result, the distance protection relay can mal-operate and predict the distance of the fault to be outside the zone of protection. To rectify this problem, two solutions are possible.

1. The operating logic of the relay can be changed to dynamically incorporate the additional impedance of the modules in the zone of protection. The operating logic

would then calculate the number of active modules on the line from the measurement of the operating line current value. The relay would adjust for the compensated line impedance and modify the zone of protection dynamically. Though the solution is viable, it introduces additional complexity in the network.

2. DSR modules are by-passed in a time much faster than the operating time of the fault detection algorithm of the distance relay. This will ensure that the relay only sees the uncompensated impedance of the line under a fault. This seems to be a more plausible approach for deploying DSR modules on a system wide basis.

5.3.1 Protection Algorithm Used in Distance Relays

Most available distance relays operate to detect the positive sequence impedance of the line, by decomposing the measured voltage and current signals into their fundamental orthogonal components. The fundamental orthogonal component of a periodic signal is given by equation (5.2), and can be determined in discrete time form by equation (5.3). The algorithm is described in Figure 5.3 and uses signal processing to reject harmonics or DC bias that may be introduced under transient conditions. By applying the algorithm to the voltage and current signals, the real and imaginary component of the impedance can be obtained by equation (5.4).

$$x(t) = x_d(t) + jx_q(t) \tag{5.2}$$

Here $x(t)$ is the time varying signal, and $x_d(t)$ and $x_q(t)$ are the fundamental orthogonal components of the signal

$$x_d(n) = \frac{1}{N}\sum_{m=k}^{N+k-1} x(mT/N)\ \sin\left((2\pi/N)(mn)\right)$$
$$x_d(n) = \frac{1}{N}\sum_{m=k}^{N+k-1} x(mT/N)\ \cos\left((2\pi/N)(mn)\right) \tag{5.3}$$

Here T is the time period of the signal, n is the time index in the discrete domain, and N is the number of samples per second.

$$R = \frac{V_d I_d + V_q I_q}{{I_d}^2 + {I_q}^2}$$
$$X = \frac{V_q I_d - V_d I_q}{{I_d}^2 + {I_q}^2} \tag{5.4}$$

Here R is the resistance and X is the reactance seen by the distance relay.

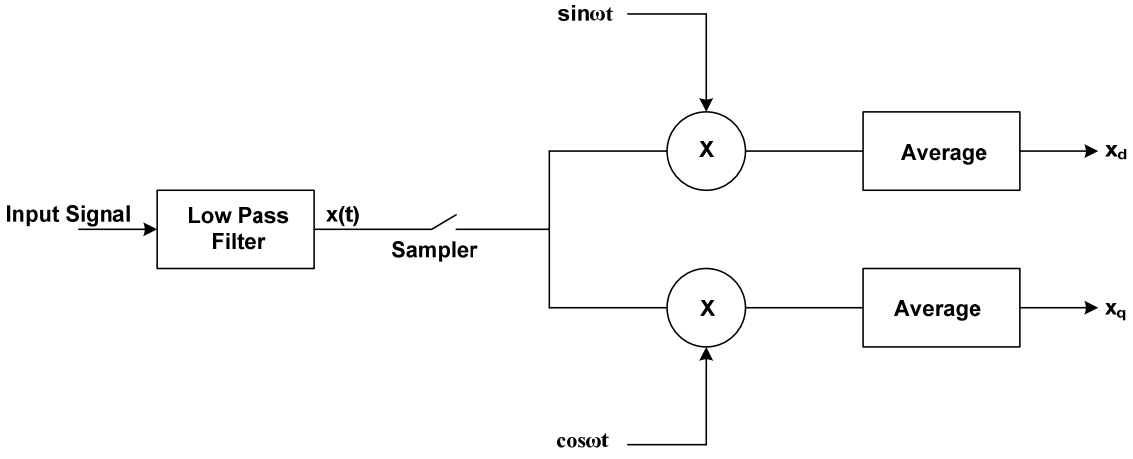

Figure 5.4 Algorithm for detecting orthogonal signal components

5.3.2 Fault Detection Algorithm Used in DSR

The fault detection algorithm of the DSR modules is based on comparing the instantaneous value of line current against a threshold. Once the instantaneous line current is detected to cross this value, the micro-controller waits for three sampling periods, under a sampling frequency of 6 kHz. After this waiting period, it again compares the measured line current value against the threshold. If the line current is still detected to be above the threshold, then the module is by-passed by shorting the secondary of the transformer. The code can be accessed from Appendix B. The thyristor pair is closed first, followed by the electromechanical relay. The waiting period of three samples allows the micro-controller to filter out any noise peaks and avoid erroneous firing of the thyristors or the relay.

Figure 5.5 shows the experimental set-up for validating the by-pass feature of DSR module under fault conditions. The DSR is seen to carry two wires through it: one operating at steady state current levels of 300-400 A and the other operating at fault currents of up to 10,000 A. The cable carrying the steady state current is series connected to a 240 V source through a variable inductor; while cable carrying the fault current is directly connected across an AC voltage source of 600 V to generate the required fault current. The electronics, which include the DC power supply, thyristors, and micro-controller, are powered from the cable carrying the steady state current.

Figure 5.6 shows the operation of DSR module under a fault current of 10,000 A. The module is initially in injection mode with the relay turned on. This can be confirmed from the secondary voltage (500 V peak-to-peak) that can be seen in the blue waveform. The fault current is given by the green waveform, with a RMS value of 10,000 A for 11

cycles. Once the fault is induced, DSR module takes only **600 µsec** to detect the fault, after which the transformer is shorted by closing the relay.

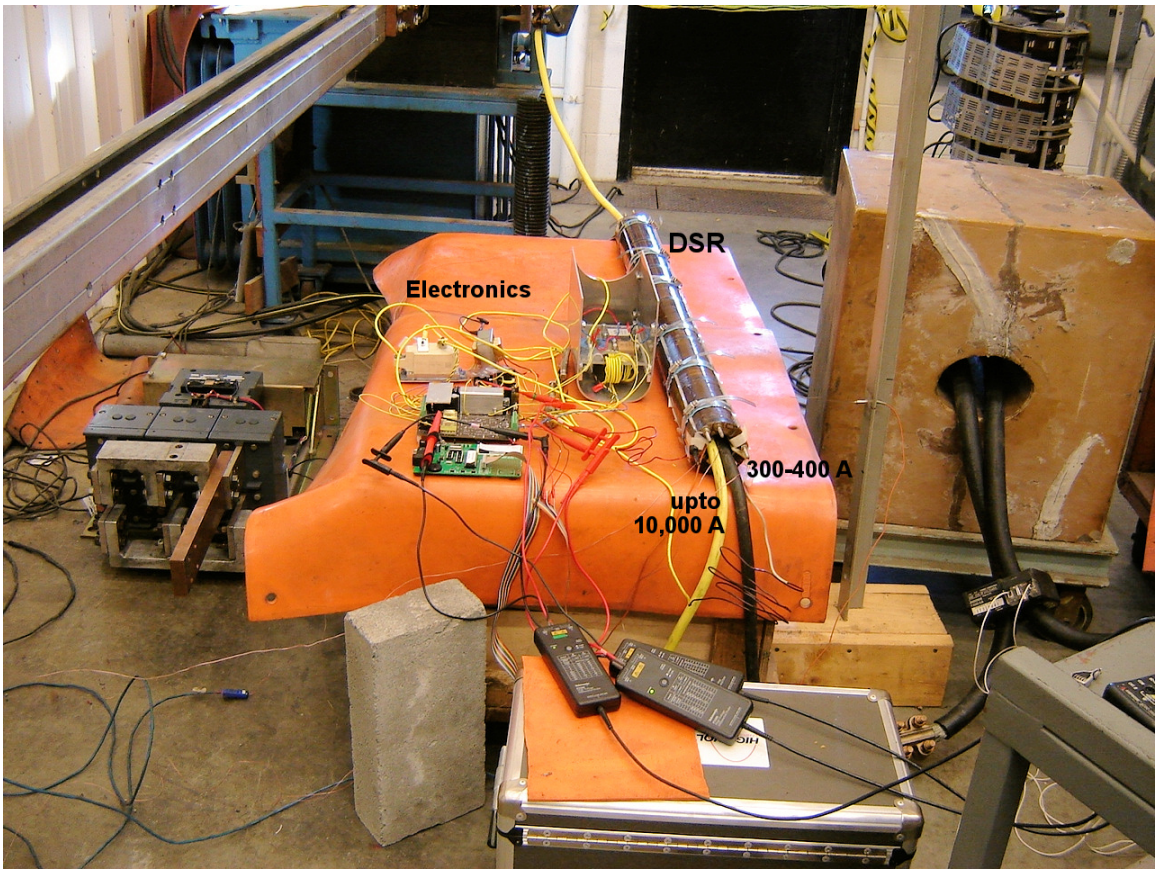

Figure 5.5 Experimental set-up for operation of DSR modules under fault currents

The thyristor pair is activated first (seen in the orange waveform) because of its fast response time (~20 µsec). It also helps the relay to make a smooth transition from the 'open' to 'close' state. The actuating signal for the relay is shown by the purple curve. It can be seen that no voltage transients/spikes are observed and the module is by-passed almost instantaneously after the inception of the fault. The relay is kept in the closed position for the next 30 cycles following the detection of fault so as to give sufficient

time for the system protection devices to clear the fault. After the elapse of this period, normal operating conditions resume and the relay is seen to revert to its original open state, with the assistance from thyristor pair to make the transition.

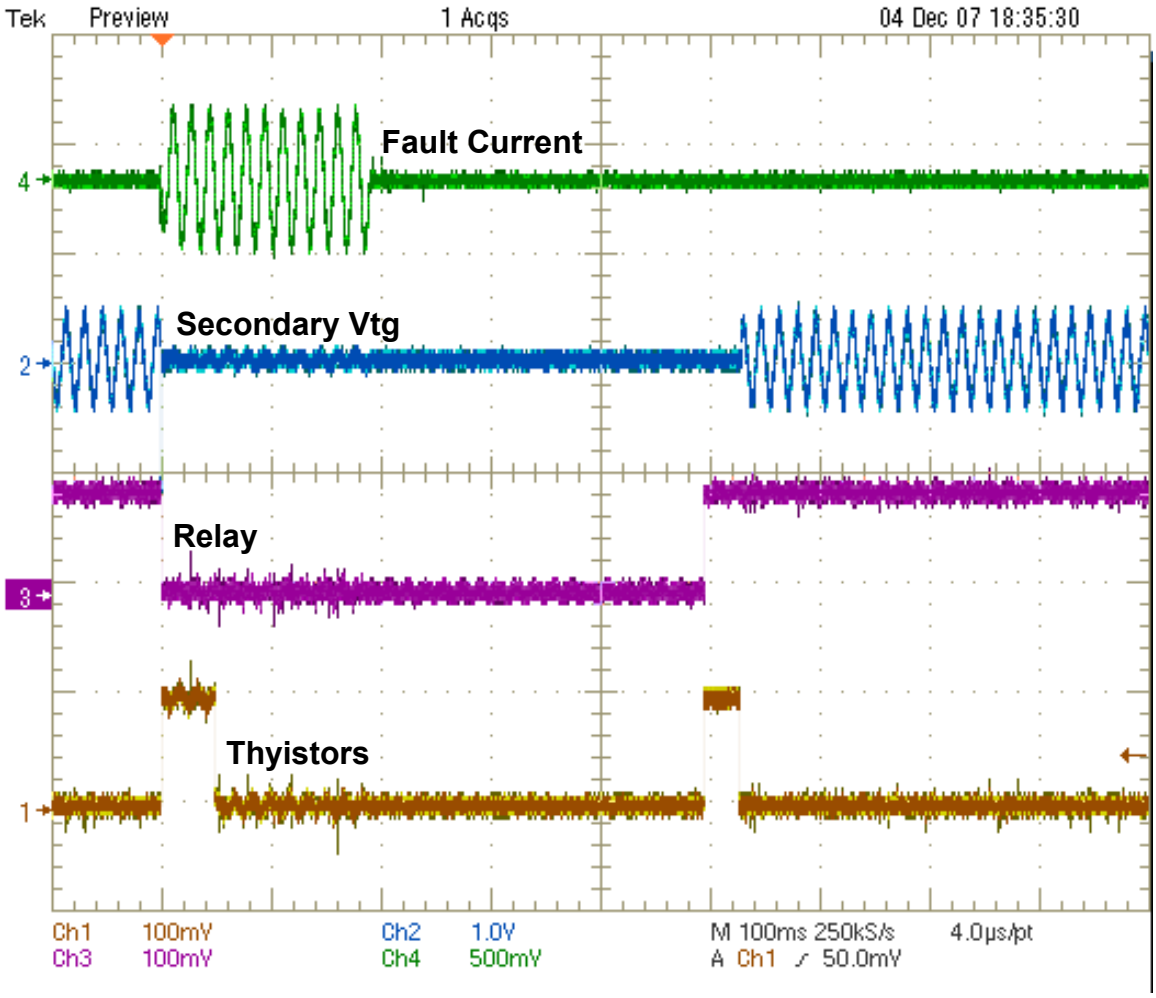

Figure 5.6 DSR module operation under a fault current of 10,000 A

Commercially used distance protection relays operate with a window of one cycle (16.67 msec) to detect a fault on the system. It can be seen that with a by-pass time of 600

μsec for DSR modules, no practical interference will be seen with the operation of protective relaying on the system.

5.4 Impact on Transient System Stability

Transient stability refers to the ability of the system to handle rapid changes in power flow associated with severe disturbances such as load changes or faults. Transient stability, among other system parameters, depends on the series line reactance. This is shown by way of an example. Consider a generator connected to an infinite bus through a reactance X_L, as shown in Figure 5.7. The power angle curve of the system in plotted in Figure 5.8 for two different values of line reactance. A decrease in the maximum power flow or the stability limit of the system is observed as the line reactance is increased from 1 pu to 1.5 pu.

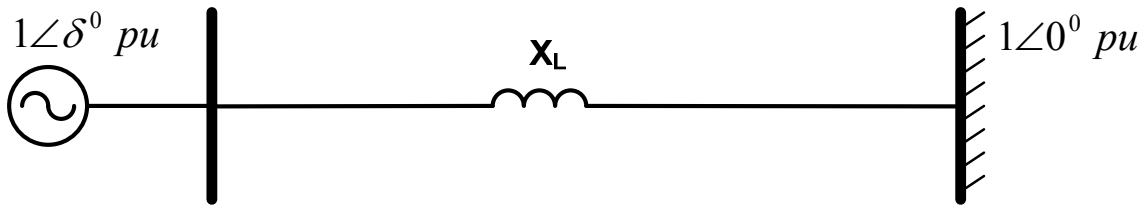

Figure 5.7 Generator connected to infinite bus

Next, assume an initial operating condition with the generator delivering active power given by '$P_{M.}$' This is shown by the horizontal line in Figure 5.9. The intersection of the power angle curves with horizontal line gives the operating points under the two scenarios. These are denoted by 'A_0' and 'B_0' respectively. When a three phase fault is

induced at the infinite bus, the trajectories are seen to follow the dotted lines. The power flow through the system is zero under the fault and would restore to 'P_M' after the fault is cleared. The system oscillates (accelerate and decelerate) around the new equilibrium points that are given by 'A_1' and 'B_1,' before settling down. The maximum swing that can be allowed without loss of synchronism is given by points 'A_2' and 'B_2' for the two scenarios. As can be seen, the system with a smaller series inductance has a bigger swing margin or a higher accelerating region, which is shown by the shaded area. The overall stability of the system thus degrades as the reactance of the line is increased.

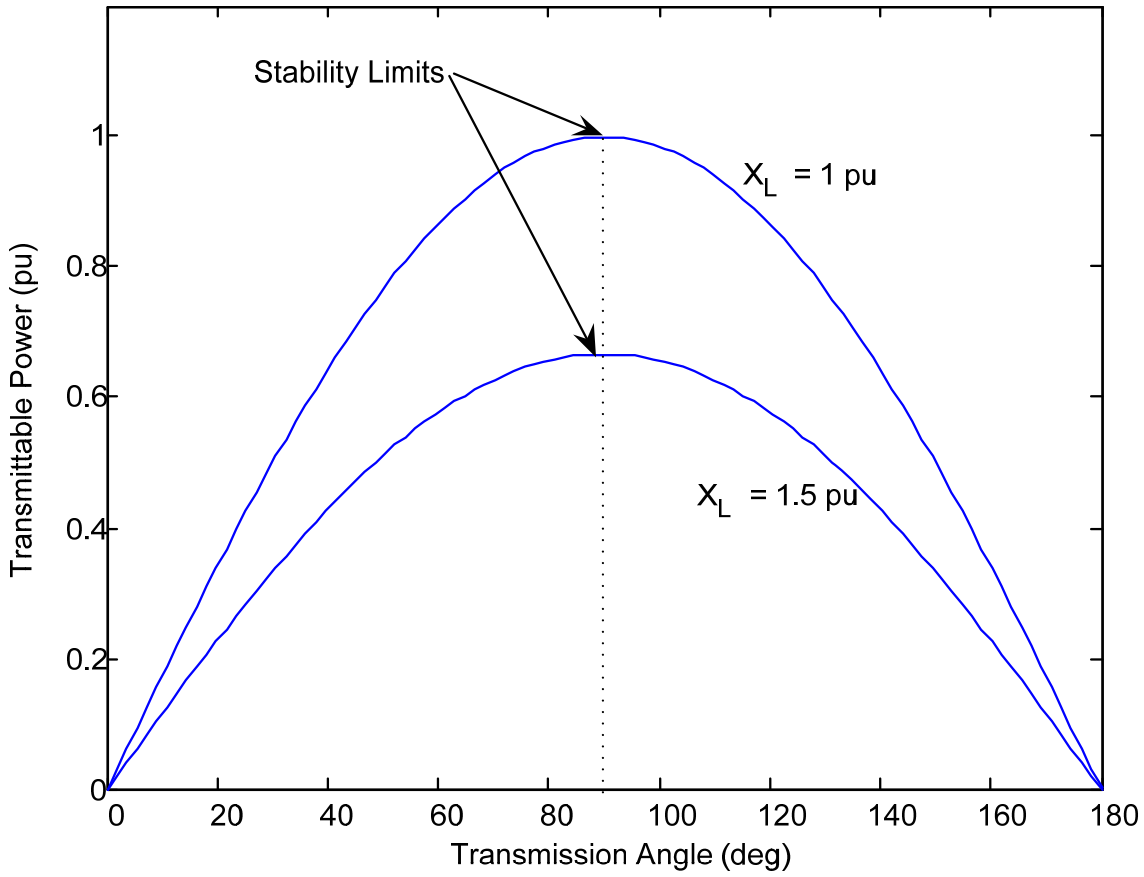

Figure 5.8 Impact on steady state stability with increase in line inductance

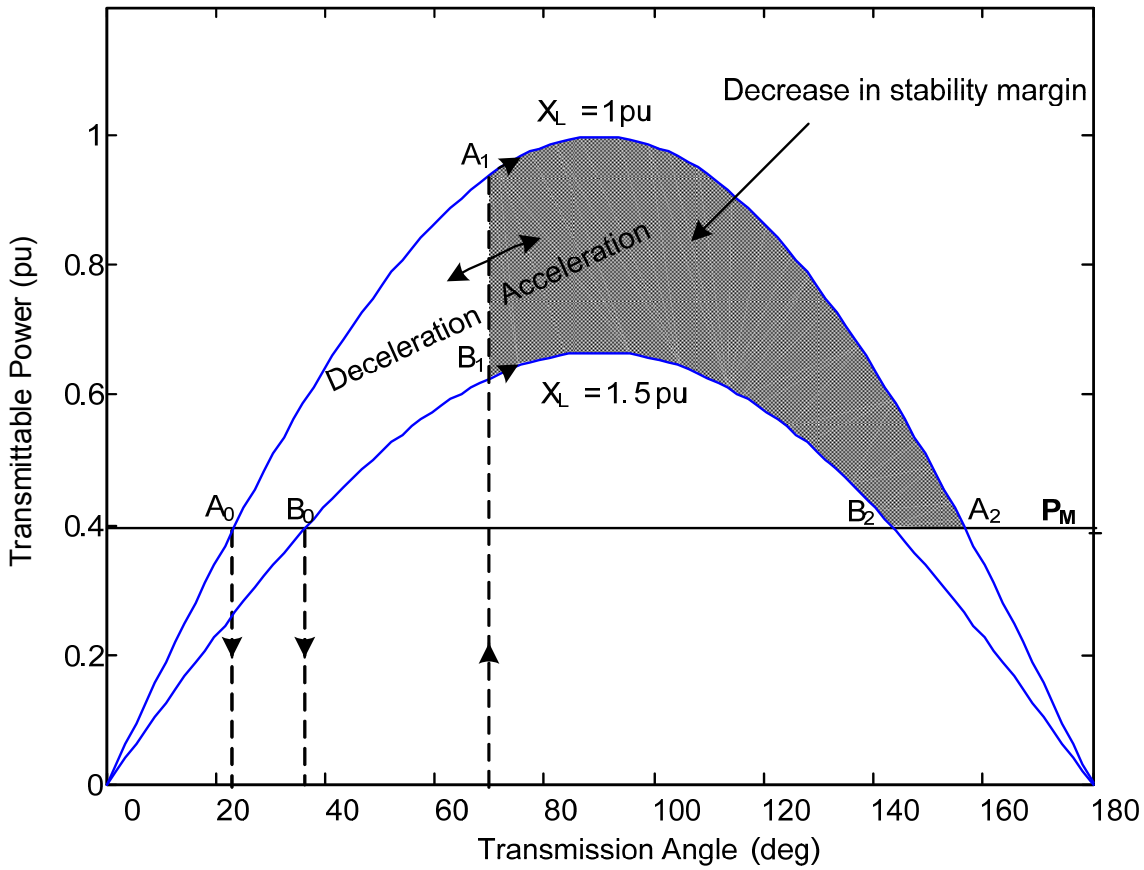

Figure 5.9 Impact on transient stability with increase in line inductance

As stated in the preceding section that DSR modules are by-passed when a fault is detected. With lower system inductance, it is intuitive to think that the system will have a higher stability margin. A simulation study was conducted on the four bus system to analyze the transient stability with the DSR modules. The modified four bus system is shown in Figure 5.10. Generator 1 was modeled as a constant voltage source to represent an infinite bus, while generator 2 was configured as a synchronous machine, controlled by an exciter and a governor. The control parameters and associated transfer functions are given in Appendix C.

DSR modules are deployed on Line 1, Line 2, and Line 5 and compensation is raised to as high as 100% of line reactance. This is an unusually higher level of injection and the purpose was to study the effect on transient stability under worst case conditions.

A three phase-to-ground fault is induced at the infinite bus, which lasts for 100 msec. Two scenarios are simulated. In the first scenario, DSR modules are allowed to remain active on each of the lines during the fault. Figure 5.11.a shows that generator active power drops to zero during the fault, but again settles down to the pre-fault value of 1900 MW. The settling time is observed to be 5 sec.

In the second scenario, DSR modules are by-passed in 600 μsec after the fault is induced on the system. The simulation results are presented in Figure 5.11.b. The settling time of the system is now seen to decrease to 4 sec. The only visible impact of DSR modules is on the settling time of the system when a three phase fault is induced. Further, under nominal injection levels of ±10% of line impedance, it can be visualized that even if DSR modules are not by-passed under fault, virtually no change will be observed.

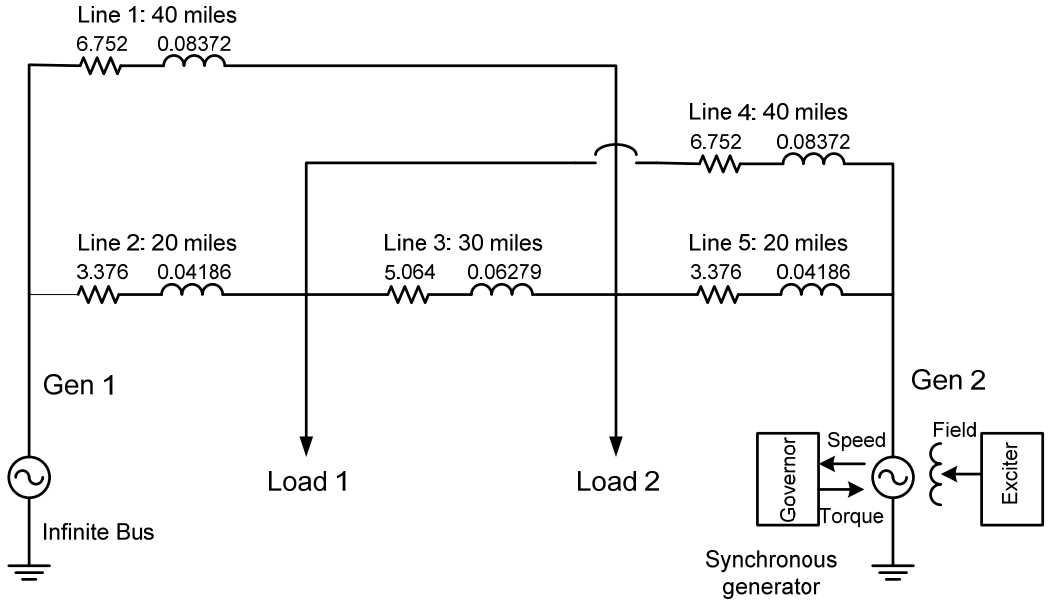

Figure 5.10 Four bus system modeled with a synchronous generator

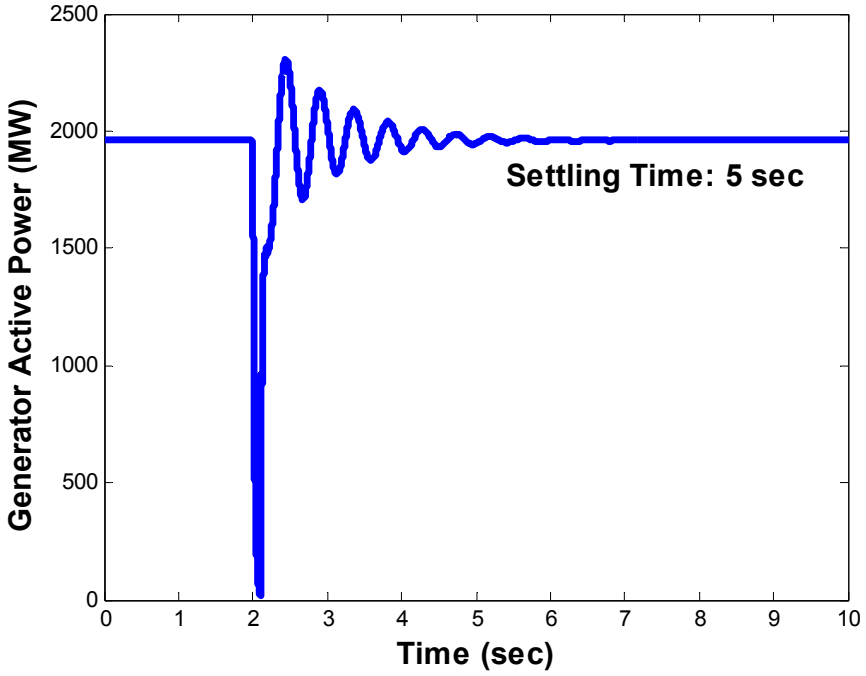

Figure 5.11.a System transient stability with DSR modules active during the fault

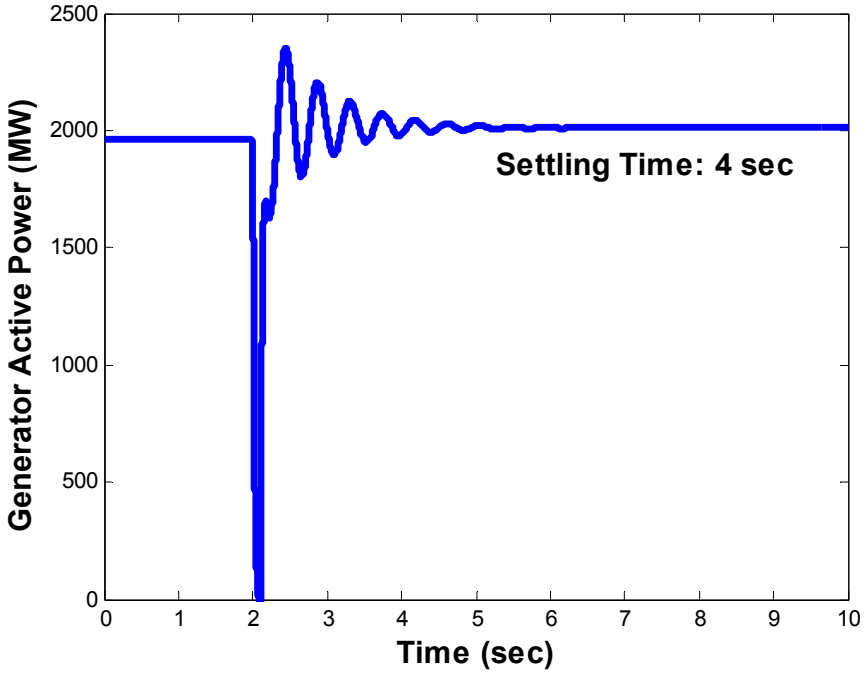

Figure 5.11.b System transient stability with DSR modules by-passed during the fault

However, there may be certain operating conditions, when DSR modules may impact the stability of the system. This can only be verified if specific operating conditions of the system are made available, under which the transient stability needs to be studied. Transient stability studies with DSR modules on utility power networks remains as a future work.

5.5 Conclusion

The introduction of a new technology on the grid always raises a myriad of questions. This chapter highlights the major issues of concern with the application of DSR technology to the power system.

Front and foremost is the issue of voltage regulation. System voltage profile is seen to droop with the use of DSR modules. However, DSR technology operates with a very high initial performance index and can realize the required gains with small series compensation. Simulation studies on the four bus and the IEEE 39 bus system indicate that most of the bus voltages are seen to remain in the acceptable voltage regulation band when the DSR modules increase the system capacity by 33%. Only three buses are seen to marginally cross the regulation band and the voltage could be easily restored with shunt VAR compensation at these locations. It is shown that load voltage regulation under series injection can easily be solved by coordinated shunt VAR injection, without any interference between the two control functions.

Distance protection relays operate on the measured series impedance of the line under fault conditions. DSR modules are programmed to by-pass quickly once a fault is detected, so that the protective relaying can operate with nominal system parameters.

Experimental results indicate a by-pass time of 600 μsec, which is seen to be much faster than the operation time of conventional power system relays. This suggests that no interference will be seen between the operation of DSR modules and the distance protection relays.

The by-pass of the DSR modules under fault conditions also indicates that there will be no degradation of the transient stability of the system. Simulation studies on the four bus system show that DSR modules only impact the settling time of the faulted system. However, studies on real power systems with specific operating conditions can provide more insight to the issue of transient stability. Exhaustive system stability studies with DSR modules remains as a future research work

The next chapter discusses the economic impact of the DSR technology on the market stakeholders. Under current regulated market conditions, it is not clear how investment opportunities for such advanced transmission technologies can be generated. The chapter puts forward some social business models and public finance mechanisms for the adoption of the DSR technology.

CHAPTER 6

ECONOMIC IMPACT OF REAL-TIME INCREMENTAL CHANGES IN LINE CAPACITY

6.1 Introduction

The objective of this chapter is to present the impact of incremental improvement in system transmission capacity on the economic position of various stakeholders. Transmission congestion restricts the ability of the market to use the available generation resources at a lower cost. Under such conditions, the consumer welfare decreases as they end up paying higher electricity costs. The low cost generators are not able to realize the additional profits they could have made by supplying power to the consumers across constrained transmission links. As a result the overall welfare of the society is seen to decrease and inefficient market equilibrium is obtained.

DSR technology offers a low cost solution to reduce system congestion. Relieving congestion through building additional transmission lines is an expensive process. This is a long term solution because of regulatory delays in the siting process and environmental impact factors. DSR technology can be used with the existing utility infrastructure and is thus ideally suited for investments in the short term as well as the long term. Further, as the congestion pattern in the network changes, possibly as a result of increased load growth in certain areas or with the building of new lines, the modules can be redeployed from one part of the network to the other to obtain maximum economic benefit. This is not possible with the conventional solution of reinforcing system capacity by laying

parallel transmission lines, which can only statically relieve congestion in one part of the network.

In a regulated market environment, increase in societal welfare forms the basis of any policy initiative. Increased societal benefits in terms of lower consumer prices and increased market efficiency can be realized from DSR technology. However, it is not clear how the investments can be initiated and who should bear the costs. This chapter attempts to understand the impact of incremental congestion relief on different market participants and suggests possible social-business models that can be used for market adoption of such advanced transmission technologies.

6.2 Historical Overview of the US Electric Power Sector

The US power sector has gone through a series of changes brought about by legislation and federal regulations over the last 100 years. In the early 1900's, large private companies controlled the US electric-power industry. They were responsible for generating 94% of the US electricity needs with the rest 6% covered by public utilities [42]. The underlying reason for the existence of such a structure was the fact that large generating plants were considered to have economies of scale. The companies were making huge profits by charging excessive electricity rates to the end consumers. These monopolistic practices were cut down with the introduction of Public Utility Holding Company Act (PUHCA) of 1935. Large electricity companies were divided into smaller public utilities and came directly under the control of federal government. The utilities were given a particular geographical area to operate and had full control over the generation, transmission, and distribution assets.

Another major step towards the restructuring of power sector came in 1978. With the passage of Public Utility Regulatory Policies Act (PURPA), the utilities were required to reduce dependence on the conventional sources of energy and increase efficiency of their power plants [43]. This led to the emergence of small non-utility power producers who were either able to produce power through alternative sources of energy or could produce power more efficiently. Their access to the market was limited and they could only sell power to the utilities.

The entry of non-utility power producers to the energy markets was made easier with the Energy Policy Act (EPACT) of 1992. The order provided non-discriminatory access to the utility transmission system at federally regulated rates. This led to the emergence of wholesale markets, wherein the non-utility power producers could sell energy to the retailers (distributing companies) or to the utilities directly.

6.3 Current Structure of the Electric Power Sector

Over the years, legislators and law makers have introduced reforms to make the power sector more competitive, with a view to introduce more choice for the customers. The three sectors of the industry, namely: generation, transmission, and distribution have been unbundled from each other. The current market-operating structure of each of these sectors is outlined below:

- Generation sector: Independent power producers are now allowed to sell electricity on the grid. The power producers (generators) can trade freely with bulk electricity buyers (distribution companies or distcoms). The wholesale price of electricity is set by the power-system operators at the price where the bulk demand equals the bulk

supply of electricity.

- Transmission sector: Utilities still continue to own the transmission lines. However, to prevent partisan practices by the utilities that own generation facilities, the operation of the transmission system has been given to independent system operators (ISOs) or regional transmission operators (RTOs). These are non-profit organizations, which create the market by accepting bids from the producers and consumers, and setting the market price taking into account physical-operating constraints of the system. Transmission fee is regulated by FERC and the state governments and is set to a price that covers the operating cost of the existing assets plus the cost of capital investment (which includes depreciation, interest, taxes, etc) [44].
- Distribution sector: This sector is regulated by state Public Utility Commissions (PUCs), who control the retail price of electricity. The retail prices are discriminated between commercial, industrial, and residential consumers.

6.4 Electricity Market Operation

As mentioned earlier, the US electric-power market is operated by the RTOs and ISOs who accept bids from producers and consumers and set the market price as the lowest price that clears the demand. Economic theory based on supply and demand functions provides the basis for understanding the market operation.

6.4.1 Demand Side

At a simplified level, the demand of electricity is almost inelastic. The variation in the price of electricity has no or minimal effect on the demanded MWs. For all practical

purposes, the demand is modeled as a fixed MW independent of the variations in electricity prices. The consumers pay the market clearing price set by the market operators.

6.4.2 Supply Side

A typical generator-supply curve looks like the one shown in Figure 6.1[1]. The marginal cost of providing additional MWs is almost flat at the fuel cost, and the offer-price primarily includes the generator start-up costs. However, once the generator hits its capacity, the marginal cost of providing an additional MW increases very sharply.

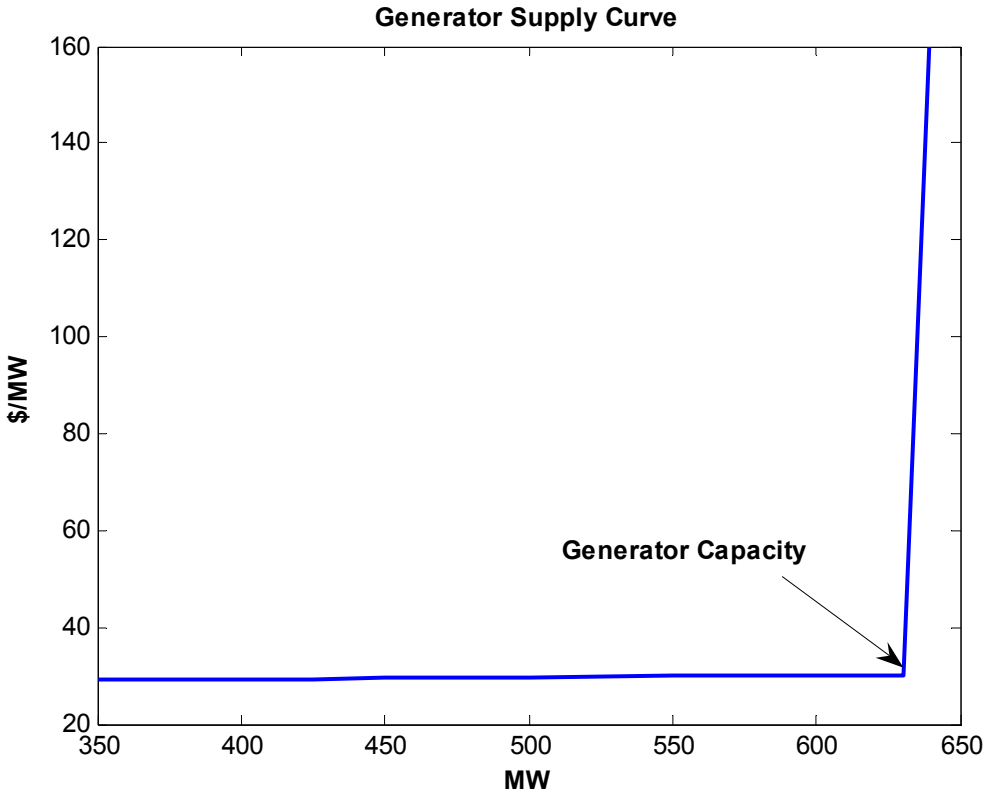

Figure 6.1 Typical generator-supply curve

[1] Courtesy PJM (Gen. code 12MG). [Online] www.pjm.com/pub/account/bids-emarket

In a multi-generator market, the aggregate market-supply curve has the shape of a staircase, as shown in Figure 6.2. The additional MWs are provided by the next out-of-merit (high cost) generator, once the low cost generator hits the capacity. GC_1 to GC_4 represents the bid-price of the last unit from the low cost generator (Gen. 1) to the high cost generator (Gen. 4). In practice, additional MWs from a generator can have increasing marginal cost associated with them. The price-offer curves from the individual generators will therefore have a small rising slope, as illustrated in Figure 6.3.

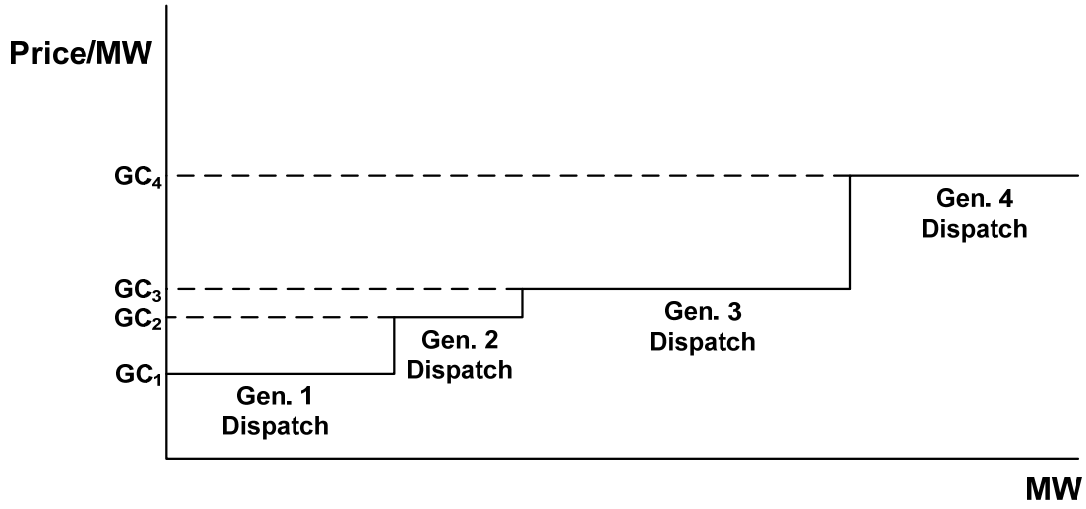

Figure 6.2 Aggregate supply curve

The aggregate market-supply curve can have a continuum of values with some discrete jumps, depending upon the individual generator-supply curves. Here we have assumed linear price-offer curves of the generators. However, individual generator price-offer curves can assume any shape and correspondingly it is possible for aggregate market-supply curve to have any shape. One approach that allows quantitative analysis is

to model the aggregate market-supply curve through a polynomial curve fitting of order N, if enough data points are available.

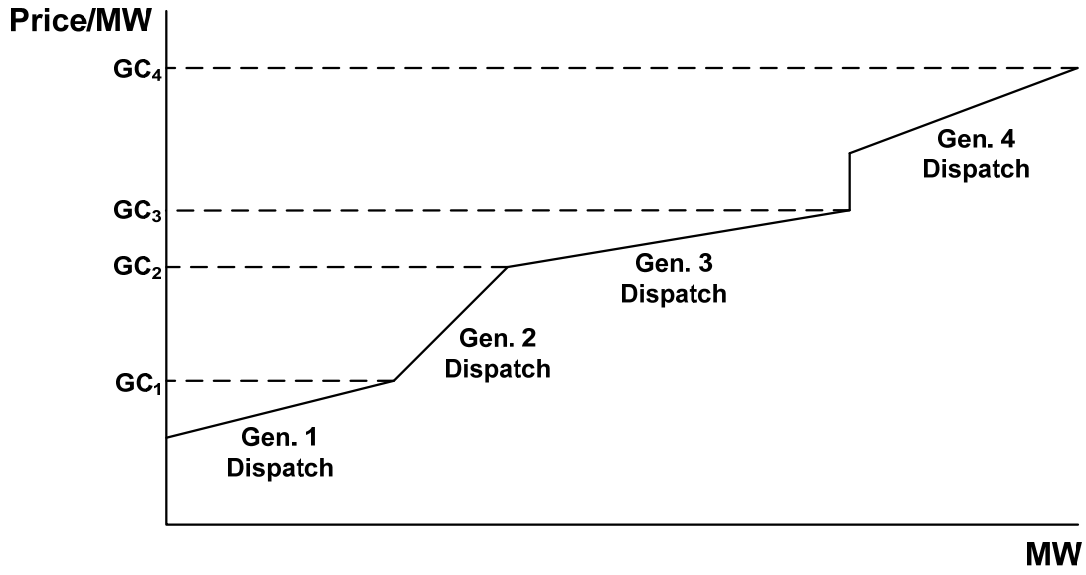

Figure 6.3 Aggregate supply curve with rising marginal cost

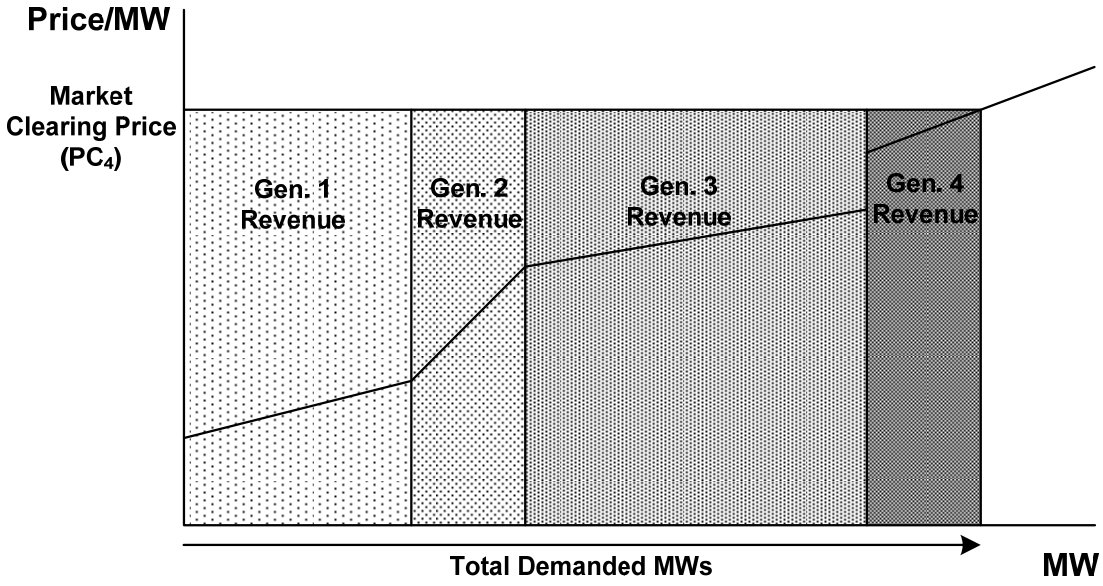

Figure 6.4 Market clearing price and generator revenue

The market clearing price is set at the lowest price where supply equals demand. All the generators receive the same price for all units they sell. In Figure 6.4, the market clearing price is set at the offer-price of the last unit (PC_4) bid by Gen. 4 that clears the market. The revenues of the different generators are also highlighted in the figure.

6.5 Electricity Pricing Methodology

In the previous section, it was said that at market equilibrium only one price of electricity exists. All the producers get the same price for their supply of electricity and all the consumers have to pay the same price for their demand of electricity, irrespective of their geographical location. This method of electricity pricing is commonly referred to as Uniform Marginal Pricing [45]. This pricing approach works fine if there is ample transmission and generation capacity, implying that a single low-cost generator is able to satisfy the total demanded MWs. However, under practical conditions, with constraints on the capacity of transmission lines, high cost generators have to be dispatched to meet the requirements of the loads locally. Charging a uniform electricity price to all the consumers turns out to be economically inefficient, as the consumers in the low-cost region end up paying a higher price. With this thought in mind, a new pricing method was coined. This method assigns a price to each node on the grid, which is representative of the generation costs in that region, thus allowing the consumers to avail the electricity at the true energy price. The electricity price at each node is referred to as Locational Marginal Price (LMP).

6.5.1 Locational Marginal Pricing (LMP)

LMP is defined as the marginal cost of supplying the next increment of electric energy at a specific bus, taking into account the fuel price and physical aspects of the transmission system that include line losses and congestion [46]-[47]. Every node on the grid has a LMP under equilibrium, given by equation (6.1)

$$LMP = P_r + P_{losses} + P_{congestion} \tag{6.1}$$

Here, P_r is the marginal energy price in \$/MWHr, P_{losses} is the marginal cost of losses with respect to the reference bus, and $P_{congestion}$ is the marginal cost of congestion with respect to the reference bus.

The marginal cost of losses is calculated using equation (6.2) and the marginal cost of congestion is calculated using equation (6.3) [48]. These prices are calculated with respect to a reference bus in the system, which is usually the bus with the lowest marginal price of energy. The loss and congestion costs at a reference bus are zero, by definition.

$$P_{losses} - \frac{\partial L}{\partial P_i} \times P_{ref} \tag{6.2}$$

Here, $\partial L/\partial P_i$ measures the change in total system losses with injection of 1 MW of power at node 'i' and P_{ref} is the marginal price of energy at the reference bus

$$P_{congestion} = -\frac{\partial G_{ik}}{\partial P_i} \times P_{ref} \tag{6.3}$$

Here, G_{ik} measures the increase in the value of constraint 'k' with injection of 1 MW of power at node 'i'.

Without line losses and transmission capacity constraint, all nodes will have the same price, which is the marginal price of energy (assuming the fuel and plant start-up costs are equal). LMP of a node will be higher than the reference bus if the dispatch of energy from that location has to account for the line losses. An increase in the LMP will also be observed if the dispatch of energy constraints the network.

When transmission capacity is constrained, out-of-merit generator must be dispatched to meet the demand locally. The LMP of the region increases and extra cost is incurred by the consumers in that region. Difference in the LMP in the two regions is just equal to the marginal value of transmitting an additional unit through the transmission link and is commonly referred to as congestion cost [49]. Equation (6.4) gives the congestion costs as the difference between the LMPs in the two regions times the transmitted MWs.

$$CONGESTION\ COST = \left(LMP_B - LMP_A\right) T_C \tag{6.4}$$

Here LMP_A is the locational marginal price in a low cost region (region A), LMP_B is the locational marginal price in a high cost region (region B), and T_C is the transmission capacity.

Under congestion, the available resources are not fully utilized and the market equilibrium is inefficient. The low cost generators with spare capacity are not able to transfer the MWs across the congested link. Consumers on the other hand, have to pay higher electricity charge to the out-of-merit generator. It is thus believed that with congestion mitigation, the overall societal welfare and market operations can be improved.

6.6 Cost of Transmission Congestion

Transmission congestion puts a hard constraint on the ability of a low cost generator to access the market across the congested links. The residual demand is then met through dispatch of the next out-of-merit generator. As a result, the electricity price is seen to increase and a price differential develops across the congested link. This is illustrated with a two bus example shown in Figure 6.5.

Here Gen. A is a low cost generator and Gen B is the out-of-merit generator. The demand in region A is given by X_A MWs and that in region B is given by X_B MWs. Gen. A supplies the load in region A as well as in region B, until the transmission capacity (T_C) is reached. The additional MWs (X_B - T_C) are then supplied by Gen. B. The transmission system is modeled with two lines, $Line_1$ and $Line_2$. $Line_1$ represents the first line to reach capacity that prevents transmission of additional power through the corridor and $Line_2$ represents other parallel power flow paths that are not, and cannot be fully utilized.

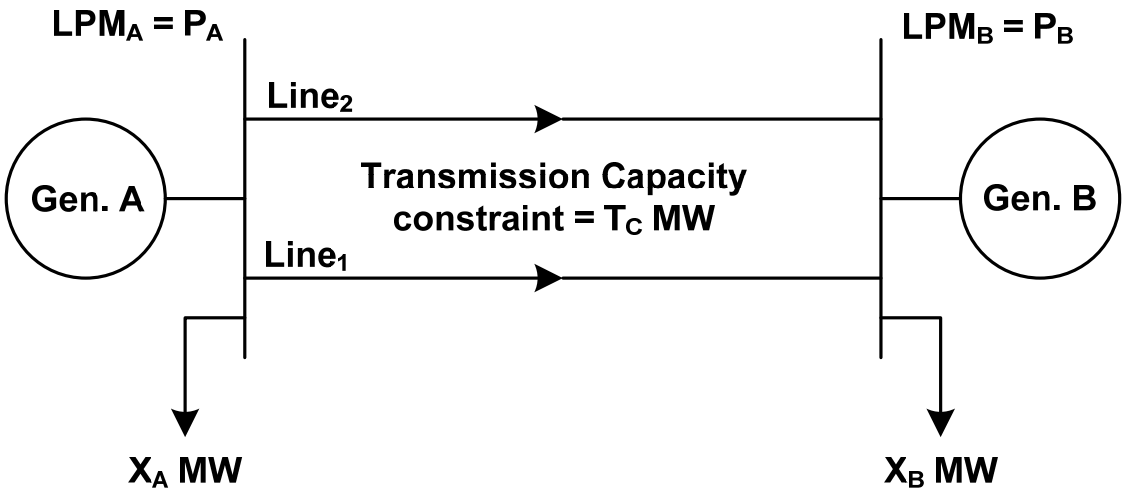

Figure 6.5 Two bus example to illustrate market operation under congestion

The LMP in regions in A and B are given by LMP_A and LMP_B respectively. The consumers in region A pay a price equal to LMP_A for their demand of X_A MWs, while consumers in region B pay LMP_B for their demand of X_B MWs. It must be noted that consumers in region B pay a higher cost for their total demand even though a part of the demanded (T_C) MWs are supplied at a lower cost. Under an unconstrained system, the electricity price paid by consumers in region B would be lower and equal to LMP_A. The market equilibrium under congestion is described by Figure 6.6.

The previous discussion highlights that a congested system decreases the welfare of the society. The consumers have to pay more and the revenue of the low cost generators gets limited. The economics clearly demands an increase in system capacity to move towards an efficient equilibrium.

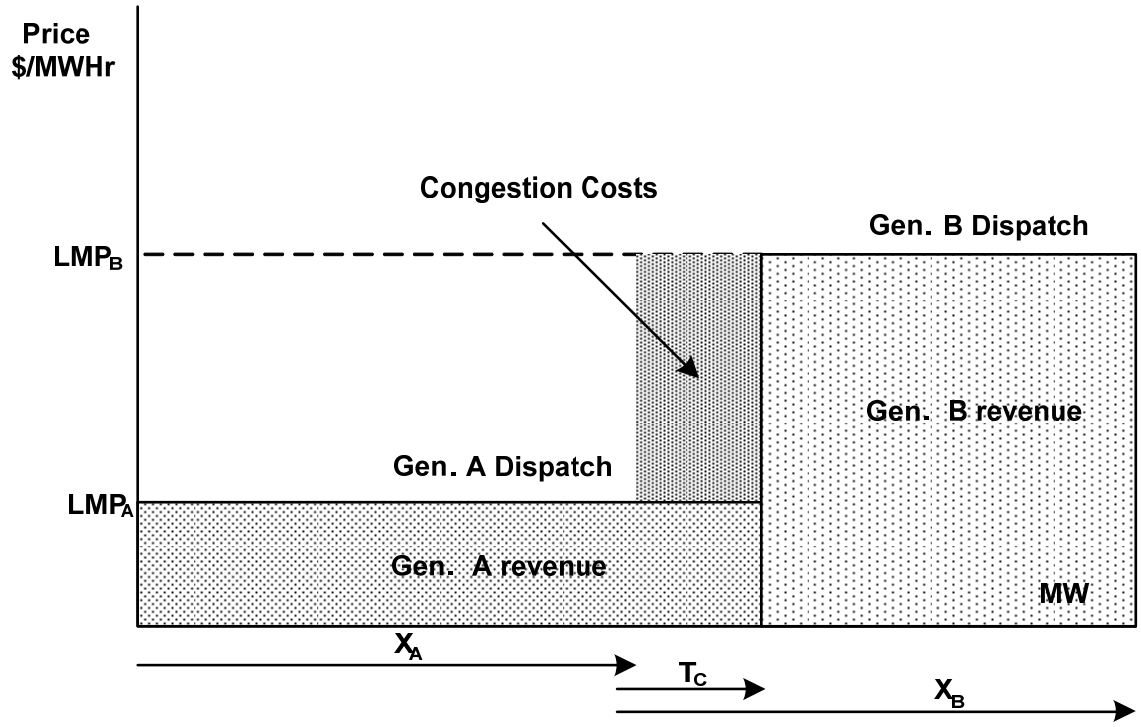

Figure 6.6 Market equilibrium under congestion

Under the conditions of a free market, it can be very easily seen that transmission investments, besides sitting issues, are driven by the LMP signals in different regions. A difference in the LMPs would imply that a low cost generator can capture the market across the congested link and make higher profits by selling electricity at a price just below that of a high cost generator in that region. A part of these profits can be used to finance transmission investments to increase the capacity of the congested link. This becomes clear from the following example.

Table 6.1 assigns numerical quantities to the two bus system of Figure 6.6. The low cost generator (Gen. A) has a capacity of 500 MWs and the total system demand is 300 MWs (150 MWs in each of the regions). The transmission capacity constraint limits

the dispatch from Gen. A into region B to 100 MWs. The residual demand of 50 MWs is met by the dispatch of the high cost generator (Gen. B). The LMPs in the two regions under such conditions are 25 $/MW and 50$/MW respectively.

Next, if we assume that the transmission capacity of the link is increased by 50 MWs, then Gen. A can satisfy all of the demand in region B at a price anywhere between 25 $/MW to 49 $/MW. A part of the increased profits ($11100-$6250 = $4850) can be used to invest in transmission upgrades to improve the capacity of the congested link. It must also be noted that under such conditions consumers in the high cost region (region B) benefit from lower energy prices (49 $/MW compared with 50 $/MW), and the consumer welfare increases by $150 ($7500-$7350).

Table 6.1 Conditions before and after congestion relief in an open market

	With Congestion	**With Complete Congestion Relief**
LMP_A ($/MW)	25	25
LMP_B ($/MW)	50	49
X_A (MW)	150	150
X_B (MW)	150	150
T_C (MW)	100	150
Consumers costs in region A ($)	3750	3750
Consumers costs in region B ($)	7500	7350
Gen. A revenue ($)	6250	11100
Gen, B revenue ($)	2500	0
Revenue for transmission Inv. ($)	0	4850

6.7 Economic Impact of Incremental Improvements in Capacity

Market operation is complex, and does not easily provide a basis for understanding how transmission investments for congestion mitigation could be supported. Under regulated market conditions, increase in public welfare should drive all policy initiatives. It thus seems desirable to make a case for the adoption of DSR technology on the basis of improvement in societal welfare. In this section, change in the welfare of consumers and producers, before and after a transmission capacity increase is compared to analyze the economic impact of congestion relief. With reference to the two bus system of Figure 6.6, the share of different market participants under transmission congestion is depicted in Table 6.2.

Table 6.2 Baseline costs for different participants under congestion

Consumer costs in region A	$LMP_A X_A$
Consumer costs in region B	$LMP_B XB$
Total consumer costs	$LMP_A X_A + LMP_B X_B$
Gen. A revenue	$LMP_A (X_A+T_C)$
Gen. B revenue	$LMP_B (X_B-T_C)$
Total Producer revenue	$(LMP_A X_A + LMP_B X_B) - (LMP_B - LMP_A) T_C$
Congestion cost	$(LMP_B-LMP_A) T_C$

Next, incremental improvement of Δx in the transmission capacity is assumed. Market situation with transmission capacity improvement is shown in Figure 6.7 and the change in the welfare of the participants is shown in Table 6.3. It can be seen that under the LMP model, the congestion costs increase with incremental increase in congestion relief. These congestion revenues are collected by RTOs/ISOs and are allocated back to

the holders of FTRs (financial transmission rights), if any, while the excess revenues are disbursed to the consumers according to some formula, which varies from RTO to RTO. The revenue of the producer increases in the low cost region, while it decreases in the high cost region; with the total producer welfare showing a decline. The consumers are made better off by the transfer of welfare from the generators; in particular from the out-of-merit generator.

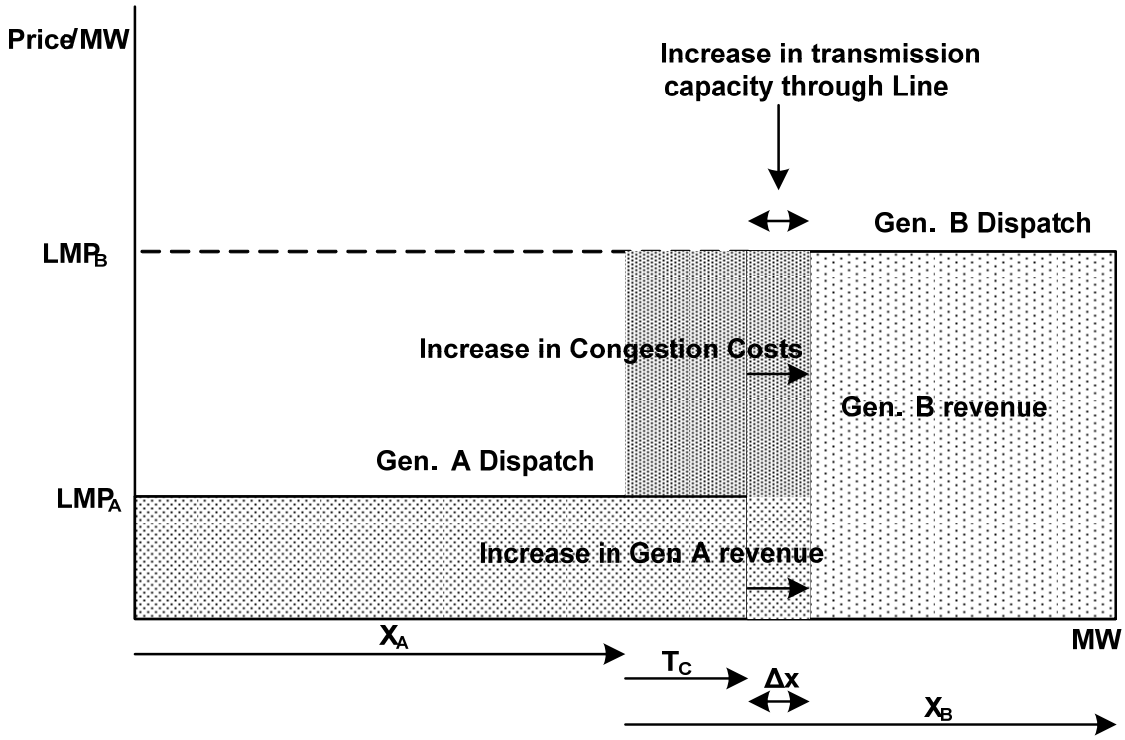

Figure 6.7 Market situation with incremental improvement in transmission capacity

Transmission rights protect the market participants against volatility of electricity prices under congestion. A market participant can hedge against price variations, by reserving a desired capacity of electricity at a predefined price. It must be noted that the

economic value of the transmission right is non-zero only under congestion; when it is equal to the transmitted MWs between the source and the sink times the LMP difference between them. To obtain a transmission right, bids are submitted to the system operators. A feasibility test is run to confirm that all the granted rights can be simultaneously honored under any system condition [50]. This essentially makes sure that the system is always revenue adequate and the collected congestion charges can be used towards payments of transmission rights.

Table 6.3 Change in societal welfare after transmission capacity improvement

Participants	**Change in Welfare**
Consumers	0
Producers	$-(LMP_B - LMP_A)\,\Delta x$
Congestion Costs	$(LMP_B - LMP_A)\,\Delta x$

Flat generator dispatch curves imply zero marginal cost of production. To realistically portray the market situation and to make the discussion more general, Gen. A is modeled with a linear dispatch curve and Gen. B is modeled with a quadratic dispatch curve, as shown in Figure 6.8. The associated values for the dispatch curves as well as for the system, as illustrated by Table 6.4, were chosen to make the conditions as close as possible to a practical scenario. A reference to these values can be obtained from the report on congestion costs by Eto, et al. [49].

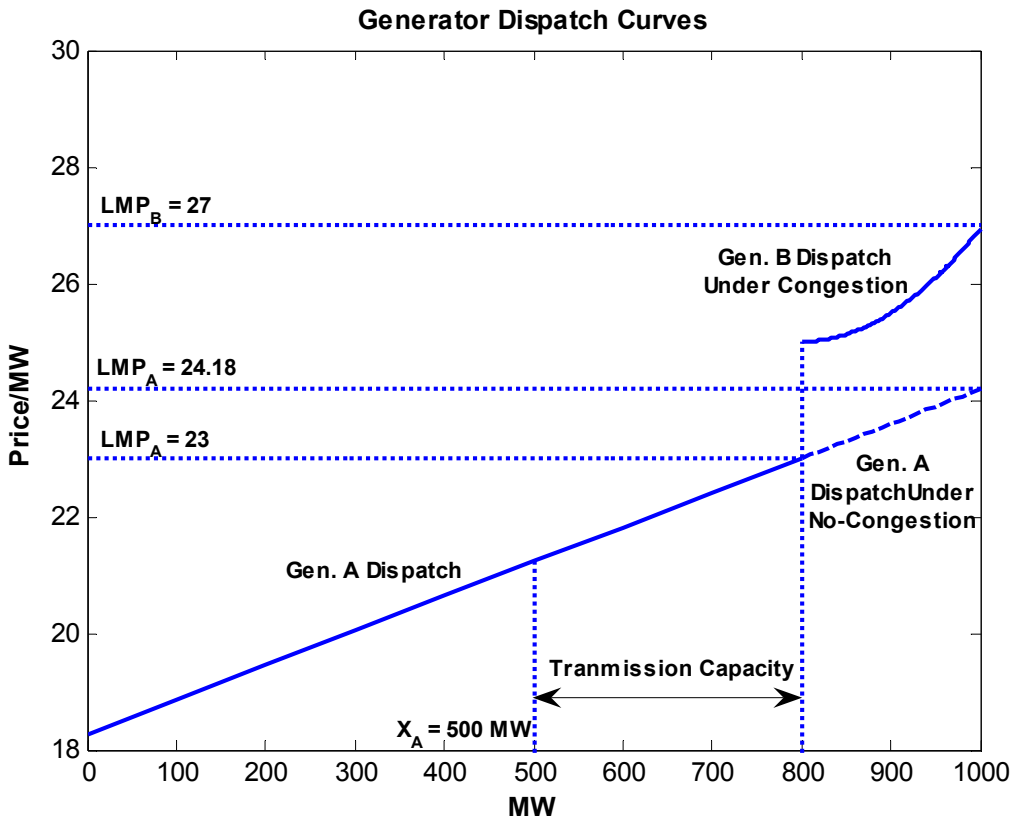

Figure 6.8 Modeling generator dispatch curves for quantitative analysis

Table 6.4 Operating conditions for the two bus example

Load A (X_A)	500 MW
Load B (X_B)	500 MW
Transmission Capacity (T_C)	300 MW
LMP_A	23 \$/MW
LMP_B	27 \$/MW

Table 6.5 shows the impact on the welfare of market participants with incremental increase in transmission capacity. Congestion mitigation has the most favorable impact on the low-cost generator, i.e. Gen. A, and has the most negative impact on Gen. B. The

total consumer welfare is seen to increase, but at the expense of the consumer welfare in the low cost region.

Table 6.5 Change societal welfare with incremental increase in transmission capacity

Change in Producer Revenue			
Δx (MW)	ΔRev. (Gen. A) ($)	ΔRev. (Gen. B) ($)	Net Change
5	138.7	-167.2	-28.5
10	277.8	-313.4	-35.6
50	1400.8	-1486.9	-86.1
Change in Consumer Costs			
Δx (MW)	ΔCosts (Cons. A) ($)	ΔCosts (Cons. B) ($)	Net Change
5	14.8	-82.7	-67.9
10	29.5	-114.3	-84.8
50	147.5	-456.4	-308.9

The increase in dispatch from the low cost generator (Gen. A) reduces the electricity costs in region B. However, an increasing marginal cost associated with the dispatch of Gen. A increases the electricity price in region A. This suggests that under current regulations, consumers may not provide a uniform and strong voice in driving policy makers to promote investments for congestion mitigation. However, the policy decisions are always made by looking at the aggregate welfare of the society. In this case, the cumulative consumer welfare shows an increase as well as the welfare of the low cost

generator. Under this simplified model, the decrease in the welfare of the high cost generator suggests possible elimination of this generator in the long run.

6.8 Cost of Congestion Relief with DSR

In this section, the cost of congestion relief with DSR is compared with the conventional method of congestion mitigation through building of additional transmission lines. The study can be extended further to include other available power flow controllers, outlined in Table 6.6 [51]. However, in this section we would limit the comparison between DSR technology and building of parallel transmission lines. The investment cost for laying transmission lines is assumed to be $500,000 per mile, while the estimated cost of DSR technology is conservatively assumed as $1000 per module (also $100/kVA), with a redeployment cost of 30%.

. The IEEE 39 Bus system is used as a representative case study for comparing the costs of the two techniques. The load growth in the system is assumed to be uniform and it is observed that under such conditions the original transfer capacity of the system is limited to 1904 MW. As the load grows, the network demands transmission upgrades at regular intervals to relieve congestion. Figure 6.9 compares the investment costs of the two techniques for relieving congestion. The investment cost curve for laying additional transmission lines can be seen to have discrete jumps at points when a particular line sees congestion. The height of each step is equal to the cost of a line. On the other hand, the investment cost curve of DSR technology shows a continuous rise, with a very small slope in the beginning, implying high initial returns. The cost of the DSR technology can be obtained by multiplying the total injection with the cost per unit of injection. Here

injection refers to the reactive VARs, and is given by equation (6.5). The cost per unit of injection was defined earlier as $100/KVA.

Table 6.6 Cost of available solutions for congestion mitigation

Solution	**Cost**	**Limitations**
HVDC Transmission	$500,000/mile, Converter Stations $250M	• Cannot provide full control over the power flowing in a particular AC line • ROW and siting issues
Phase Shifting Transformers	$100/KVA	• Large investment • Slow and manual control • Poor dynamic response
Shunt FACTS	$60-$120/KVAR	• Weak influence on active power flow control • Bulky solution
Series FACTS	$60-$160/KVAR	• High cost • Difficult fault management • Bulky solution

$$Injected\ VARs = I_{Line}^{\ 2} \times (2\pi f) \times X_{Module} \times n \tag{6.5}$$

Here I_{Line} refers to the line current, f is the nominal frequency of 60 Hz, X_{module} is the inductance of each module, and n is the total number of modules on the line.

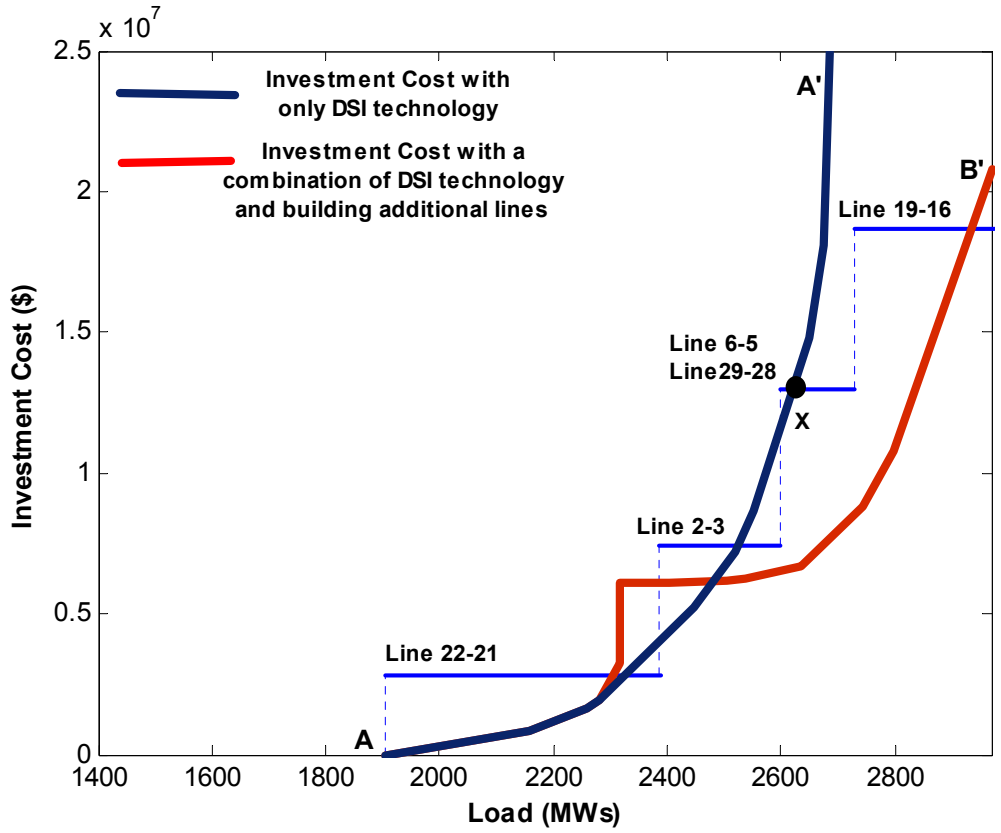

Figure 6.9 Comparison of transmission investment costs for congestion relief

DSR modules offer a very high performance index initially, capturing the capacity of the under-utilized lines at a lower cost. For example, the DSR technology can realize 7.4 MWs of increase in capacity with an investment of $740,000. On the other hand, a cost of $2,800,000 has to be incurred to build an additional line when the network sees congestion for the first time. With the DSR technology, the transfer capacity of the system can be increased by as much as 700 MW before it becomes unattractive (point X on the curve A-A'), with the exception of some instances when the investment cost curve of DSR lies above the cost curve of building additional transmission lines.

This also suggests that a combination of these technologies can prove to be more cost effective. DSR modules can be deployed on congested lines initially to capture the gains from a high performance index. As the cost of deploying additional modules becomes more than cost of laying additional lines, transmission lines can be built and DSR modules can be redeployed on other lines to again capture the gains at a higher performance index. This is shown by the red line (curve A-B') in Figure 6.9. The DSR modules are initially deployed on the congested line (Line22_21). A new line is built at a system load of 2300 MW, when for the first time the cost of deploying DSR modules is seen to be more than cost of laying a line. The redeployment cost of DSR modules is assumed to be 1/3'rd the original cost of the module. With this strategy, the aggregate investment cost curve (curve A-B') is seen to lie well below the individual cost curve of the DSR technology as well as that of building additional lines.

DSR technology turns out to be even more attractive under contingency conditions. Planning for contingency requires system operators to make reservation for spare system capacity. Under such conditions, the need for transmission upgrades may occur earlier than under nominal operating conditions. As an example, Line19_16 was taken out to realize a (N-1) contingency condition. This was the worst case contingency condition, and it limits the transfer capacity of the network to 1469 MW. DSR technology now provides an attractive investment for the first 871 MW of load growth. A performance index of 22 is observed initially, suggesting even higher returns in this case. If a line is again built at a network load of 2300 MW, the performance index of DSR modules again increases, providing improvement in transmission capacity at a lower cost. This is shown by the red curve in Figure 6.10.

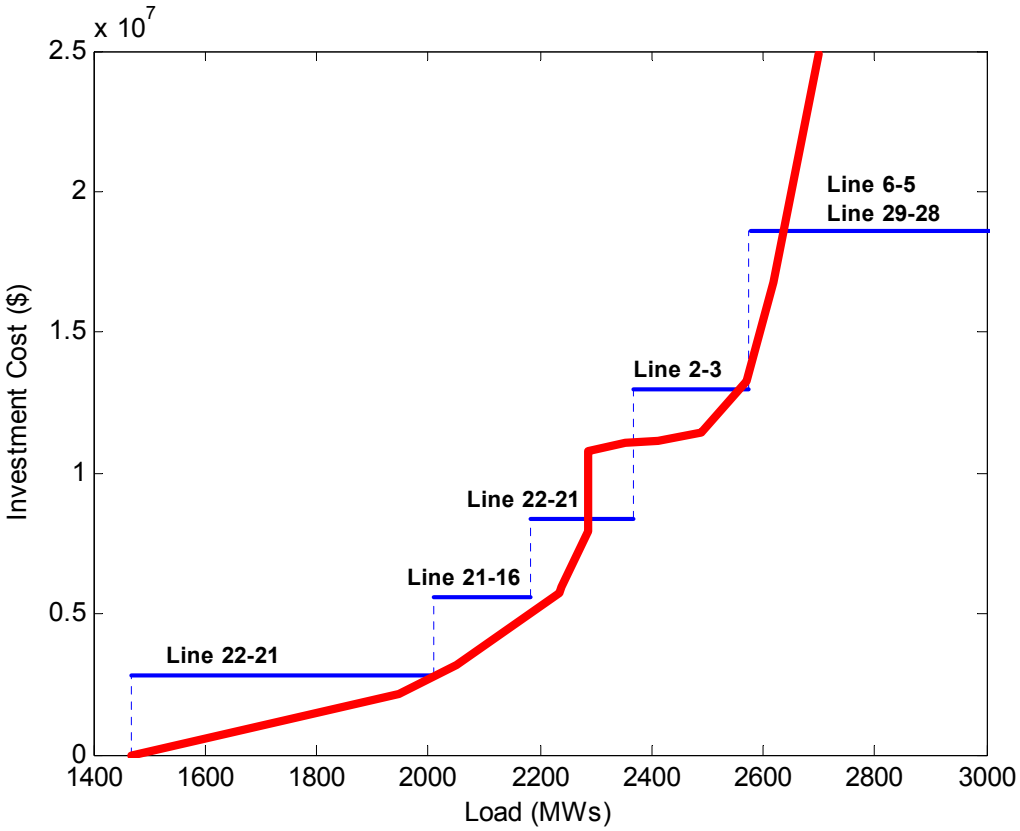

Figure 6.10 Investment cost curve under contingency condition

The model presented above does not capture the time value of money. It is assumed that a transmission line can be build with zero lead time, where in fact it takes about 10-12 years for a project to get approved. The opportunity value of money invested should be reflected in the total cost to give a true economic analysis. So for the sake of argument, if we assume an annual interest rate of 10%, the total cost of laying a transmission line should be $550,000 per mile instead of $500,000 per mile. The effect of this on the investments cost graphs will be to increase the height of each of the steps proportionally; thus making the investment cost curve of DSR technology even more attractive.

DSR technology is thus seen to have significant impact on reducing the cost of transmission investments in the short run as well as the long run. The significant results from the above discussion can be summarized as below:

- DSR technology provides incremental investment opportunities, compared with conventional solution of building additional, which requires a fixed lump sum investment.
- A very high initial performance index suggests the capability to realize system wide benefits at a lower initial cost
- Provision for redeployment of the modules allows dynamic congestion management.
- DSR technology can be combined with other solutions of congestion mitigation to provide a slew of investment opportunities, as the operating conditions or the topology of the network changes.

6.9 Market Challenges

The restructuring of the power sector was started with a view to improve the operational efficiency of the market. Deregulation of generation has been the first step towards making the power sector more competitive. Free market economics governs the operation of generators to produce electricity at cheaper and competitive rates. However, the lower cost of electricity can only be passed successfully to the end consumers if sufficient transmission and distribution capacity is made available. The current electricity-market structure is in a transitory phase, with strict regulations in the transmission and distribution sector. The problems and issues presented in the succeeding sections highlight the difficulty in creating a marker for a new transmission and

distribution technology that can have significant impact on improving grid-capacity and reliability.

6.9.1 Reliability Drives Investments

The transmission and distribution sector is heavily regulated with the transmission owners receiving a fixed tariff for their services. Any investment activity in these sectors is only directed towards securing a reliable operation of the system. The market has been averse to create investment opportunities by synergistically relating economic and reliability benefits.

Under current market operating conditions it is difficult to justify T&D investments due to congestion. On the other hand, a reliability constraint makes it easier to get the PUC's approval for the proposed investments. Public policies are required that can support finance mechanisms to induce economic based investment activity.

6.9.2 Decreased Economic Interaction between Sectors

A vertically integrated utility, owning and controlling generation, transmission, and distribution services would come up with a unified investment plan to maximize its profits. If fuel costs are cheaper in one region, it would be in the interest of such an organization to set up a generating plant at that place to produce electricity at lower cost. Similarly, if fuel costs are higher, the utility might benefit by building additional lines into that region from a remote generating facility. With the unbundling of generation from transmission and distribution, the internalization of this investment process is completely lost. The economic signals to induce investment activity can no longer be

exchanged between the different sectors. Moreover, the current market rules and strict regulations on transmission fees and pricing do not support independent investment activity.

6.10 Initiatives to Improve T&D Infrastructure

A study conducted by DOE estimates the cost of congestion because of a single constraint in California region to be around $222 million for a period of 16 months, prior to December 2000 [1]. Transmission congestion and insufficient capacity is detrimental for a reliable operation of the grid. The blackout of August 2003, which resulted in a loss of $7-$10 billion dollars [52], is reminiscent of the fact that we need to strengthen the power-transmission structure. Various policies have been formulated and studies have been conducted to emphasize the importance of strengthening the existing transmission and distribution network.

6.10.1 Energy Policy Act of 2005

The Energy Policy Act of 2005 emphasizes the modernization of existing transmission structure to reduce transmission constraints and relieve congestion [53]. The act specifically encourages the development of advanced transmission technologies that can improve the capacity, efficiency, or reliability of the existing transmission structure. Examples of advanced transmission technologies, as outlined by the act, include flexible AC transmission system, superconducting cables, and optimized line configurations.

The act further suggests the promotion of performance based transmission-rate treatment. Performance based regulations can include rewards based on increasing

market efficiency, creating timely investments for enhancing T&D infrastructure, and ensuring greater system reliability. The act calls for establishing a rule that will "promote capital investment in the enlargement, improvement, maintenance, and operation of all facilities for the transmission of electric energy in interstate commerce." The provision of a return on the equity that attracts new investments is also included in the act.

6.10.2 National Transmission Grid Study (Department of Energy)

The national transmission-grid study conducted by the Department of Energy recommends the congress to direct appropriate federal agencies to take necessary actions to remove transmission constraints. The study suggests the incorporation of operational reliability with economic efficiency. It proposes the use of advanced pricing methods to include information about transmission congestion, so that economic signals for new transmission projects can be generated. It also promotes for higher rates of return to foster transmission investments and for reduction in regulatory uncertainty. It further underlines the importance of advanced transmission technologies for enhancing reliability and for reducing the costs to customers.

6.10.3 Energy Independence and Security Act of 2007

This act envisages the creation of a smart grid, with emphasis on grid sensing, communications, and power flow control to improve system performance and reliability [54]. The act authorizes $100,000,000 for each of the fiscal years 2008 through 2012, for such demonstration projects.

6.11 Business Case for DSR Technology

DSR technology offers significant economic benefits in terms of improved market efficiency. These can be listed as below:

- Decrease in consumer costs by allowing the dispatch from the low cost generator
- Increase in market competition by making the most economical generator as the dominant market player
- Savings in cost and money from the regulatory delays in building of additional transmission lines. With the time value of money included, the investment cost graphs look even more attractive
- Opportunity of incremental and reconfigurable investments for maximum budget flexibility

All these features make a strong business case for the DSR system. However, the current market structure does not suggest how transmission investments for DSR technology can be supported. A public finance mechanism is clearly required to support such investments. One possibility can be a profit sharing mechanism between an investor and consumers. The investor makes the upfront investment in building transmission lines. The increase in welfare gain from congestion relief can be in part used to pay for the investor's efforts and the rest can be translated to lower electricity costs for the consumers. This is illustrated by way of an example. Assume that a transmission link is congested for 500 hours in a year with congestion costs amounting to 25 $/MWHr. Congestion relief for each MW could increase consumer welfare by $12,500. As stated earlier, in a meshed system such as the IEEE 39 bus system, the DSR technology can

increase system capacity by each MW with just 0.125 MVar of control effort (which translates to a performance index of 8). In other words, incremental congestion relief of 1 MW would need an investment of ~ $13,000 (equivalent to 13 modules). A profit sharing formula can be devised such that the consumers and investors share 50-50 benefits from the technology till the break even point for the investment and in the ratio 25-75 from that point onwards. This would result in a payback period of two years, as is shown by the profit of the investors in Table 6.8. The cumulative welfare of consumers is shown in the last column of Table 6.8, which is seen to increase continuously.

Table 6.7 Cost sharing formula to support transmission investments

Congestion Costs	**Congested Hours/year**	**Increase in welfare**	**Investments with DSR (assuming a PI of 8)**	**Profit-sharing Formula (consumer-investor)**
25 $/MWHr	500 hours	12,500 $/MW	13000 $/MW (cost for 13 modules)	I. 50-50 till break even II. 25-75 after break even

Table 6.8 Consumer and producer welfare under cost sharing formula

Time	**Investment Costs**	**Investor profit**	**Consumer welfare**
12 months	$ 13000	- $ 6250	$ 6250
24 months	-	- $ 500	$ 12500
36 months	-	$ 3645	$ 21875

Another possibility can be a contract path based business model. A transmission path can be defined between a generator and a load, and the electrons be transported over the specified path. This technique is presented in chapter 8 and can be implemented with communication enabled DSR technology. The transmission access fee can be charged directly to the users of the service on a MWhr-Mile basis, similar to how oil pipeline markets operate. Today, a new oil pipeline project is initiated as a Master Limited Partnership (MLP), wherein the master starts the partnership with a small share of investment overhead and is responsible for the operation of the pipeline. Transmission charge is based on per unit volume of liquid transported. These partnerships are attractive because they provide a steady stream of revenue for the investors and avoid corporate income tax. A business model like this can allow a business entity, such as Wall Street, to initiate transmission investments at a lower risk and create a market for the technology.

6.12 Conclusion

This chapter gives an overview of the structure and operation of the power sector in US. With a view to increase economic efficiency, vertically integrated utilities have been disintegrated and a complete unbundling of the generation, transmission, and distribution sectors has been done. While the generation market is now governed by the free market economics, the transmission and distribution markets are still heavily regulated. Introduction and adoption of a new transmission technology under these conditions seems to be very difficult.

System reliability is of paramount importance and is a major driver for transmission investments. Sufficient reserve margins are allocated to the critical lines of

the network to secure a reliable system operation under all contingency conditions. In the past, building of new transmission lines was the only way to secure system reliability and improve network capacity. With the emergence of technologies such as DSR, transmission investments can be decreased considerably to realize the same benefits. Further, as the system conditions change, DSR modules can be redeployed to relieve congestion at particular points to obtain maximum economic gains.

DSR technology increases market efficiency by allowing the most competitive generator to supply MWs to the end consumer. Theoretical analysis based on market supply curves is provided to show the change in societal welfare with incremental increase in transmission capacity. With congestion relief, aggregate consumer welfare is seen to increase as well as the welfare of the low cost generator. The market equilibrium is thus seen to move to a more efficient point.

A truly competitive market would easily realize investment opportunities for such a technology. However, under a regulated market structure, policy decisions are made with a view to increase the overall welfare of the society. Increased societal benefits in terms of lower consumer prices and increased efficiency of wholesale and retail markets can be realized from DSR technology. This chapter presents economic benefits of incremental increase in transmission capacity and suggests some possible public finance mechanisms that can be used to create a market for such advanced transmission technologies.

CHAPTER 7

DSR MODULE IMPLEMENTATION

7.1 Introduction

Application of DSR technology to the utility transmission and distribution network requires in depth analysis of some of the practical limitations. The most important issues concerning the design of such modules are driven by the unique aspects of the application. The issues of total module weight, mechanical clamping, potential for conductor damage, heat removal, extreme environments, corona discharge, fault currents, and lightning strikes are all critical issues to resolve. Further to make the modules operate in an autonomous manner, a self sustainable power supply is required for the controls and electronics. This chapter addresses these design considerations, and presents a detailed magnetic, electrical, and mechanical design of the module.

7.2 System Specifications

For a typical high voltage transmission line operating at 138 KV level, the line parameters are shown in Table 7.1 [55]. The critical parameter for realizing a DSR module is its weight; targeted at 120 lb per module. This is based on the discussions with transmission engineers, who suggested that this would be a reasonable weight for the modules to float mechanically on a transmission line. A realistic system would be rated at approximately 10 kVA per module, injecting for instance 14 volts at 750 A. This corresponds to a magnetizing inductance of 50 uH per module. One DSR module per phase per mile could change the line impedance by roughly 2%. A number of such

standard modules can be suspended from the power-line, floating both electrically and mechanically, to realize the required change in the line impedance.

Table 7.1 Line parameters for a typical 138 kV system

Operating Line Voltage	Current Capacity	Outside radius of conductor	Impedance per mile
138 KV	750 A*	0.033 m	0.168+j 0.789

* Maximum current can be as high as 1000 A

The series injection of impedance at each module is accomplished through a single-turn transformer (STT), which uses the line conductor itself as a winding of the transformer. To simplify the installation process, STT must have two separable cores that can be clamped around an existing line. The desired injection can be achieved by tuning the air gap of the separable core to realize a magnetizing inductance of 50 uH. The leakage inductance of the transformer must be made as small as possible to have minimal impact on the system when the module is by-passed.

Handling high levels of fault current and transient voltages during turn-on/off is typically a challenging problem for series connected devices. This must be coordinated with the overall protection of the module. Further, the module must act as a self sustained unit with the ability to power the switches and relays from the power-line itself. Other important issues include operation in high E-fields and minimization of corona discharge, effective heat removal from the module, sealing of the unit against rain and moisture, and protecting the line conductor against any damage during installation or operation. Each of these will be discussed in detail in the following sections.

7.3 Magnetic Design

The single-turn transformer design perhaps plays the most important part in the overall design of the module. The transformer core consists of two parts that can be physically clamped around a transmission line, forming a complete magnetic circuit, as shown in Figure 7.1. The magnetic path of the core has a small air gap, as a result of the separable cores needed for clamp-on. The air gap is desired and can be tuned to get the final value of magnetizing inductance. The power-line itself functions as one of the windings of the transformer. The other winding is wound on the cylindrical core with multiple turns so as to transform the operating line amperes to lower value sustainable for the switches.

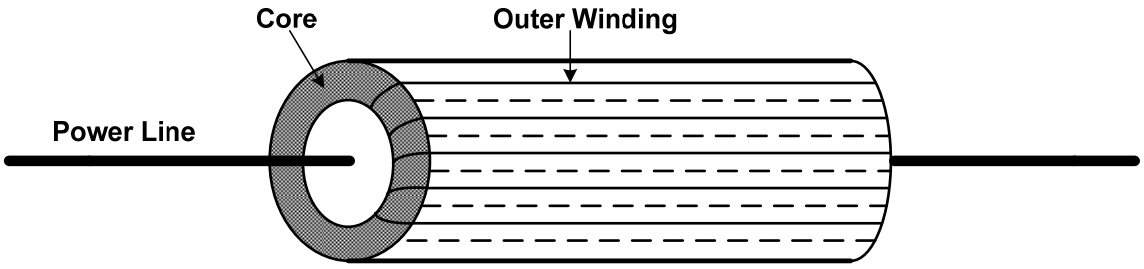

Figure 7.1 Single-turn coaxial transformer

The transformer operation can be categorized under two different operating conditions: by-pass mode and injection mode. In the by-pass mode, the output of the transformer is shorted by an electromechanical relay to cancel the power-line mmf and therefore only the leakage inductance is injected into the line. The leakage inductance of the STT is very small, which can be primarily attributed to the flux from the end turns, and has practically no effect on the operation of the transmission line. In the injection

mode, the electromechanical relay is opened and the magnetizing inductance X_M (or the self inductance of the primary winding) is injected into the line.

As the nominal operating line current can be as high as 1000 A, the core material of choice is silicon steel with a saturation flux density of ~1.6 T. Further, as the current flowing in the power cable produces flux lines tangential to circular paths around the cable, silicon steel with the grains oriented in the direction of flux is a more preferred material. If the permeability of silicon steel is assumed to be much higher than the air, then most of the flux lines can be assumed to be concentrated in the core. The concentration of flux lines in the magnetic core tends to increase the self inductance of the power-line, which in turn has the effect of increasing the overall line inductance.

The self inductance of the power-line with a magnetic core around it can be calculated from the inverse of the total reluctance faced by the magnetic flux lines. The reluctance of the magnetic path with a thickness 'Δr' and at a distance 'r' from the power-line is given by equation (7.1). The total reluctance is given by the parallel combination of all such reluctances of thickness 'Δr', over the width of the core.

$$R = \frac{2\pi r}{\mu(\Delta r * l)} \tag{7.1}$$

Where μ is the permeability of silicon steel and l is the length of the conductor

The weight of the STT is the most critical design parameter. As the reluctance depends on the radial thickness and the length of the core, the design must be optimized to obtain the required magnetizing inductance at the smallest weight of the core. The

desired inductance can be obtained by making the core thinner and longer or by making it thicker and shorter. The volume of a cylindrical object varies linearly with the length but with the square of the radius. Therefore, a lower weight of the core can be obtained if the length is made much longer than the radius, for a given volume. Added advantages of this design are larger surface area for heat convection and radiation, and a smaller leakage reactance from the end windings [56].

The power-line conductor used in the design process was ACSR (Aluminum Conductor Steel Reinforced) 'Drake', with an outside diameter of 795 kcmil or 2.81 cm. To protect the power-line from any damage during installation, aluminum armor roads would be wrapped around the line before the DSR module can be clamped-on. This is a desirable and standard operating practice for most utilities. After allowing margin for the secondary winding, armor rods and mechanical clearance, it was seen that the inside diameter of the cylindrical core could not be reduced below 5 cm. As a first order design procedure, various core geometries were simulated in MATLAB using equation (7.1), with a constant relative permeability of silicon steel as 5000. Table 7.2 shows the core geometries and their impact on the weight of the system. It is seen that the core weight can vary from 52.2 lbs to 250 lbs, a significant variation, to realize a magnetizing inductance of 50 uH. The selected core geometry is highlighted in the table and gives 46.7 uH of magnetizing inductance at 86.6 pounds. The basis for selecting this particular geometry was to keep the weight of silicon steel less than 90 lbs, so as to achieve the target weight of 120 lb for the entire unit and still keeping the length manageable around 1 meter.

Table 7.2 Core geometries for realizing a magnetizing inductance of 50 μH

Rel. Perm.	MATLAB Inductance	Inner Radius	Outer Radius	Air Gap	Height	Weight
	(uH/m)	(cm)	(cm)	(cm)	(cm)	(Pound)
5000	12.3	2.5	3	0.05	359.7	52.3
	23.9	2.5	3.5	0.05	206.1	65.3
	35.37	2.5	4	0.05	148.6	76.6
	46.7	2.5	4.5	0.05	117.1	86.6
	57.93	2.5	5	0.05	97.8	96.9
	69	2.5	5.5	0.05	84.9	107.7
	80	2.5	6	0.05	75.6	118.9
5000	6.63	2.5	3	0.1	472.1	68.6
	12.65	2.5	3.5	0.1	296.7	94.1
	18.64	2.5	4	0.1	224.2	115.5
	24.59	2.5	4.5	0.1	185.2	137.0
	30.51	2.5	5	0.1	158.7	157.3
	36.4	2.5	5.5	0.1	141.6	179.6
	42.25	2.5	6	0.1	130.5	205.2
5000	12.13	3	3.5	0.05	372.9	64.0
	23.605	3	4	0.05	209.6	77.5
	34.95	3	4.5	0.05	151.6	90.1
	46.16	3	5	0.05	119.0	100.6
	57.26	3	5.5	0.05	99.0	111.1
	68.23	3	6	0.05	85.5	122.0
5000	6.56	3	3.5	0.1	479.4	82.3
	12.55	3	4	0.1	301.2	111.4
	18.5	3	4.5	0.1	226.2	134.5
	24.42	3	5	0.1	185.8	157.1
	30.31	3	5.5	0.1	158.6	178.1
	36.17	3	6	0.1	140.1	200.0

The selected core geometry was then simulated in MAXWELL finite element package to validate the design. Again a constant permeability of 5000 was assumed for silicon steel. With this, the magnetizing inductance of the core was obtained as 48.5 uH at 750 A. To make the analysis more exact, the actual non-linear B-H curve of the commercially available grain oriented silicon steel was used to account for the saturation effect at high currents. The data for the B-H curve is available in D. The magnetizing inductance of the transformer was now found to be 47.15 uH at a peak current of 750 A.

A peak flux density of 1.55T was observed at the inner circumference (Figure 7.2) of the core.

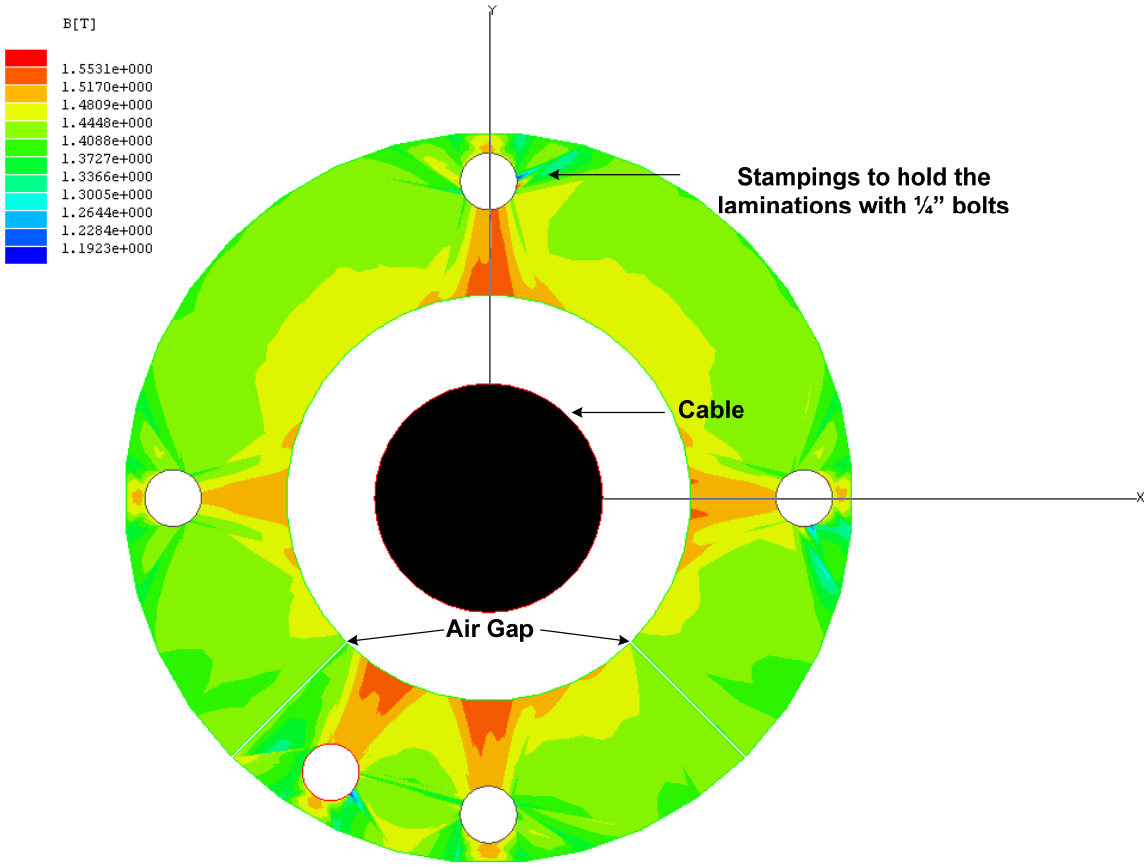

Figure 7.2 Cross sectional view of the core showing magnetic field density

As will be discussed in the next section, the core is in the form of laminations that are stacked together. Five stampings can be seen in Figure 7.2 and these are provided to hold the laminations with bolts. These bolts were modeled as low grade steel in the MAXWELL simulations. Preliminary design was based on custom laminations being die-

cut. Design was finalized with help from Paul Springer and Frank Lambert of NEETRAC.

7.3.1 Lamination Design

As the transformer core consists of two parts that needs to be physically clamped around a transmission line, the laminations must be stamped out in the form of two sectors of a circle, with a desired material-loss of not more than 0.25 mm on either side to account for the air gap. The lamination design is presented in Figure 7.3.

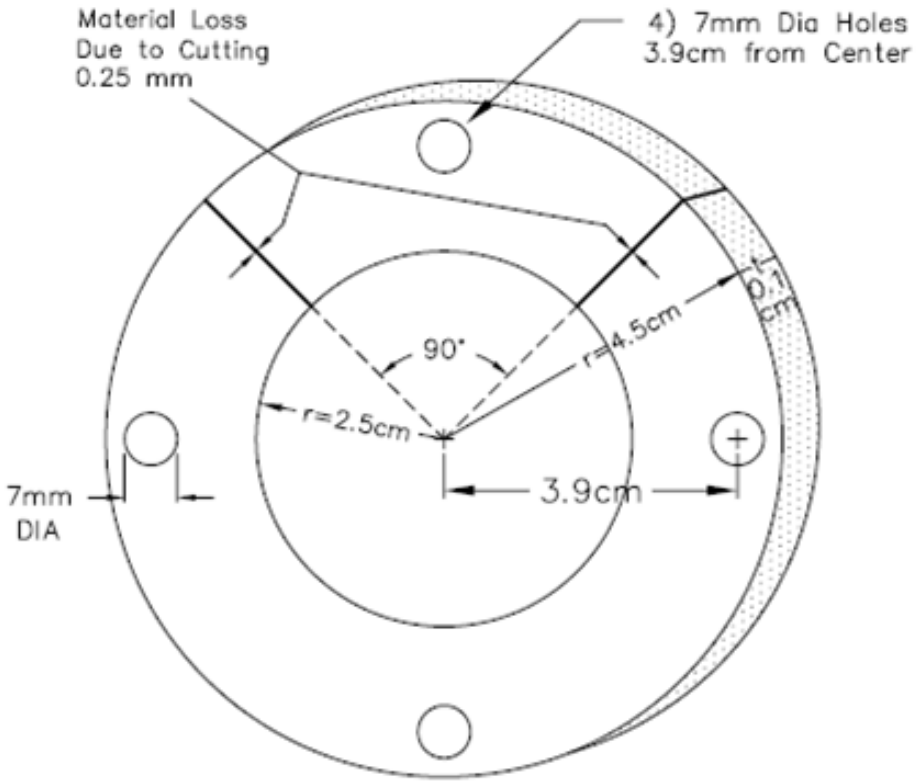

Figure 7.3 Lamination design

Commonly available silicon steel comes with a thickness of 0.27mm. This requires a total of 4333 laminations to be stacked together to get the required core length of 117 cm. To hold the laminations together, four stampings for 1/4" Alloy Steel bolts are provided. Extra compression can be provided by end plates on both sides of the stack. To reduce the magnetic flux-loss, the stampings are displaced towards the outer edges of the laminations. This is because the reluctance increases radially from the center and therefore any material-loss on the inner edge has a more drastic effect on the flux-loss as compared to an equivalent material-loss on the outer edge. An improved lamination design is shown in Figure 7.4, where an extra stamping is provided to reduce the bend-back of the laminations.

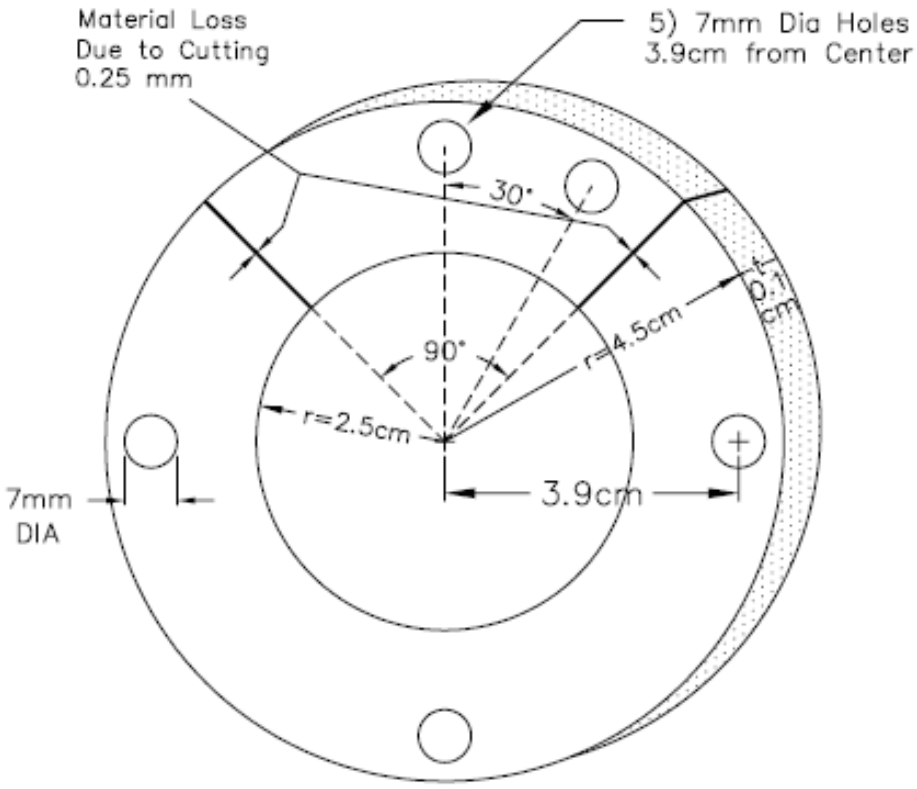

Figure 7.4 Improved lamination design

In the next generation prototype, laminations would be rolled to form the transformer core; unlike the design presented here, wherein individual laminations are cut and stacked together. This would help in lowering material loss, and reducing complexity and cost of the manufacturing process.

7.3.2 Transformer Winding Design

The design of the transformer winding is primarily governed by the open circuit voltage that the switches can withstand and the sustainable level of current under normal and faulted conditions. The electromechanical relay is the most critical component, as the electrical rating of the relay has a direct bearing on its size and weight. Relays compatible with the size and weight considerations for the DSR unit can withstand an off-state voltage of 480 V and a continuous current of 30 A. A turns ratio of 25:1 is sufficient to reduce the line current from 750 A to 30 A. With an operating current of 750 A, 47.15 uH of primary inductance reflects as 13.3 volts on the primary, and as 333.5 V on the secondary, well within the blocking capability of the relay. Under fault conditions, a Metal Oxide Varistor (MOV) will provide protection against excessive voltages. This will be connected across the secondary winding.

A circumference utilization factor of 0.75 together with a wire lay factor of 0.8 was used in the design process of the secondary winding. With these constraints, 25 turns of AWG 10 can be easily accommodated on the inner circumference of the core to sustain the steady state current of 30 A. Further the insulation of the wire must also have sufficient margin to ride through fault currents of 2000 A (equivalent to 50,000 A on the primary side). Under these transient conditions, all the energy dissipated by the winding

resistance is absorbed by the wire insulation. This is an adiabatic loading of the line and is governed by equation (7.2) [57]. The formula can be re-written in terms of the wire cross section as described by equation (7.3).

$$I^2 Rt = H_c \theta \tag{7.2}$$

Where, I is the current flowing in the wire, R is the resistance of the wire, t is the time during which the current flows, H_c is the thermal capacity of the wire, and θ is the temperature rise of the wire in ^{0}C

$$\left[\frac{I}{CM}\right]^2 t = 0.0297 \log\left(\frac{T_2 + 234}{T_1 + 234}\right) \tag{7.3}$$

Here, CM is the wire cross section in circular mils, T_1 is the temperature of the wire before the fault, and T_2 is the temperature of the wire after the fault.

A fault current of 2000 A flowing through the secondary winding for 3 cycles results in a temperature rise of 51 ^{0}C. As the operating temperature inside the unit can be as high as 100 ^{0}C, it is required to use a wire insulation that belongs to 200^o C temperature class, or above. Polyurethane-amid-imide is one such possibility [58].

Table 7.3 summarizes the design of the secondary winding. The complete STT unit is pictorially shown in Figure 7.5; while Figure 7.6 shows the aluminum casing for the module with a small enclosure at one end to accommodate the electronics.

Table 7.3 Secondary winding design

Wire AWG	Number of Turns	Insulation Class	Weight
10	25	Polyurethane-amid-imide	3 lbs

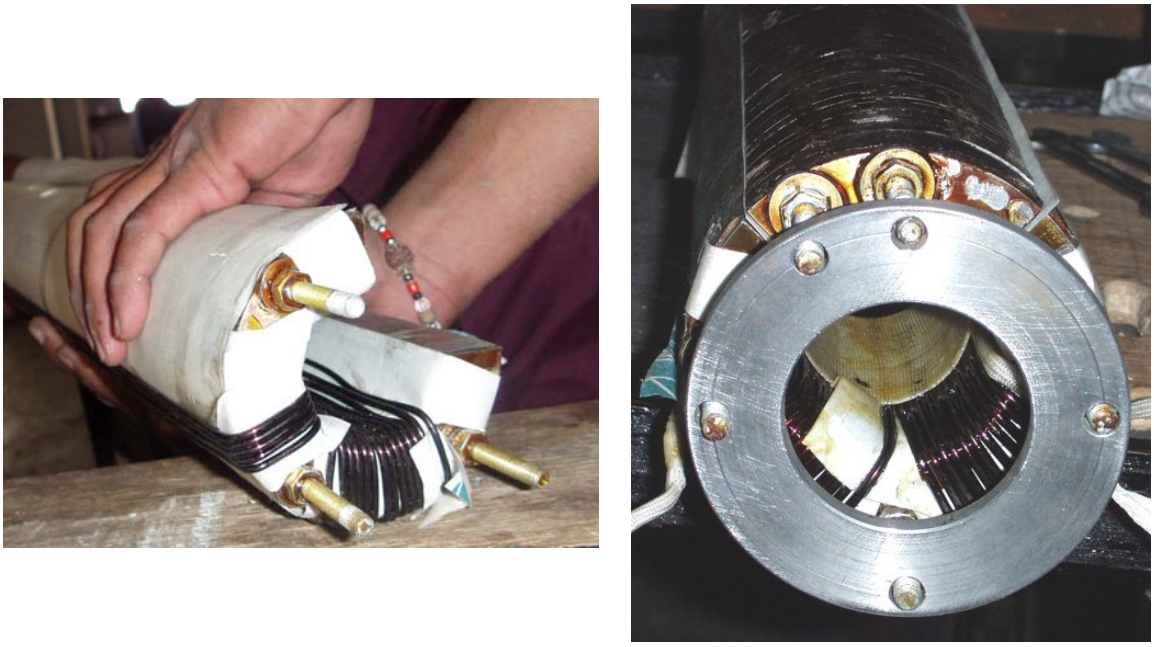

Figure 7.5 DSR prototype

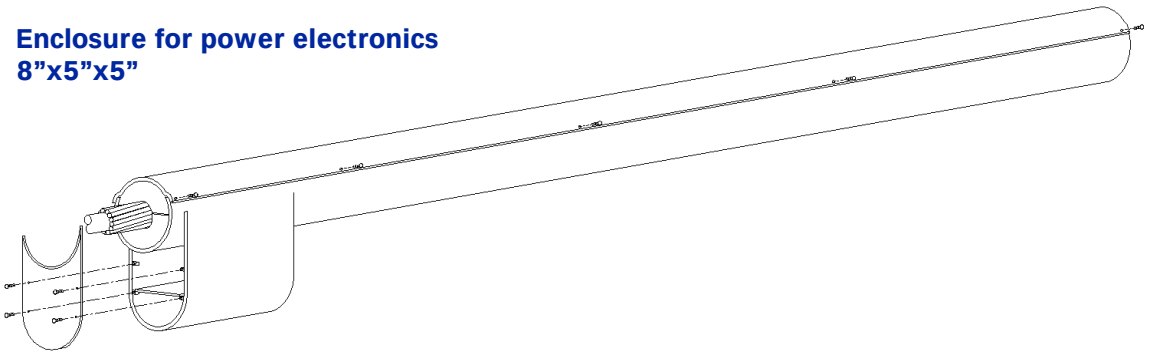

Figure 7.6 Module casing with an enclosure for electronics

7.3.3 Magnetic Forces on the Transformer

Magneto-mechanical forces are developed in the transformer core that tries to increase the flux linkage through the system. Such forces are generated only during the injection mode of operation. During the by-pass mode, the transformer operates under zero flux and hence no magneto-mechanical forces can be set-up.

A virtual force of attraction, described by equation (7.4), is developed during injection mode. The force tries to pull the two lamination stacks towards each other so as to reduce the reluctance of the air gap. A two dimensional model of the transformer core was duplicated in MAXWELL to study the magnetic forces on the core under nominal and fault conditions. The simulations indicated that a magneto-mechanical force of 20,000 N is exerted on the lamination stack when the power line current is 1000 A and can increase up-to 51,240 N under a fault of 50,000 A on the power-line.

$$F_{mech} = -\frac{dW}{dl} \tag{7.4}$$

Here, dW is the amount of energy required to move the system by a distance dl, against a magneto-mechanical force of F_{mech}.

Under by-pass mode, electro-magnetic force is generated by the magnetic field of the power-line on the current-carrying secondary winding, and is given by equation (7.5). This force has a tendency to push-out the windings on the inner surface of the core and to pull-in the windings on the outer surface of the core. This force is negligible under steady state conditions but can increase up to 680 N/turn under fault currents of 50000 A.

$$F_{mag} = \left(\vec{I}.\vec{dl}\right) \times \vec{B} \tag{7.5}$$

Here, F_{mag} is the electro-magnetic force developed on a secondary winding of length *dl* and carrying a current of *I* in the presence of a magnetic field *B* that is generated by the power line.

The results are summarized in Table 7.4 and 7.5. The magento-mechanical or the virtual force acts on the lamination stack with a tendency to pull the two cores towards each other. The direction of the net force is towards the center. The electromagnetic force acts on the secondary windings in a way that the windings on the inner surface of the core experience a net outward pull, while the windings on the outer surface of the core experience a net inward pull. The direction of the resulting force is outwards. The leakage flux from the end turns results in slightly higher forces at the edges of the core and the windings.

Table 7.4 Magnetic forces under steady state operation at 1000 A

	Virtual Force	**Electromagnetic Force**
Laminations	16.5 N/lamination towards center (20000 N total)	N/A
Winding	N/A	0.305 N outwards (0.488 N at the sides)

Table 7.5 Magnetic forces under transient operation at 50000 A

	Virtual Force	**Electromagnetic Force**
Laminations	42 N/lamination towards center (51240 N total)	N/A
Winding	N/A	680 N outwards (1215 N at the sides)

7.3.4 Heat Dissipation and Losses

Heat generated in the DSR module must be transferred to the surroundings effectively to maintain safe operation of the windings, magnetic core, and the power electronics. There are four different sources of heat generation in the transformer: primary winding losses, secondary winding losses, core losses, and losses in the control circuitry and switches.

Primary winding losses include the conduction losses in the portion of the cable enclosed within the module. We need to factor-in these losses as they are handled through the module. The losses in the primary winding are present in the injection as well the by-pass mode and are given by equation (7.6). The resistance of the cable is 0.128 Ω/mi [59], which should result in a maximum power loss of 93.1 W at 1000 A. Experimental results are shown in Figure 7.7, which indicate a power loss of 75 W at 1000 A.

$$Q_{cable} = I^2 \times R_{per\ unit\ length} \times Module\ Length = 93.1W \tag{7.6}$$

Here Q_{cable} is the heat dissipated in the primary winding, I is the current flowing through the winding, and $R_{perunitlength}$ is the resistance per unit length of the winding.

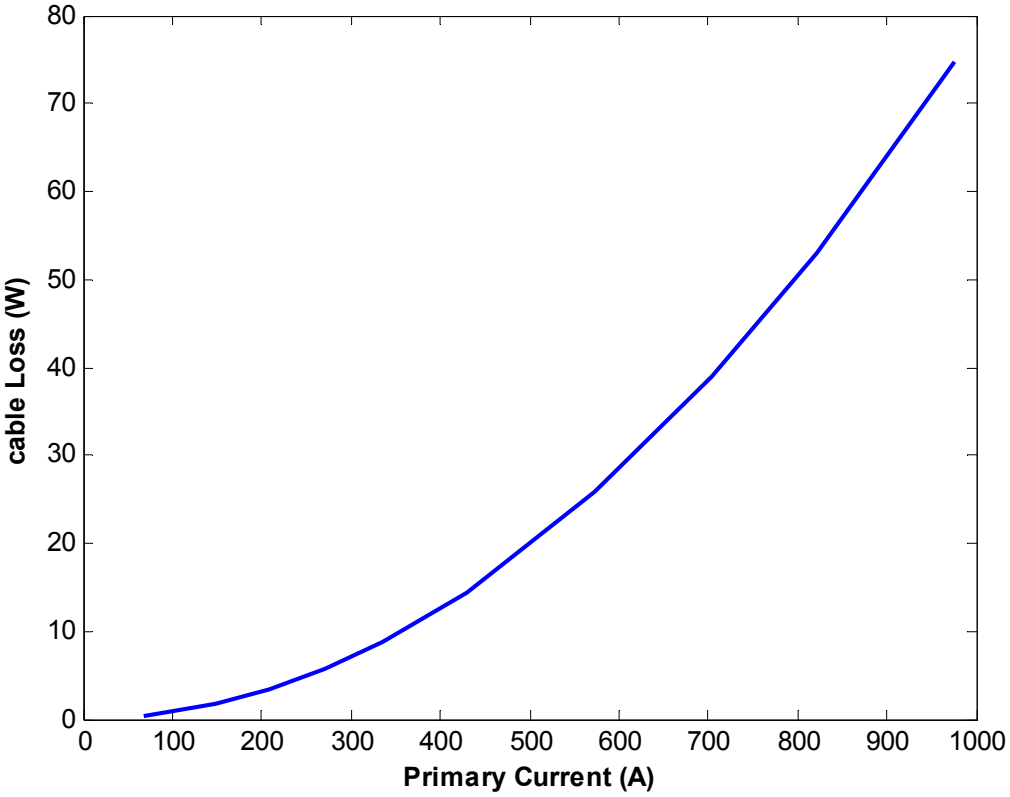

Figure 7.7 I^2R loss in the power-line

Core losses occur in the STT primarily during the injection mode and are given by equation (7.7). Under by-pass mode, the flux in the core is almost zero and thus the core losses are negligible. With a specific loss of 3.5 W/Kg [60] and an operating magnetic field of 1.5 T, the total core losses for a length of 117 cm equal 137.7 W. Experimental measurement for core losses was performed by creating a magnetic field corresponding to 1000 At on the STT core. In other words, 40 A of current was made to pass through 25

turns on the STT core. The power consumed by the laminations was measured through a power analyzer as the dot product between the voltage induced across the winding and the current flowing through it. Figure 7.8 shows core losses in the lamination stack with an air gap 0.7mm to be 137 W at 1000 A.

$$Q_{core} = Specific\,loss_{W/Kg} \times Core\,Weight = 137.7\,W \tag{7.7}$$

Here Q_{core} refers to the heat dissipated in the core.

Copper losses in the secondary winding of the transformer occur only during the by-pass mode. With 25 turns of AWG 10 wire, the total resistance of the secondary winding comes to be 0.1556 mΩ [59]. Equation (7.8) gives the I^2R loss in the secondary winding to be 155.6 W, when 1000 A of current is flowing in the power cable. Losses in the switches and control circuitry are small and do not impact the operation of the unit in any significant way. Table 7.6 gives the summary of the total heat losses in the module.

$$Q_{\text{sec}} = I^2 \times R_{\text{sec}} = 155.6\,W \tag{7.8}$$

Here, Q_{sec} refers to the heat losses in the secondary winding, I is the current flowing through the winding, and R_{sec} is the resistance of the secondary winding.

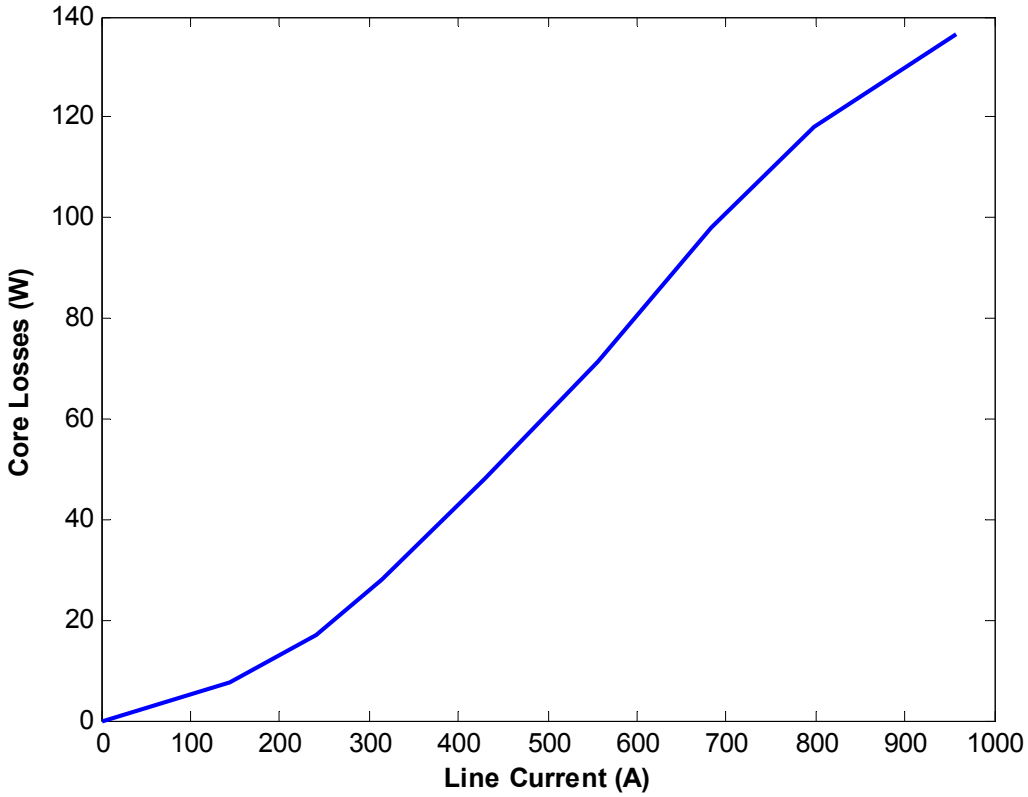

Figure 7.8 Core Losses with air gap of 0.7 mm

Table 7.6 Heat losses in the module

Heat Source	Injection Mode	By-pass Mode
Primary Wdg. Copper Loss	93.1 W	93.1 W
Secondary Wdg. Copper Loss	0 W	155.6 W
Core Loss	137.7 W	0 W
Losses in relay	2 W	1.5 W
Losses in electronics	2 W	2 W
Total	232.8 W	252.2 W

It can be seen that under nominal operating conditions, maximum heat generation occurs during the by-pass mode. Also under faults, the module is by-passed and heat is primarily generated by the losses in the primary and secondary winding. To analyze the heat transfer process in the by-pass mode, a steady state thermal model of the module is developed, as shown in Figure 7.9. The heat is transmitted radially through the transformer core and laterally through the power cable. Table 7.7 explains the notations that are used to define the temperatures at different points in the module; while Table 7.8 summarizes the geometrical parameters of the module, which are used to calculate the thermal resistances.

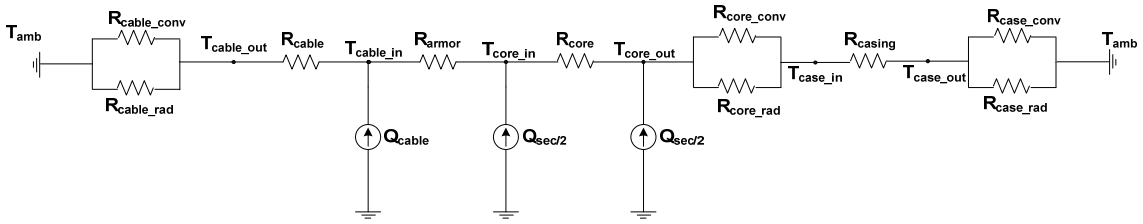

Figure 7.9 Thermal model during by-pass mode

The heat generation sources are I^2R losses in the cable, represented by Q_{cable}, and I^2R losses in the secondary winding, represented by Q_{sec}. The heat generated by the secondary winding is split into two equal heat sources to account for the winding on the inner and outer side of the core respectively. The direction of heat flow is from the cable to the ambient.

Table 7.7 Temperatures at different points inside the module

Notation	Explanation
T_{cable}_in	Temperature of the cable inside the module
T_{cable}_out	Temperature of the cable outside the module
Tcore_in	Temperature of the inner surface of the core
Tcore_out	Temperature of the outer surface of the core
Tcase_in	Temperature of the inner surface of the module casing
Tcase_out	Temperature of the outer surface of the module casing
Tamb	Ambient temperature

Table 8.8 Geometrical parameters of the module

Geometrical Parameters	Value
Radius of the cable (r_{cable})	1.4 cm
Inner radius of the core (r_{ci})	2.5 cm
Outer radius of the core (r_{co})	4.5 cm
Length of the module (L_c)	117 cm
Inner radius of the casing (r_{di})	5.85 cm
Outer radius of the casing (r_{do})	6.35 cm
Length of the casing (L_d)	154 cm

The transfer of heat occurs radially through the module as well as laterally through the power line. The temperature gradient between the cable enclosed within the

module and the cable outside the module creates a path for conductive heat flow. The heat is then transferred to the surroundings by radiation and convection from the cable.

The heat is also transmitted radially through conduction from the cable within the module to the transformer core. Aluminum armor rods will be wrapped around the conductor to protect against damage during installation. Thermal conductivity of aluminum is very high and majority of heat will be conducted through it. The heat then flows through the body of the core, by the process of thermal conduction. The heat from the outer surface of the core gets transferred to the module casing through convection and radiation. Finally, the heat is conducted through the module casing, before being transferred to the surroundings through convection and radiation. Table 7.9 gives the thermal resistances for different modes of heat flow through the module. Detailed explanation for thermal resistances can be found in the Appendix E.

Figure 7.10 shows the experimental test set-up for the thermal testing of the module. The set-up is powered through a 480 V feeder, which passes through an auto-transformer to supply 0-480 V of controlled voltage. A step-down transformer, with a turns ratio of 10:1, is used to provide 0-48 V of voltage on the secondary. ASCR Drake conductor closes the loop on the secondary with an inductive load of 120 μH connected in series. DSR module is clamped on to the ASCR Drake conductor. The set-up is capable of delivering up to 1500 A of continuous current through the ASCR conductor.

Table 7.9 Thermal Resistance Values

Thermal Resistance	Heat Transfer Process	Value (^{0}C/W)
R_{cable}	Conduction through cable	$R_{cable} = \frac{d}{\lambda_{cable} A}$
R_{cable_conv}	Convection through cable outside the module	$R_{cable\_conv} = \frac{1}{1.34\, A_{cable}} \left(\frac{d_{cable}}{T_{cable\_out} - T_{amb}} \right)^{0.25}$
R_{cable_rad}	Radiation through cable outside the module	$R_{case\_rad} = \frac{\left(T_{case\_out} - T_{amb}\right)}{5.7\, \varepsilon\, A_{core}} \frac{1}{\left(\left(\frac{T_{case\_out}}{100} \right)^4 - \left(\frac{T_{amb}}{100} \right)^4 \right)}$
R_{amrmor}	Conduction through armor rods	$R_{armor} = \frac{\ln\left(r_{ci} / r_{cable}\right)}{2\pi\, \lambda_{armor} L_c}$
R_{core}	Conduction through core	$R_{core} = \frac{\ln\left(r_{co} / r_{ci}\right)}{2\pi\, \lambda_{core} L_c}$
R_{core_conv}	Convection from outer surface of core	$R_{core\_conv} = \frac{1}{1.34\, A_{core}} \left(\frac{d_{core}}{T_{core\_out} - T_{case\_in}} \right)^{0.25}$
R_{core_rad}	Radiation from outer surface of core	$R_{core\_rad} = \frac{\left(T_{core\_out} - T_{case\_in}\right)}{5.7\, \varepsilon\, A_{core}} \frac{1}{\left(\left(\frac{T_{core\_out}}{100} \right)^4 - \left(\frac{T_{case\_in}}{100} \right)^4 \right)}$
R_{case}	Conduction through module casing	$R_{case} = \frac{\ln\left(r_{do} / r_{di}\right)}{2\pi\, \lambda_{case} L_d}$
R_{case_conv}	Convection from outer surface of casing	$R_{case\_conv} = \frac{1}{1.34\, A_{case}} \left(\frac{d_{case}}{T_{case\_out} - T_{amb}} \right)^{0.25}$
R_{case_rad}	Radiation from outer surface of casing	$R_{case\_rad} = \frac{\left(T_{case\_out} - T_{amb}\right)}{5.7\, \varepsilon\, A_{case}} \frac{1}{\left(\left(\frac{T_{case\_out}}{100} \right)^4 - \left(\frac{T_{amb}}{100} \right)^4 \right)}$

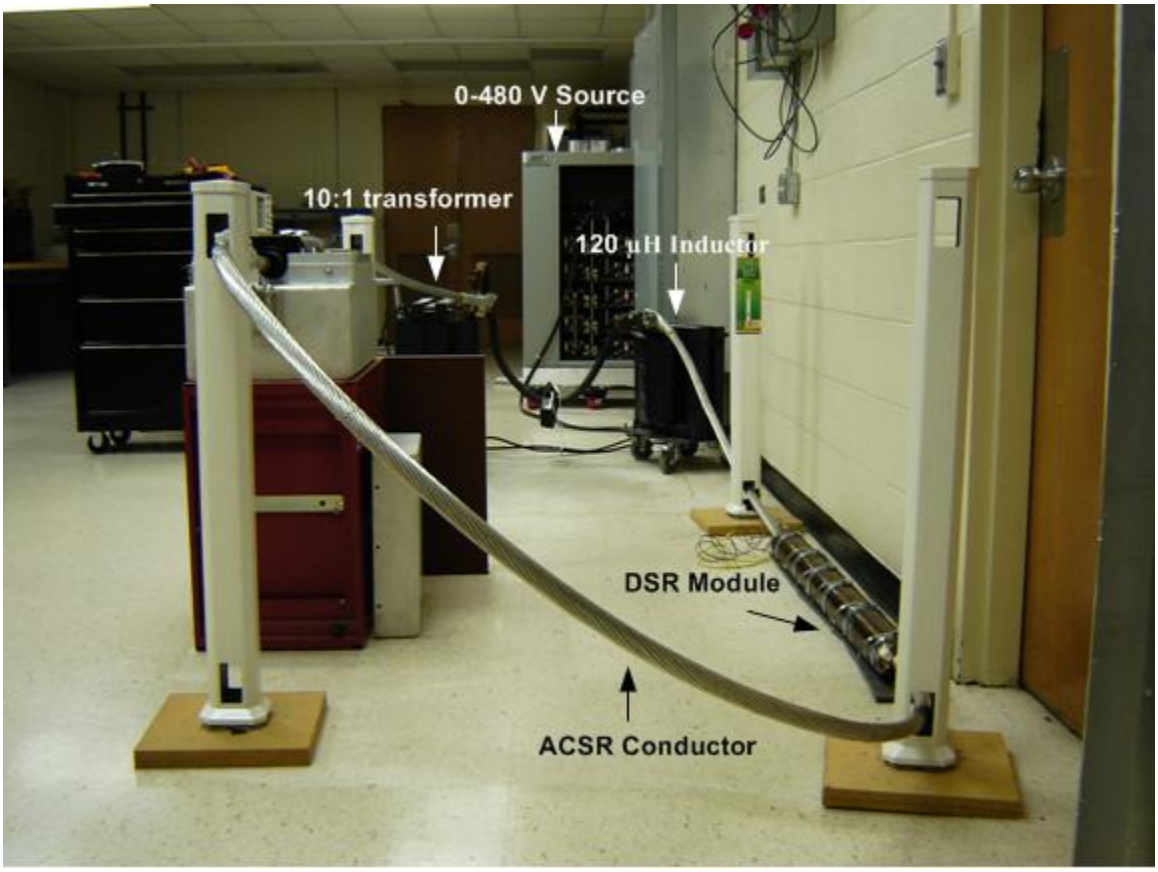

Figure 8.10 Lab set-up for experimental testing of DSR prototype

The temperature rise of the module was studied by passing 750 A of continuous current through the set-up for one hour. A thermocouple was placed at the inner surface of the STT core, where the temperature is predicted to be the highest. Another thermocouple was attached to the cable outside the module to record the operating temperature of the cable.

The results showed a temperature of 85 ^{0}C inside the module when the cable was operating at 60 ^{0}C. The ambient temperature of the room was recorded to be 23 ^{0}C. The utility engineers have indicated that the power cable can operate at temperatures of up to 100 ^{0}C. Under such conditions, a temperature rise of 25-40 ^{0}C is expected for the module.

This sets the benchmark for sizing the electronics and the wiring insulation for 200 ^{0}C, or above.

7.4 Electrical Design

To enable a self-sustained operation of the DSR unit, a DC power supply is needed for the relay, thyristor switches, and the microcontroller. The power supply must be able to derive the input power from the line itself, so as to allow the unit to operate on a stand-alone basis. To meet this criterion, the input power must be obtained from the voltage induced on the secondary winding during injection mode and from the current flowing through the shorted secondary winding during by-pass mode.

The power requirement for the control circuitry and the switches is shown in Table 7.10. A regulated 24 V DC power supply is required at all times to power the relay and the thyristors. Power supply for control circuitry and microprocessor (5-10 V) is obtained by stepping down the voltage from 24 V, using a DC-DC buck converter.

Table 7.10 DC power supply requirements of the DSR unit

Device/Circuit	**Injection Mode**	**By-pass Mode**
Relay	24 Vdc, 2 Watts	-
Thyristor Pair	24 Vdc , 1.2 Watts for 1 cycle	24 V dc, 1.2 Watts for 1 cycle
Control Circuitry	10 Vdc, 2 Watts	10 Vdc, 2 Watts
Microprocessor	5 Vdc, 1 Watt	5 Vdc, 1 Watt

As the module is designed to operate between line currents of 0-1000 A, the transition point from the by-pass to the injection mode may be selected as 500 A. It must be noted that this transition point is not fixed, and is only used as a reference. Power electronics can be designed to sustain a variable transition point.

7.4.1 Power Supply Design under By-pass Mode

In the by-pass mode, 0-20 A of current flows through the secondary winding, corresponding to 0-500 A of current flowing on power line. A current transformer, denoted by 'T_2' is used to step down the secondary current to 0-0.33 A, which is used as the input signal for the closed loop controller (Figure 7.11). Switch 'M_1' is used to regulate the output voltage to 24 V DC. The switch is opened when the output voltage falls below 24 V and the input current starts charging the capacitance 'C' to 24 V DC. The switch is closed when the output voltage exceeds 24 V providing a shunt path to the flow of input current. A hysterisis comparator 'C_1' controls the switching of the converter. Figure 7.12 shows the experimental results during by-pass mode. The experimental set-up shown earlier in Figure 7.10 was used for the electrical testing of the module. The converter gives a regulated voltage of 24 V DC, with a ripple of less than 5%. The power supply picks-up when the line current becomes greater than 140 A.

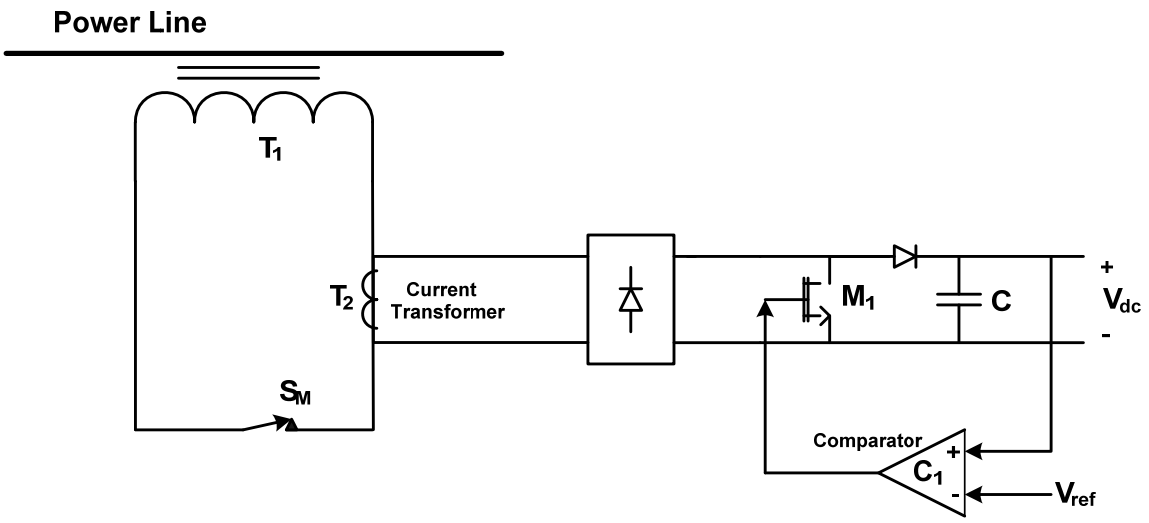

Figure 7.11 Power supply design under by-pass mode

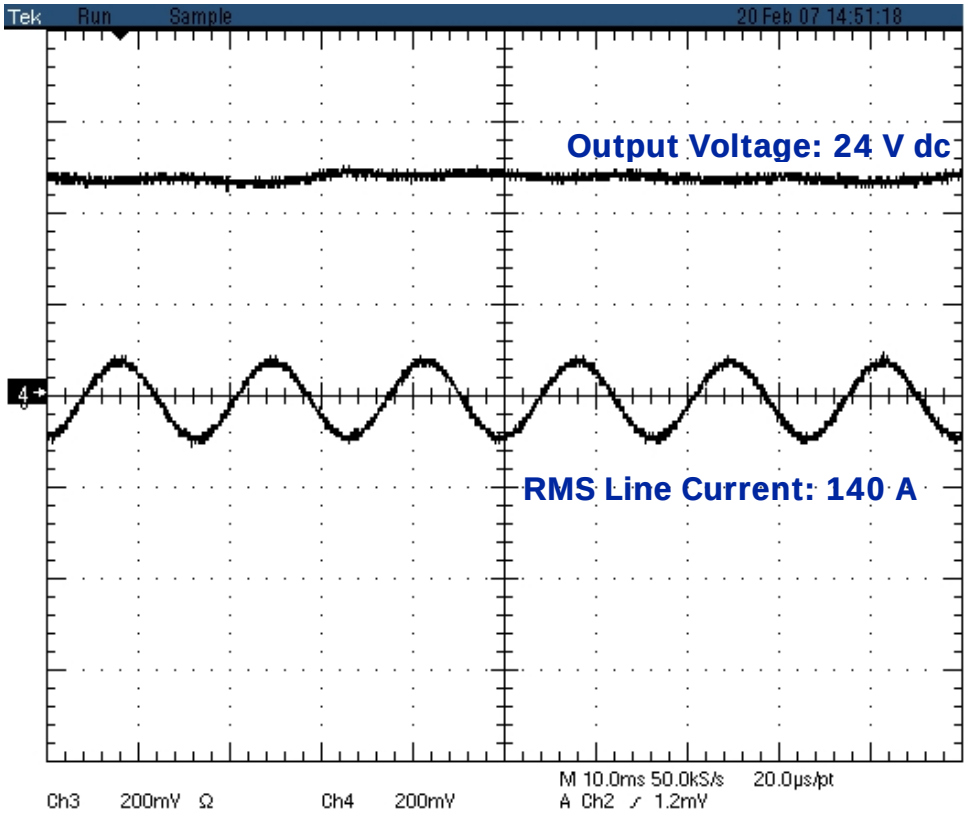

Figure 7.12 Experimental results showing a regulated DC voltage at 140 A

7.4.2 Power Supply Design under Injection Mode

In the Injection mode, 235-480V of voltage is generated across the secondary winding of the STT, which corresponds to 500-1000 A of current flowing on power line. A voltage transformer, denoted by 'T_3,' is used to step down the voltage to 9-18 V and a boost converter is used to regulate the output voltage to 24 V DC, as shown in Figure 7.13. Switch 'M_1' is now opened when the output voltage exceeds 24 V DC and is closed when the output voltage falls below 24 V DC to provide the conventional boost functionality. A PWM chip is used to control the switching of the converter with a frequency of 20 kHz. Figure 7.14 shows the experimental results during injection mode. The converter gives a regulated voltage of 24 V DC, with a ripple of less than 5%. The two circuits are integrated to provide an uninterrupted DC voltage over the current range of 140-1000 A. A printed circuit board design of the power supply is presented in Figure 7.15. The circuit layout is provided in Appendix F.

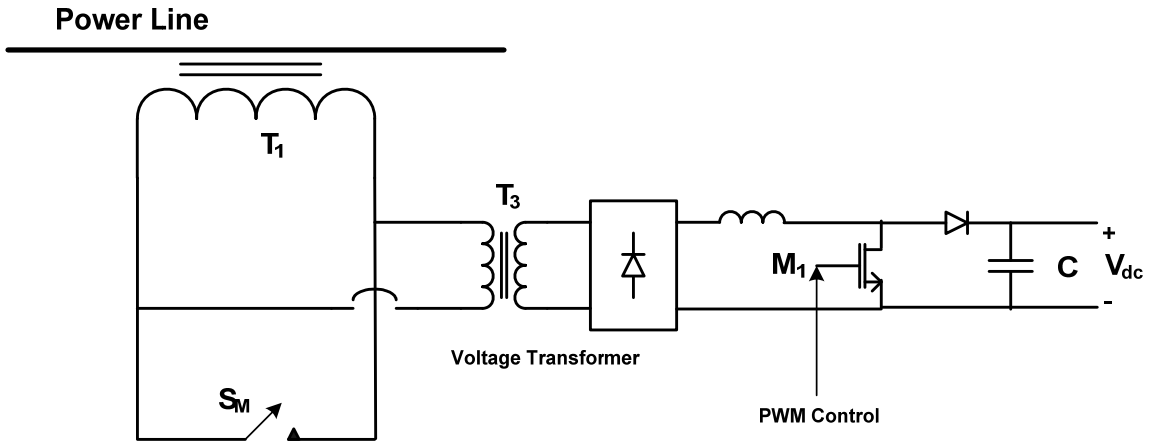

Figure 7.13 Power supply design under injection mode

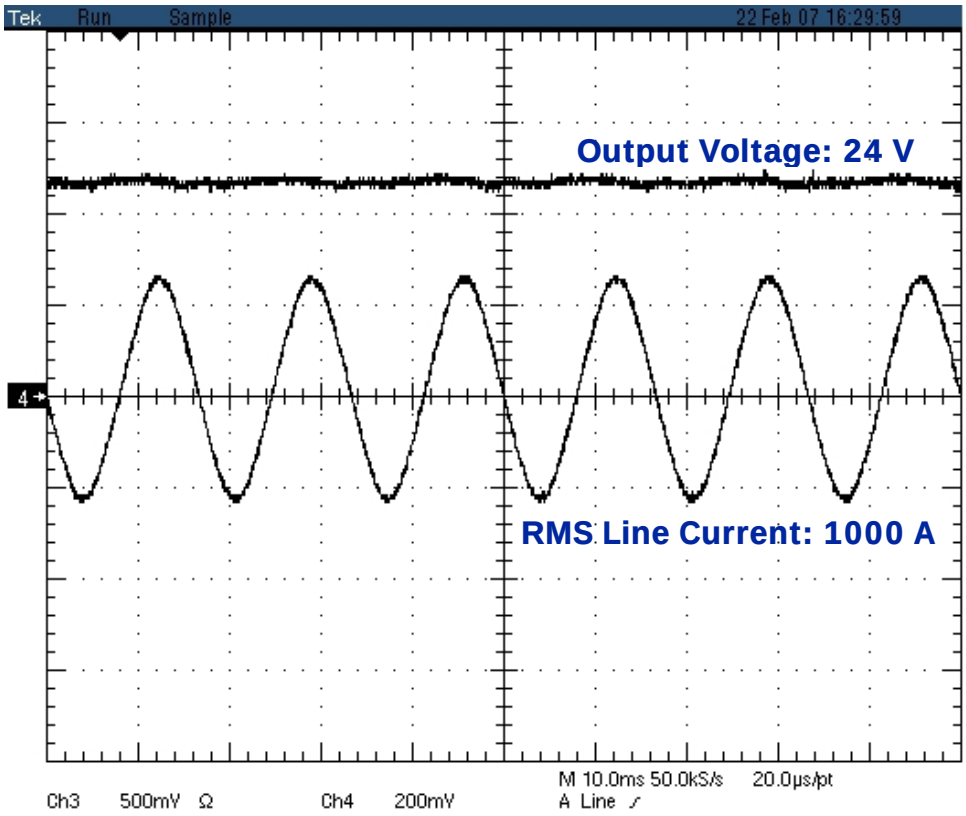

Figure 7.14 Experimental results showing a regulated DC voltage at 1000 A

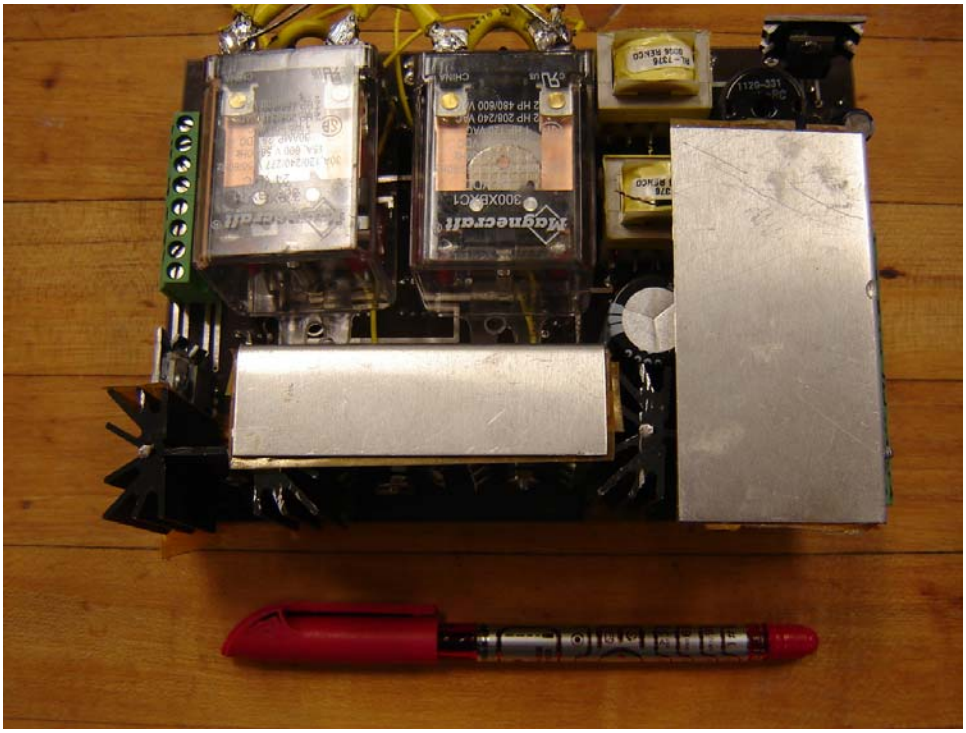

Figure 7.15 Printed circuit board layout of the power supply

7.4.3 Controller Operation

As discussed in chapter 3, the actuating signal for the turn-on and turn-off of the module is based on the current flowing through the power line. This requires an additional current transformer on the power-line, to provide the feedback signal to the controller. Besides increasing the total cost of the module, it also complicates the installation process. It is thus desired to obtain the actuating signal based on easily-accessible quantities, which are secondary current and voltage.

During the by-pass mode, circulating current flowing in the secondary is equal to the power line current times the turns-ratio of the transformer. The trigger for the turn-on of the module can thus be generated by measuring the secondary current. Under injection mode, the secondary voltage can be obtained from equation (7.9). Therefore, the trigger for the turn-off of the module can be generated by translating secondary voltage to an equivalent value of the power line current. A current transformer and a voltage transformer are attached to the secondary winding to provide control signals to the micro-controller for the turn-on and turn-off of the module.

$$V_{\text{sec}} = I_{line} \times X_{mag} \times N \tag{7.9}$$

Here, V_{sec} is the voltage induced on the secondary winding, I_{line} is the current flowing through the power-line, X_{mag} is the magnetizing inductance of the STT, and N is the turns ratio of the STT.

Figure 7.16 shows the control of the module based on the secondary current and voltage. The turn-on of the module is governed by the curve a-a', which gives the relation between the current on the STT secondary winding and on the power-line. As the secondary current crosses point A, the module is turned-on at a line current value of I_{on}. The turn-off of the module is governed by the curve b-b', which gives the relation between the transformer secondary voltage and the power-line current. As the secondary voltage drops below point B, the module is turned-off at a line current value of $I_{off.}$ The integrated power supply and control schematic is shown in Figure 7.17.

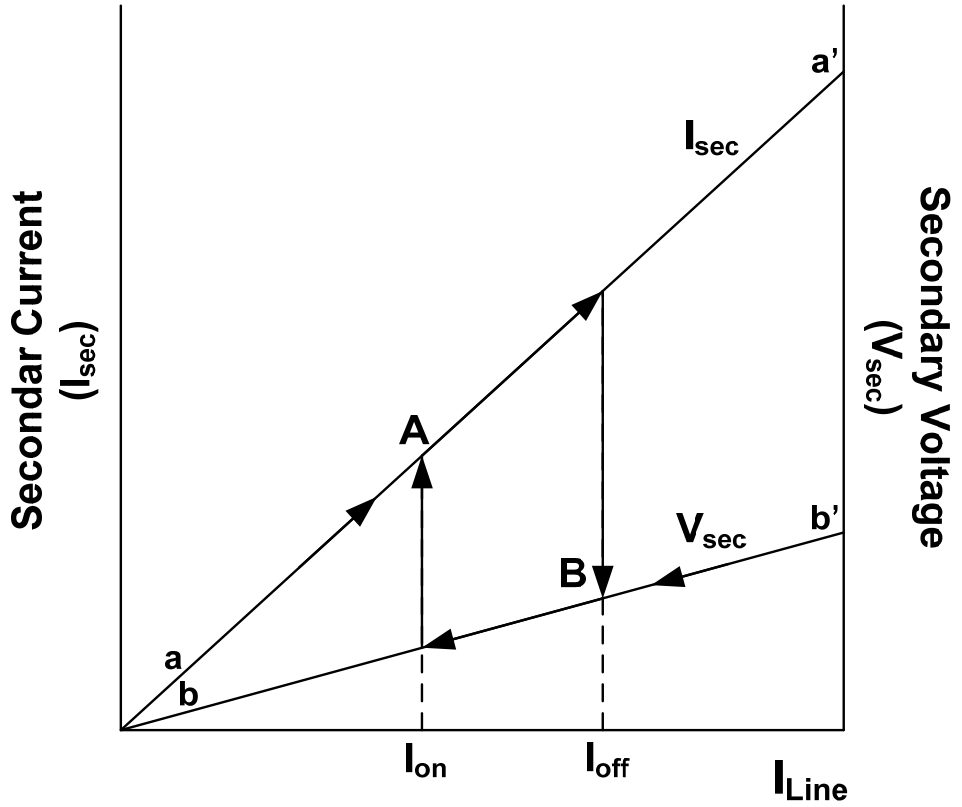

Figure 7.16 Secondary current and voltage governing the turn-on/off of the module

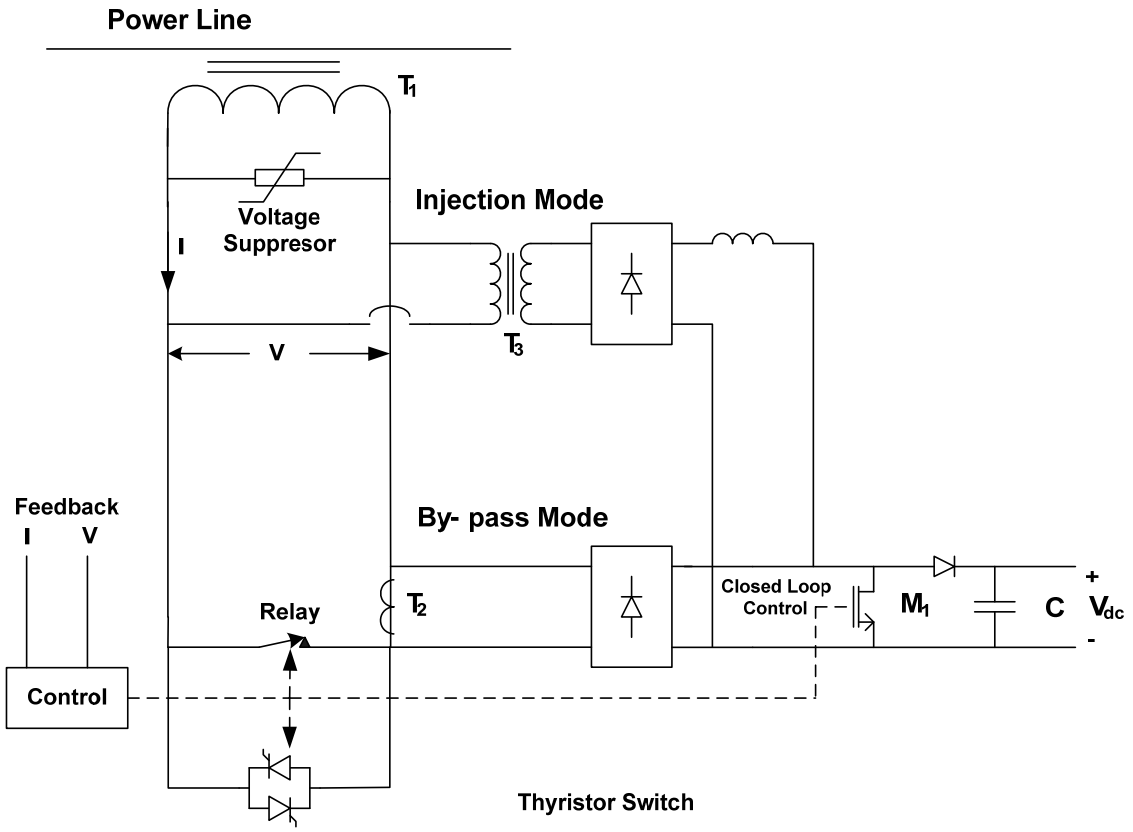

Figure 7.17 Integrated power supply schematic

Figures 7.18 and 7.19 show the transition of the module from injection mode to by-pass mode and vice versa, as it receives actuating signals from the micro-controller, which is a 8 bit PIC18F1320 MCU [62]. The code for micro-controller operation can be accessed from Appendix B. Details on control transformers and other power supply components are available in Appendix F.

Again, the test set-up of Figure 8.10 was used for conducting the experiment. A transition point of 300 A was selected between the by-pass and the injection mode. The power line current is seen to increase from 300 A to 400 A as the transition is made from injection mode to by-pass mode. This occurs because the injection level of DSR module

(50 µH) is comparable to the inductive load (120 µH) on the test set-up. The power line current is seen to vary as the total impedance on the circuit changes between the two modes.

The control signal for the transition is shown by the green line, which triggers the relay to go from closed (low) state to open (high) state. The relay transition is assisted by turning on the thyristors for 3 cycles during each transition. This helps to reduce voltage stresses across the relay and increase its operational life. A slight change is seen in the output voltage as the module transitions between the two modes. This is associated with a small shift in the reference voltage under injection mode of operation, which occurs because of the inaccuracies in the values of capacitors and resistors. Such a slight variation in the output DC voltage has no effect on the operation of the unit.

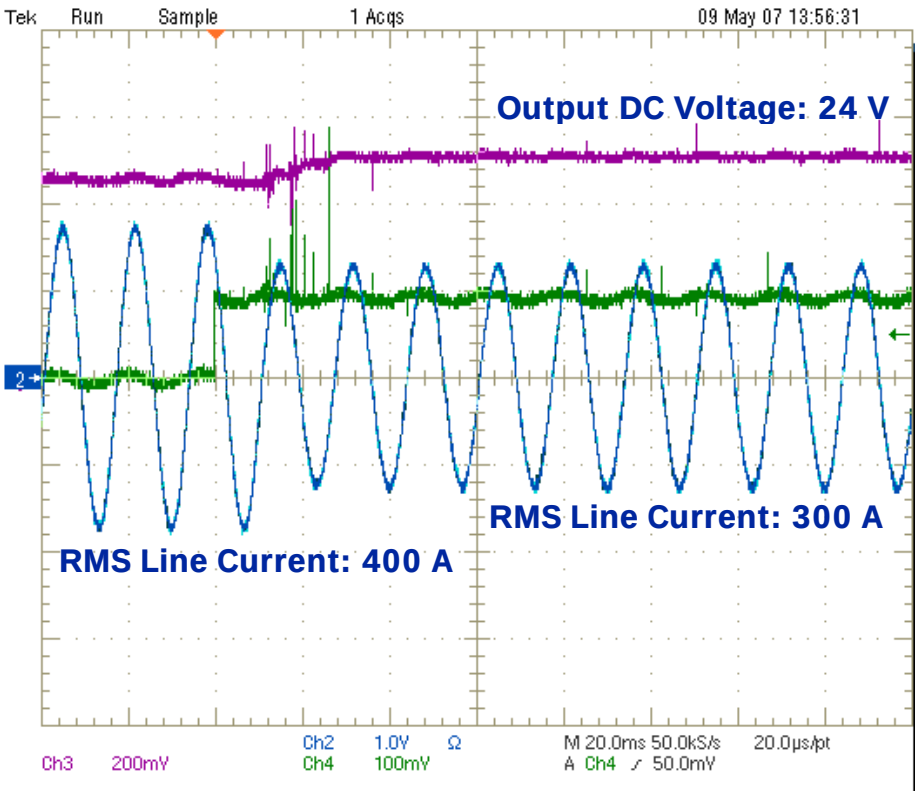

Figure 7.18 Module transition from by-pass to injection mode

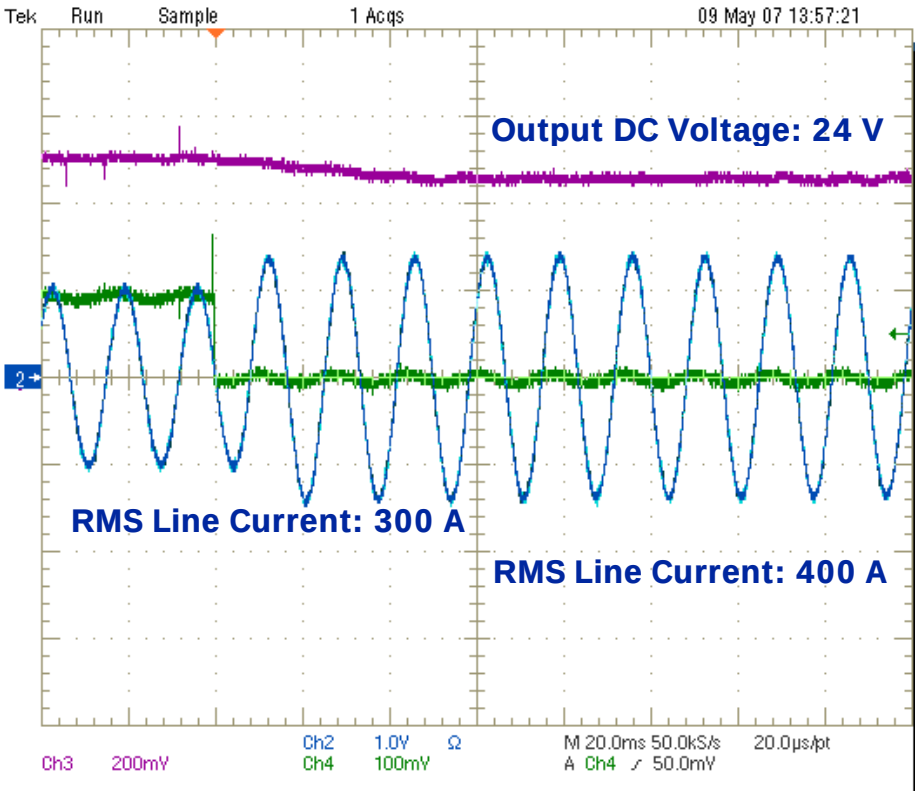

Figure 7.19 Module transition from injection to by-pass mode

7.4.4 Fault Management and Lightning Strikes

Fault currents can be as high as 50,000 A, which can cause big voltage spikes on the secondary winding of the transformer. These voltage transients can be damaging for the switches and control circuitry. Thus, it is desirable that the module switches over to by-pass mode, once a fault is detected. A thyristor-switch is used to quickly by-pass the module under such conditions. Saturation of the transformer also provides a benign layer of protection. Though undesirable under steady state conditions, transformer saturation aids in limiting the voltage induced on the secondary winding under high currents. However, one must be careful to take into account the voltage spike that may be generated as the transformer comes out of saturation, after the fault is cleared.

Figure 7.20 shows the simulation results during by-pass, normal injection and fault conditions for a DSR device. When a fault is detected, the system automatically switches over to by-pass mode. However, a large voltage-transient occurs on the secondary of the STT as this transition is made. Voltage suppressors will be provided across the secondary winding, as shown in Figure 7.17, to limit such transient voltages so as to protect the semiconductor switches, electronics, and the relay.

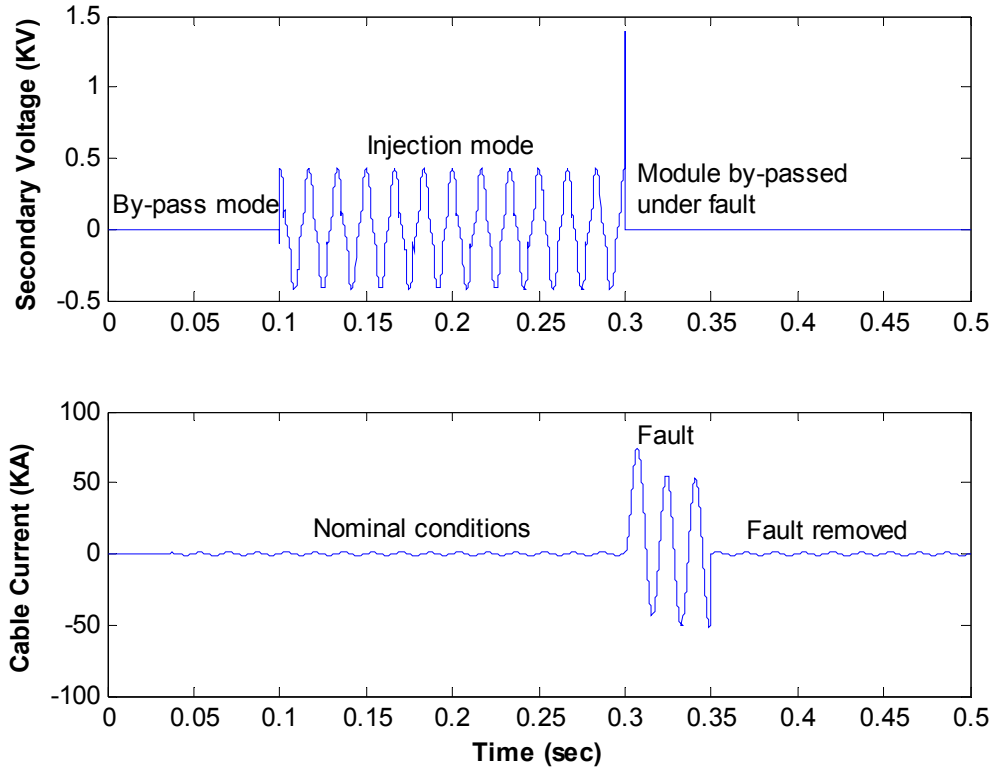

Figure 7.20 Module operation under by-pass mode, injection mode, and fault

A Secondary protection is also provided in terms of a break-over device, attached between the outer casing of the transformer and the cable. This provides an alternate path

for the current flow under fault conditions or lightning strikes. As shown in Figure 7.21, one end of the transformer is clamped at line voltage while the other end is insulated and a MOV is provided between the transformer casing and the power-line. When a large current flows through power-line, the MOV breaks-over. As a result, the line current starts flowing through the skin of the transformer, by-passing the unit. The skin of the module creates a Faraday shield, protecting the electronics.

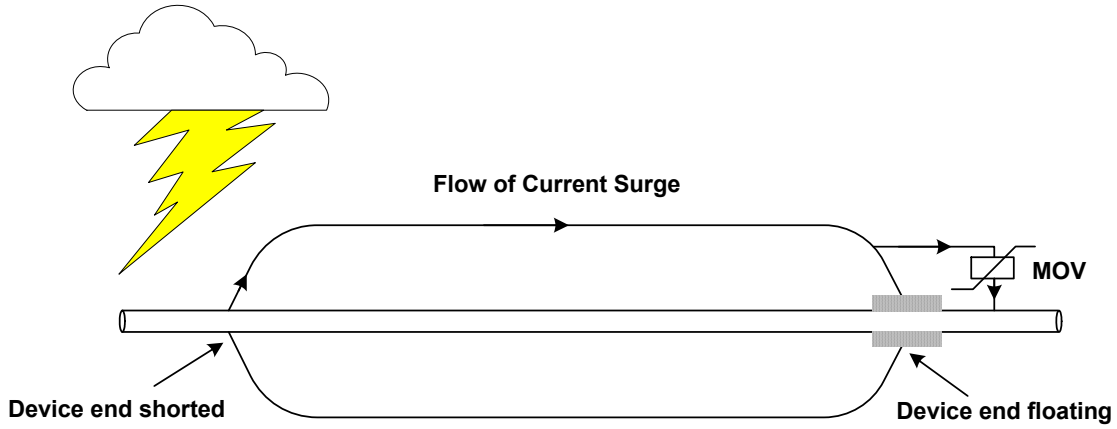

Figure 7.21 Use of a MOV to protect the module under lightning strikes

7.5 Mechanical Design

As the proposed technology has to operate in the harsh utility environment, a good mechanical design is deemed essential for the proper functioning of the unit. The mechanical design considerations have been outlined at the beginning of this chapter and are discussed in detail in the following sections.

7.5.1 Module Weight

The module is designed with a target weight of 120 lb, which is comparable to the mass of sag modifiers and de-tuning pendulums that are used on the transmission lines to correct line-sag and to reduce conductor-galloping. Table 7.10 shows the weight of the module in terms of individual components. The total estimated weight is seen to be within the threshold of 120 lbs.

Table 7.10 Weight of different components of a DSR unit

Component	**Weight (lb)**
STT Core	86.6
STT Winding	6
Switches and Control Circuitry (*estimated*)	7-8
Casing, Clamps, and Armor Rods (*estimated*)	15-18
Total	114.6 - 118.6

7.5.2 Conductor Damage

ACSR conductors are fragile and must be protected against damage during installation as well as during the operation of the DSR unit. Line guards or aluminum armor rods will be wrapped around the power-line before the module is clamped-on to prevent any damage to power lines. The additional strength provided by the line guards would also help to correct for mechanical fatigue, which is introduced by the weight of the DSR unit on the line.

Another important design consideration relates to limit the participation of the DSR modules with conductor motion. Examples of conductor motion are galloping during bird or ice jumps, excursions during turbulent winds, and oscillations under fault conditions. To limit the participation of DSR unit under such events, it is suggested to clamp the modules near transmission towers and on shorter line spans. Further, it is thought that the increased mass of the DSR unit will offset the increase in sail area, which would further be helpful to reduce conductor excursions and swings.

7.5.3 Corona Discharge

High electric fields can sometimes lead to ionization of the air, resulting in an electrical discharge; which is more commonly referred to corona. Corona can cause electromagnetic interference, audible noise and damage to insulating equipment. The probability of discharge is highest in the vicinity of sharp corners or edges. The casing of the module must therefore be designed to ensure that the electrical field around the edges is always less than the breakdown strength of the air.

Equation 7.10 gives the strength of electric field at a distance ‘r’ from a conductor that is operating at a voltage ‘V.’ For example, under an operating voltage of 161 kV, the electric field in the vicinity of a conductor can be as high as 1.835 kV/cm and can be an order of magnitude higher around sharp edges. The breakdown strength of air, under dry conditions, is 30 kV/cm [63]; implying an electric field of 30 kV/cm or greater would result in a corona discharge.

$$E = \frac{V}{r \ln\left(\frac{R}{r_0}\right)} \tag{7.10}$$

Here, R is the distance of the reference potential from the conductor and r_0 is the conductor radius

To identify corona hot spots, DSR unit was clamped on a high voltage transmission line. Figure 7.22 shows the schematic of the test set-up. The test was conducted in accordance with NEMA 107 for measurement of Radio Influence Voltage (RIV) of high voltage apparatus. Complete details about the test set up are available in Appendix G.

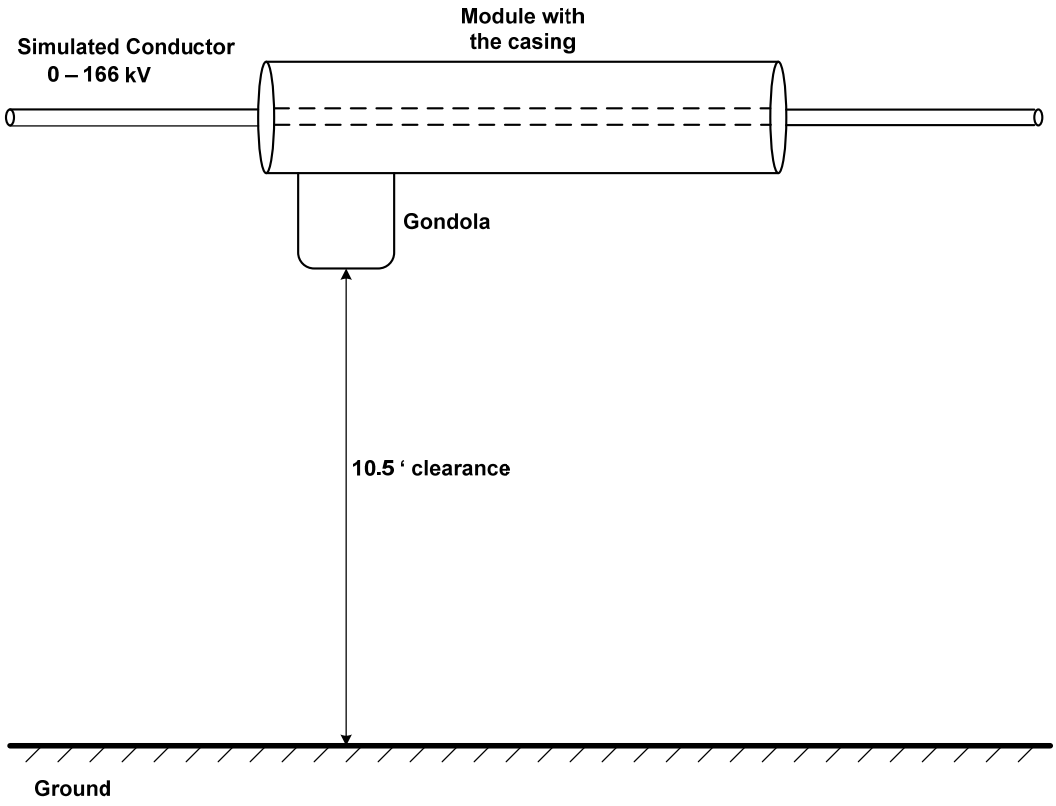

Figure 7.22 High voltage test set-up

The test voltage was varied from 35 kV – 166 kV. The inception of corona was first seen to occur at a voltage of 125 kV. Figure 8.23 shows the picture of the module at a line voltage of 166 kV. The bright spots show the occurrence of corona at these locations.

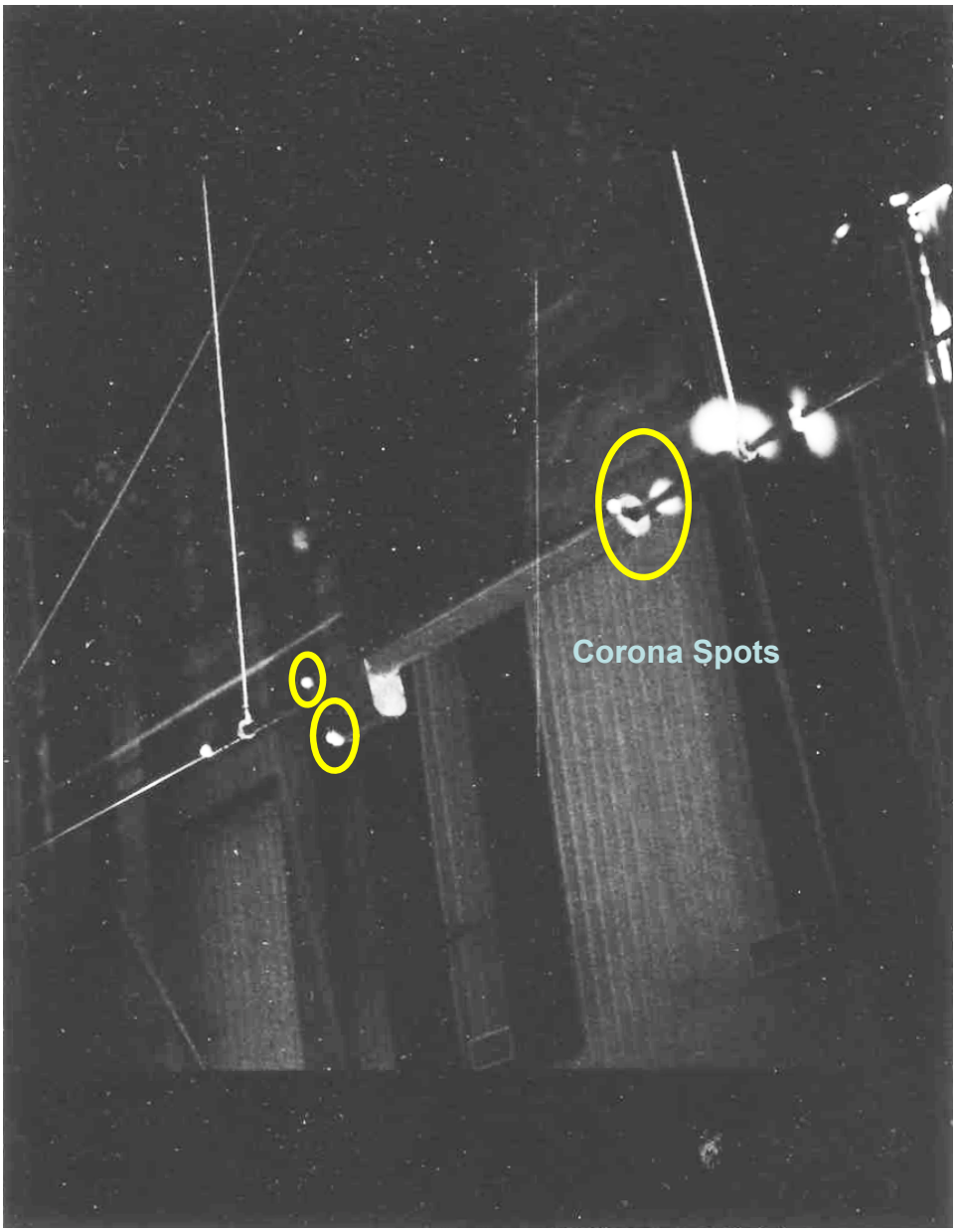

Figure 7.23 Corona spots near the edges of DSR module

Most of the corona is seen to occur at the line guards and at the ends of the hook up wire that was used to suspend the conductor. A few corona spots are also visible on the module. These are seen at the following locations:

1. Bolts at the end of the top housing on either side
2. At the bottom of the gondola that holds the electronics

The geometry at these locations will be revised to reduce the intensity of electric field strength. However, with the current module design, field testing at 138 kV is perceived to be possible, when the corona activity is just seen to initiate.

7.6 Conclusion

This chapter presents the details on the implementation of a DSR module. Each module is rated for 10 KVA, 750 A, based on the given system specifications and the weight constraint. At this rating, the injection from each module can change the line impedance by roughly 2% per mile. The electrical specification is fairly simple but all practical issues of implementation must be simultaneously handled. A detailed magnetic, electrical, and mechanical design is presented that addresses all the major considerations.

The magnetic design of the module is primarily governed by the magnetizing inductance of the single-turn transformer, which is designed to be 50 μH. The lamination design of the transformer is complicated by the special mechanical requirements of clamping around an existing power-line. The proposed laminations are in the form of two sectors of a circle with stampings near the outer edges, to hold the stack with bolts. The secondary winding of the transformer is designed to reduce the operating current and voltage to a level sustainable for the electronics and the switches. The wire size is

selected on the basis of fusing time of the insulation under fault conditions. The issue of heat transfer is very important and is discussed with a steady state thermal model of the system. Quantitative analysis on the mechanical forces impressed on the laminations and windings is also presented.

A self sustainable power supply is designed to meet the requirements of the electronics and the controls. The power supply is driven off-the-line, by the secondary current in the by-pass mode and open circuit (secondary) voltage in the injection mode. Experimental results indicate that a regulated DC power supply of 24 V, 10 W is available at all times. To protect the electronics during faults and lightning strikes, the module is rapidly by-passed and an external MOV provides an alternate path for the current through the casing of the module.

Important mechanical design considerations such as module weight, conductor damage during installation, and operation in high electric fields have been discussed. The mechanical design of the module will be augmented as further inputs become available from the field testing of the module. Alpha testing of the technology is planned at sub-transmission level (138 kV) and at distribution level (4 kV) for this year.

CHAPTER 8

CONTROLLING POWER FLOW ON SPECIFIC LINES

8.1 Introduction

The use of DSR modules has shown that current can be diverted in case of line overload. The broader problem is concerned with being able to control power flow through the lines so as to support market functions. Currently, the end user is indifferent between consuming electrons from carbon sources (‘black’ electrons) or from non-carbon sources (‘green’ electrons). The reason being that once an electron is dispatched from a generator, there is no control over how it flows and at which load point it gets consumed.

It is the role of public policy to look to the longer term, and to ensure that societal welfare is its overriding objective. For instance, reducing our dependence on oil becomes necessary, both from an energy security and sustainability perspective. This can be achieved through economic disincentives for carbon-generation through a carbon-tax or a carbon cap and trade policy. A fixed resource or scarce commodity typically experiences high price volatility (e.g. oil prices today). For instance, a ‘black’ electron produced from a coal generating plant, would be subject to constraints linked to Green House Gas (GHG) emissions, and may have very high marginal pricing as carbon limits were approached. On the other hand, a ‘green’ electron from a renewable resource would have no limits on generation or use, and could be supplied from a willing generator to consumer. However, this is difficult to accomplish in a real system today as it is not possible to control what path an electron takes once it enters the electrical network. This

then results in overloading and congestion along unintended paths, and creates a convoluted and poorly functioning market structure.

This chapter presents an approach for controlling the flow of electricity along a specified path or a pipeline between a generator and a consumer. In an oil pipeline, each molecule of oil can be tagged according to the grade: gasoline, kerosene, fuel oil, etc, and by ownership. Similarly, creating a pipeline flow of electrons would provide a mechanism for specifying and validating the path taken by 'green' electrons, enabling investments and market operation, allowing taxation of 'black' electrons, or incentivizing the consumption of 'green' electrons.

8.2 Controlling the Flow of Electrons

Power in a networked system flows along the path of least impedance. Thus, once the electrons are injected into the system by a producer, there is no control over the actual path taken by them to reach the end user. Figure 8.1 shows a diagram of power flow from Wisconsin to Tennessee. It shows that the related power flows as far away as Texas, and contributes to overloading of lines, loop-flows and congestion on a large number of unintended power lines. This dramatically demonstrates the issues surrounding lack of power flow control.

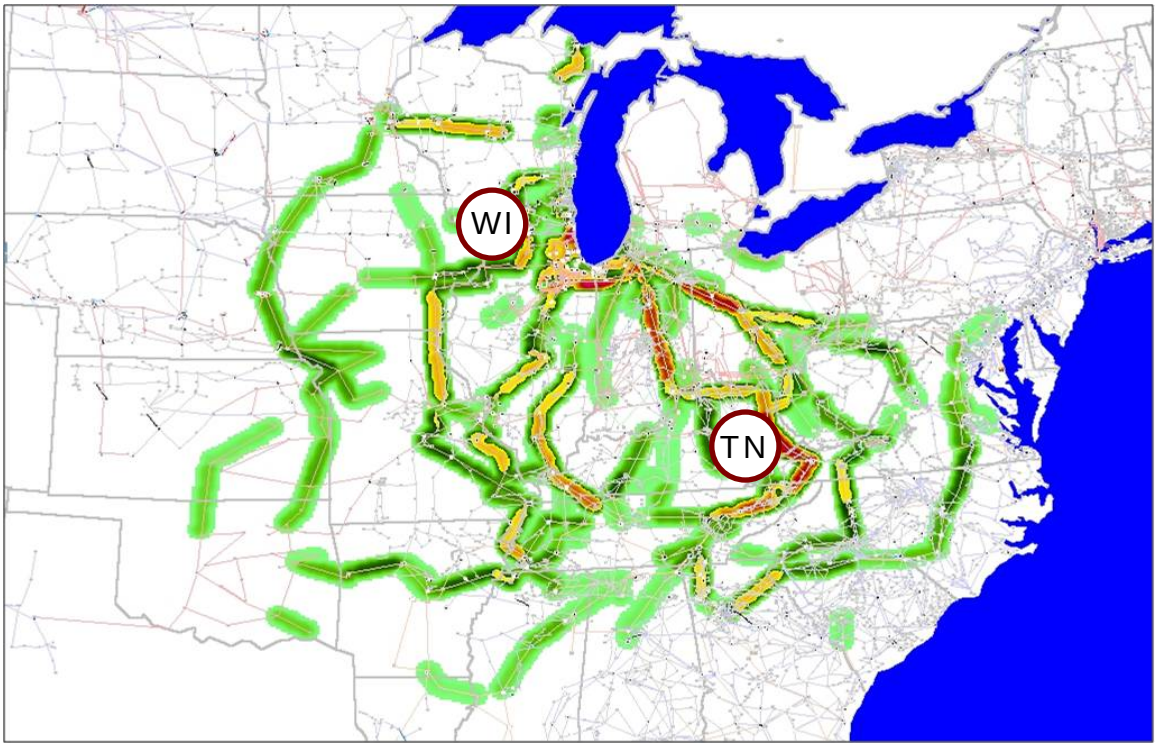

Figure 8.1 Power flow from Wisconsin to Tennessee[2]

Figure 8.2 shows an IEEE 39 bus system as a representative transmission/distribution network in which such a dispatch scenario has been simulated. In the example shown, Gen 6 (a 'green' provider) dispatches 3.4 MW of additional power to serve demand at the Load Bus. It is seen that with no controls only 0.34 MW actually reach the intended target. The balance, 3.06 MW flows through nine different transmission lines, as shown by the dark red lines in Figure 8.2, before getting consumed at different load points.

[2] Courtesy: Tom Overbye – Powerworld Corporation

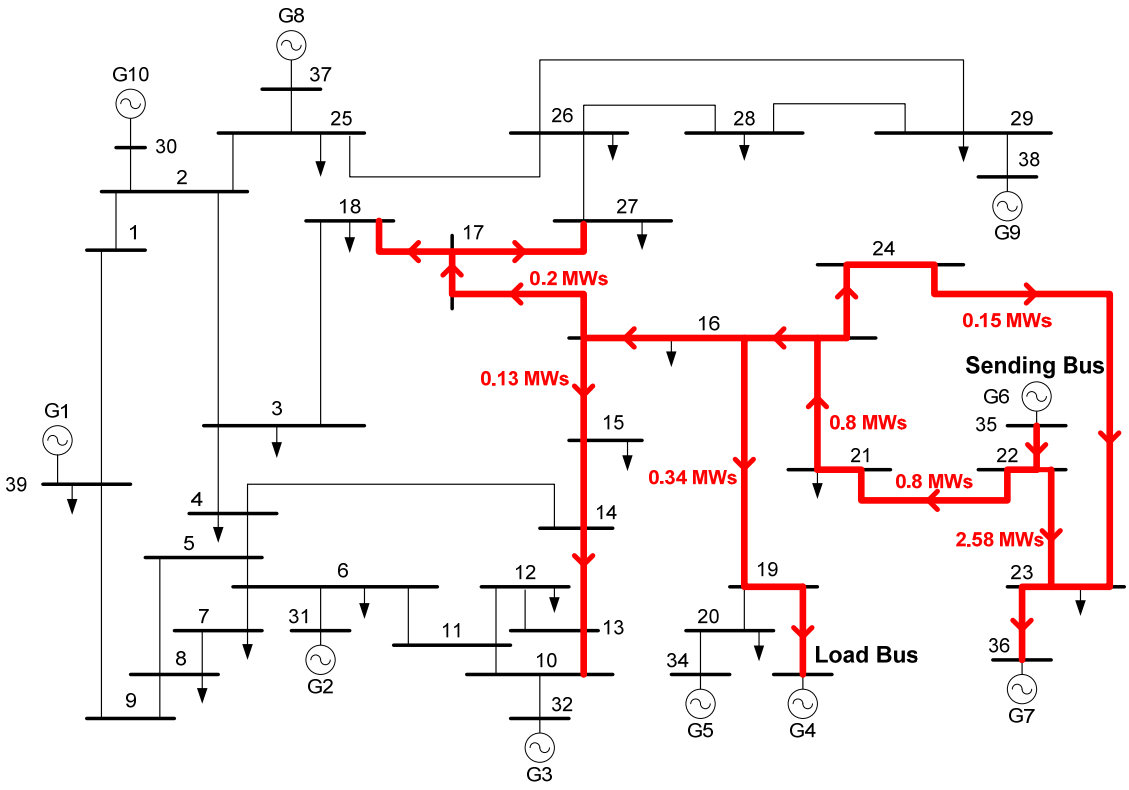

Figure 8.2 Line flows associated with 3.4 MWs of dispatch from Gen. 6

As current flows on a transmission path, additional voltage drop is caused along series line reactance, which changes the node voltages on the transmission path. As a result, the power lines branching out from these nodes see a different voltage gradient, causing a change in the current flow on these branches. Therefore, additional power pumped from a generator, which is intended to flow on a designated path, ends up flowing on all the branches of the transmission path.

To maintain power flow along a predefined path between a generator and a load, the transmission lines branching out from the path must be compensated to keep the same node voltages at the respective branch-out points. This would ensure that there is no

change in the potential gradient along the branches and thus no current would leak into them.

This is shown by way of an example in Figure 8.3. Let ΔI represent the additional electrons per second that need to be transported over the path. There are two branches, which divide the impedance of the path into Z1, Z2, and Z3. Further, assume that ΔV is the forcing function that is causing additional electrons to flow on the path. ΔV can result from a change in angle or magnitude of the generator voltage. It is also possible to cause additional current to flow on the path by decreasing the series impedance. The analysis would be similar. As ΔI flows through the path, it causes additional voltage drop across Z1, Z2, and Z3. This changes the node voltages at the two branch-out points by (ΔV - ΔI*Z1) and (ΔV - ΔI*{Z1+Z2}) respectively. To maintain a pipeline flow of electrons without any leakage, the two branches are compensated with series voltage injection, as shown in Figure 8.3. The voltage injections are of the same magnitude as the change in the respective node voltages, but of opposite polarity.

Several approaches are possible to realize series injection of voltage. DSR technology offers the simplest implementation, but can only provide reactive voltage compensation. Alternatively, the use of series injection voltage sources, such as Unified Power Flow Controller (UPFC) or a Controllable Network Transformer (CNT), can be used to inject fully controllable real and reactive voltage components into the line.

Further, as the system operating conditions change, the series injection must be altered to maintain the same node voltages at the branch-out points. A central command dispatcher and a communication infrastructure are required to realize such a controllable network, as shown in Figure 8.3. Sensing instruments on the branches transmit system

information, such as line current magnitude and phase angle to the central command dispatcher. The required injections are then calculated and transmitted back to the voltage sources. Power line communication is one possibility to realize a bi-directional communication infrastructure [64].

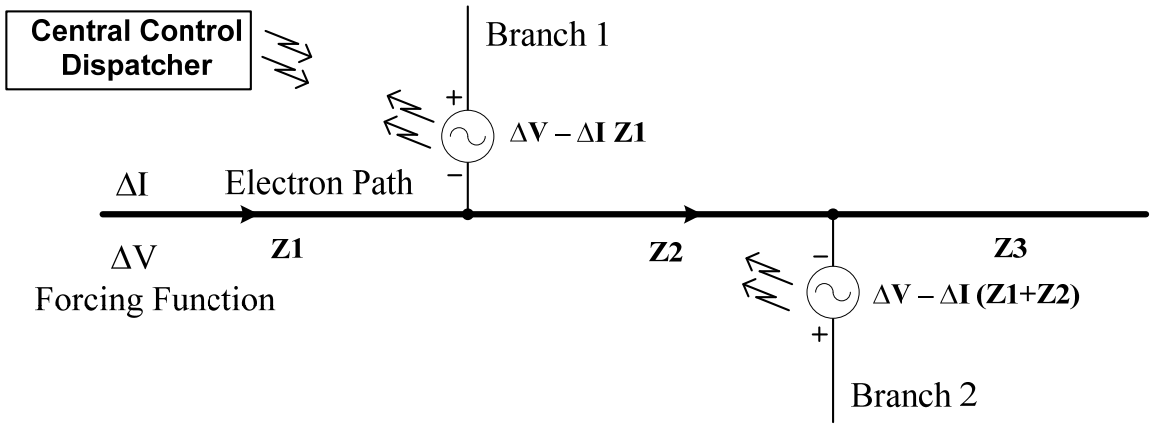

Figure 8.3 Branches with controllable voltage sources to realize a pipeline flow

8.3 Creating a Pipeline Flow of Electrons

Taking the same example of Figure 8.2, a path is now defined between the Sending Bus (Gen. 6) and the Load Bus, as shown in Figure 8.4. Node 22, Node 21, and Node 16, are the branch-out points on the defined path. Figure 8.4 also shows series compensators deployed on the branches emanating from these nodes. In the first scenario, DSR technology is used for series voltage compensation, as it is the simplest to implement. The series injection from DSR modules only compensate for the reactive voltage change at the respective nodes.

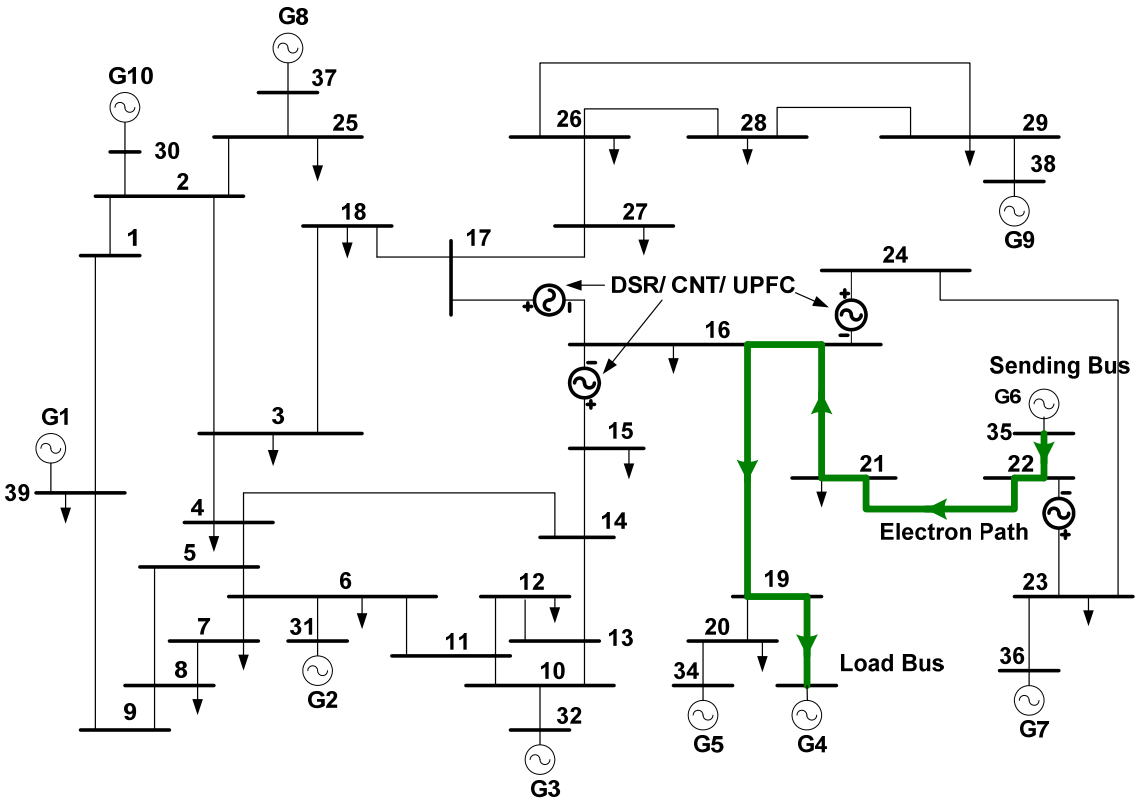

Figure 8.4 Directed flow path from Gen. 6 to Gen. 4

Table 8.1 shows the required series inductance and the MVAR for injection on each of the branches. The inductance is calculated by dividing the reactive component of the required voltage injection by the line current. The MVAR represent the control effort, which is essentially the reactive power consumed by the series inductance. The last column of the table shows the leakage power associated with each of the branches. A positive sign indicates power being leaked into the branch from the pipeline, while a negative sign signifies power being sucked into the pipeline from the branch.

In this case, 2.16 MW (or 63% of the dispatch) are seen to reach the Load Bus. The leakage of the rest 1.24 MW to the branches occurs because the series reactance only compensates for the reactive voltage at the respective nodes. The in-phase voltage change

at the respective nodes is left uncompensated. Although, a significant level of improvement is seen, as compared to the base case, high levels of leakage still occurs and limits the usefulness of this approach.

Table 8.1 DSR technology to realize a pipeline flow of electrons

Branches	**Injected Inductance (H)**	**Injected MVAR**	**Leakage Power (MW)**
Line 22-23	0.0846	0.059	+1.3
Line 16-24	0.246	0.0075	+0.08
Line 16-17	0.009	0.307	-0.46
Line 16-15	0.0119	0.213	+0.32

In the next scenario, a controllable voltage source, which can be implemented using a UPFC or a CNT, is used to control the node voltages to the desired magnitude and angle. Table 8.2 shows the voltage magnitudes and MVA required to realize a fully controllable path. The MVA is calculated as the product of the line current magnitude and the injected voltage magnitude, and it represents the control effort required for the series injection. In this case 3.05 MW dispatched from Gen. 6 reach the Load Bus. Lines losses are seen to constitute the residual 5% of the dispatch (~0.15 W). It must be noted that the loads connected at the branch-out points are left uncompensated. This is because the compensating voltages, show in Table 8.2, are much smaller than the load voltage (80 kV) and has virtually no effect on power drawn by the load.

Table 8.2 UPFC/CNT technology to realize a pipeline flow of electrons

Branches	Injected Voltage (kV)	Injected MVA
Line 22-23	2.22 ang(89.22^0)	0.095
Line 16-24	1.075 ang(88.5^0)	0.01
Line 16-17	1.075 ang(88.5^0)	0.32
Line 16-15	1.075 ang(88.5^0)	0.24

The results are summarized in Table 8.3. In the base case only 0.34 MW or 10% of the dispatched power flows along the designated path. The DSR technology helps to realize a partially controllable flow path and is able to steer 2.16 MW or 63% of the dispatched power along the specified path. Finally, the UPFC/CNT technology is able to realize a fully controlled pipeline flow, requiring only 0.665 MVA of control effort to deliver 3.4 MW of power.

Table 8.3 Summary of results

	Base Case	DSR Technology	UPFC/CNT Technology
MWs Dispatched	3.4	3.4	3.4
MWs Received	0.34	2.16	3.4
MVARs Injected	-	0.586	0.665

8.3.1 Controlling Multiple Pipeline Flows

In a real utility network with multiple generators and load points, multiple pipeline flows can co-exist that may share the same node(s) of the network. It must be demonstrated that these pipelines can be controlled independently and electrons can be

delivered verifiably from the designated generator to the designated load along the specified path. Figure 8.5 shows one such example with four energy transactions being satisfied simultaneously.

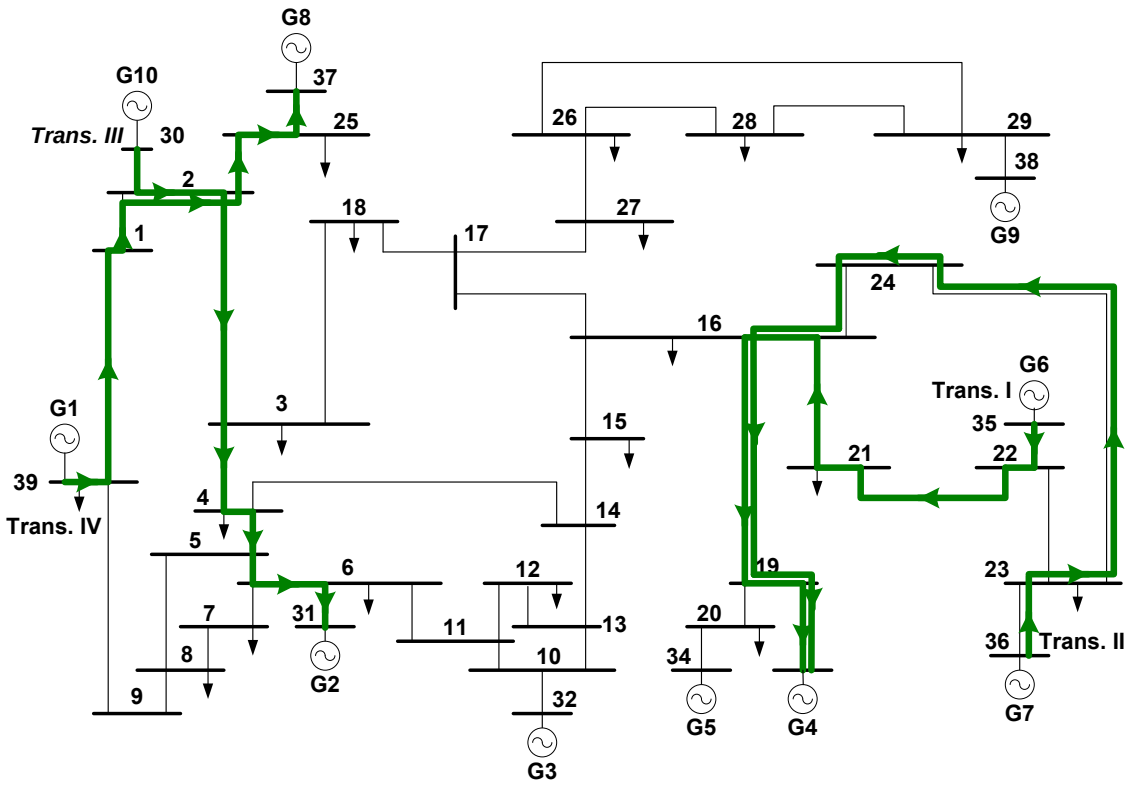

Figure 8.5 Four energy transactions/pipelines being simultaneously satisfied

Table 8.4 outlines the associated paths, generators, and loads with each of the transactions. Nodes 16, 19, and 33 are highlighted in blue color and are shared by Trans. I and Trans. II. Node 2 is highlighted in golden color and is shared by Trans. III and Trans. IV. Using the approach outlined in the preceding section, each of the transactions is controlled by injecting voltages on the branches of the designated transmission paths so as to keep the node voltages unaltered. The results are shown in Table 8.5.

Table 8.4 Transaction details

Transaction #	Generator Bus	Load Bus	Designated Path
Trans. I	35	33	22_21→21_16→16_19→19_33
Trans. II	36	33	36_23→23_24→24_16→16_19→19_33
Trans. III	30	31	30_2→2_3→3_4→4_5→5_6→6_31
Trans. IV	39	37	39_1→1_2→2_25→25_37

Table 8.5 Summary of results on realizing multiple transactions

Transaction #	Transmitted Power (MW)	Voltage Injection (kV)	Total Control Effort (MVA)	Performance Index
Trans. I	3.4	22_23: ***2.2 ang(89.2^0)*** 16_24: ***1.1 ang(88.5^0)*** 16_17: ***1.1 ang(88.5^0)*** 16_15: ***1.1 ang(88.5^0)***	0.665	5.1
Trans. II	2.7	22_23: ***2.5 ang(89.1^0)*** 16_21: ***0.8 ang(88.3^0)*** 16_15: ***0.8 ang(88.3^0)*** 16_17: ***0.8 ang(88.3^0)***	0.85	3.2
Trans. III	2.7	2_1: ***2.4 ang(83.2^0)*** 2_25: ***2.4 ang(83.2^0)*** 3_18: ***1.7 ang(83.5^0)*** 4_14: ***0.7 ang(83.4^0)*** 5_8: ***0.2 ang(82.7^0)***	1.0	2.7
Trans. IV	2.1	*39_9*: ***2.5 ang(79.9^0)*** *2_30*: ***0.4 ang(50.8^0)*** *2_3*: ***0.4 ang(50.8^0)***	0.46	4.5

Table 8.5 presents the MW transmitted over each path and the corresponding control effort required. The last column specifies the performance index for each of the four transactions, which is measured as the ratio of transmitted MW to the total control effort (MVA) required. A higher performance index greater than one indicates that for

each MW transmitted over the 'pipeline,' the total MVA required from the controllable voltage sources is less than one; suggesting a higher benefit to cost ratio. It can be seen that for all four transactions the performance index is around 3-5, implying that pipeline flows can be realized at a much smaller control effort.

8.3.2 Generic Formulation for Branch Injections

The discussion can be generalized to control 'N' transactions that share one or more buses/nodes of the network. Figure 8.6 shows one such scenario, where 'N' electron pipelines pass through a common node. A generic equation is formulated for the required injections on the branches emanating from the common node so as to realize pipeline flows on all of the 'N' paths.

To begin the formulation, let's assume that only one energy transaction is being handled and that is through Path 1. The electron flow on this path results in a voltage change of 'V_1' at the common node. Therefore to realize a pipeline flow through Path 1, without any leakage, all the other branches emerging from the common node must be series compensated with a voltage 'V_1.'

Next, a second energy transaction is allowed through Path 2, which causes an additional voltage change of 'V_2' at the common node. Now to realize pipeline flows through the two paths, Path 1 must be compensated with voltage 'V2,' while Path 2 should be compensated with voltage 'V1,' and all the remaining paths should be compensated with voltage 'V1+V2.' The summation here refers to a vector sum of the two voltages.

Following the argument, if 'N' energy transactions are allowed to share a common node, then each of the branches emanating from the node must be compensated with a voltage that is the vector sum of the voltage changes seen at the node by the electron flow on all the other pipelines. A generic formula for injection on each of the branches is presented by equation (8.1).

$$V_{i^{th}branch} = \sum_{j=1; j\neq i}^{N} V_j \tag{8.1}$$

Here, $V_{i}^{th}{}_{branch}$ refers to total voltage injection on ith branch, V_j is the voltage change caused by the electron flow on the j'th path, and subscripts j and i refer to the different branches emanating from the node.

In a targeted application, say providing power from a renewable source in Iowa to Chicago, one can identify lightly loaded line(s) and provide the control effort required to channel the desired power flow. The investments would be fully controlled, and would not provide broad benefits to other users. Further, the ability to provide verified 'green' electrons with no carbon limits can open up new markets. For instance, electric or plug-in hybrid cars fueled from such 'green' electrons would have no limits on their use.

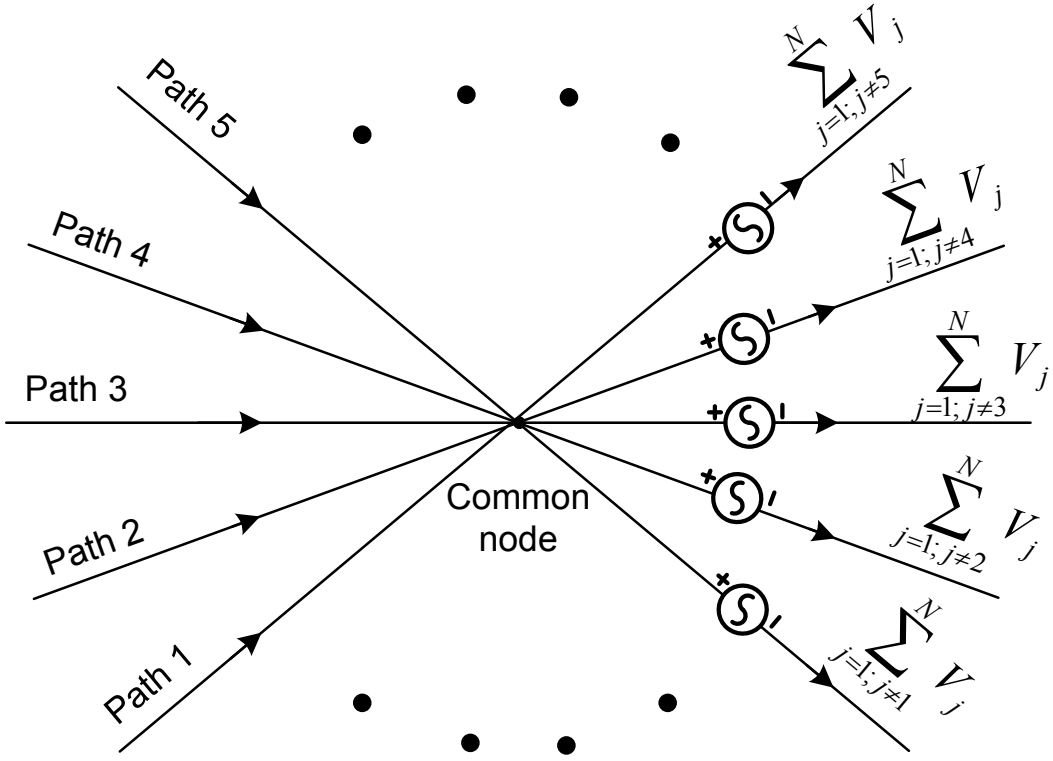

Figure 8.6 Realizing 'N' pipeline flows that share a common node

8.4 Conclusion

As the society transitions towards a sustainable energy, the electricity grid will become the primary preferred energy delivery infrastructure. The ability of the grid to accommodate a variety of flexible non-carbon generation sources ranging from solar, wind, hydro, and nuclear and to integrate demand management and load control provides unprecedented ability to coordinate operations across large geographical regions. A carbon cap and trade policy is imminent as a measure to curb GHG emissions, to wean society from over-use of irreplaceable fossil fuels, and towards a more sustainable future.

In such an environment, ‘green’ electrons from non-carbon sources such as hydro, wind or solar will have no limitation on their generation or use, and will have a higher value than ‘black’ electrons from fossil fuel burning generators.

A new technique is presented by which power-lines on the existing grid can be turned into ‘pipelines,’ causing specified electrons to flow along a specified contract path. To realize a sustainable energy infrastructure, policy changes are imminent that will shape consumer demand for higher utility from consumption of ‘green’ electrons. The approach presented here provides a tool for implementation of such an energy infrastructure, allowing system operators to track the delivery and consumption of ‘green’ electrons on the network.

CHAPTER 9

CONTRIBUTIONS AND FUTURE WORK

9.1 Introduction

The work in this thesis introduces a new technology that can improve the capacity and reliability of the existing grid. The technology is intended to realize a controllable transmission and distribution network that can steer the flow of current form the overloaded lines to the under-utilized lines.

The core of the technology is based on the concept of power flow control through change of the series line reactance. A distributed model makes the system practically feasible, at a lower cost and with high reliability. Various power flow controllers have been proposed in the past but have had limited penetration in the market, primarily because of their high cost, low reliability, and long build and repair times. Distributed Series Reactance (DSR) devices are seen to potentially overcome the shortcomings of the conventional power flow control devices.

9.2 Conclusions

9.2.1 Development of a Distributed Modular Solution

A distributed modular solution is proposed that uses low cost components and can increase system transfer capacity dramatically, using only local current measurements and without any communications. The distributed nature of the solution offers higher reliability as the failure of a single component or even a complete device is seen to have

limited impact on the overall functionality of the solution. The cost of the technology is lower, as off-the-shelf components can be used to meet the rating of the individual controllers/devices and can be further scaled down with volume production. The module is self-powered off the power line and operates autonomously without any centralized control or communication.

9.2.2 Homeostatic Control Strategy for System-wide Implementation

A strategy is proposed to control large number of distributed modules on the power grid. The proposed controller allows the DSR modules to reach the desired state asymptotically over time, without the need of communications. The implementation is simple as the feedback to each individual controller is based on local measurement of line current. Identical controller is used for all the DSR modules on a power line but with different switching values of line current.

The controller calculates the desired injection at each sampling instant, based on the measured line current and then self-adjusts the injection rate according to an exponential time decay function. In this way, at each sampling instant the rate of injection is updated, allowing the controllers to adjust their actions according to the dynamics of the system. At a system level, DSR modules can be switched in a coordinated manner, without any line interactions. An important design parameter is the time constant of the exponential estimator, which is designed to be much larger than the sampling time period; otherwise the controller might not able to vary the injection in sympathy with the changes in line current.

9.2.3 Unlocking Unused Grid Capacity and Improvement in System Reliability

DSR technology has been shown to increase the transfer capacity and reliability of a system by automatically diverting current flow from congested parts of the network to underutilized lines of the network. Benchmark studies on a four bus and the IEEE 39 bus system have depicted that DSR modules are effective in increasing the capacity of a networked system by as much as 33% from the base capacity. As the DSR modules redistribute the current through the system, utilization of the existing lines is also seen to increase. Without the use of DSR technology, additional transmission lines would be required to reinforce the capacity of the system. However, this does not promise an increase in the utilization of the lines of the system.

Another important aspect of the DSR modules is the capability to automatically and dynamically redistribute the line current under unanticipated contingencies. The DSR modules make the network 'self-healing' by allowing the system to share the overload and settle to a new operating point. While a significant number of papers have discussed the desirability of 'self-healing' networks, this is possibly the first example of an autonomously operating 'self-healing' network. Studies on Staten Island distribution grid confirmed that reasonable level of injection can secure system operation and reliability under (N-X) contingency conditions and can alleviate a cascading failure.

Performance of the DSR technology is topology-dependent and this has a very important economic bearing on the system. When the planning studies predict a change in the topology or operating conditions of the system, DSR modules can be redeployed on the system to extract maximum benefits at a lower cost. Reconfigurable investment

opportunities can change the dynamics of the current transmission market and help to create investment opportunities for DSR technology.

9.2.4 Economic Benefits and Market Impact

DSR is a low cost technology that allows the possibility of incrementally increasing the transmission capacity of a network in the short run and at a low cost. Investment behavior of the utilities is based on long term planning for building additional transmission lines, which usually takes years. With DSR technology, market dynamics can be shrunk to days and even to hours, allowing the possibility of short run congestion relief, dynamic contract management, and improving market efficiency.

In a regulated market environment, increase in societal welfare forms the basis of any policy initiative. Increased societal benefits in terms of lower consumer prices and increased market efficiency can be realized from the DSR technology. Simulation studies on the IEEE 39 bus system indicate that the cost of relieving congestion through DSR is much smaller than by building additional transmission lines. However, the current regulated market structure does not suggest how transmission investments for DSR technology can be supported. Some possible public finance mechanisms are suggested that can be used to create a market for such an advanced transmission technology.

9.2.5 Module Design to Minimize Interference with System Operation

Anticipated interactions between the operation of DSR modules with that of the power system have been discussed and design solutions are proposed to minimize interference with the two.

System voltage profile is seen to droop with the use of DSR modules. However, DSR technology operates with a very high initial performance index and can realize the required gains with small series compensation. Simulation studies on the four bus and the IEEE 39 bus system indicate that most of the bus voltages are seen to remain in the acceptable voltage regulation band when the DSR modules increase the system capacity by 33%. Further, it was shown that load voltage regulation under series injection could be easily be solved by coordinated shunt VAR injection.

DSR modules are programmed to by-pass quickly once a fault is detected, so that the protective relaying can operate with nominal system parameters. Experimental results indicate a by-pass time of 600 μsec, which is seen to be much faster than the operation time of conventional power system relays. This suggests that no interference will be seen between the operation of DSR modules and the distance protection relays. The by-pass of the DSR modules under fault conditions also indicates that there will be no degradation of the transient stability of the system. Simulation studies on the four bus system show that DSR modules only impact the settling time of the faulted system. The transient stability is seen to remain unaffected.

9.2.6 Prototype Development and Experimental Validation

The DSR module is designed for 10 KVA, 750 A, based on the given system specifications and the weight constraint. At this rating, the injection from each module can change the line impedance by roughly 2% per mile. A detailed magnetic, electric, and mechanical design is outlined to address all major considerations of operation in a utility environment.

The magnetic design of the module is primarily governed by the magnetizing inductance of the single-turn transformer, which is designed to be 50 μH. The lamination design of the transformer is complicated by the special mechanical requirements of clamping around an existing power-line. The proposed laminations are in the form of two sectors of a circle with stampings near the outer edges, to hold the stack with bolts. The secondary winding of the transformer is designed to reduce the operating current and voltage to a level sustainable for the electronics and the switches. The wire size is selected on the basis of fusing time of the insulation under fault conditions. The issue of heat transfer is very important and is discussed with a steady state thermal model of the system. Quantitative analysis on the mechanical forces impressed on the laminations and windings is also presented.

A self sustainable power supply is designed to meet the requirements of the electronics and the controls. The power supply is driven off-the-line, by the secondary current in the by-pass mode and open circuit (secondary) voltage in the injection mode. Experimental results indicate that a regulated DC power supply of 24 V, 10 W is available at all times. The module is controlled to switch from by-pass mode to injection mode based on the secondary voltage and current signals, eliminating the need for a separate current transformer on the power line. Power electronics is designed to sustain a variable transition point between the by-pass and injection mode. To protect the electronics during faults and lightning strikes, the module is rapidly by-passed and an external MOV provides an alternate path for the current through the casing of the module.

Important mechanical design considerations such as module weight, conductor damage during installation, and operation in high electric fields have been discussed. The corona activity is just seen to initiate at a voltage of 125 kV, and it is perceived that a field testing of the module is possible at such voltages. Alpha testing of the technology is planned at sub-transmission level (138 kV) and at distribution level (4 kV) for this year.

9.2.7 Creating a Pipeline Flow of Electrons

A technique is presented through which power-lines on the existing grid can be turned into 'pipelines,' causing specified electrons to flow along a specified contract path. DSR technology is proposed as a cost effective and simple approach, but can only realize a partially controllable path for electron flow. A fully controlled pipeline flow of electron flow can be realized through UPFC or CNT technologies that are capable of providing both real and reactive voltage compensations.

To realize a sustainable energy infrastructure, policy changes are imminent that will shape the consumer demand for higher utility from consumption of 'green' electrons. Creating a pipeline flow of electrons would provide a mechanism for specifying and validating the path taken by 'green' electrons, enabling investments and market operation, allowing taxation of 'black' electrons, or incentivizing the consumption of 'green' electrons.

9.3 Contributions

A paper titled "Current Limiting Conductors: A Distributed Approach for Increasing T&D System Capacity and Enhancing Reliability", was published in the *IEEE*

T&D Conference and Exposition 2005/06. This was the preliminary paper that presented DSR modules as a low cost solution to improve system utilization and reliability.

Another paper titled "Distributed FACTS: A New Concept for Realizing Grid Power Flow Control", was published in the *IEEE Power Electronics Specialist Conference* in June 2005. This paper received the best paper prize award in the conference and has been published in the *IEEE Transactions on Power Electronics*.

A third paper, based on the design of DSR system was published in the *Industrial Applications Society Conference* in October 2005. The paper is titled "Design Considerations for Series Connected Distributed FACTS Converter", and has also been published in the *IEEE Transactions on Industrial Applications*.

The research outlined in chapter 3, 4, 5, and 7 is submitted as a two series paper to *IEEE Transactions on Power Deliver*. The first paper is titled "Implementation and Operation of DSR Modules: Part I." This paper outlines the control strategy and module design to minimize interference with the system operation. The second paper is titled "Implementation and Operation of DSR Modules: Part II." This paper outlines details of the magnetic, electric, and mechanical with experimental validation under specified operating conditions.

Based on the research outlined in chapter 6, a paper titled "Economic Impact of Real-time Incremental Changes in Line Capacity," has been submitted to the *IEEE Transactions on Power Delivery*. Another paper titled, "From Power Lines to Pipeline: Creating a Sustainable Energy Infrastructure," will be submitted to *IEEE Transactions on Power Electronics*. This paper is based on the research presented in chapter 8.

The contributions of the proposed research, as a new power flow control technology are summarized as below:

- Development of a distributed modular solution that operates at a lower cost, higher reliability, with minimal power electronics, and without the need of communications.
- Proposed a strategy to control large number of distributed modules and minimize line interactions
- Demonstrated the efficacy and impact of DSR modules on real scale complex systems
- Proposed design solutions to allow DSR modules to operate with minimum interference to system operation
- Design of a module to realistic specifications (138 KV/1000A) and experimental validation under specified utility operating conditions.
- Understood the impact of DSR modules in simplified but realistic market conditions and proposed public finance mechanisms to create investment opportunities for the technology.
- Proposed a technique to control the flow of electrons on designated paths, to facilitate electricity contract management between a specified generator and a specified consumer.

9.4 Recommendations for Future Work

The research presented in this thesis advances a new concept of improving asset utilization and reliability of a power system. The proof of concept has been shown with simulation studies on realistic power networks. A detailed design and experimental

validation of the module is also presented. However, further research work is required on various aspects of the technology.

9.4.1 Mathematical Proof for the Optimality of the Proposed Control Strategy

It has been shown that the proposed control strategy gives better response with no overshoot or transient oscillations even when large numbers of modules operate simultaneously. The controllers approach the desired objective asymptotically over time, giving the necessary damping required for a stable response. However, no mathematical proof has been included in the document that verifies that the proposed control strategy is optimum for this application. Investigation of a similar control strategy is required, exploring the conditions under which instability can be initiated.

9.4.2 Transient Stability Studies on Utility Network

Simulation studies on the four bus system have shown that the DSR technology has no impact on the transient stability, with the only visible effect on the settling time of the system. Transient stability studies are specific to the operating conditions of the system. As a part of the pilot study of DSR modules on the Staten Island distribution grid, simulation studies must be performed to assess the affect on transient stability of the network.

9.4.3 Improving Mechanical Design of the Module

Mechanical design of the module was based primarily on keeping the total weight of the module within 120 lbs and to minimize corona activity. The first pass of the design has met these criteria to a reasonable extent. However, the design must be augmented to reduce corona activity further around the sharp edges of the gondola. Another important criterion that needs to incorporated into the design of the casing is to provide an easy exit path for the water that enters the unit. It is impossible to provide complete sealing against seepage of water into the module and therefore the only way to protect the electronics and the transformer against moisture is to make sure that whatever water enters into the unit also leaves it.

9.4.4 Module Re-design for Distribution Voltage Application

The module has been designed for overhead conductors for sub-transmission voltages at 138 kV. As the field testing of the technology is being proposed at 4 kV level for the Staten Island distribution grid, the module must be re-designed for the particular application. Preliminary discussions have suggested that a pole mounted design would best suit the application. A design blueprint is shown in Figure 9.1. Four series connected transformer modules, each rated for 38 kVA, will be used in each pole to give a total series injection of 152 kVA. Three such pole mounted units will be required per phase.

Two wires pass through a disconnect switch and series connect the primary side to the power line, as shown in Figure 9.1. On the secondary side, two sets of wires from the high side of each 38 kVA transformer unit will connect to protection devices and controls. Disconnect switch, relays, thyristor pairs, MOVs, and control will be placed in

housings on the casing of the pole-type transformer. The design is in the preliminary stages as further details are being made available from the utility engineers.

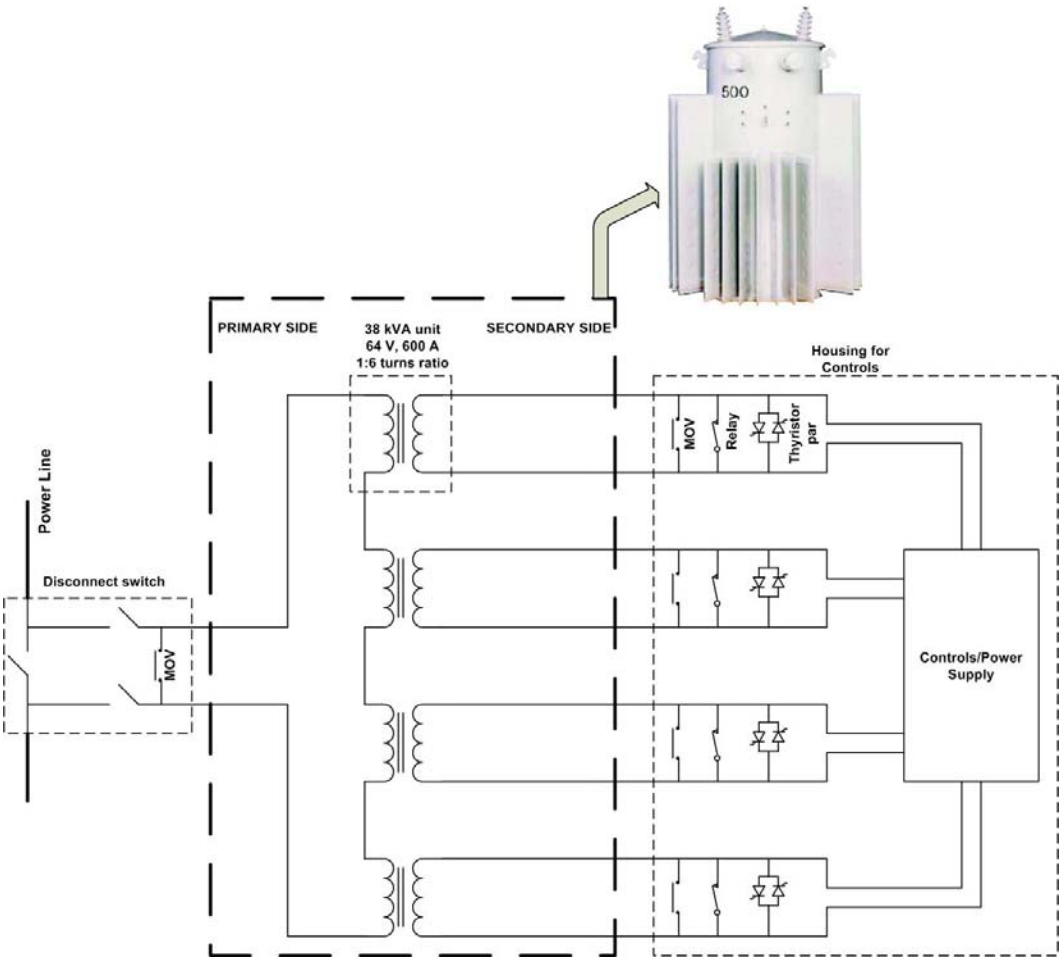

Figure 9.1 Pole-type transformer design for 4 kV grid

9.4.5 Creating a Market for DSR by Converting Power Lines to Pipeline

Controlling the flow of electrons on a designated path can help to create a market for DSR technology on the lines of how cellular companies or the oil pipeline markets operate. Creating a pipeline flow for electricity provides a mechanism for tagging the

electrons as ‘green’ or ‘black.’ Electric or plug-in hybrid cars fueled from such ‘green’ electrons can open up new markets. Business case needs to be developed that can be adopted into the current semi-regulated market environment, which will help utilities and independent business entities to initiate and participate in the investment activity.

9.5 Concluding Remarks

DSR technology is a step towards creating a sustainable T&D infrastructure and an efficient market design for the US power industry. Incremental changes over the existing legacy investments to realize improvement in system performance is the philosophy outlined in this thesis. All major industrial sectors are seen to be moving towards distributed systems; satellite networks in cell phone industry, cluster computing in IT industry, etc. The commercial success of these sectors can be attributed to the increased reliability and availability of operation, and reduced cost of operation. It is envisioned that a distributed power flow controller will also help to enhance control and operation of power system and realize the objective of restructuring that began more than a decade ago.

APPENDIX A

FORTRAN CODE FOR IMPLEMENTING EXPONENTIAL ESTIMATOR

```
        Irms = sqrt(60*Ir)


!       Initialize Controller
        ************************************************

        If ($Time.EQ.0) then
                $L2 = 0.000000001
                ind_prev = 0.000000001
        endif
!       Discrete Inductance Injection Following a Exponential Curve
!
        subroutine Controller_Line2($Ia,$L2,$Time)

        real                                    :: $Ia,$L2,$Time
        integer, parameter                      :: n_samples=667
        real, parameter                         :: Ts =25*0.000001
        real, parameter                         :: Lf = 0.0005
        real, parameter                         :: I0 = 0.7
        real, parameter                         :: It = 0.8
        integer, parameter                      :: device_num = 2


        real                                    :: Ir,Irms,inj,ind,ind_prev,ind_dig
        integer                                 :: a,b,c,step,counter,step_check,check
        real                                    :: devices_on,device
        real, dimension(n_samples)              :: Iin


!       Variable Initialization
        ***********************************************
        data step /0/
        data counter /0/
        data step_check/1/
        data check /1/
        data inj /0.000001/
        data ind_prev /0.0000001/
        data ind /0.00000001/
        data ind_dig /0.000001/
        data devices_on /0/
        data device /0/


        if ($Time==0.0) then
        do a =1,n_samples,1
        Iin(a) = 0.0
        end do
        end if

        do b = 1,n_samples-1,1
        Iin(n_samples-b+1) = Iin(n_samples-b)
        end do
        Iin(1) = $Ia


        Ir = 0
        do c = 1,n_samples,1
        Ir = Ir + (Iin(c)*Iin(c)/40000)
        end do


        Irms = sqrt(60*Ir)


!       Initialize Controller
        ************************************************

        If ($Time.EQ.0) then
                $L2 = 0.000000001
                ind_prev = 0.000000001
        endif
```

```
!       Induce Injection with an Exponential Profile
        ********************************************
        if ($Time.GT.0) then

                if (step.LT.(step_check+200)) then
                        if ((Irms.LE.0.8).AND.(Irms.GE.0.7)) then
                                inj = ((Irms-0.7)/(It-I0))*Lf
                                ind = (inj-ind_prev)*(1-exp(-10*((counter-step_check)*Ts))) + ind_prev
                                devices_on = ind/0.00005
                                devices_on = devices_on - mod(devices_on,1.0)
                                if (ind.GE.ind_prev) then
                                        if (mod(Irms*100,10.0).GE.1) then
                                                device = devices_on
                                        elseif (mod(Irms*100,10.0).LT.1) then
                                                if (devices_on.EQ.0) then
                                                        device = 0
                                                else
                                                        device = devices_on - 1
                                                endif
                                        endif
                                elseif (ind.LT.ind_prev) then
                                        if (mod(Irms*100,10.0).GE.9) then
                                                device = devices_on + 1
                                        elseif (mod(Irms*100,10.0).LT.9) then
                                                if (devices_on.EQ.0) then
                                                        device = 0
                                                else
                                                        device = devices_on
                                                endif
                                        endif
                                endif
                                if (check.EQ.0) then
                                        if (device.GE.device_num) then
                                                $L2 = 0.00005
                                        else
                                                $L2 = 0.000000001
                                        endif
                                endif


                        elseif(Irms.GT.0.8) then
                                inj = Lf
                                ind = (inj-ind_prev)*(1-exp(-10*((counter-step_check)*Ts))) + ind_prev
                                devices_on = ind/0.00005
                                devices_on = devices_on - mod(devices_on,1.0)
                                if (check.EQ.0) then
                                        $L2 = 0.00005
                                endif


                        elseif (Irms.LT.0.7) then
                                $L2 = $L2
                        endif
                        check = check + 1
                else
                        ind_prev = ind
                        $L2 = $L2
                        step_check = step
                        check = 0
                endif
        counter = counter + 1
        endif


        step = step + 1


!       open(21,FILE='L2.txt')
!       write(21,'(f12.6)')$L2


        return
        end
```

APPENDIX B

C CODE FOR MICRO-CONTROLLER OPERATION

```
#include        <p18f4520.h>
#include        <timers.h>
#include        <delays.h>
#include        <stdlib.h>
#include        <stdio.h>
#include        <string.h>
#include        <usart.h>
#include        <adc.h>
#include        <math.h>
#include        <usart.h>


//#define CLEAR_DISPLAY 0x01
#define size 0x064      // 100 samples per period
#pragma udata big_array
static long int volt[size];
#pragma udata

#define size 0x064      // 100 samples per period
#pragma udata big_array1
static long int volt1[size];
#pragma udata


void initializeADC1 (void)
{
OpenADC(ADC_FOSC_64 &
                ADC_RIGHT_JUST &
                ADC_4_TAD,
                ADC_CH1 &               // Channel 0 is anlalog input
                ADC_INT_OFF, 12);       // AN0,AN1,AN2 is analog; all other are digital
ADCON1 = 0x01;
}


void initializeADC2 (void)
{
OpenADC(ADC_FOSC_64 &
                ADC_RIGHT_JUST &
                ADC_4_TAD,
                ADC_CH2 &                // Channel 0 is anlalog input
                ADC_INT_OFF, 12);        // AN0,AN1,AN2 is analog; all other are digital
ADCON1 = 0x01;
}

void initializePORTB (void)
{
TRISB = 0;
PORTB = 0;
}

void initializePORTA (void)
{
TRISA = 1;
}

void initializePORTC (void)
{
TRISC = 0;
PORTC = 0;
}
```

```
void initializeUSART (void)
{
        // configure USART
        /* USART Transmit Interrupt OFF
                USART Receive Interrupt OFF
                USART in Asyncronous mode
                USART 8 bit 0 parity
                USART Continuous Receiving
                Baud Rate = High
                Baud Rate = 9600 */
        OpenUSART( USART_TX_INT_OFF &
                                USART_RX_INT_OFF &
                                USART_ASYNCH_MODE &
                                USART_EIGHT_BIT &
                                USART_CONT_RX &
                                USART_BRGH_HIGH,
                                25 );
}
/************************** main starts here **************************/

void
main (void)

{

        unsigned long int result = 0;   // Holds the conversion result of ADC
        unsigned long int result1 = 0;
        near long int ram *voltarray = &volt[0];
        near long int ram *voltarray1 = &volt1[0];
        unsigned long int temp=0;
        unsigned long int RMSS = 0;
        unsigned long int RMS = 0;
        unsigned long int temp1=0;
        unsigned long int RMSS1 = 0;
        unsigned long int RMS1 = 0;
        unsigned char i;
        unsigned char step=1;
        unsigned char step_check=1;

        unsigned int If = 32;
        unsigned long int If_sq = 94372; // 32*32*size
        unsigned int I0 = 28;
        unsigned long int I0_sq = 82208; // 28*28*size
        unsigned long int inj = 0;
        unsigned long int ind = 0;
        unsigned long int ind_prev = 0;

        unsigned int V = 0;
        unsigned int V_prev = 0;
        unsigned long int fault_slope = 100000;
        unsigned char fault = 0;
        unsigned long int slope = 0;
        unsigned int thy = 0;
        unsigned int rel = 0;
        unsigned int rel_flag = 0;
        unsigned int thy_flag = 0;


        unsigned char current_trig = 710; // (If^2-I0^2)/number of devices
        unsigned char Hyst = 4;
        unsigned long int Ihyst_upper = 3000000;        // (current_trig+Hyst/2)^2
        unsigned long int Ihyst_lower = 1000000;        // (current_trig-Hyst/2)^2
        unsigned char L = 0;
        unsigned char L_prev = 0;

        unsigned char clic = 0;
        unsigned int counter = 0;
        unsigned char flag = 0;
        unsigned char flag2 = 0;

        unsigned char unit_digit = 0;
        unsigned char one_tenth_digit = 0;
        char string1[] = "abc\r\n";
```

```
/********Initialization*********/
        for (i=0; i<size; i++)
        {
                voltarray[i] = 0;
                voltarray1[i] = 0;
    }

//      initializeADC();
        initializePORTA ();
        initializePORTB ();
        initializePORTC ();
//      putrsUSART((const far rom char *)"Working\r\n");
        L = 0;

        Delay10TCYx(8); // 16 usec of delay for the acquisition time of ADC

        i = size-1;
        while(1)
        {

/********ADC Conversion*********/
                initializeADC1();
//              Delay10TCYx(4);
                ConvertADC();   //Start AD Conversion
                while(BusyADC());       // Wait until conversion is complete
                result = ReadADC();
//              result = 200;
                CloseADC();


                initializeADC2();
                ConvertADC();
                while(BusyADC());
                result1 = ReadADC();
                V = result1;
                slope = fabs((V-V_prev)*6000);
                CloseADC();


/********Fault Detection*********/

if ((slope>fault_slope)|(fault==1))
{
        thy_flag=1;
                if ((thy_flag==1)) //Thyristor firing
                {
                        PORTC = 1;
                        thy = thy+1;
                        rel_flag = 1;
                        fault = 1;

                }
                else
                {
                        Delay10TCYx(2);
                        Delay1TCY();
                        Delay1TCY();
                        Delay1TCY();
                        Delay1TCY();
                        Delay1TCY();
                        Delay1TCY();
                        Delay1TCY();
                }


                if (thy==300)   // thyristor opened after 3 cycles
                {
                        thy=0;
                        PORTC = 0;
                        thy_flag = 0;
                        fault = 0;
                }
                else
                {
                        Delay10TCYx(1);
                }
```

```
                if ((thy==200)) // relay firing delayed by a cycle
                {
                        PORTB = 0;
                        rel_flag = 0;
                }
                else
                {
                        Delay1TCY();
                        Delay1TCY();
                        Delay1TCY();
                        Delay1TCY();
                        Delay1TCY();
                        Delay1TCY();
                        Delay1TCY();
                }
        V_prev = V;
        Delay100TCYx(5);
        Delay10TCYx(3);

}


/********RMS Calculation*********/
 if (fault==0)
{
                temp = voltarray[i];
                voltarray[i] = result*result;
                RMS = RMS + voltarray[i]-temp;
//              RMS = RMSS;  // pri. current sq {(5/1024)^2/0.0039^2/size}

                temp1 = voltarray1[i];
                voltarray1[i] = result1*result1;
                RMS1 = RMS1 + voltarray1[i]-temp1;

                if (i==0)
                {
                        i = size;
                }
                i =i-1;
/********Exponential Function*********/
                if ((RMS>7500000))  //7500000
                {
                        L = 1;
                        clic = 1;
                }
                else
                {
                        Delay10TCYx(1);
                }

                if ((clic==1)|(flag==1))
                {
                        flag = 1;
                        counter = counter+1;
                }
                else
                {
                        Delay10TCYx(1);
                        Delay1TCY();
                }

                if (counter>1000)
                {
                        counter=0;
                        flag = 0;
                        if((RMS1<3300000))
                        {
                                L = 0;
                                clic = 0;
                        }

                }
```

```
                else
                {
                Delay10TCYx(1);
                Delay1TCY();
                Delay1TCY();
                Delay1TCY();
                Delay1TCY();
                }

/********Trigger*********/

                if (((L==1)&(L_prev==0))|((L==0)&(L_prev==1))|(thy_flag==1)) //Thyristor firing
                {
                        PORTC = 1;
                        thy = thy+1;
                        thy_flag = 1;
                        rel_flag = 1;

                }
                else
                {
                        Delay10TCYx(3);
                        Delay1TCY();
                        Delay1TCY();
                        Delay1TCY();
                        Delay1TCY();
                }
                 if (thy==150)   // thyristor opened after 3 cycles
                 {
                         thy=0;
                         PORTC = 0;
                         thy_flag = 0;
                 }
                 else
                 {
                         Delay10TCYx(1);
                 }


                 if ((thy==5))   // relay firing delayed by a cycle
                 {
                         PORTB = L;
                         rel_flag = 0;
                 }
                 else
                 {
                         Delay1TCY();
                         Delay1TCY();
                         Delay1TCY();
                         Delay1TCY();
                         Delay1TCY();
                         Delay1TCY();
                         Delay1TCY();
                 }

        L_prev = L;

        }       //end of fault bracket
        }
```

APPENDIX C

SYNCHRONOUS GENERATOR MODELLING

Table C.1 Generator Parameters

Rated line-to-neutral voltage (Vt)	79 kV
Regulator time constant (Ia)	45 kA
Base angular frequency (w)	377 rad/sec
Inertia constant	1.7 sec
Iron loss resistance	300 p.u.
Mechanical friction and windage	0 p.u.
Neutral series resistance	1E+05 p.u.
Neutral series reactance	0 p.u.
Armature resistance (Ra)	0.002 p.u.
Potier reactance (Xp)	0.13 p.u.
Unsaturated reactance (Xd)	0.92 p.u.
Unsaturated transient reactance (Xd')	0.3 p.u.
Unsaturated transient time (Tdo')	5.2 sec
Unsaturated sub-transient reactance (Xd'')	0.22 p.u.
Unsaturated sub-transient time (Tdo'')	0.029 p.u.
Unsaturated reactance (Xq)	0.51 p.u.
Unsaturated sub-transient reactance (Xq'')	0.29 p.u
Unsaturated sub-transient time (Tqo'')	0.034 sec
Air gap factor	1.0

Table C.2 Exciter Parameters

Regulator gain (Ka)	400 p.u.
Regulator time constant (Ta)	0.02 s
Rate feedback gain (Kf)	0.03 p.u.
Rate feedback time constant (Tf)	1 s
Exciter time constant (Te)	0.8 s
Exciter constant related to field (Ke)	1 p.u.
Field circuit commutating reactance (Kc)	0.2 p.u.
Demagnetizing factor (Kd)	0.38 p.u.
Saturation at VE1	0.1 p.u.
Exciter voltage for SE1	4.18 p.u.
Saturation at VE2	0.03 p.u.
Exciter voltage for SE1	3.14 p.u.

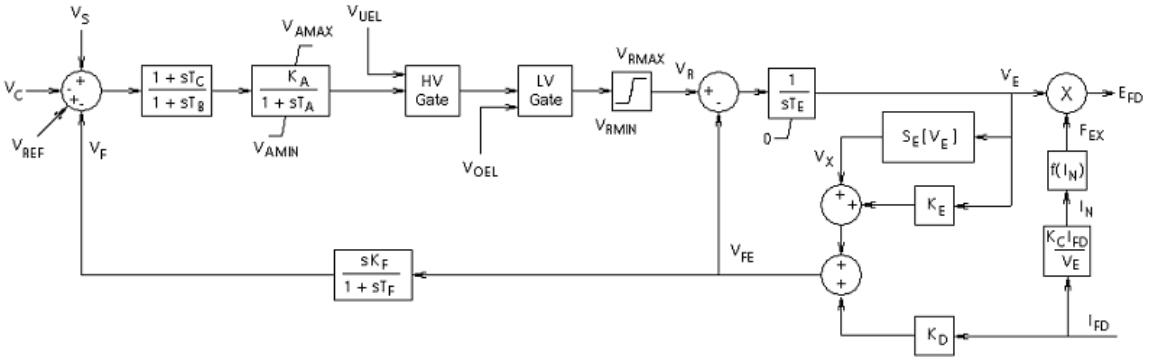

Where,

V_C = Output of terminal voltage transducer and load compensation elements [pu]

V_{REF} = Voltage regulator reference (determined to satisfy initial conditions) [pu]

V_S = Combined power system stabilizer and possibly discontinuous control output after any limits or switching, as summed with terminal voltage and reference signals [pu]

V_F = Excitation system stabilizer output [pu]

V_{AMAX}, V_{AMIN} = Maximum and minimum regulator output limits [pu]

K_A = Voltage regulator gain [pu]

T_A, T_B, T_C = Voltage regulator time constants [s]

V_{UEL} = Under-excitation limiter output [pu]

V_{OEL} = Over-excitation limiter output [pu]

V_{RMAX}, V_{RMIN} = Maximum and minimum regulator output limits [pu]

V_R = Voltage regulator output [pu]

V_{FE} = Signal proportional to exciter field current [pu]

T_E = Exciter time constant, integration rate associated with exciter control [s]

V_E = Exciter voltage back of commutating reactance [pu]

K_E = Exciter constant related to self-excited field [pu]

K_D = Demagnetizing factor, a function of exciter alternator reactance [pu]

K_F = Excitation control system stabilizer gain [pu]

V_X = Signal proportional to exciter saturation [pu]

$S_E \cdot [V_E]$ = Exciter saturation function value at the corresponding exciter voltage, V_E, back of commutation reactance [pu]

K_C = Rectifier loading factor proportional to commutation reactance [pu]

I_{FD} = Synchronous machine field current [pu]

I_N = Normalized exciter load current [pu]

V_{RMAX}, V_{RMIN} = Maximum and minimum regulator output limits [pu]

V_R = Voltage regulator output [pu]

V_{FE} = Signal proportional to exciter field current [pu]

T_E = Exciter time constant, integration rate associated with exciter control [s]

V_E = Exciter voltage back of commutating reactance [pu]

K_E = Exciter constant related to self-excited field [pu]

K_D = Demagnetizing factor, a function of exciter alternator reactance [pu]

K_F = Excitation control system stabilizer gain [pu]

V_X = Signal proportional to exciter saturation [pu]

$S_E \cdot [V_E]$ = Exciter saturation function value at the corresponding exciter voltage, V_E, back of commutation reactance [pu]

K_C = Rectifier loading factor proportional to commutation reactance [pu]

I_{FD} = Synchronous machine field current [pu]

I_N = Normalized exciter load current [pu]

F_{EX} = Rectifier loading factor, a function of I_N [pu]

E_{FD} = Exciter output voltage [pu]

Figure C.1 Transfer function for Exciter model

Table C.3 Governor Parameters

Servo gain (Q)	5 p.u.
Servo motor time constant (Tp)	0.05 s
Main servo time constant (Tg)	0.2 s
Temporary droop (Rt)	0.4 p.u.
Reset time constant (Tr)	5 s
Dead band value	0 p.u.
Permanent droop (Rp)	0.04 p.u.
Maximum gate position (Gmax)	1 p.u.
Minimum gate position (Gmin)	0 p.u.
Maximum gate opening rate	0.16 p.u./s
Maximum gate closing rate	0.16 p.u./s

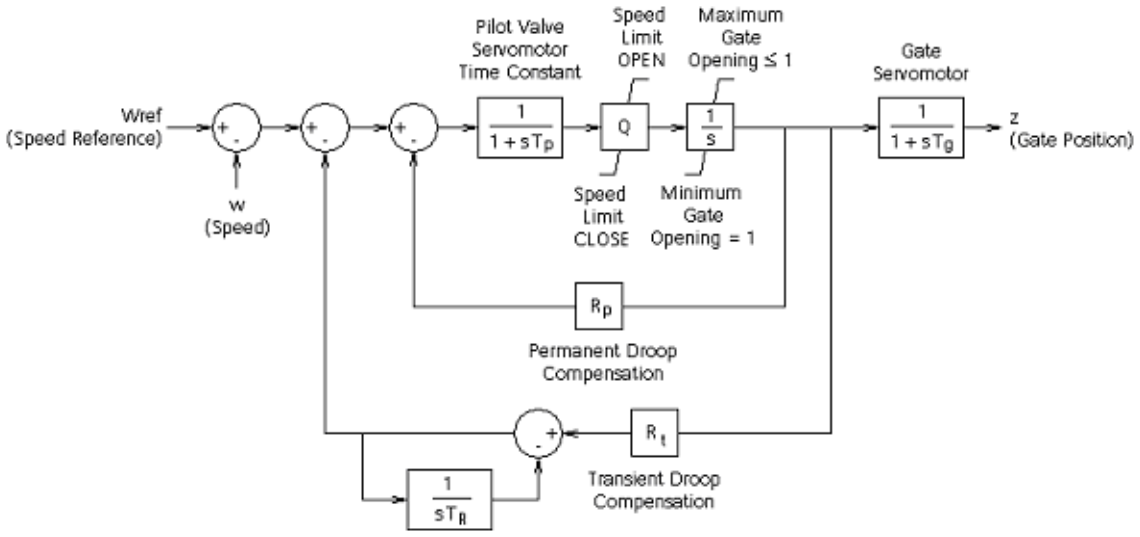

Where,

$Q =$ Servo gain [pu]

$R_p =$ Permanent Droop [pu]

$R_t =$ Temporary Droop [pu]

$T_g =$ Main Servo Time Constant [s]

$T_p =$ Pilot valve and servo motor time constant [s]

$T_R =$ Reset or Dashpot Time Constant [s]

Figure C.2 Transfer function for Governor model

Table C.4 Turbine Parameters

Head at rated conditions	1 p.u.
Output power at rated conditions	1 p.u
Initial output power	1 p.u.
Initial operating head	1 p.u.
Turbine damping constant	0.5

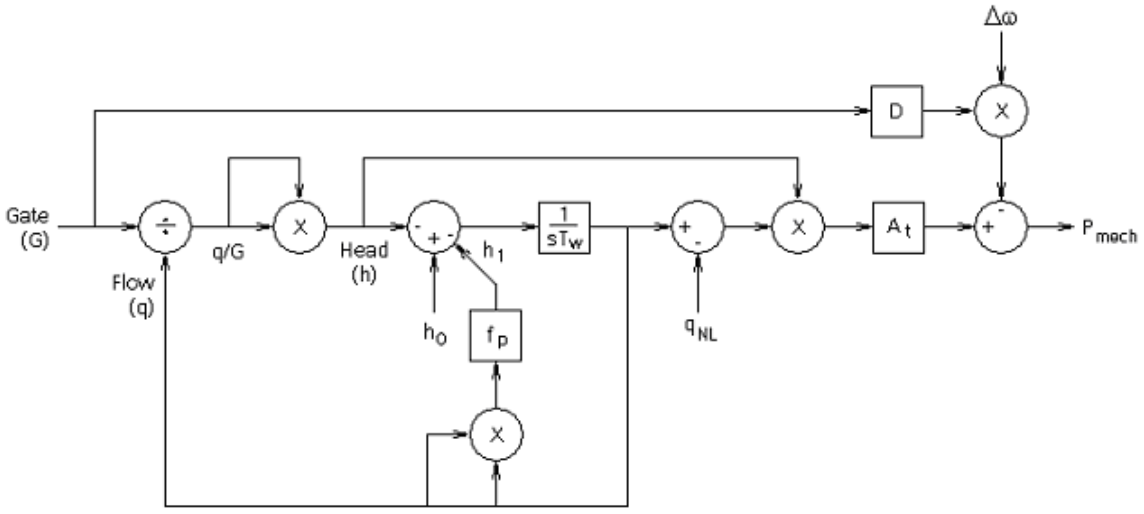

Where,

A_t = Turbine Gain Factor Flow

f_p = Penstock Head Loss Coefficient [pu]

G = Gate Position [pu]

q = Turbine Flow Before reduction by Deflector and Relief valves [pu]

q_{NL} = No load water flow [pu]

T_w = Water Starting Time [s]

Figure C.3 Transfer function for Turbine model

APPENDIX D

B-H Data FOR GRAIN ORIENTED SILICON STEEL

POGGEN - AMP NAGARSHETH POWERTRONICS LTD

Sample data

Coil : Epstein 50 Hz

Identification

Name	:	PAN364	
Mass	:	260	g
Density	:	7,75	g/cm³
Length	:	280	mm
Width	:	30	mm
Thickness	:	499	µm
Number	:	8	
Quality	:		

Operator : Administrator
Date : 26/09/2002
Time : 10:20:27

Info

Measuring results

Mess.	Freq. [Hz]	Jd [mT]	Je [mT]	Jr [mT]	Hd [A/m]	Hc [A/m]	Ps [W/kg]	Ss [VA/kg]	FF	µ	DC [%]	Richt.	He [A/m]
1	50	999,88	708,0	804,0	159,58	81,87	1,927	3,005	1,113	4988	0,74	Misch	104,62
2	50	1099,91	779,0	883,0	191,38	86,47	2,288	3,755	1,113	4575	0,45	Misch	118,81
3	50	1199,82	850,0	957,0	240,97	91,01	2,694	4,764	1,113	3963	0,24	Misch	138,76
4	50	1299,75	922,0	1024,0	328,1	95,83	3,16	6,388	1,114	3152	0,12	Misch	170,97
5	50	1399,8	992,0	1081,0	524,32	100,01	3,699	9,48	1,113	2124	0,98	Misch	235,78
6	50	1499,46	1063,0	1115,0	1144,5	102,29	4,344	19,127	1,113	1042	0,52	Misch	443,83
7	50	1599,93	1136,0	1141,0	2975,52	104,56	5,034	51,962	1,115	427,0	0,15	Misch	1128,53
8	50	1699,32	1208,0	1147,0	6235,21	111,38	5,62	123,559	1,117	216,0	0,03	Misch	2521,8
9	50	1457,81	1033,0	1103,0	799,56	101,72	4,066	13,677	1,113	1451	0,85	Misch	326,54
10	50	1580,72	1122,0	1132,0	2504,95	104,56	4,911	42,926	1,114	502,0	0,11	Misch	943,92
11	50	1660,74	1180,0	1140,0	4864,47	106,83	5,395	91,892	1,116	271,0	0,07	Misch	1920,53
12	50	1778,04	1267,0	1155,0	9869,92	109,11	6,044	214,814	1,119	143,0	0,02	Misch	4182,36

FREQUENCY
PEAK VALUE INDUCTION
EFFECTIVE INDUCTION
REMANENT INDUCTION
PEAK FIELD STRENGTH
COERCITIVE FIELD STRENGTH
CORE LOSS
APPARENT POWER
FORM FACTOR
PERMEABILITY
ASYMMETRY
MEASURING DIRECTION
EFFECTIVE FIELD STRENGTH

APPENDIX E

THERMAL RESISTANCES UNDR BY-PASS MODE OF OPERATION

In chapter 7, a steady state thermal model of the DSR unit was developed. The explanation of various thermal resistances is presented here.

The temperature gradient between the cable enclosed within the module and the cable outside the module creates a path for conductive heat flow. Equation (E.1) gives the thermal resistance for conduction of heat through the cable.

$$R_{cable} = \frac{d}{\lambda_{cable} A} \, {}^{0}C/W \tag{E.1}$$

Here, λ_{cable} is the thermal conductivity of the ACSR cable, A is the area of cross section of the cable in m^2, and d is the length of the cable over which conductive heat flow occurs.

The heat is then transferred to the surroundings by radiation and convection from the cable. Equations (E.2) and (E.3) give the thermal resistances for convective and radiative heat transfer to the ambient.

$$R_{cable\_conv} = \frac{1}{1.34 A_{cable}} \left(\frac{d_{cable}}{T_{cable\_out} - T_{amb}} \right)^{0.25} {}^{0}C/W \tag{E.2}$$

Here, R_{cable_conv} refers to the thermal resistance for convective heat transfer from the cable, A_{cable} refers to the surface area of the cable, and d_{cable} refers to the outer diameter of the cable.

$$R_{cable\_rad} = \frac{\left(T_{cable\_out} - T_{amb}\right)}{5.7\,\varepsilon\, A_{core}} \frac{1}{\left(\left(\frac{T_{case\_out}}{100}\right)^4 - \left(\frac{T_{amb}}{100}\right)^4\right)} \ {}^0C/W \tag{E.3}$$

Here, R_{cable_rad} refers to the thermal resistance for radiative heat transfer from the cable and ε is the emissivity of ACSR conductor.

The transfer of heat also occurs by conduction from the cable enclosed within the module to the transformer core. Aluminum armor rods will be wrapped around the conductor to protect against damage during installation. Thermal conductivity of aluminum is very high and majority of heat will be conducted through it. Equation (E.4) gives the thermal resistance of the armor rods, which accounts for the heat transfer from the cable to the inside surface of the core.

$$R_{armor} = \frac{\ln\left(r_{ci} / r_{cable}\right)}{2\pi\, \lambda_{armor} L_c} = 3.8 \times 10^{-4} \ {}^0C/W \tag{E.4}$$

Here, λ_{armor} is the thermal conductivity of aluminum armor rods and is equal to 206 W/m/^{0}C [61].

The heat then flows through the body of the core, by the process of thermal conduction. R_{core} refers to the thermal resistance of the core and is given by (E.5). The thermal conductivity of the core is assumed to be that of steel, which is 45 W/m/^{0}C [61].

$$R_{core} = \frac{\ln(r_{co}/r_{ci})}{2\pi\,\lambda_{core} L_c} = 1.8\times10^{-3}\ {}^0C/W \tag{E.5}$$

Here, λ_{core} is the thermal conductivity of the steel core.

The heat from the outer surface of the core gets transferred to the module casing through convection and radiation. The thermal resistances for natural convection and radiation are given by (E.6) and (E.7) respectively.

$$R_{core\_conv} = \frac{1}{1.34\,A_{core}}\left(\frac{d_{core}}{T_{core\_out} - T_{case\_in}}\right)^{0.25} = \frac{1.2356}{\left(T_{core\_out} - T_{case\_in}\right)^{0.25}}\ {}^0C/W \tag{E.6}$$

Here, R_{core_conv} refers to the thermal resistance for convective heat transfer from the outer surface of the core, A_{core} refers to the surface area of the core and is calculated to be 0.3308 m^2, and d_{core} refers to the outer diameter of the core and is equal to 0.09 m.

$$\begin{aligned} R_{core\_rad} &= \frac{\left(T_{core\_out} - T_{case\_in}\right)}{5.7\,\varepsilon\,A_{core}} \frac{1}{\left(\left(\frac{T_{core\_out}}{100}\right)^4 - \left(\frac{T_{case\_in}}{100}\right)^4\right)} \\ &= \frac{2.6517\left(T_{core\_out} - T_{case\_in}\right)}{\left(\left(\frac{T_{core\_out}}{100}\right)^4 - \left(\frac{T_{case\_in}}{100}\right)^4\right)}\ {}^0C/W \end{aligned} \tag{E.7}$$

Here, R_{core_rad} refers to the thermal resistance for radiative heat transfer from the outer surface of the core and ε is the emissivity of the steel core, which is equal to 0.2 [61].

Finally, the heat is conducted through the module casing, before being transferred to the surroundings through convection and radiation. Equations (E.8) – (E.10) give the thermal resistances associated with each of these modes of heat transfer.

$$R_{case} = \frac{\ln\left(r_{do} / r_{di}\right)}{2\pi \lambda_{case} L_d} = 4.12 \times 10^{-5} \ {}^0C/W \tag{E.8}$$

Here, R_{case} refers to the thermal resistance of heat conduction of the casing, and λ_{case} is the thermal conductivity of the aluminum casing and is equal to 206 W/m/^{0}C.

$$R_{case\_conv} = \frac{1}{1.34\, A_{case}} \left(\frac{d_{case}}{T_{case\_out} - T_{amb}} \right)^{0.25} = \frac{0.7266}{\left(T_{case\_out} - T_{amb}\right)^{0.25}} \ {}^0C/W \tag{E.9}$$

Here, R_{case_conv} refers to the thermal resistance for convective heat transfer from the outer surface of the case, A_{case} refers to the surface area of the casing and is calculated to be 0.6131 m^2, and d_{case} refers to the outer diameter of the casing and is equal to 0.127 m.

$$R_{case\_rad} = \frac{\left(T_{case\_out} - T_{amb}\right)}{5.7\,\varepsilon\, A_{core}} \frac{1}{\left(\left(\frac{T_{case\_out}}{100}\right)^4 - \left(\frac{T_{amb}}{100}\right)^4\right)}$$

$$= \frac{0.3198\left(T_{case\_out} - T_{amb}\right)}{\left(\left(\frac{T_{case\_out}}{100}\right)^4 - \left(\frac{T_{amb}}{100}\right)^4\right)} \ {}^0C/W \qquad \text{(E.10)}$$

Here, R_{core_rad} refers to the thermal resistance for radiative heat transfer from the outer surface of the casing and ε is the emissivity of black oxidized aluminum surface and is equal to 0.9 [61].

APPENDIX F

PCB LAYOUT OF POWER SUPPLY

The Printed circuit board is designed as a four layer board[3] (Figure E.1). The copper layers on the top and bottom are shown in Figure E.2 and Figure E.3 respectively. The middle two layers are designed to be the ground and the 24 V DC. Table E.1 explains the different components of the PCB.

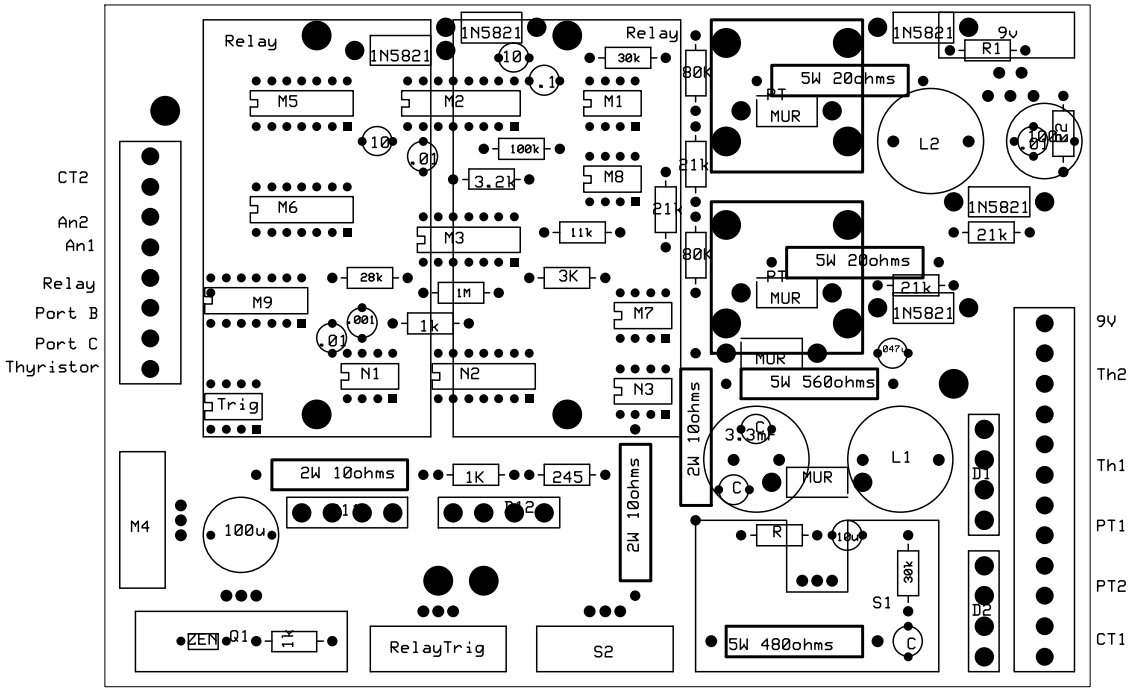

Figure F.1 PCB Layout

[3] Debrup Das, Georgia Tech

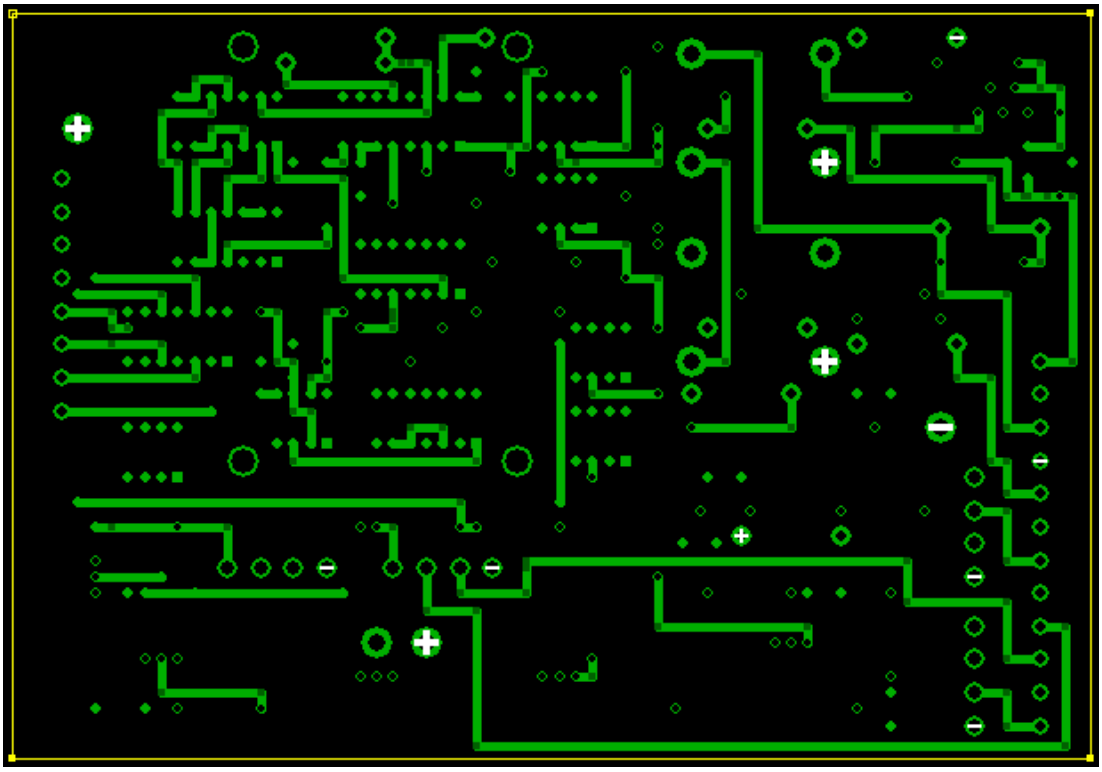

Figure F.2 Top layer

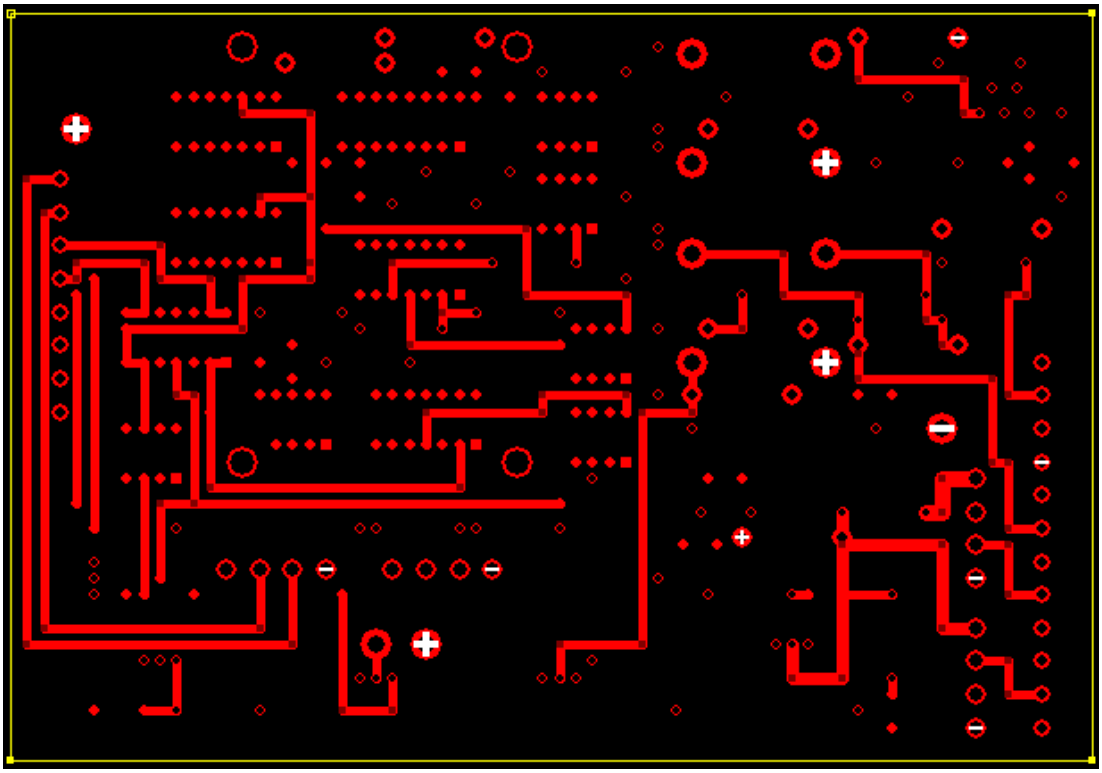

Figure F.3 Bottom layer

Table F.1 PCB Component Details

Component Name	Description	Specification
PT1	Power supply voltage transformer	460:25 V, 24 VA
PT2	Control voltage transformer	460:32 V, 10 VA
CT1	Power supply current transformer	150:3 A, 24 VA
CT2	Control current transformer	10:1 A, 10 VA
PT	Pulse transformer	RL-7376 0306 Renco
S1, S2	Mosfet	STP80 NF1
Q1	NPN Transistor	TIP 81A
Thyristor	Thyristor pair	SKKT 250/16E
L1	Inductor	560 μH, 5A
C1	Electrolytic capacitor	3.3 mF, 100 V
Zen	Zener diode	IN5240BT
MUR	Fast recovery diode	MUR405
9 V	9 VDC Regulated supply	LM2595T
L2	Inductor	68 μH, 1 A
C	Ceramic Capacitor	0.1 μF, 100 V
Relay	Normally closed electro-mechanical relay	300XBXC1
M1	Op-Amp	TL082ACP
M2	PWM controller	UC2823AN
M3	Comparator	LM339
M4	5 VDC Voltage regulator	LD1084 V50
M5	NAND gate	MC14011BCP
M6	NOR gate	MC14001BCP
M7	Mosfet driver	UC3710N
M8	Op-Amp	TL082ACP
M9	Op-Amp	TLV2474
N1	Timer	LM555
N2	NAND Gate	MC14011BCP
N3	Mosfet Driver	UC3710N
D1, D2	Rectifier bridge	GBU 8B
D11, D12	Rectifier bridge	GBU 8B
Th1	Signal for gate 1 of thyristor pair	-
Th2	Signal for gate 2 of thyristor pair	-
Port B	Port B of μ-controller (Relay signal)	-
Port C	Port C of μ-controller (Thyristor signal)	-
AN2	Analog port of micro-controller	-
AN1	Analog port of micro-controller	-

APPENDIX G

HIGH VOLTAGE TEST DATA AND RESULTS

National Electric Energy Testing Research & Applications Center
NETRAC
A Research Center in the School of Electrical and Computer Engineering at the Georgia Institute of Technology

Corona & RIV Test Data Sheet

Manufacturer: Georgia Tech	Date: 12/20/2007
Project: 07-079	
Sample Description: First generation prototype of a fault current limiter/power flow controller	
Test Standards: NEMA 107	ASTM STP 669
RIV Factor: 0.286	
Barometric Pressure: 736.4 mm Hg @ 20 °C	Wet Bulb: 56 °F
Vapor Pressure: in. Hg	Dry Bulb: 69 °F
Distance to Ground: 11' from simulated conductor, 10' 5~~7~~" from lowest point on device	

Test Voltage (kV)	Peak RIV Reading on Meter (μV)	Actual RIV (μV)	Comments
140	42	14685	40 dB scale
130	42	14685	40 dB scale
120	42	14685	40 dB scale
110	42	14685	40 dB scale
86	400	13986	20 dB scale
80	400	13986	20 dB scale
75	10	350	20 dB scale
55	50	175	0 dB scale
35	14	49	0 dB scale
HV ON 3600/15kV	2.5	1	-20 dB scale
HV OFF	2.5	1	-20 dB scale

Notes: Internal wiring is floating and possibly sparking
Ground Plane Distance: 11' from 1" OD simulated conductor
Corona Inception: 125 kV
Corona Extinction: 123 kV
Bolt on top of housing holding housing together see corona photo on North end

Photo #6, 166kV, 4min exposure, f/4.5 east facing
#5, 166 kV, 4min exposure, f/4.5 west facing

REFERENCES

[1] National Transmission Grid Study, US Department of Energy. May 2002. Available: http://www.pi.energy.gov/documents/TransmissionGrid.pdf. Accessed: May 2006.

[2] National Electric Transmission Congestion Study, US Department of Energy. 2006. Available:http://www.oe.energy.gov/DocumentsandMedia/Congestion_Study_2006-9MB.pdf. Accessed: May 2006.

[3] M. J. Museler, President and CEO of the New York Independent System Operator (NYISO), presentation. May 22, 2003. Available: http://www.nyiso.com/topics/articles/news_releases/2003/pa3_presentation.pdf. Accessed: Jan 2006.

[4] W.F. Tinney and C.E. Hart, "Power Flow Solution by Newton's Method," in IEEE Transactions on Power Apparatus and Systems, vol. 86, issue 11, Nov. 1976, pp. 1449- 1460.

[5] B. Stott and O. Alsac, "Fast Decoupled Load Flow", in IEEE Transactions on Power Apparatus and Systems, vol. 93, issue 3, May 1974, pp. 859- 869.

[6] O.J.M. Smith, "Power System State Estimation," in IEEE Transactions on Power Apparatus and Systems, vol. 89, issue 3, March 1970, pp. 363- 379.

[7] H.M. Merrill and F.C. Schweppe, "Bad Data Suppression in Power System Static State Estimation," in IEEE Transactions on Power Apparatus and Systems, vol. 90, issue 6, Sept. 1973, pp. 2718- 2715.

[8] H.W. Dommel and W.F. Tinney, "Optimal Power Flow Solutions," in Power System Static State Estimation," in IEEE Transactions on Power Apparatus and Systems, vol. 87, issue 10, Sept. 1968, pp. 1866- 1876.

[9] W.R. Barcelo, W.W. Lemmon, and H.R. Koen, , "Optimization of the real-time dispatch with constraints for secure operation of bulk power systems," in IEEE Transactions on Power Apparatus and Systems, vol. 96, issue 3, part 1, May 1977, pp. 1866- 1876.

[10] G. Hadley, Nonlinear and Dynamic Programming. Reading, Mass.: Addison-Wesley, 1964. pp. 60.

[11] H. A. Spang, "A review of minimization techniques for nonlinear functions," IAM Review, vol. 4, pp. 343-365, October 1962.

[12] H. Harsan, N. Hadjsaid, and P. Pruvot, "Cyclic security analysis for security constrained optimal power flow," in IEEE Transactions on Power Systems, vol. 12, issue 2, May 1997, pp. 948- 953.

[13] P. W. Sauer and M. A. Pai, Power System Dynamics and Stability. Upper Saddle River, NJ: Prentice-Hall. 1998.

[14] L. Gyugyi and E.R. Taylor, "Characteristics of Static, Thyristor-Controlled Shunt Compensators for Power Transmission System Applications," in IEEE Transactions on Power Apparatus and Systems, vol. 99, issue 5, Sept. 1980, pp. 1795- 1804.

[15] C. W. Edwards, K.E. Mattern, E.J. Stacey, P.R. Nannery, and J. Gubernick, **"**Advanced state VAR generator employing GTO thyristors," in IEEE Transactions on Power Delivery, vol. 3, issue 4, Oct 1988, pp. 1622-1627.

[16] L. Gyugyi**, "**Power electronics in electric utilities: static VAR compensators," in Proceedings of the IEEE, vol. 76, issue 4, April 1988, pp. 483-494.

[17] H. Liu, Z. Xu, and Z. Gao, **"**Study on SSR characteristics of power systems with static VAr compensator," in the proceedings of AC-DC Power Transmission, Nov. 2001, pp. 193-198.

[18] L. Gyugyi, "Dynamic compensation of AC transmission lines by solid-state synchronous voltage sources," in IEEE Transactions on Power Delivery, vol. 9, issue 2, April 1994, pp. 904-911.

[19] A.F.J. Keri, et al., "Improved Transmission System Performance Using Controlled Series Capacitors," CIGRE Paper 14/37/38-07, 1992.

[20] S.G. Helbing and G.G. Karady, "Investigations of an advanced form of series compensation," in IEEE Transactions on Power Delivery, vol. 9, issue 2, April 1994, pp. 939-947.

[21] E.V. Larsen, K. Clark, S.A. Miske, and J. Urbanek, "Characteristics and rating considerations of thyristor controlled series compensation," in IEEE Transactions on Power Delivery, vol. 9, issue 2, April 1994, pp. 992-1000.

[22] J. Urbanek, R.J. Piwko, E.V. Larsen, B.L. Damsky, B.C. Furumasu, W. Mittlestadt, and J.D. Eden, "Thyristor controlled series compensation prototype installation at the Slatt 500 kV substation," in IEEE Transactions on Power Delivery, vol. 8, issue 3, July 1993, pp. 1460-1469.

[23] A.L. Courts, N.G. Hingorani, and G.E. Stemler, "A New Series Capacitor Protection Scheme Using Nonlinear Resistors," in IEEE Transactions on Power Apparatus and Systems, vol. 97, issue 4, July 1978, pp. 1042-1052.

[24] IEEE Subsynchronous Resonance Working Group of the System Dynamic Performance Subcommittee, "Series Capacitor Controls and Settings as Countermeasures to Subsynchronous Resonance," in *IEEE* Transactions on Power Apparatus and Systems, vol. 101, issue 6, July 1982, pp. 1281-1287.

[25] L. Gyugyi, C.D. Schauder, and K.K. Sen, "Static synchronous series compensator: a solid-state approach to the series compensation of transmission lines," in IEEE Transactions on Power Delivery, vol. 12, issue 1, Jan. 1997, pp. 406-417.

[26] J. Verboomen, D. Van Hertem, P.H. Schavemaker, W.L. Kling, and R. Belmans, "Phase shifting transformers: principles and applications," in International Conference on Future Power Systems, Nov. 2005.

[27] B.K. Patel, H.S. Smith, T.S. Hewes, and W.J. Marsh, "Application of Phase Shifting Transformers for Daniel-McKnight 500kV Interconnection," in IEEE Transactions on Power Delivery, vol. 1, issue 3, Jan. 1986, pp. 167-173.

[28] J.K. Bladow and A.H. Montoya, "Experiences with parallel EHV phase shifting transformers," in IEEE Transactions on Power Delivery, vol. 6, issue 3, Jan. 1991, pp. 1096-1100.

[29] M.R. Iravani and D. Maratukulam, "Review of semiconductor-controlled (static) phase shifters for power systems applications," in IEEE Transactions on Power Systems, vol. 9, issue 4, Nov. 1994, pp. 1833-1839.

[30] K.K. Sen and M.L. Sen, "Introducing the family of "Sen" transformers: a set of power flow controlling transformers," in IEEE Transactions on Power Delivery, vol. 18, issue 1, Jan. 2003, pp. 149-157.

[31] D. Divan and J. Sastry, "Controllable Network Transformers," in IEEE Proceedings of Power Electronics Specialist Conference, June 2008, pp. 2340- 2345.

[32] D. Divan and J. Sastry, "Voltage Synthesis using Dual Virtual Quadrature Sources," Controllable Network Transformers," in IEEE Proceedings of Power Electronics Specialist Conference, June 2007, pp. 2678- 2684.

[33] L. Gyugyi, "Unified power-flow control concept for flexible AC transmission systems," in IEE Proceedings – Generation, Transmission and Distribution, vol. 139, issue 4, July 1992, pp. 323-331.

[34] L. Gyugyi, "Dynamic compensation of AC transmission lines by solid-state synchronous voltage sources," in IEEE Transactions on Power Delivery, vol. 9, issue 2, April 1994, pp. 904-911.

[35] C. Schauder, E. Stacey, M. Lund, L. Gyugyi, L. Kovalsky, A. Keri, A. Mehraban, and A. Edris, "AEP UPFC project: installation, commissioning and operation of the ±160 MVA STATCOM (phase I)," in IEEE Transactions on Power Delivery, vol. 13, issue 4, Oct. 1998, pp. 1530-1535.

[36] D.M. Divan, W.E. Brumsickle, R.S. Schneider, B. Kranz, R.W. Gascoigne, D.T. Bradshaw, M.R. Ingram, and I.S. Grant, "A Distributed Static Series Compensator System for Realizing Active Power Flow Control on Existing Power Lines," in IEEE Transactions on Power Delivery, vol. 22, issue 1, Jan. 2007, pp. 642-649.

[37] R.C. Arkin, "Dynamic replanning for a mobile robot based on internal sensing," in Proceedings of the International Conference on Robotics and Automation, vol. 3, May 1989, pp. 1416-1421.

[38] R.C. Arkin, "The impact of cybernetics on the design of a mobile robot system: a case study," in IEEE Transactions on Systems, Man, and Cybernetics, vol. 20, issue 6, Dec. 1990, pp. 1245- 1257.

[39] F.C. Schweppe, R.D. Tabors, J.L. Kirtley, H.R. Outhred, F.H. Pickel, and A.J. Cox, "Homeostatic Utility Control," in IEEE Transactions on Power Apparatus and Systems, vol. 99, issue 3, May 1980, pp. 1151- 1163.

[40] EPRI Report, Electricity Technology Roadmap: 1999 Summary and Synthesis. Report CI-112677-V1, EPRI, Palo Alto California. Available: http://www.epri.com.

[41] M. A. Pai, Energy Function Analysis for Power System Stability. Boston: Kluever Academic Publishers. 1989.

[42] Status of State Electric Industry Restructuring Activity, US Energy Information Administration. Available: http://www.eia.doe.gov/cneaf/electricity. Accessed: June 2006.

[43] R. Munson, **"**Deregulation and the power struggle," IEEE Spectrum**,** vol. 25, issue 5, April 1988, pp. 61-63.

[44] Operating Agreement of PJM Interconnection, PJM Interconnection. [Online]. Available: http://www.pjm.com/documents/downloads/agreements/oa.pdf

[45] M. Xingwang, D.I. Sun, and K.W. Cheung, "Evolution toward standardized market design," in IEEE Transactions on Power Systems, vol. 18, issue 2, May 2003, pp. 460-469.

[46] Congestion Workshop, "A Discussion of Locational Based Marginal Pricing, Transmission Congestion Contracts, and Congestion in New York," National Grid Transmission Regulation and Commercial, Aug. 26 2004.

[47] J. Frame, "Locational marginal pricing," in the proceeding of IEEE Power Engineering Society, Winter Meeting, vol. 1, Jan. 2001, pp. 377-382.

[48] NYISO attachment B. Available: http://www.nyiso.com/public/archive/webdocs/committees/Market%20Structure%20WG/2001-07-27/mst_attchmnt_b_103_vb.pdf. Accessed: May 2007.

[49] B.C. Lesieutre and J.H. Eto, "Electricity Transmission Congestion Costs: A Review of Recent Reports." Available: http://certs.lbl.gov/pdf/54049.pdf. Accessed: May 2006.

[50] M. Zeng, L. Wang, Z. Liu, W. Zhou, and X. Chen, "Research on the Theory of Financial Transmission Right and its Application in the Electricity Market," in the Proceedings of International Conference on Power System Technology, 2006, pp. 1-5.

[51] Estimated costs of conventional and FACTS devices, EPRI Report. Accessed: Jan. 2006.

[52] Report of Electric Consumers Resource Council, 2004. Available: www.elcon.org/Documents/EconomicImpactsOfAugust2003Blackout.pdf. Accessed: Aug. 2004.

[53] Energy Policy Act of 2005. Available: www.epa.gov/oust/fedlaws/publ_109-058.pdf. Accessed: Aug. 2005.

[54] Energy Independence and Security Act, 2007. Available: http://www.pserc.org/docsa/Energy_Independence_Security_Act.pdf. Accessed: Jan. 2008.

[55] Arthur Bergen, Power System Analysis. Prentice Hall. 1986.

[56] Mark Rauls, 'Analysis and Design of High Frequency Co-Axial Winding Transformers', MS Thesis. University of Wisconsin Madison. 1992.

[57] R.C. Mullin and R.L. Smith, Electrical Wiring Commercial. pp. 309.

[58] Colonel McLyman, Transformer and Inductor Design Handbook, Marcel Dekker Inc.

[59] G.R. Jones, M.A. Laughton, and M.G. Say, Electrical Engineer's Reference Handbook. Butterworth-Heinemann Ltd. 1993.

[60] Philip Beckley, Electrical Steels for Rotating Machines, IEE Power and Energy Series 37. 2002

[61] Frank Kreith, Principles of Heat Transfer. International Text book Company. 1958.

[62] PIC18F1320 Datasheet. Microchip. Available: http://ww1.microchip.com/downloads/en/DeviceDoc/39605F.pdf

[63] J.D. Cobine, Gaseous Conductors: Theory and Engineering Applications, 3rd edition New York: Dover. 1958. pp. 173-177.

[64] Ferreira, H.C.; Grove, H.M.; Hooijen, O.; Han Vinck, A.J., "Power line communications: an overview," in IEEE AFRICON, vol. 2, Sep. 1996, pp. 558-563.